The C M D S Flow-Rate and Conductivity Transducer:
Design, Manufacture and Testing

by

Peter William George Byrnes
B.Sc., University of Victoria, 1989

A Thesis Submitted in Partial Fulfillment of the
Requirements for the Degree of

MASTER OF APPLIED SCIENCE

in the Department of Mechanical Engineering

We accept this thesis as conforming
to the required standard

[redacted]

Dr. G.W. Vickers, Supervisor (Department of Mechanical Engineering)

[redacted]

Dr. N. Djilali, Member (Department of Mechanical Engineering)

[redacted]

Dr. T.M. Fyles, Outside Member (Department of Chemistry)

[redacted]

Dr. P.M. Wild, Additional Member (Queen's University)

[redacted]

Dr. M. Miller, External Examiner (Department of Computer Science)

Supervisor: Dr. G.W. Vickers

Abstract

Beginning from preliminary design constraints and functional requirements, a custom Flow-Rate And Conductivity Transducer (FRACT) was conceived, designed, and built for use in situ aboard the spinning rotor of the Centrifugal Membrane and Density Separation (CMDS) Research centrifuge. It was subjected to rigorous laboratory simulation of the centrifuge environment for structural and operational validation. The original prototype underwent incremental development, was installed on the newly completed centrifuge rotor, and was calibrated and commissioned. It performs liquid flow-rate measurement in the 1–20 mL/min range to better than 2% accuracy and precision. Conductivity measurement is attainable to similar accuracy and 0.3% precision across two ranges: 0–340 µS/cm and 0.44-5 mS/cm, corrected for temperature. Operation has been proven to rotor speeds imposing 3100 G centripetal acceleration upon the device. A suite of control and data acquisition "Virtual Instrumentation" software was also developed to complete the measurement system.

Examiners: [redacted]

Dr. G.W. Vickers, Supervisor (Department of Mechanical Engineering)

[redacted]

Dr. N. Djilali, Member (Department of Mechanical Engineering)

[redacted]

Dr. T.M. Fyles, Outside Member (Department of Chemistry)

[redacted]

Dr. P.M. Wild, Additional Member (Queen's University)

[redacted]

Dr. M. Miller, External Examiner (Department of Computer Science)

Table of Contents

Chapter 1: Introduction

Chapter 2: Flow-Rate Measurement

Chapter 5: Commissioning and Calibration

Chapter 6: Control and Data Acquisition Software

Chapter 7: Example Results from C•M•D•S and Conclusions

List of Tables

List of Figures

Nomenclature

f	oscillator frequency
g	acceleration due to "gravity"
$h_{surface}$	fluid surface height
k	polarization slope
l	electrode separation
m_{net}	net mass
n	number of engaged threads
r	radius
$v_{surface}$	fluid surface velocity
y_d	discharge orifice height
y_L	fluid surface height
A	area
A_d	discharge orifice sectional area
C	constraint
C_d	discharge coefficient
DP	design parameter
FR	functional requirement
G	conductance
G_r	centrifugal acceleration
K_c	cell constant

L................conductivity, characteristic length
L_M..............measured conductivity
L_{25}.............. specific conductivity (at 25°C)
M_{full}............full chamber fluid mass
P................pressure
R_{calc}............radial position for centrifugal pressure calculations
R_M.............. measured resistance
R_T..............true (electrolyte) resistance
S_S.............. shear stress
T................temperature
V................volume
α................coefficient of linear thermal expansion
ρ_{fluid}............fluid density
ω............... rotation speed
Γ_T..............temperature compensation coefficient

Acknowledgements

I wish to acknowledge first the privilege of returning to the University of Victoria to pursue graduate studies, which was made possible by Dr. Geoffrey Vickers.

The camaraderie of the C•M•D•S Research team and of my colleagues in the Advanced Manufacturing Laboratory made it a pleasure to spend time working on this project. In particular, my supervisory committee was supportive yet properly demanding.

Finally, I gratefully acknowledge the unqualified support, patience, and encouragement of my family, and of my dear friend Alison Bird.

Dedication

I dedicate this work to my parents: Olga Emily Byrnes, and Earl Madigan Byrnes, P.Eng., (Queen's: Science '49), who presented to me the Iron Ring.

1 Introduction

1.1 PRELIMINARIES

Production of potable water from seawater or other brackish stocks has been a technological capability for decades, but with the peopling of desert territory the world over, the depletion of natural fresh water sources, and the need to restrict discharges of contaminated effluents, has now grown into an industry of colossal proportions. This trend shows no sign of slackening. Distillation is perhaps the most familiar purification process, but has been supplanted in recent years by membrane processes, which provide considerable operating cost savings.

The mainstream membrane separation industry offers purification plants in various capacities, cataloging infrastructure such as pumps, valves and, most significantly, membrane cartridges, in many standard sizes and configurations. Recent research and development activity, however, has sought to further improve on membrane separation yields and cost effectiveness at a systemic level, by fundamentally altering the process energetics and infrastructure.

One of the most promising of these activities replaces much of the conventional equipment with a single part: a spinning centrifuge rotor. This technology has recently been the subject of further interest, as refinement to the very membrane configuration is being investigated for truly optimizing the approach.

These topics will be sketched in greater detail en route to asserting the motivation for the research and development undertaken in this thesis: development of a measurement system allowing quantitative evaluation of such membrane configurations.

1.1.1 Overview of Reverse Osmosis

In conventional Reverse Osmosis (RO) for seawater purification, a specially treated substrate forms a membrane which is permeable to pure water but which impedes the transfer of other chemical species. If seawater under pressure is brought into contact with such a membrane, pure water may be transmitted through the sheet while dissolved and suspended contaminants remain in the feed stream. The minimum pressure required to accomplish this mass transfer is 2.6MPa (374 psi) and in working apparatuses generally greater pressures are used: 5.5 to 6.9 MPa (800 to 1000 psi), typically accomplished by means of a high pressure pump, often of reciprocating piston design.

The RO process works best if only a small fraction of pure water is extracted from the feed; fortunately seawater is abundant and this is not wasteful of raw material. The exhaust fluid, however, possesses the stored energy of its 6 MPa process pressure. A portion of this energy can be recovered by complex and expensive turbomachinery or, as is often done in small and medium scale plants, merely dissipated across a throttling valve. A new technology which systemically conserves this fluid energy clearly should find demand as water treatment requirements escalate worldwide. This technology substitutes a simple spinning centrifuge rotor for both the high pressure pump and energy recovery turbine.

1.1.2 Centrifugal Reverse Osmosis Fundamentals

The pressure field present at radial distance r within fluid of density ρ_{fluid} contained in a centrifuge spinning at angular speed ω is given by equation 1.1.

$$P(r,\omega) = (1/2)\cdot\rho_{fluid}\cdot\omega^2\cdot r^2 \text{............................} 1.1$$

By introducing feed water at the axis of a centrifuge and passing it into a radial column this pressure may be brought to bear upon a membrane located at the centrifuge's periphery. Moreover, if the exhaust stream is carried back to the centrifuge axis before discharge, the energy associated with the osmotic process pressure is recovered; only a low pressure pump is required to maintain flow and overcome fluid energy losses.

Considerable work has been done [1.1] in implementing this theory in a viable Centrifugal Reverse Osmosis (CRO) plant. A crucial limitation of the current technology however is its reliance on membrane cartridges developed for the conventional RO industry. An important next step in refinement of CRO is the innovation of a new cartridge design, making full use of the specific flow characteristics within a centrifuge to enhance productivity. Much of this initiative is spawned from the desire to exploit the tremendous accelerations available to avoid certain deleterious effects at present only partially overcome, and often at considerable energy wastage, by both conventional RO and basic CRO technologies. The principal effect in question here is concentration polarization. It is the attacking of these issues which identifies C•M•D•S: Centrifugal Membrane and Density Separation.

1.2 OVERVIEW OF THE C•M•D•S RESEARCH CENTRIFUGE: NOVEL ISSUES

To investigate the full gamut of such possibilities the C•M•D•S Research Centrifuge has been built. It may be regarded as a flexible centrifuge test-bed whose payload is the process cell, containing a membrane cartridge arranged to examine RO process performance under a specific set of variables. These include three angles of membrane orientation (pitch, roll and yaw), feed-flow rate and direction, feed stream composition and concentration, and particular membrane and spacer mesh materials.

The centrifuge (Figure 1.1) is housed within a five-foot diameter vacuum housing which is integral with the supporting frame, secured to the laboratory floor by four vibration mounts. Access to the chamber's interior is provided through a full-sized hinged door with O-ring seal. The process cell, radial arm, counterweight, hub, allied fluid and electrical conduits and couplings, and main shaft comprise the rotor, shown in Figure 1.2, supported in cantilever fashion and equipped with dynamic vacuum seals about the shaft. The rotor is belt driven by a ten horsepower electric motor, and is also equipped with a pneumatic disk brake. Chamber vacuum is established and maintained by a liquid ring vacuum pump; other pumping equipment includes an adjustable speed low-pressure feed circulation pump and a simple centrifugal cleanup pump. A heat exchanger, particle trap and a panoply of valves complete the fluid handling equipment, much of which is visible in Figure 1.3.

In order to quantify the influence of the variables mentioned above, the membrane cartridge is strictly constrained and consists of a stack of ten Lexan disks, each disk comprising a membrane, associated feed flow channel, a permeate flow spacer, and seals and porting to isolate and gather the permeate fluid. In Figure 1.4 this assembly is shown in isometric quarter section; the ten membrane modules[1] including feed channels, and one permeate port are visible. Its configuration ensures that a useful area of membrane is both subjected to comparatively uniform centrifuge effects, while also is well supported mechanically and contained in a vessel of reasonable size and bulk. The latter is a very important consideration for, unlike most rotating machinery such as turbine blades having a tapered profile, this significant terminal load exerts tremendous stress upon the centrifuge arm, serving as a structural member in tension.

---

[1] of which nine have active membrane areas, the tenth merely providing a feed channel for its neighbour.

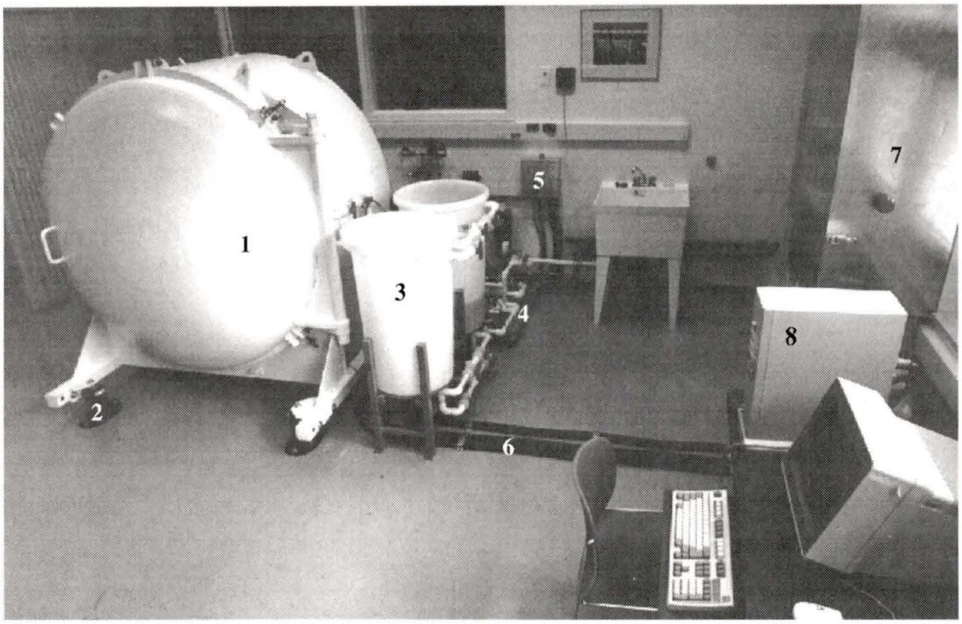

LEGEND			
1	Vacuum housing	5	Electronics cabinet
2	Vibration mount (four)	6	Electrical conduit
3	Feed tanks	7	Main junction box & controllers
4	Pump and valve equipment	8	Control and DAQ computer

Figure 1.1: The C•M•D•S Research Centrifuge and Supporting Systems

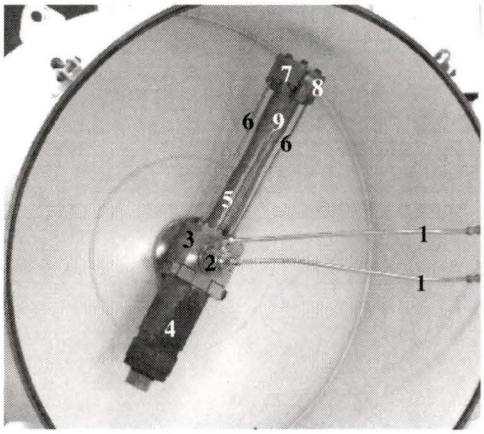

LEGEND	
1	Feed & retentate piping
2	Dual-passage rotary union
3	Hub
4	Counterweight
5	Titanium rotor arm
6	Feed & retentate piping
7	RO process cell
8	Flow-rate & Conductivity X-ducer
9	F•R•A•C•T electrical conduit

Figure 1.2: Detail of Housing Interior and Rotor Assembly

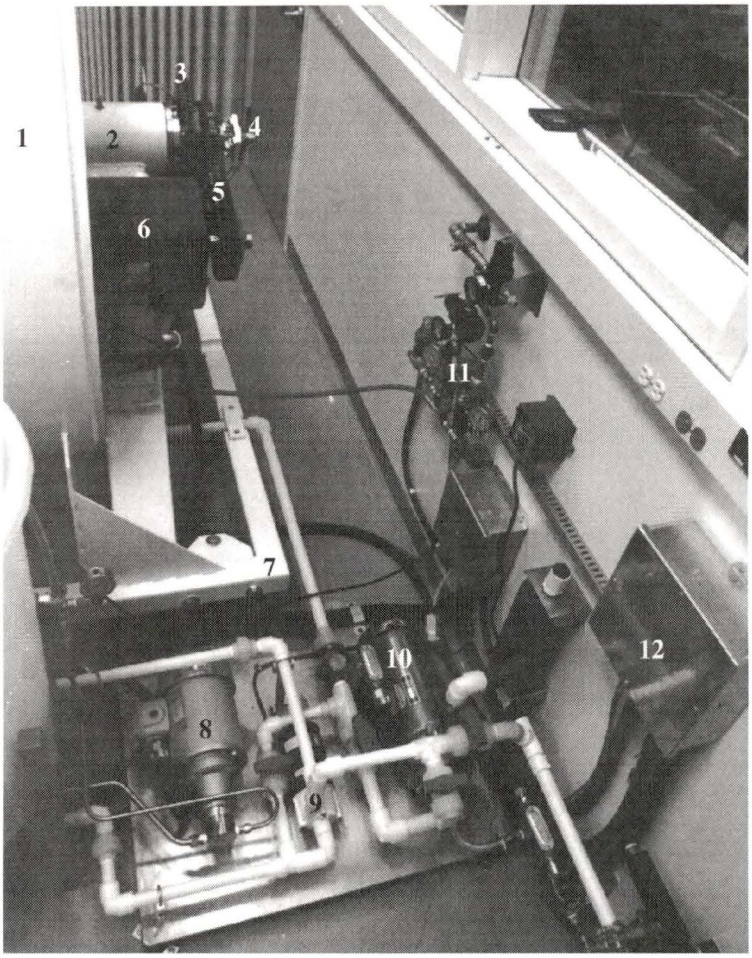

Figure 1.3: Centrifuge Rear View, Showing Allied Equipment

LEGEND			
1	Vacuum housing	7	Frame
2	Bearing tunnel	8	Feed pump
3	Disk brakes (air)	9	Cleanup pump
4	Slip ring assembly	10	Vacuum pump
5	Dual drive belts	11	Air and vacuum valves
6	Electric motor (10hp)	12	Electronics cabinet

An isometric exploded view of the rotor, found in Appendix I, illustrates how the process cell, individual membrane modules and cartridge are assembled and installed. The Flow-Rate and Conductivity Transducer (hereafter referred to by the acronym "FRACT" for brevity), installed on the process cell holder, is also visible in this drawing.

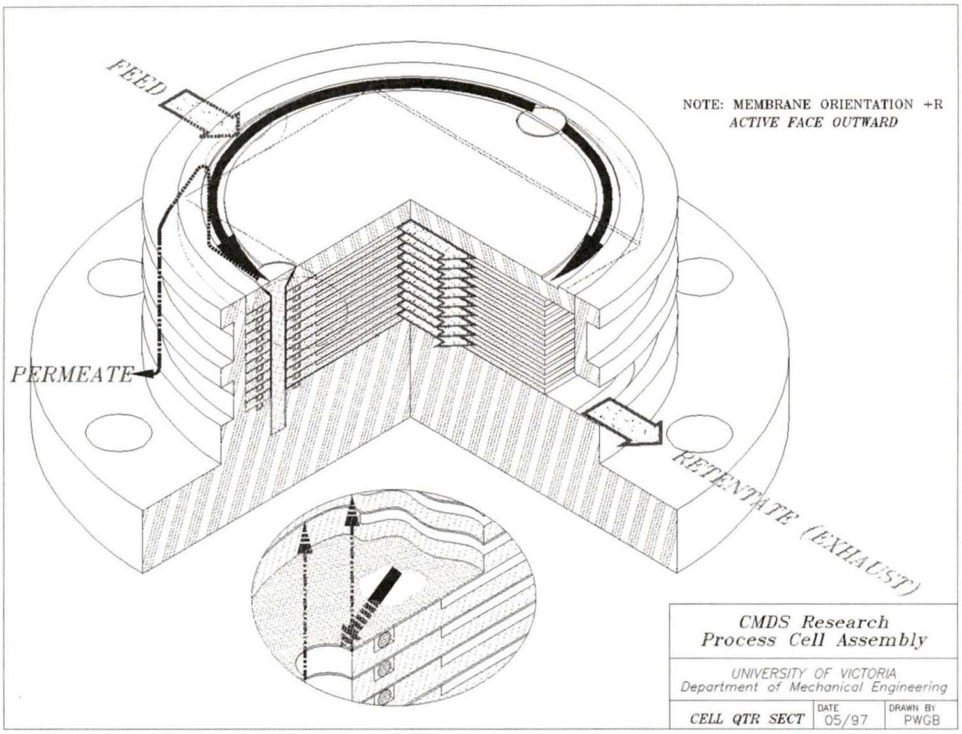

Figure 1.4: Isometric Quarter Section View of Assembled RO Process Cell
Feed fluid enters the cell through a slot (upper left) from a circumferential channel. It then flows across the membranes in the shallow rectangular channel of the adjacent membrane module, and exits via a slot and circumferential passage similar to the inlet (lower right). Permeate, having passed through the membrane and across the spacer mesh, is accumulated in a port coaxial with and surrounding the locating screw (inset), and exits the cell via a shallow groove in the cover plate. A dotted line then indicates the conduit leading into the FRACT, within which the fluid path is indicated by a dash-dot line. 26 O-rings prevent mixing of the fluid streams with one another.

1.3 C•M•D•S EXPERIMENTAL AGENDA

The C•M•D•S centrifuge has been designed to fulfill a variety of research goals. The FRACT device of this thesis is involved in the first phase of this agenda: intimation of the optimal orientation for a RO membrane in a centrifuge installation.

In its initial form, the rig is configured to subject the membrane cartridge to uniform, but adjustable, pressure and centrifugal influences for the purpose of converging on an optimal orientation. This is in part to be accomplished by the use of different RO cell holders, and in part by variation of the orientation of the cell within a given holder. Stress magnitudes have prohibited the development of a single fully gimballed RO cell holder.

The experimental agenda adopts a three pronged attack on this problem: static, dynamic and numerical simulation. Provision has been made for the entire RO cell from the

C•M•D•S rig (dynamic) to be transferred, without disturbing the membrane cartridge inside, to the static reverse-osmosis test apparatus of Fyles [1.2]. This apparatus is equipped with a high-pressure feed pump and throttle valve to develop the process pressure, and has been used in a number of successful research ventures. In this manner, experiments may be duplicated in close analogy with those performed on the dynamic rig, but with deliberate exclusion of centrifugal effects.

The results of both these experiments may furthermore be simulated numerically, and these results also compared. The development of a robust approach to numerical simulation, which in turn will be used to explore the question of optimal membrane orientation in greater detail, is one goal of this exercise. Specific potentially optimal orientations will then be validated experimentally on the dynamic rig, at great savings in time.

A later phase of the project will see the present rotor replaced with an annular rotor incorporating the optimal membrane orientation as determined by phase I but filling the available swept volume to the maximum allowable extent with membrane material. This maximum extent is constrained by the tolerable load of the cantilever drive shaft and is smaller than the overall chamber volume, however the effective membrane area of this form of the centrifuge will be comparable to the prototype apparatuses of Wild [1.1].

1.3.1 Concentration Polarization

Consider a suitable membrane against one side of which a concentrated (feed) solution resides and which separates this feed from a volume of less concentrated (permeate) solution. A chemical potential energy difference is present, tending to cause the migration of solvent through the membrane from permeate to feed, in a natural process intent on equalizing solvent concentrations and eliminating the chemical potential difference. This is osmosis. The reverse-osmosis process utilizes the application of pressure, upon which chemical potential energy depends, to reverse this gradient and drive solvent to the permeate side of the membrane.

As permeate is transported across the membrane boundary the nearby feed solution experiences a concentration increase owing to the net loss of solvent. This is depicted in Figure 1.5. Hence, the net chemical potential gradient across the membrane is attenuated; this phenomenon is called concentration polarization. Its effect is to lessen the flux of solvent through the membrane, or to demand greater process pressure be delivered to maintain a set flux. Clearly, this effect is undesirable in a reverse-osmosis plant.

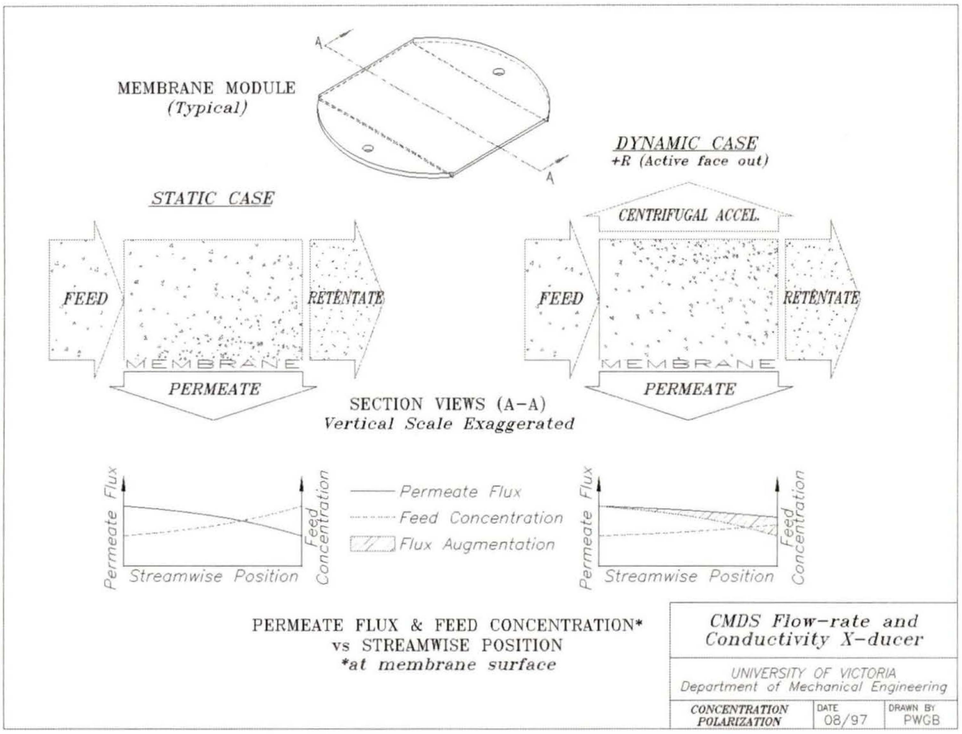

Figure 1.5: Static versus Dynamic Reverse Osmosis - Illustration of Concentration Polarization Abatement by Centrifugal Acceleration
In simple RO, the streamwise increase in feed concentration at the membrane surface results in a permeate flux decline (left); selective orientation of the membrane with respect to the centrifugal force direction (right) lessens the concentration increase and thus augments the permeate flux (graph, hatched area); the optimal orientation to maximize this area is a central goal of C•M•D•S.

Conventional RO technologies employ tightly wound or densely stacked membrane material spaced by a mesh which permits feed solution to pass between layers. This mesh also induces turbulence in the feed flow which is one way to dispel the concentrated boundary layer and mitigate concentration polarization to a degree. Energy supplied by the pumping apparatus, however, is dissipated by this turbulence.

C•M•D•S offers a different means of concentration polarization abatement as a fringe benefit of the heretofore unexploited centrifugal field. By judicious choice of membrane orientation, the concentrated brine proximate the membrane surface may be stripped away; its increased solute proportion having given rise to greater density which, given the magnitude of centrifugal acceleration existent within the centrifuge, results in tangible body forces and induced circulation. Permeate flux is hence augmented.

It is this selection of membrane orientation that the C•M•D•S agenda seeks to intimate.

1.4 SURVEY OF MEASUREANDS AND RELEVANCE TO RESEARCH GOALS

Independent variables include process pressure (imparted by rotor speed), three angles specifying the membrane cell orientation, the membrane active surface orientation within the cell and direction of feed flow. Temperature may also be regarded as an independent, though controlled, variable. Membrane material, sandwich construction and feed solution composition and concentration are other independent variables potentially to come under investigation.

There are two important dependent variables in the experiment space described above. These are permeate flow-rate and conductivity, which when compared to feed flow-rate and conductivity indicate the recovery ratio and rejection ratio respectively. The recovery ratio and/or production rate is expected to be a strong indicator of the relative merits of various membrane orientations as detrimental effects such as concentration polarization are manifested therein. This can be likened to a clogging of the membrane by build up of concentrated brine, the feed fluid proximate thereto having been deprived of some fraction of solvent by the trans-membrane migration of those molecules preferentially. Conductivity is another indicator of membrane performance, and of experimental soundness; while most membranes nominally operate at a specific rejection ratio the CMDS process has the potential to influence this parameter. Moreover the general performance of the experimental apparatus (leaks etc.) can be revealed by monitoring this output.

This assertion provides the motivation for the work of this thesis. During early conceptual stages of the test rig design it became apparent that the permeate flow-rate would be small, inviting the challenge of devising a means to measure this important variable. Various schemes were entertained, some occurring in situ aboard the centrifuge rotor while others posited the notion of gathering or somehow transferring the permeate from the rotor to the laboratory frame. The case for installation of measuring equipment aboard the spinning rotor became stronger as alternatives were fraught with difficulty. In order to permit unabated progress on the design issues specific to the centrifuge infrastructure, its containment, shaft and hub, arm, counterweight and cell, and fluid couplings, the task of delivering a workable flow-rate and conductivity transducer was delegated to the author. Approximate design constraints for physical size and mass were proposed. Operation at high acceleration was the preeminent functional requirement.

1.5 NEED FOR AND IMPLICATIONS OF INSTRUMENTATION AT ROTOR PERIPHERY

There are three fundamental approaches to obtaining physical data concerning the permeate fluid.

- Permeate recovery from the spinning rotor
    - by skimmer tip method,
    - by pneumatic slug approach.
- Permeate recovery from the stationary rotor.
- Instrumentation aboard the spinning rotor
    - commercially available device(s),
    - custom made device(s).

While the membrane area of 47 cm^2 (comprised of nine modules of 0.0052 m^2 each) is adequate to generate measurable amounts of permeate fluid as in the static test rig of Fyles, permeate production is three orders of magnitude smaller than that of the CRO prototype and six orders less than any proposed production equipment. This fact has the important ramification that the novel skimmer tip permeate recovery scheme of Wild [1.1] is not viable. Production rates are too small to sufficiently fill the collection annulus and overcome losses due to overspray and evaporation. Nor is the option of merely collecting the permeate discharge in the rotor containment vessel viable; fluid loss through surface coating, evaporation and aspiration, and contamination by oil or leaked feed/retentate fluid being the petitions against this avenue. Collection of permeate aboard the rotor for later recovery is severely restricted by rotor imbalance concerns, which would compel the frequent interruption of the experiment to stop the rotor and drain the permeate. Not only would this be inconvenient once spin-down, chamber repressurization and re-evacuation times are combined, but the very act of interrupting a membrane chemistry process introduces unreconcilable time dependent behaviours. One final possibility is recovery of the permeate sample from the spinning rotor. This might be accomplished by pneumatically forcing the sample to the axis through a capillary. The enormous pressures required and need for a rotary coupling capable of handling such pressures make this apparently simple approach virtually impossible.

By process of elimination, flow-rate determination therefore must occur in-situ aboard the centrifuge rotor. The ramifications of this fact bear mainly upon two areas: greatly elevated body forces acting upon the entire instrumentation unit, arising from the high centripetal accelerations, and interfacing of the data channels from within the rotating frame to the stationary laboratory frame.

A liberating consequence of this approach is, having obtained the desired physical data concerning the permeate sample, it may be discharged into the environment which, in this case, is the rotor enclosure. Retrieval of this material is thereafter not a concern.

1.5.1 General Design Requirements of Instrumentation Unit

The conceptual design of a rotor borne instrumentation package is influenced chiefly by the constraints of size, weight and strength, themselves all ramifications of the intense centripetal field to be experienced by the device. Secondary constraints stem from the chemical environment: the presence of brine mist in a largely evacuated housing, and significantly, that the device being inaccessible to attention or even inspection while in use. Moreover, owing to the low pressure dual passage rotary fluid coupling, the RO process cannot even be simulated with the rotor stationary for testing and demonstration.

- Rotating frame of reference
    - acceleration related phenomena
        - a) centripetal acceleration of ~3000 G (30000 $m \cdot s^{-2}$),
        - b) coriolis acceleration,
    - other phenomena
        - a) vibration,
        - b) signal interface.
- Evacuated housing
    - limited convection.
- Enclosed location
    - inaccessible during operation.

1.5.2 General Design Strategy

The design and development of the FRACT was pursued for the most part with only projections to the functional requirements and physical constraints, as the C•M•D•S rig too was still at a conceptual design phase when the FRACT project was undertaken. This influenced the design and development in that it was endeavoured to maintain flexibility in the prototype to allow emergent C•M•D•S rig criteria to be incorporated without setback.

The embodiment was envisioned to proceed through two prototype stages, the second of which was expected to include design revisions stemming from tests performed on the initial prototype, and eventually to be installed on the C•M•D•S rig. Subsequent to actual centrifuge testing, it was anticipated that (given the success of the general principle of operation) an operational version would be constructed to synthesize the totality of experience through both prototype and testing stages.

Nonetheless, the prototype was subjected to extensive and rigorous laboratory testing; efforts were made to simulate the centrifuge environment as closely as possible particularly as manifested by body force loadings. Moreover the prototype, having been designed with development flexibility anticipated, was modified in several crucial ways. One such example was the provision of oversize length dimensions to allow attachment of fittings for laboratory testing. Later final machining to size removed all vestiges of this adaptation and incorporated the attachment features whose dimensions were accepted once the cell holder design was complete.

The sole prototype served through a battery of laboratory tests before eventually being installed on the C•M•D•S rig for actual centrifuge testing. Moreover, it underwent stringent commissioning tests and has served as an operational unit for bona fide C•M•D•S experiments. Although subsequent embodiments will no doubt incorporate several modifications suggested by experience with the prototype, the usefulness of the prototype is testimony to the success of the adopted design strategy.

1.6 SCOPE AND STRUCTURE OF THIS THESIS

1.6.1 Organization of Material

In describing the research and development work, two complementary approaches were considered: chronological, and subject grouping by sub-system (flow-rate, conductivity, temperature and level-sensing). Strong lateral ties across subject categories exist representing the transfer of critical data required for further progress to have ensued. Between such links, progress on many issues may be regarded as having occurred concurrently. C•M•D•S rig development proper also took place in concurrent fashion until late stages, when FRACT integration concerns reached a culmination. Prior to this, FRACT development was largely independent and reliant solely upon initial constraints imposed by early conceptual studies for the C•M•D•S rig design.

To highlight the concealed interdependency that surfaced during development the following example is offered. Although the measurement of flow-rate and conductivity appears to be uncoupled, this is in fact untrue. The ultimate choice of level-sensing by electrical means irrevocably couples these measurements owing not only to the potential dependence of the level-sensing system performance on sample conductivity, but also arising from the interaction of level-sensing system with the conductivity measurement channel. For the latter reason, development of the electronics portion of the level-sensing system, though functionally associated with the flow-rate measurement objective, occurred mainly in association with conductivity cell and its prototype circuit development.

These points are broached here because, in the interest of clarity, this work has adopted the approach of discussion by sub-system category. Unfortunately, doing so may have obfuscated the critical linkages between sub-systems and their impact on the priority of development and continuity of the timeline. Wherever possible and necessary, such linkages have been highlighted; occasionally this has resulted in topics being touched upon without the expected preamble. Any sacrifice in clarity in such cases has been a judicious compromise.

Design, development and testing emphasized the flow-rate measuring function since structural and operational issues exerted strenuous constraints on this portion of the embodiment. Though significant development and testing were also required for the conductivity, temperature and level-sensing functions, insofar as the physical form of the FRACT was concerned, expediency was gained by integrating these functions subsequent to establishing a viable basic device.

1.6.2 Some Useful Nomenclature and Conventions

During the course of the following chapters it will be useful to have clarified certain nomenclature and conventions, particularly with regard to coordinate systems. The rotor provides a basis for such: its radial direction. The centrifugal pseudo-force is aligned with the radial direction $+R$. The centripetal force is in the $-R$ direction. Hence, as perceived by the FRACT, affixed to a rotating frame of reference, body forces, which are in fact due to restraint, occur in the $+R$ direction.

A second coordinate system may be attached to the FRACT. This will prove useful in describing relative positions and directions of motion on and about the FRACT. The orientation of body forces mentioned above is defined as being the $-z$ or "down" direction. This is a convenient convention because, throughout laboratory testing the FRACT must be placed in a manner that Earth gravity is aligned with this direction. The remainder of this rotating Cartesian system can be seen in Figure 1.6. Thereby, the terms top, bottom, left, right, front and back assume an unambiguous meaning when applied to the FRACT, as is also shown.

Three angles which define the orientation of the RO process cell are indicated in Figure 1.6. Of these, only yaw variation is supported by the present cell configuration; roll and pitch are fixed and will be explored in the future using a cell holder designed especially for that purpose. The reference sphere (beach-ball) residing within the cell volume specifies the approximate centroid of the membrane stack and the position at which many design calculations dependent upon radial position, such as process pressure, were calculated.

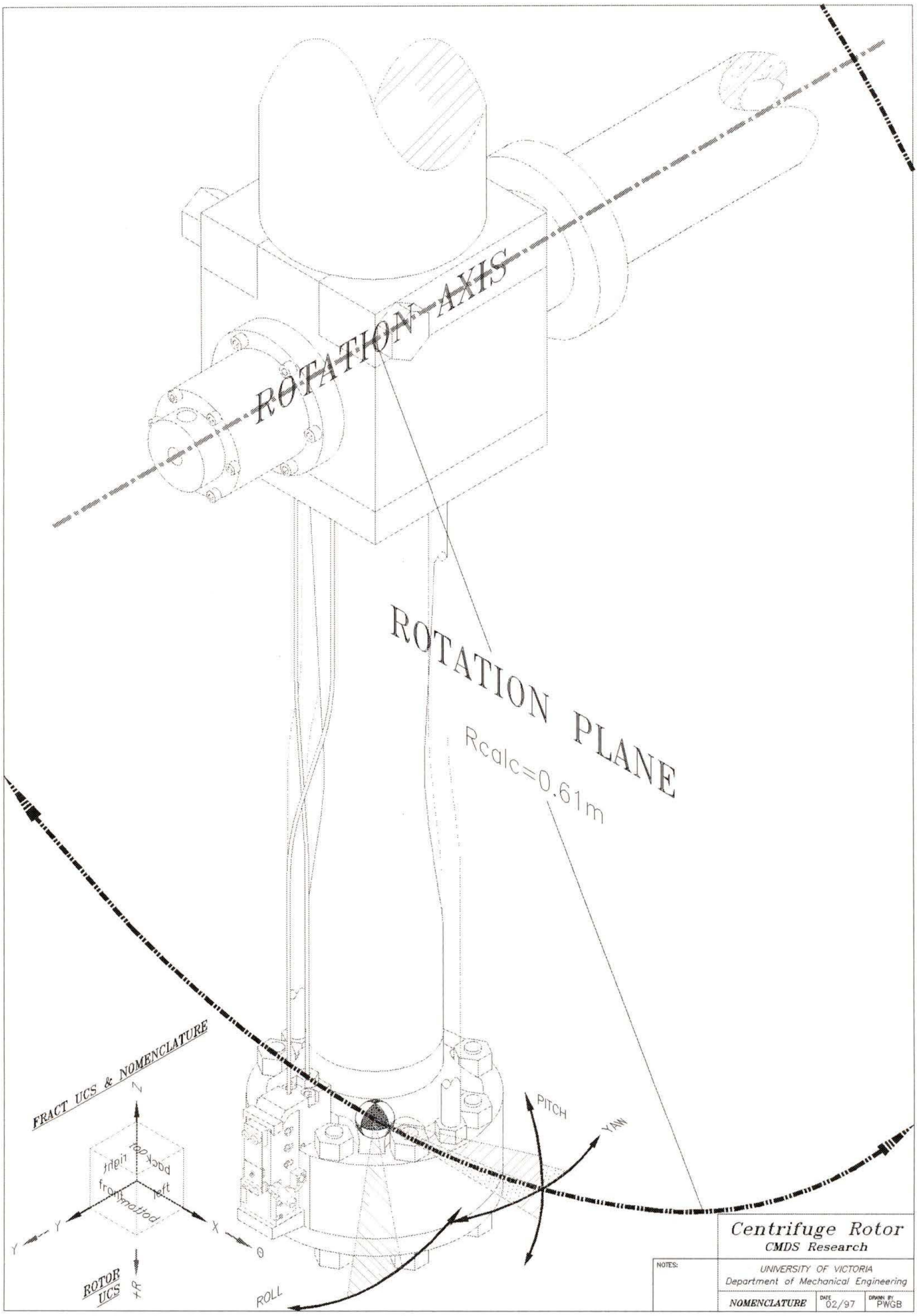

Figure 1.6: Nomenclature and Conventions

1.6.3 Intention and Synopsis

This thesis is intended to chronicle, as fully as is appropriate, the process undertaken to deliver a functional flow-rate and conductivity measuring system for the C•M•D•S Research Project.

A survey of the potential avenues for obtaining the desired physical data concerning the RO process led to the collective decision to develop a proprietary device for this purpose. This material is mainly developed in chapter 2: Flow-Rate Measurement. The conceptual stages of design benefited from consultations and ongoing dialogue, as initial designs for the C•M•D•S apparatus were also then taking shape.

The specific design and refinements thereto were within the purview of the author, as was the conception and execution of the prototype testing, and development activity arising from it. This applies particularly to the structural and mechanical facets of the embodiment, which is to be found mainly in chapter 4: Prototype Testing. The associated electronic prototyping, however, involved numerous consultations. Chapter 2 and chapter 3: Conductivity Measurement, both broach this topic. A significant but very different aspect of the author's work was the devising and incremental development of a suite of computer software applications upon whose existence the FRACT heavily relies, described fully in chapter 6: Control and Data Acquisition Software.

The stage of final integration of the FRACT and C•M•D•S apparatus heralded a highly cooperative stage of the project: dynamic testing and calibration. Though largely planned and orchestrated as part of the FRACT design and development thread, these tasks involved considerable expertise from other team members. Nowhere was this more apparent than in the refinement of the supporting electronics hardware systems. Discussion of these issues is to be found principally in chapter 5: Commissioning and Calibration. In chapter 7: Example Results from C•M•D•S and Conclusions, some recent experimental and theoretical work is summarized and future directions outlined.

1.6.4 Summary

Flow rate measurement in situ aboard the spinning rotor is undeniably the main challenge addressed by this work. The FRACT embodiment was largely shaped by this assertion and other required functions were merged to conform with the prime configuration dictated by it.

2 Flow-rate Measurement

2.1 SURVEY OF COMMERCIALLY AVAILABLE DEVICES

Commercially available flow meters employ a variety of operating principles, but can coarsely be categorized as either additive energy or extractive energy [2.1]. Additive energy devices include magnetic, sonic and thermal types, which operate by various principles involving propagation or dissipation of externally supplied energy. Extractive energy devices such as head or pulse types harness energy present in the fluid sample to perform actions indicating rate of flow.

Commercially available offerings are typically not built with a view to low mass nor structural and functional integrity under anything other than normal ambient laboratory conditions. Moreover, liquid flowmeters for the 10 mL/min order of magnitude are uncommon. Popular varieties which are capable of measurement in this range are summarized in Table 2.1.

Conventional laboratory practice for measurement in this range is the manual capture of a known liquid volume over a measured time. Such "primary" methods, which include positive displacement meters, are preferred for high accuracy situations. The simplicity of this approach has appeal and was the method chosen for development. "Secondary" or rate measurements, though often more expedient particularly in high flux instances, usually exhibit lower accuracy and rangeability. With the exception of the true mass classification, Table 2.1 describes only secondary measurements.

Class	Type	Range [L/min]	Rangeability	Repeatability
variable head	Orifice Plate	0-1900000	20:1	0.25%
variable gap	Glass tube	0.0001-4000	6:1-10:1	2.00%
	Metal tube	0.001-15000		4.00%
obstructionless	Ultrasonic	≤75000	300:1	1% F.S.D.
	True mass	0-22700 kg/min		0.50%

Table 2.1: Popular Flow-rate Instrument Classifications (with Low Range Capability) [2.2]

The premiere selection criterion was the anticipated flow-rate range: 1-20 mL/min. This had been estimated based on approximate projected membrane area and experience with typical membrane yields in the static test rig. The transducer mass was also considered, whose bearing on the overall load in the main structural member of the centrifuge was judged a truly significant issue. Physical dimensions must fall within feasibility constraints. A prevailing, but largely subjective concern was reasoned to be the compatibility of the meter's principle of operation under high accelerations in a rotating frame of reference. Operation in vacuo, and interfacial compatibility, it being necessary to obtain experimental data from within the sealed centrifuge chamber, were regarded as additional selection criteria.

Rotameters, though popular for many laboratory applications, are infeasible. These are extractive energy, secondary measurement devices. Their principle of operation relies on the equilibrium position of a shuttle, sometimes incorrectly called a float, under the opposing influences of hydrodynamic pressure and gravity. Effective gravity varies with speed of rotation and radial position in the centrifuge, and moreover at high acceleration the supporting pressure requirements are unreasonable. Additionally, rotameters are usually direct reading.

Extractive energy, primary measurement types such as vane or positive displacement meters are not invalidated by virtue of their principle of operation but they contain moving parts operating in close tolerance and having delicate bearing surfaces. It is very unlikely any such contrivance would operate in, let alone survive, the intensely destructive centrifugal field.

Two potentially feasible commercially available devices were researched, and are shown in Figure 2.1 along with a pair of rotameters.

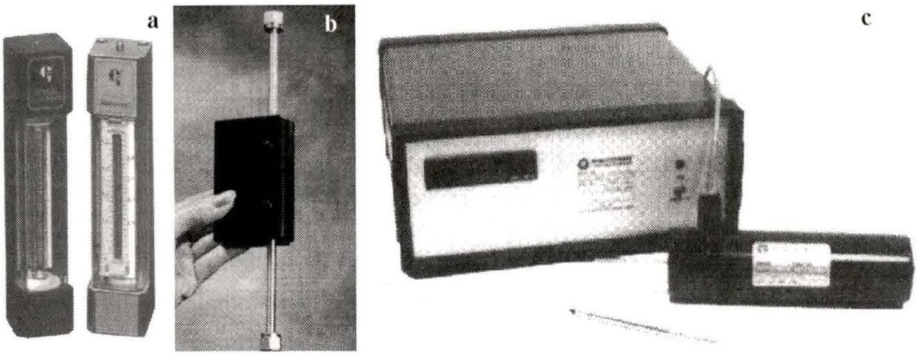

Figure 2.1: Four Commercial Flow-meters
a) Two rotameters, b) M-Tek Thermal Pulse flow-cell, c) INTEK Rheotherm with TU-transducer [2.3, 2.4].

2.1.1 M-Tek Thermal Pulse Time-of-Flight Flowmeter

One promising commercial flow meter which claims to operate in the required range is the thermal pulse time of flight device offered by M-Tek [2.3]. This is an additive energy, thermal, secondary measurement device. It was scrutinized in some detail because it emerged as one of only two commercial technologies potentially useful in the centrifuge application.

This device avoids moving parts altogether but rather introduces a heat impulse into the flowing liquid within a capillary of assured laminar flow properties. The arrival of this heat pulse some fixed distance downstream is detected by a sensor, and through the use of aggressive signal conditioning the time interval between generation and reception of this heat pulse reveals the liquid flow rate [2.5].

The useful range of such a device is governed chiefly by the capillary bore and length, selected to promote laminar flow. For different expected flow-rate ranges, a variety of "flow-cells" are available. The basic construction appears adequately robust for centrifuge use, and remote installation of the flow cell and computer interfacing capability are both supported. The "flow-cell" probe unit is approximately 15 centimetres in length and has a mass of 180 grams These characteristics suggest such a device might be acceptable for the C•M•D•S application.

Examining the principle of operation, it was observed the heated parcel of fluid attains a temperature approximately 0.5-1.0°C greater than the bulk flow. Such a fluid parcel experiences a small buoyant force owing to its reduced density. Were the buoyant tendency of the heated fluid parcel aligned with the bulk flow, the regular laminar transport through the capillary might be convoluted. Therefore it would be preferable for the capillary to be oriented in alignment with the centrifuge axis. This compromises the full versatility of the test rig by sacrificing adjustment of the yaw angle, which would reorient the capillary in other directions.

An issue which further instills doubt over the performance of this device, even if it were possible to ensure this preferred capillary orientation, is the effect of convection, normal to the laminar flow direction and amplified by a factor of up to 3000, upon the heated parcel of fluid. The detection circuitry is intended to filter and condition the smeared signal under normal operating conditions and it is presumably this aspect of the design which defines its lower bound of operation. Buoyant effects would worsen the sharpness of the thermal pulse and likely reduce accuracy to an unacceptable level.

2.1.2 Intek Rheotherm Thermal Flow Meter

Another commercially available thermal additive-energy flowmeter claiming to operate in the low flow-rate regime is the Rheotherm device [2.4] manufactured by Intek, Inc. This device operates on a principle of operation similar to a hot wire or hot film anemometer, but places the heater and sensor components out of direct contact with the liquid flow [2.6].

Probes are available in a variety of shapes and sizes and like the M-Tek device previously described, these are intended for remote location. The “TU-type” probe recommended for flow-rates of 0.8 to 30 mL/min outwardly resembles the time-of-flight probe, having a capillary bore with allied elements disposed along it; it differs however in mode of operation.

An upstream temperature sensor monitors the bulk flow temperature. Downstream, a heater and second temperature sensor are situated near one another such that the variation of temperature induced by the heater recorded at the this sensor is a function of flow-rate. The entire active portion of the sensor is insulated from ambient conditions. Detection and signal processing circuitry complete the device.

Although the principle of operation appears alluring and seems to avoid the potential difficulties of buoyancy induced phenomena assessed likely with the M-Tek device, as manufactured the probe is physically large, leading to grave concerns over installation feasibility and structural integrity.

2.1.3 Commercial Survey: Conclusions and Recommendations

No method to simulate the influence of the centrifugal field could be envisioned for these devices, making their recommendation unconscionable. Table 2.2 reviews the physical comparison amongst commercial and custom devices.

Device	Range [mL/min]	Length [mm]	Width [mm]	Mass [g]
Intek 'TU'	0.8-30	330	76	?
M-Tek	0.2-20	155	40	180
FRACT	0.7-20	76	32	100

Table 2.2: Comparison of Intek and M-Tek Thermal Additive Energy Probes and FRACT [2.3, 2.4]

2.2 PROTOTYPE CONCEPTION

2.2.1 Early Conceptual Designs and Ideas

At very early stages, a number of potential avenues for development were considered. These included: deduction of permeate mass from precision measurements of feed and retentate amounts, self-activating direct mass devices, and pneumatic propulsion of sample fluid slugs into the laboratory frame for capture. Each of these, and numerous other options, were rejected from further development when compromising deficiencies were encountered. To summarize:

- Deduction of permeate mass from feed and retentate amounts
    - required inline mass measurement accuracy unattainable,
    - rotary fluid coupling leaks would be mistaken for permeate production.
- Pneumatic slug transfer to laboratory frame
    - requires high pressure rotary air coupling to convey propulsive charge,
    - requires lossless dedicated rotary fluid coupling to channel sample recovery.
- Self-activating direct mass devices
    - delicate bearings incompatible with centrifuge loadings.

2.2.2 Theory of the Design Process: The Functional Domain

"Functional requirements are defined to be the minimum set of independent requirements that completely characterize the design objective for a specific need" [2.7].

Functional requirements as stated belong in the "functional domain." Their independence from plausible physical solutions, many of which might exist for a single objective, is semantically apparent via this construct. In the axiomatic design process, functional requirements are mapped into the physical domain by "design parameters." Design parameters suggest physical embodiments that address specific functional requirements. Different design parameters which satisfy the same functional requirements represent different candidate physical embodiments which may be evaluated at the design stage.

To develop a complete design, a hierarchy of functional requirements and associated design parameters may be constructed. Such a process aids in revealing design conundrums before parts are manufactured and avoids the need to develop every imagined candidate design for comparison before convergence upon the favoured design takes place.

The device chosen, be it in situ or remote, must satisfy the following functional requirements:

FR_1 Measure permeate flow-rate in 1-20 mL/min range (nominal 10 mL/min).
FR_2 Measure conductivity in range of 50 (+200, -40)[1] μS/cm, corrected for temperature influences.

Constraints are a part of every design. Identification of constraints narrows the eligible design parameters to a manageable set. For the FRACT, size, weight and strength comprise the principal design constraints. Presuming the device is to be mounted in situ aboard the spinning rotor, these include:

C_1 Minimal mass.
C_2 Structural integrity under severe centripetally induced body forces.
C_3 Small physical dimensions.
C_4 Shape and form compatible with RO cell
  a) fluid porting,
  b) mechanical attachment.
C_5 Moving parts
  a) no degrees of freedom influenced by centrifugal acceleration,
  b) no bearing surfaces subject to centrifugally induced loading.
C_6 Operation in vacuo.
C_7 Mass variation during operation minimal (imparted vibration) +/- ~3 grams.
C_8 Corrosion proof and chemically inert where in contact with permeate.
C_9 Capable of repeated measurements.
C_{10} Adjustability and interchangeability of key components for development and maintenance reasons.

The natural process of design is rationalized in the axiomatic regime by an iterative process wherein each functional requirement is paired with a proposed design parameter intended to fulfill it. A hierarchy emerges as design parameters themselves spawn subordinate functional requirements, until a level is reached where the design parameters cease to be abstractions but instead map directly into the physical domain. At this level, the design is

---

[1] later extended to exceed 5mS/cm once experimental objectives were more clearly defined

complete, and may be compared with other meritorious candidate designs. Based on the emergence of a preferred design from this process, the manufacture of a prototype then finally ensues.

This formalism permits the statement of the design solution in terms of its design parameters. For the design championed in this work, several important secondary functional requirements were identified by this process, among them the need for a reliable and positively activated drain valve, and the need for detection of fluid level within the sampling chamber. Alternate design parameters for both these FRs were considered, and in the former case a creative implementation permitted many secondary design ramifications to be optimized.

2.2.3 Convergence on a Design for Further Development

The principle of operation selected for implementation and development is a primary, direct volume measurement. A known volume of fluid is captured, the time to capture measured, yielding an average flow-rate over that time. This cycle is repeated following discharge of the sample chamber. The mechanical design challenges of this approach were considered tractable, and a methodology was envisioned for adequately simulating the centrifuge environment as an aid to testing and development.

This strategy eliminated the need for calibrated orifices, capillaries, vaned wheels, venturis, or other commonly used elements which might work poorly or not at all under conditions of such low flow-rates and high accelerations, and whose performance in the centrifuge would be difficult or impossible to simulate in the laboratory.

Functional requirement FR_1 is satisfied by the design parameter DP_1 suggesting timed capture of a known fluid volume. Predicated by this in the hierarchy are the secondary functional requirements:

$FR_{1.1}$ Drain valve permitting control and repetition of fluid capture.
$FR_{1.2}$ Fluid level sensing means for volume mensuration.
$FR_{1.3}$ Data acquisition and processing means.

The formulation and development of design parameters satisfying each of these requirements under the stipulated constraints C_1 through C_{10} has been the definitive objective of this thesis.

2.2.4 Candidate Conceptual Designs

The flow-rate measuring function was viewed as the most formidable of the design challenges faced. In particular, the design of a positively activated discharge valve capable of establishing a reliable seal against high fluid pressure while also enduring the stresses of the centrifuge environment, was critical.

Two exclusive design parameters addressing $FR_{1.1}$ may be envisioned, wherein actuation is presumed to be accomplished electromagnetically:

$DP_{1.1.a}$ Valve seal opened by actuator (seal augmented by vessel pressure).
$DP_{1.1.b}$ Valve seal closed by actuator (seal drawn against vessel pressure).

$DP_{1.1.a}$ offers an obvious advantage. The tendency to leak at elevated pressure is automatically combatted through augmented sealing force, however it has two debilitating disadvantages which undermine it in this application:

- Valve, seal, and actuator components must be situated internal to sampling chamber, influencing chamber dimensions contrary to other functional requirements.
- Valve state switching occurs at maximum pressure; requiring maximum servo force to be generated under least favourable electromechanical conditions.

$DP_{1.1.b}$ allows valve and seal components to be situated accessibly for manufacturing, assembly, inspection, adjustment and service convenience, and moreover permits a sampling chamber section area chosen chiefly to satisfy flow-rate resolution issues. Additionally, valve closure is achieved by the engagement of the electromagnetic actuator and maximum required force is achieved at maximum available force, i.e. when the air-gap shrinks to zero. The disadvantages of this implementation include:

- The need for a continuous duty electromagnet (electromagnet current on during lengthy filling phase).
- Remote electromagnet location with flux conveyance by soft-alloy poles, increasing flux leakage: reducing actuator efficiency.

The disadvantage of continuous duty is partially overcome by the relatively low closure sustaining current enabled by matching required to peak available pulling force.

Implementation of $DP_{1.1.b}$ has been the thrust of the initial prototype and proposed operational version. $DP_{1.1.a}$ has undergone a phase of conceptual design which offers potential for a future embodiment. In this eventuality the two units could be interchangeable and require only modified control software.

2.2.5 Genesis of the Prototype

The FRACT embodiment ultimately developed had its genesis in the adoption of electromagnetic actuation for valve closure. Preliminary investigations had converged on the primary volume measurement principle and the use of a non-binding servo-driven valve. Electromagnetic actuation, piezo-electrics, mechanical couplings and pneumatic servos were among the means proposed for valve operation, however most reasoning placed the actuator in the role of forced valve opening, rather than closing. Conceptual designs (Figure 2.2) were formulated, which championed the following features:

- Non-metallic machine figured body with internal porting.
- Separate electromagnet with flux conveyance by pole tip extensions.
- Pull-closed type pendant valve with attached armature.
- Interchangeable drain valve seal assembly.
- Fluid level-sensing by electrical means.
- Inlet with intrinsic hydraulic damping (promoting stable fluid sample surface).
- Control and data acquisition by remote computer.

Solids modeling was performed to aid in interference checking; refinements to the initial design ensued and most significantly included:

- Fully supported electromagnet assembly.
- Integration of continuously-flushed conductivity cell.
- Integration of temperature measurement means.
- Choice of stock threaded fasteners for level-sensing electrodes; redundant system.
- Detailed design of doubly-supported interchangeable seal assembly.

Many of these features were later the subject of specific consideration and revision, and many smaller issues were introduced or analyzed before submitting shop drawings for component manufacture.

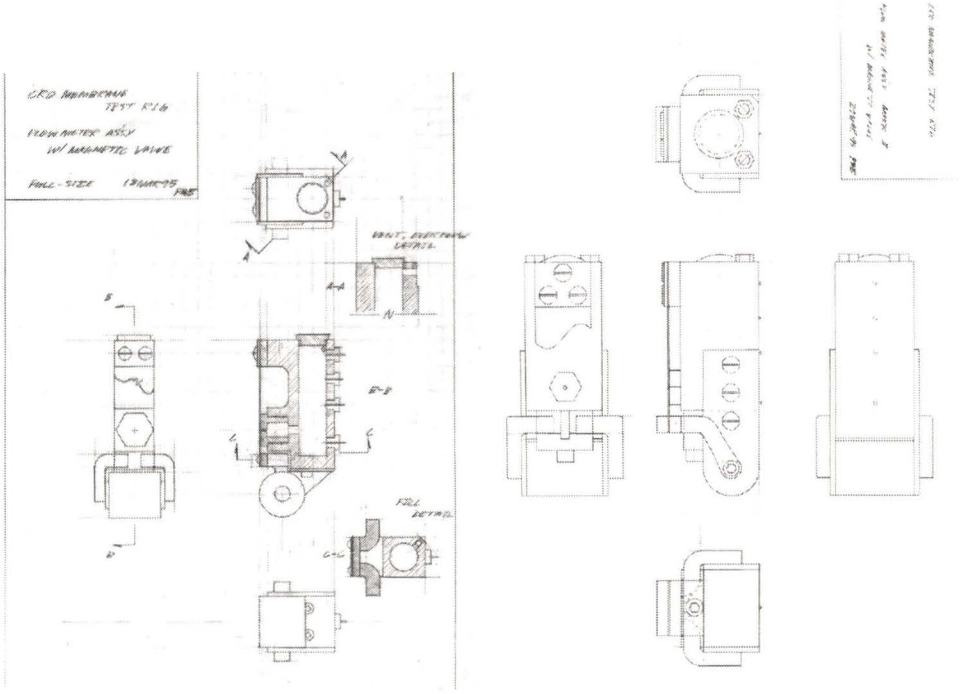

Figure 2.2: Two Early Conceptual Designs of FRACT

2.2.6 Design of the Prototype

The general dimensions and proportions of the FRACT converged with early constraints from the conceptual design of the RO cell which, at that time, was to be a fork and clevis type arrangement. A key design parameter of a CRO apparatus is the critical radius of the permeate outlet. This dimension arises due to the need to employ permeate back pressure, acting on the membrane, to compensate for the radial dependency of the feed pressure, allowing the entire span of membrane to experience a uniform process pressure not exceeding its absolute limit [1.1]. The critical permeate outlet radius is therefore close to the innermost radial position of the membrane stack. This gives rise to an upper limit on the necessary size of the FRACT, since the sampling chamber cannot naturally fill inward of this location. The opposite extremity of the FRACT is dictated by the dimensions of the RO cell, it being necessary to support the unit near this position by some mechanically sound attachment.

The alternating fill-drain cycles will result in mass variation of the rotor and concomitant vibration. Hence, the sample mass must be restricted to the order of a few grams. This constrains the maximum volume of the sampling chamber. The aspect ratio of the chamber has a profound effect on flow-rate resolution and instrumental range. Fluid level sensing measures the discrete height of the captured sample fluid surface. This measure yields flow-rate information when divided by elapsed time. At a given flow-rate, the fluid surface height rate-of-change is greater for a slender chamber than a squat one and enhances device resolution for low flow rates, but cycle frequency may become too rapid for higher flow rates. In addition, time resolution complications to be discussed later make rapid chamber filling undesirable. To compromise among these many constraints, a chamber with undersquare proportions of approximately 2.3:1 was selected. Its capacity of 2.7 mL (including inlet passages) was deemed acceptable for rotor balance concerns. The option of installing a sleeve to increase the aspect ratio was maintained if permeate flow-rate fell below the expected value and resolution enhancement was necessary.

Integration of the conductivity cell involved an analysis of the appropriate cell constant for the anticipated nominal permeate conductivity, an important step at this early stage in order to ensure the operational cell resistance would be amenable to detection by conventional electronic means. The physical dimensions and style of the cell were thereby selected and the system integrated within the FRACT design. Likewise, the function of temperature measurement was addressed via the use of a precision IC temperature chip, the installation requirements for which were incorporated at this stage.

A prototype electromagnet assembly was first produced, allowing performance and weight expectations to be empirically validated prior to further component manufacture.

2.3 MATERIALS SELECTIONS

2.3.1 FRACT Body and Ancillary Components

Use of a non-metallic material for the FRACT body was desirable due to the generally lower density of engineering plastics. The electric potential imparted upon the fluid sample by the conductivity and level-sensing electrodes moreover compelled this choice as it provides isolation for these important systems. An acetal resin, commonly known as Delrin, was selected. Delrin has excellent mechanical characteristics, offering high strength and stiffness, dimensional stability, resistance to creep, and fatigue endurance. Additionally, it is a good insulator, tolerates moisture and many chemicals, has a suitable and wide end-use temperature range and is easily machinable to high tolerance with good surface finish [2.8]. Delrin is available in bar, rod and sheet stock, and was also used for a number of ancillary components where its properties were similarly beneficial.

2.3.2 Engineering and Design Concerns Specific to Manufacture with Plastics

The Machinery's Handbook [2.8] states "in setting safety factors for plastic parts there are no hard and fast rules." The handbook proceeds to assert that the consequences of failure should serve as a guide in converging upon meaningful safety factors. Moreover, it is emphatically suggested that rigorous testing be the overruling authority in determining the fitness of a part, particularly a critical one.

This philosophy has been adopted in the development of the FRACT. Key locations were identified and stress calculations for them advanced. The consequences of failure at these locations were considered, and stringent tests conceived and executed to validate the design and calculations.

2.3.3 Electromagnet

One FRACT sub-system with very special material requirements is the electromagnet assembly: the core, poles and armature must be made from a “soft magnetic” material. Such materials convey magnetic fields that are induced upon them without themselves becoming permanently magnetized to any significant degree. The FRACT application imposes the additional requirement that the finished assembly be corrosion resistant. Non-resistant parts might be viable if well treated with a protective coating. Typical of such materials is the ubiquitous electrical iron, a low carbon iron widely used in low-cost electromagnetic applications where corrosion resistance and strength are not prevailing concerns.

A wide selection of soft magnetic alloys is available from various manufacturers for specialized purposes. The Carpenter Steel Division of Carpenter Technology Corporation offers several [2.9] which were considered for this application. Free samples of two were provided for evaluation; indeed the quantity of material was far in excess of the amount needed for several complete assemblies.

Material properties germane to magnet design include several in addition to those familiar from general mechanical design: permeability, residual magnetism, and saturation flux density being principals. Permeability relates magnetic flux density within a material to the magnetomotance that causes it, a non-linear relationship for ferromagnetic materials. Initial and maximum permeability are two often quoted properties. Residual magnetism is the flux density remanent once the magnetomotance has been withdrawn, a measure of hysteresis. Saturation flux is the flux density beyond which increased magnetomotance evokes no further additional flux density. It can be regarded as the flux attained when the permeability function diminishes to unity.

The FRACT application requires a material with good properties in all these categories. Aggressive pursuit of any one of these properties at the expense of others is not required for adequate performance. Indeed the desire for corrosion resistance led to the unambiguous choice of stainless type 430FR. This material is a free machining solenoid quality ferritic chromium-iron alloy specifically developed for such uses where excellent magnetic properties and corrosion resistance are required [2.10]. It is supplied in mill annealed form, and therefore does not usually require post-manufacture annealing to restore its magnetic properties. It is harder than many soft magnetic alloys, making it an appropriate choice for relay parts where impact can cause peening of softer materials.

High-performance alloys with various different intended purposes were researched and maintained as options if 430FR failed to prove satisfactory. A supply of high-permeability (type 49) alloy was obtained and magnet parts prepared for comparison, however 430FR was found entirely adequate and further deliberation was deemed unnecessary.

2.3.4 Other Components

Details of material selection for the many smaller components is highlighted where their engineering is described.

2.4 FRACT BODY: ENGINEERING SPECIFICS

The FRACT body is a complicated part serving various functions. The sampling chamber, permeate inlet and vent porting are integral. It also has provisions for the installation or attachment of many parts including the seal assembly, pendant valve spring, and electromagnetic actuator. It supports the weight of all these components under the centrifuge loading environment, and includes two flanges for secure attachment to the RO cell holder. Its initial form, prior to the commencement of testing and development, is presented in Figure 2.3, which also shows some of the related components. Figure 2.4 summarizes the terminology used in reference to a number of design features, depicted on an isometric view of the operational variant.

2.4.1 Manufacture

The FRACT body was made from rod-stock Delrin, milled into the basic rectangular prismatic shape required and having the various necessary features also machined. The size, cylindricity and surface finish of the sampling chamber were desired to be of a high standard. The chamber diameter was achieved to close tolerance by reaming, which also permitted the chamber bottom to be squared. This operation also resulted in the achievement of a smooth surface, resistant to contaminant adhesion. Zero taper ensured that the chamber sectional area was uniform, allowing sample volume deduction from fill-height. The relative position of the level-sensor electrode holes was also rigidly specified to facilitate partition volume calculation.

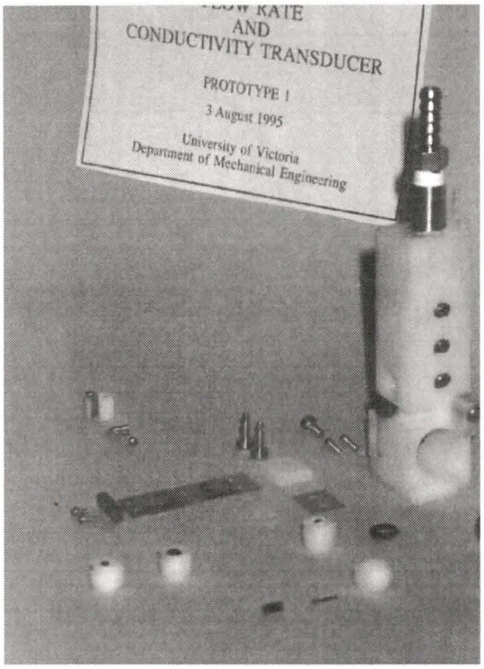

Figure 2.3: Initial Form of FRACT
Pressure test fitting attached (top). Allied components arrayed nearby, foreground to background: seal assemblies with internal components; pendant valve spring, armature, and provisional mounting; conductivity cell; magnet not shown.

The electromagnet coil is supported by a clearance hole drilled laterally through the body. The pole tips are accommodated by a faceted notch, and the entire assembly is further supported and located by end clamps fastened by machine screws to the body. These clamps are supported against centrifugal loading by flanges which extend from the body sides at its bottom plane.

The sampling chamber and inlet passages run parallel and must be connected at their bottom extremities. This was accomplished by way of a blind crossbore, drilled through from the pole relief notch. The ensuing open passage must be plugged securely, for it experiences significant pressure. A threaded plug with gasket was installed using adhesive for this purpose. Spin-welding of a Delrin plug has been investigated as a more permanent option for future devices.

The interchangeable seal assembly fits into a relief which has 7/16-20 internal bottom tapped threads. This square-bottomed relief must be milled since insufficient depth exists to accommodate the point angle of a conventional drill in concert with the need for adequate thread depth.

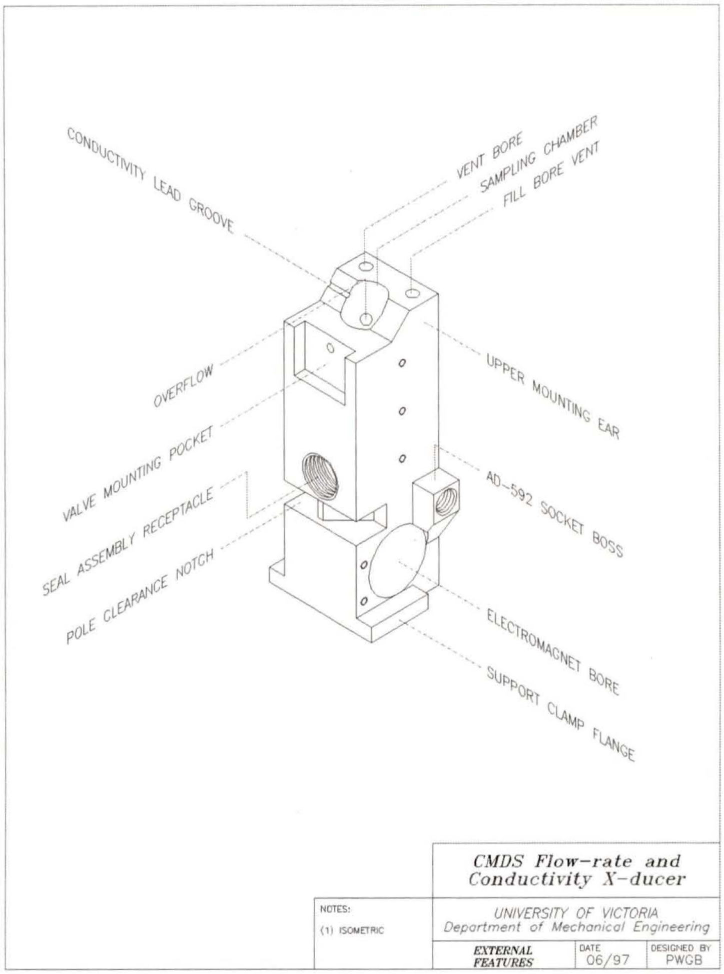

Figure 2.4: Summary of Terminology Ascribed to Various Design Features

The means of attachment of the pendant valve spring was the subject of much development and testing. The initial implementation emphasized adjustability for validation of general principles, and its evolution led to a rigid mounting arrangement amenable to functional requirements, repeated disassembly and contact stress abatement suitable for mechanical interaction with plastic.

2.4.2 Structural Integrity

All components of the FRACT are highly stressed owing to the centripetally induced body forces at play. As an assembly the Delrin body bears the totality of such loads, since it alone is supported by the mounting fixtures to the cell holder.

For the body and key components, stress calculations and testing were performed to ascertain the integrity of these parts under anticipated loadings. Moreover, operational tests were conceived and performed to simulate, as closely as possible, operation under actual service conditions.

Two loading situations were considered: maximum operational and overspeed. Operational loads correspond to the centrifugal acceleration experienced at the FRACT location under typical experimental conditions, usually the consequence of having chosen a specific process pressure for comparison with the static apparatus. A maximum operational benchmark of 3000 G was assumed. In addition, however, the centrifuge rotor and structural components of the centrifuge had been scrutinized for strength in an overspeed scenario. This was imperative for safety. Although not a structural member in the same sense, the FRACT is responsible for supporting its own sub-assemblies. Therefore, strength calculations and experimental validation were also performed for specific FRACT components under such conditions, taken to be 5000 G. In all such calculations, a conservative simplification was employed, namely that the acceleration magnitude was uniform at all positions of the FRACT. Given that the acceleration chosen corresponds to the reference radius R_{calc} for the membrane module of 0.61 m, an additional margin of safety of up to 9% is included in such calculations.

Three general stress cases may be proposed, and their ultimate ramifications identified as:

- Body stresses within a component
    - component failure.
- Contact stresses at attachment positions
    - component separation.
- Hydraulic (pressure) loadings
    - component rupture,
    - static seal leakage.

Of these, body and contact stresses were regarded and found to be most serious. Hydraulic pressure loadings are relevant merely to leakage of static components that penetrate the sampling chamber.

2.4.3 Body Stresses

Body stresses warrant examination in nearly all FRACT components. Both in tests and calculations, however, the effect of such loadings was examined proximate to each component's most vulnerable locations, usually at minimum section areas. Component failure would most likely occur at such locations, if at all.

2.4.4 Contact Stresses

Contact stresses arise where components are attached. Because of the modular design chosen for development reasons, there are several key contact stress locations. The induced weight of attached components are borne by and transferred to the FRACT body at these sites. Thereafter, such loads augment the innate stresses attributable to centrifugal effects in the body, and must be considered as part of the overall stress regime.

Contact stresses are often the most severe stresses experienced by a part. Many of the instances found in the FRACT involve joinings of metals, mainly steel, to polymers (Delrin). The process of such joints is considered challenging and two principal approaches are advocated: mechanical fastening and adhesive bonding. Messler [2.11] warns, however, "the viscoelastic behaviour of polymers versus the elastic-plastic behaviour of metals means that the stresses imposed by mechanical attachments must be kept low, otherwise severe deformation and loss of integrity can occur."

"The shear strength achieved with most adhesives is only 2-10% of the available shear strength of Delrin" [2.12] Typical adhesive performance for a stainless steel to Delrin joint is approximately 1.7 MPa (250 psi) in shear. Therefore, load bearing adhesive joints in the FRACT have been avoided except for non-structural instances where unavoidable, for example locational control during assembly, and where load levels are acceptably low.

2.4.5 Adhesives Selection

For these particular instances, a number of adhesives were investigated and tested. These included: Loctite 454, with and without 770-Primer "adhesion promoter for plastics", Ciba-Geigy Araldite 2041, Miller-Stevenson Epoxy 907.

Loctite 454 is a surface insensitive instant adhesive of the cyanoacrylate family, and is a gel which facilitates its use in many situations where liquid adhesives would be unmanageable. Potential shear strength can reach 24 MPa (3500 psi) with optimum substrate type and preparation. Primer 770 is a treatment which activates the substrate surface in preparation for use of an anaerobic adhesive, and which improves curing qualities where tight joint gaps are not achievable [2.13].

Epoxy 907 is a two-part epoxy with a 24 hour cure time. Owing to the high rigidity of the cured adhesive, epoxies suffer from low peel strength, particularly when employed with substrates having a degree of flexibility, such as plastics [2.8].

Ciba-Geigy Araldite 2041 is a two-part high-strength polyurethane adhesive, intended for use with plastic substrates. The chief benefit of the polyurethane family of adhesives is their improved peel strength compared to epoxies. Araldite 2041 is recommended for use with Nylon, another difficult to bond plastic [2.14].

For close fitting joints, the combination of Loctite 454 and 770-Primer was found preferable. Araldite 2041 provided excellent adhesion and gap filling ability, but possesses resilience. Where this property is desired, it is the adhesive of choice. Where gap filling ability is needed in concert with rigidity, Miller-Stevenson Epoxy 907 was found to be acceptable. Roughening of the Delrin surface is beneficial to bond strength in all three cases. Table 2.3 identifies and describes the sites of adhesive usage in the FRACT.

Assembly	Substrates	Adhesive	Joint type	Stress [psi]
Cond'y cell	Pt-Delrin	Araldite 2041	Shear	15 @ 5000G
Seal ass'y	Viton-Delrin	907 Epoxy	Locational	not load bearing
E/M coil ends	Phenolic-430FR	454 Loctite	Locational	not load bearing
Pole shims	Delrin-Delrin	454 Loctite+770	Locational	not load bearing

Table 2.3: Adhesive Usage

2.4.6 Separate Fasteners

A number of parts are attached to the FRACT body by separate fasteners, however of these only the valve mounting block retaining screw is a truly load bearing member of some concern. The coil end supports, for example, are retained by threaded fasteners, but these serve in mainly a locational capacity, for centrifuge induced loads are transferred to the body by normal contact with a pair of flanges.

The electromagnet poles are fastened to the core by custom made machine screws. The valve assembly is assembled and fastened with machine screws, all loaded in shear. Design calculations indicate these fasteners are well able to sustain their expected loadings.

The aluminum valve mounting block is located and restrained in the radial (centrifugal) direction by engagement with the pocket provided. A single #2-56 machine screw restrains the valve mounting block from pivotal movement and is placed under pure tensile loading. Assuming no support by tractions between the block and pocket, the magnitude of this load under overspeed conditions equals 147 N (33 pounds) resulting in a tensile stress of 57 MPa (8300 psi). Under maximum operational conditions this stress diminishes to 35 MPa (5000 psi). This was estimated by a free-body calculation treating the valve assembly as a lumped mass which imparts a moment upon the mounting block. The margin of safety, given a modest yield stress of 250 MPa (36000 psi), is greater than 4. The custom fabricated nut, made from aluminum to reduce weight, was scrutinized to ensure the thread engagement length was adequate to bear this load. Given the dimensions of the screw and the overspeed load expectation, a relationship (Equation 2.1) was derived for the shear stress S_s in the threads

$$S_s = (100\ \text{MPa})/n \qquad 2.1$$

where n is the number of threads engaged. Comparing this with the tensile yield strength of aluminum (130 MPa) and applying the conventional factor 0.57 relating shear yield strength to tensile yield strength, one may observe that no fewer than 1.4 thread pitches are required. Approximately seven full threads are in fact engaged, giving a factor of safety of five, even in the severe overspeed loading situation.

Of the separate components, by far the most massive is the coil assembly, accounting for over 25% of the total FRACT mass. Properly supporting this part bore an early influence on the general layout of the FRACT. It is located close to the bottom mounting surface, and thus transmits its full weight into a solid section of material, moderating stress levels considerably. If the upper half of the bore it which it resides is regarded as a stress free boundary (i.e. the coil assembly supports no externally imposed load) this results in the stress trajectories of the remainder of the FRACT body being disposed through the arch-shaped webs embracing the bore, the minimum section of the body component. As such, the wide-field stress experienced by the FRACT is greatest at this location, which was studied carefully before FRACT structural integrity under expected loads could be confirmed.

2.5 ACTUATOR: ENGINEERING SPECIFICS

2.5.1 Actuation and Sealing

As fluid accumulates in the sampling chamber, pressures reaching 700 kPa (100 psi) develop at the chamber drain. The means of sealing this drain must have integrity against such pressures and offer positive actuation without bearing surfaces.

The approach pursued here employs a pendant leaf spring. An adjustable needle is supported by the pendant spring, and mates with the interchangeable seal fixed to the FRACT body. Such a valve avoids the plight of component translation guided by bearing surfaces, instead its dimensional stability and stiffness allow constrained motion through a small range of displacement. In familiar installations, i.e. the two-stroke internal combustion engine, a similar leaf spring arrangement, the reed valve, establishes an adequate (though incomplete) seal by self activation in the presence of pressure. Moreover, valve opening occurs naturally once the pressure difference across it is reversed. It can be likened therefore to a check valve.

In the current application, no such pressure reversal occurs; valve state switching must occur in an opposite sense to that described above. Hence, an actuator servo must be introduced to achieve state switching.

2.5.2 Electromagnetic Servo: Principles

Many actuators (relays, solenoids) exploit electromagnetic induction as the means of coupling mechanical work with the delivery of energy by electrical means. In such devices, magnetomotance is applied to a magnetically permeable material volume which in turn produces a magnetic field. This is akin to a voltage producing an electric field. The material property relating the field strength to the magnetomotance is magnetic permeability. A class of materials known as ferromagnetic, their paradigm being soft iron, has the valuable attribute of responding in a non-linear fashion to the application of magnetomotance, producing exceptionally strong magnetic fields.

The work performed by such an actuator may be related to the change in stored energy within the magnetic field. This field passes through a volume of empty space, an air-gap; it is this gap which permits the translational or rotational movement required for mechanical work to occur. The field spanning this gap has greater energy density than within the solid soft magnetic material. Hence, a force develops in a manner resulting in the closure, or attempted closure, of this gap. Moreover, this force is proportional to the gradient of the energy density. It therefore results that increasing force occurs with diminishing air-gap. For a given actuator, the result is maximum force capability at minimum air-gap (approaching zero). The force thereby achieved is strongly non-linear. In addition, magnetic flux pervades all space and is only partially guided by permeable matter. Hence, flux leakage, which results in lost energy density in the volume of the air-gap, is a function of the design which significantly affects the achievable force for a given magnetomotance.

2.5.3 Electromagnet Design

The actuator mass is, due to metallic construction, a significant fraction of the flowmeter overall mass, and the electromagnet winding is the largest component of that portion. For this reason, the dimensions of the electromagnet were sought to be minimized.

The external location of the valve was a design option exercised to permit access to and interchangeability of key components such as the seal, valve and actuator. This also facilitates adjustment, an important consideration for a prototype design. The remote location of the coil that results, however, dictates that pole tips are required to convey the magnetic flux from the solenoidal field of the coil to the air-gap vicinity. Flux leakage and the resultant lessening of peak pulling force is a compromising result of this configuration.

The pull-closed principle of operation means the coil must serve in continuous duty, but the fortuitous circumstance that maximum sealing force requirements correspond with maximum actuator force availability means the design is optimized for performance. The drain orifice size was selected with awareness that the steady state efflux rate must allow flow-rate measurements in the desired range to occur; in turn this imparts a requirement for the pull strength of the actuator. Tabulated dimensions of commercially available tubular solenoids, which likely operate at greater efficiency (owing to smaller flux leakage) than the remote type used in this design, were consulted; it was learned that a long-life continuous duty type of similar dimensions to the projected FRACT unit develops a peak pull of 0.71 Newtons. This is approximately double the pull required to overcome the hydraulic pressure integrated over the orifice area, and hence is thought to be similar to the actual demands of the FRACT application, where seal compression is also desired.

These facts were borne in mind when the size, proportions, power requirements and materials selection for the actuator were assessed. Influential quantities like flux loss could not be feasibly calculated nor estimated, for the peculiar shape of the pole tips would have required a detailed finite element analysis to establish such parameters. Rather, priority was given to the manufacture and testing of a prototype actuator to assess performance empirically following design calculations of a simplistic nature. This approach delivered satisfactory results, and although the opportunity to further optimize coil mass and flux conveyance efficiency still exists, that the device functions adequately and meets mass constraints suggest the adopted philosophy was appropriate. Assembly views of the complete actuator are presented in Figure 2.5.

Wire specifically for use in electromagnet windings is commercially available. Attributes for this specialized application are low electrical resistivity, high tensile strength, ductility, temperature tolerance and minimal insulation thickness. The latter two criteria discriminate this class of wire, or more specifically its insulation, from most others. Neighbouring wraps in an electromagnet must be insulated from one another; the relatively durable but thick insulation of common wire however wastes volume that would be better filled with conductor. Often this insulation is also vulnerable to heat damage, particularly under pressure. Resistive heating of an electromagnet can result in high temperatures inside the coil far from radiative heat sinks, and winding tension exerts pressure. To accommodate these requirements, magnet wire has thin but tough insulative coatings. The wire selected for this application is a 28-gauge dual insulated type, rated for 130°C service; the insulation layers are polyurethane and nylon.

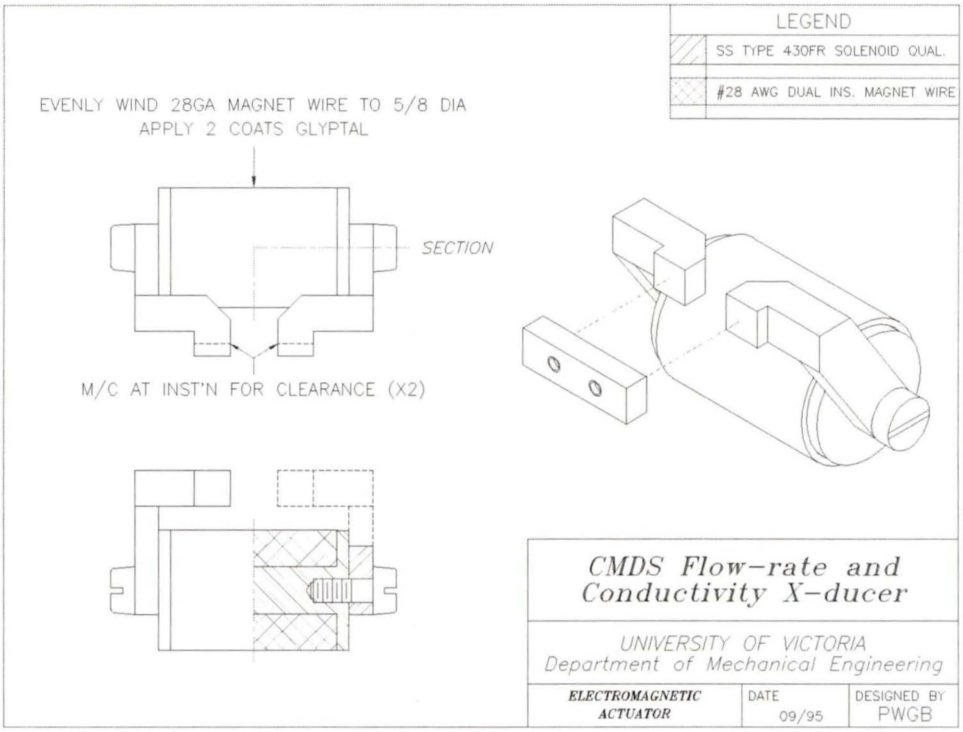

Figure 2.5: Assembly Views of the Electromagnetic Actuator

Initially, the core and end washers, made of a phenolic material, were separate parts. The washers were press fitted onto the core ends and then cemented using 454 instant adhesive. This was satisfactory for initial evaluation but an improved version, with end plates integral with the core, was later made. This revision permitted more accurate and dense winding of the coil; the original design was vulnerable to failure (washer separation) during during coil manufacture. Precise control and layering of the winding wraps helps to avoid wire breakage during centrifuge operation, which can occur where crossed wraps introduce stress raisers. To achieve this degree of quality, the winding procedure is manual: a small lathe was used to restrain the coil and was turned slowly with a variable speed drill. The number of winding turns was calculated as 790±10. Three estimates[1] of the number of winding turns, which were not counted during manufacture, comprise this value.

Were it chosen to implement the design in the alternate scenario wherein the self-exciting valve is drawn open by the actuator through a similar airgap (required to provide sufficient drainage) a pulling force equal to or greater than the sealing force would have to be developed under the least favourable circumstances of the air-gap vs force relationship. To accomplish this, the actuator coil would be required to generate a stronger field entailing that it have increased saturation flux density, greater magnetomotance and less flux leakage.

---

[1] dimensional, resistive and mass

Increased saturation flux density can only be achieved through the use of certain exotic magnetic alloys such as Carpenter HiPerCo, an iron-cobalt alloy, which affords a 64% improvement over 430FR. Greater core volume and magnetomotance both propagate a significant increase in the size and mass of the electromagnet. Reduction of flux leakage would require a coil and pole assembly design optimised for flux containment which, though probably implicit to the self-exciting valve arrangement, would compromise installation, adjustment and ease of manufacture objectives.

2.5.4 Core, Pole and Armature Design Considerations

Firm contact between the pole extensions and core is required for a good magnetic circuit. Each pole is therefore attached to the coil by a #4-40 shoulder screw engaging in a tapped hole on each end of the coil. This would be a mundane topic except that these shoulder screws are custom made from the same 430FR alloy as the rest of the magnet. The volume occupied by the fasteners is sizeable, is partially within the induction of the coil and is important for linkage of the pole with the coil in a contiguous magnetic circuit. Performance would doubtless be sacrificed if plain stainless fasteners, which are non-magnetic, were used in this crucial joint.

Flux leakage can be promoted by abrupt changes in section area in the flux path of permeable elements. To avoid unnecessary flux leakage, the core, custom fasteners, and pole tips were designed to have similar section area. The armature has somewhat less section area than the other elements in an effort to lessen supported mass, hence stress, on the valve leaf spring. This was deemed acceptable since significant flux losses will have occurred prior to the flux path encountering this component, meaning that its lesser area will not constrict the field by virtue of field saturation. A revised, improved armature incorporating counterweight and a single fastener maintains higher section area and is an option open for further refinement and eventual implementation.

2.6 VALVE: ENGINEERING SPECIFICS

2.6.1 Discharge Orifice

The sampling chamber must drain fully between measurements. Head is derived from the centripetally induced body forces acting on the column of fluid within the chamber. As the seal must be held closed against this head during the chamber fill phase, a compromise between drain rate capability and sealing force arises.

The first-order sealing force required results from the product of the drain orifice area and the hydraulic pressure. This pressure ranges from zero to 700 kPa (100 psi) with fill fraction and centrifugal loading. The drain rate varies from its maximum when the full chamber first begins to drain, to a minimum when approaching empty. Permeate flow continues to replenish the sampling chamber during the drain cycle, so steady state conditions occur when the drain and fill rates balance. The fluid level at steady state therefore is related to permeate flow rate. A vertical offset between the drain orifice and the lowest level-sensor electrode ensures sufficient head will exist to permit complete drainage at target flow rates, while allowing the level sensor and fill-timing systems to operate consistently.

2.6.2 The Interchangeable Seal Assembly

The design of the seal assembly posed unique challenges due to the tremendous lateral loadings involved. Reliable sealing is of paramount importance, because leakage would render flow-rate measurements inaccurate or impossible. For reliable sealing, an elastomeric seal element is required, however such an element must be supported to avoid distortion under its own weight at operational accelerations. The seal design conceived in this work has addressed this effect. Moreover the seal assembly was designed as an interchangeable component to permit both design refinements and replacement due to wear or damage. Although the permeate stream should be clean and clear, the discharge orifice may also be cleaned by way of this feature if it becomes clogged. The seal assembly is threaded and this opportunity for leakage guarded by a #10 O-ring in a static crush gland.

A number of conceptual ideas for the specific design and construction of the seal assembly were advanced, and prototypes made based on a interchangeable seal blank, of which several were manufactured for this purpose. The embodiment selected for further development, testing and eventual operational service emerged early as superior to the other designs under initial consideration.

The seal assembly consists of a Delrin plug incorporating the crush gland, tool flats and 7/16-20 external thread. The plug possesses additional internal features to accommodate the seal core, whose dimensions are tightly constrained to fit. The core is assembled around a short length of 19 gauge #316 stainless steel hypodermic tubing press fitted into the plug; this tubing directs the discharged permeate and prevents erosion of the surrounding Delrin. Coaxial with and supported by the rigid tubing is a length of 0.8 mm (1/32") ID Viton flexible tubing, which forms the elastomeric seal itself. Viton, a synthetic rubber, was chosen for its respected endurance characteristics; it is frequently found in seal, O-ring and peristaltic pump applications. During assembly, the Viton tubing is adjusted to protrude approximately 0.8 mm beyond the stainless tubing within, allowing for proper seal deformation during operation. This coaxial assembly is furthermore supported by an encasement of epoxy, which results in a near solid assembly well capable of enduring centrifuge loadings. Figure 2.6 illustrates this crucial component.

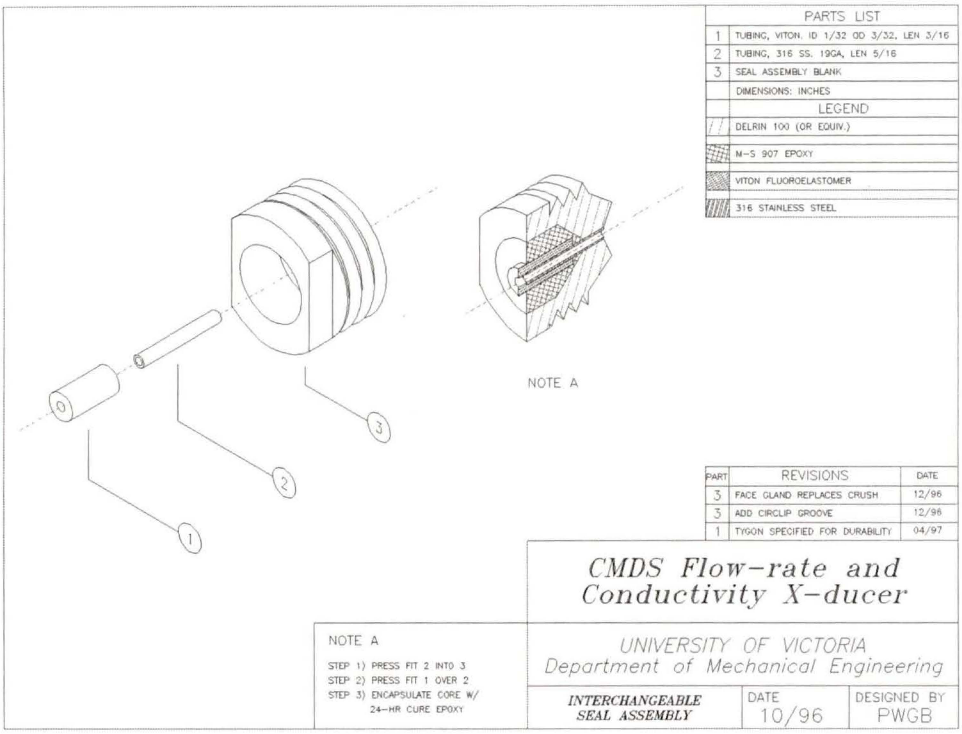

Figure 2.6: The Interchangeable Seal Assembly

2.6.3 Valve Design

A conical-tip needle is carried by the pendant valve spring component in a #2-56 internally threaded hole. This needle is aligned with the discharge orifice and when drawn in by the armature's motion, penetrates the tubular Viton element of the seal assembly and establishes a reliable seal. Stainless steel was initially specified for this component.

The valve spring need not possess any particularly strenuous spring stiffness qualities and as such was made of plain 0.3 mm stainless steel plate stock. The spring was reinforced to a total thickness of 0.9 mm in two areas. One, about the mounting holes, provides additional thickness there to give adequate sectional area, lessening stress levels where the mounting holes act as stress raisers. The second reinforcement area extends from the vicinity of the valve needle to the terminal end of the spring. This lends added stiffness through that span to reduce bending and constrain the needle's motion to near linear as drawn inward by the actuator, the armature for which is attached to the reinforced portion at its extremity. This extra thickness has the added benefit of allowing the tapped needle hole to possess sufficient depth, two full threads, for good engagement.

A closeup view of the completed valve in the open (relaxed) state, Figure 2.7, clearly shows the alignment of the needle and seat and the armature gap, which propels the valve into its closed position. A supplementary depiction of the valve in its relaxed and engaged states is presented in Figure 2.8. This entire valve assembly was mounted and located via a pair of 1/8" #4-40 stainless shoulder screws providing positive support and location, which in turn engage on a properly counterbored and threaded mounting block, affixed to the FRACT body. The valve needle, being threaded, allows for a small range of adjustment to achieve proper seal compression while exploiting the effective travel of the actuator. The relative locations of the armature and needle also result in a small force augmentation at the seal due to leverage. To ensure adequate drainage the relaxed position of the valve must return the needle a slight distance from the orifice. This is a function of the valve mounting position, an adjustable feature on initial versions of the first prototype.

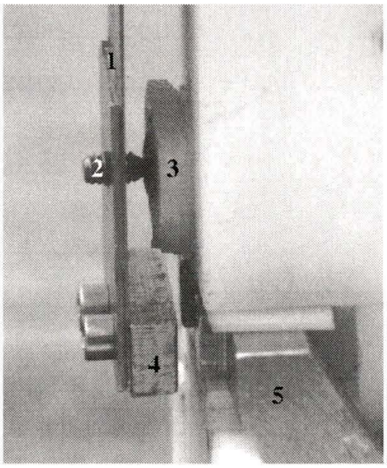

Figure 2.7: Closeup View of Valve
1) pendant spring, 2) needle, 3) interchangeable seal assembly, 4) armature, 5) electromagnet pole.

A crucial observation for this style of valve is the influence of tremendous body forces deriving from the centrifugal accelerations. These forces would render the valve inoperative if they, or any substantial component of them, were aligned parallel to the direction of free travel. This would either hold the valve open against the pull of the actuator, or force it closed, unable to open. The former case is tractable for, provided a constraint is included to limit the deflection and maintain an adequately small armature gap, actuator force should overcome the small additional load. The latter case however might cause the valve's neutral position to be in full contact and with full sealing pressure upon the seat. In this scenario the FRACT operation would be compromised.

For these arguments it is imperative that the FRACT, in its present form, be oriented such that its front face lies nearly parallel to the rotation plane. Outside this orientation, the valve relaxed position will tend to deflect away from the FRACT body. To avoid this, a restraining pin may be added; certainly this modification will be included in future versions.

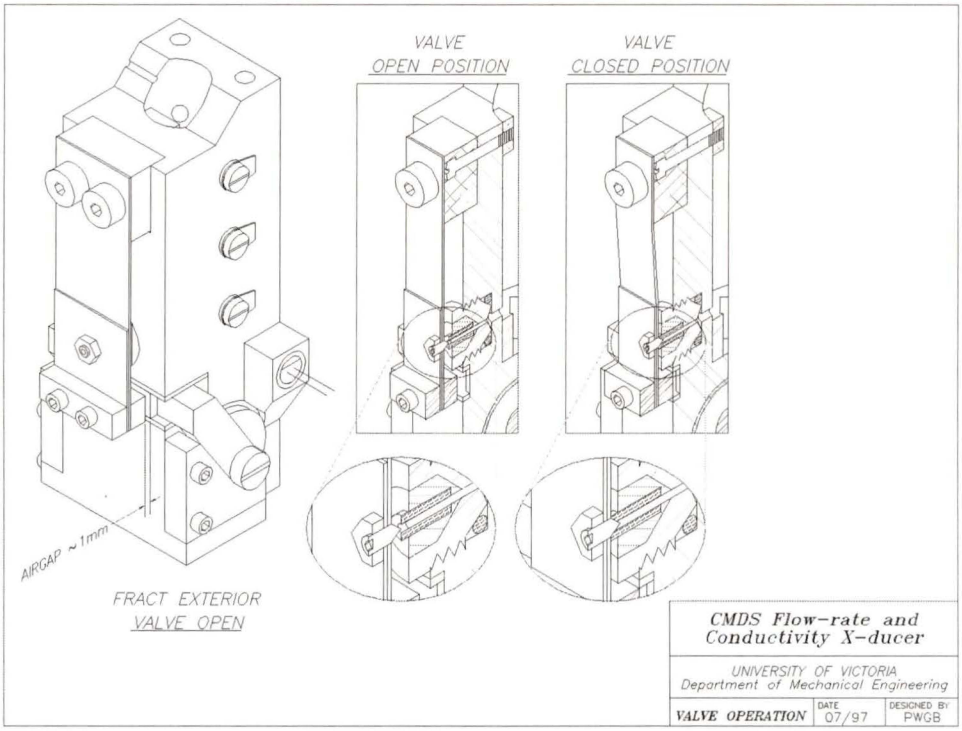

Figure 2.8: Isometric and Section Views of Valve & Seal Assembly
In this figure the airgap, residing between armature and pole tip, may be seen in the exterior view. In the section views, the valve is shown in both relaxed (open) and engaged (closed) states; note the compression of the seal and the flexure of the pendant spring.

2.7 LEVEL SENSOR SYSTEM

One of the fundamental functional requirements for flow-rate measurement using the adopted principle is the means to infer fluid level within the sampling chamber. This is in turn used to compute an average flow-rate, given the fixed chamber volume and the elapsed time to fill. The basic nature of the adopted level sensing strategy has already been broached, namely the detection of the presence of an electric signal at a specific electrode, this signal having been conveyed by circuit continuity through the entrapped fluid from a source electrode. It is a requirement of this approach that the fluid sample be electrically conductive.

2.7.1 Essential Features

The implementation of this simple requirement is subject to the same rigid constraints, particularly as pertaining to centrifugally induced loading, as the other principal elements discussed so far. The electric continuity approach benefits from a total lack of moving parts, indeed a paucity of required parts of any kind, and hence was anticipated to provide a most satisfactory implementation, adaptable to the emergent physical embodiment precipitated by other less flexible design parameters.

The minimum level sensing system consists of a pair of electrodes disposed such that they are separated by a span of sampling chamber volume in the direction normal to the entrapped fluid surface. The lower of these electrodes shall be connected externally to a signal generator, the upper to a detection circuit. Although the details of conductivity cell design will be discussed in a later chapter, it suffices here to state that such a pair of electrodes constitutes a conductivity cell. To any conductivity cell one may ascribe a gain, or cell constant, which is a measure of the cell's conductance (reciprocal resistance) given the presence of a sample of some known specific conductivity. In conductivity measuring applications the cell constant is optimised for a range of sample conductivity; often where relatively pure samples are involved this results in a low cell constant, indicative of a high gain.

Permeate is a relatively pure sample, however the level sensing electrodes are subject to constraints quite atypical from those in a measuring application. They must be of small dimensions, chiefly to resolve the fluid surface presence within a small spatial extent, and they must be situated far from one another, such that they bracket a meaningful sampling chamber volume. This results in the level sensor cell constant(s) being very large, i.e. having very low gain. Hence, the level sensor system is a poor conductivity measuring system. Fortunately, however, the system is not required to derive accurate measures of sample conductivity, but merely to indicate the presence of fluid: a binary state.

2.7.2 The Level Sensing Electrode Array

For ease of manufacture the level sensing electrodes were chosen to be simply #1-72 stainless steel binding head machine screws. The installation of each electrode therefore requires only a full-depth tapped hole in the FRACT body at the desired location. A solder tab, sealing compound and gasket complete the installation. A total of five electrodes, equally spaced 6.4 mm (0.25 in) apart, were fitted, disposed upon the two sides of the FRACT in staggered fashion. Therefore, the sampling chamber may be regarded, for the purpose of flow-rate deduction, as partitioned into four volumes bracketed by these electrodes. Screw length was selected such that each barely protrudes into the sampling chamber; the electrode is therefore formed by the circular end area, having diameter

1.7 mm. Stainless steel is adequately conductive to function in this capacity, where its corrosion resistance is an overriding requirement.

There are three options for installation of the interfacial wiring for these electrodes. The simplest is merely adhesive bonding of the individual wires to the FRACT body after each is soldered to a tab. Since the wire routing was not known at design time, this became the implemented approach. Machining of shallow fine grooves into the FRACT body into which each wire could be pressed, then glued, is a preferable approach, possible though only with a priori knowledge of wire routing. An elegant option, reserved for possible future versions, is an appliqué of polyimide flexible printed circuit, which would integrate the functions of the solder tab, and connecting lead for each level-sensor, plus all other electrical connections of the FRACT.

All five of these electrodes serve as level sensors; the conductivity cell electrodes function as source electrodes for this array. This merging of functions was envisioned at an early design stage and supported by later testing of the completed device, although a contingency involving a separate source electrode identical to the five sensors was maintained.

2.7.3 Fluid Level Detection

For samples of low conductivity, approximately 50 µS/cm for example, the resistance of the circuit formed by the individual level sensors may range between roughly 1-3 MΩ. Therefore, a detection circuit having high input impedance is required. A simple FET, whose input impedance is approximately 10 MΩ, sufficed in this capacity for testing purposes. A prototype circuit, to be described in greater detail as pertaining to conductivity sensor development, permitted basic tests to proceed.

The full development of this important system involved the commissioned electronics hardware, and the control and data acquisition hardware and software, not available until the FRACT was ultimately installed on board the centrifuge rotor and commissioning trials were imminent. These details are therefore deferred to chapter 5: Commissioning and Calibration.

2.7.4 Flow-rate Measurement

The exact function of the five level sensing electrodes in the task of flow-rate measurement is a topic of some importance. The array of electrodes is positioned such that its lowest member resides a small distance (3.2 mm between centres) above the chamber drain orifice. In this manner a short time interval shall pass between drain valve closure and detection of fluid at this zeroth electrode, which is interpreted by the control and data acquisition program as the trigger to record the initial time to be used in flow-rate calculations. The chamber proceeds to fill; the fluid surface sweeps upward within the chamber, contacting electrodes as it does so.

As each electrode becomes immersed and hence each detector in series registers the presence of fluid, absolute time is fetched and buffered in software. Once the chamber is sensed to be full, controlling action invokes the draining of the chamber and other activities proceed. Difference calculations between the individual time measures and the initial time provide elapsed times for each of the four volume partitions, which share bottom limits and overlap. Combined with a knowledge of each partition volume, the program output is a weighted average flow-rate for the measurement cycle.

2.7.5 Value of Redundant Flow-rate Data

The five level sensing electrodes clearly exceed minimum requirements for rudimentary flow-rate deduction. There is, however, an important purpose for this redundant information. The validity of the cycle average flow-rate depends on the entirety of permeate being entrapped by the measurement device during sampling chamber filling. Any leaks in the system, be they due to poor static seals or a poorly sealed drain valve, will result in spurious flow-rate deduction. In some cases, leakage might be so severe that the sampling chamber will not even fill; more invidious however would be the circumstance of a small leak, allowing the chamber to fill yet yielding incorrect flow-rate data.

Permeate enters the FRACT at low pressure. Hence, pressures endured by the various seals within the sampling chamber derive strictly from the head of fluid in the chamber applied to them. Though the dimensional extent of this head is very small, no more than 35 mm, in the presence of accelerations up to 3000 G the pressures borne may reach 740 kPa (107 psi) at the dynamic drain seal and 1 MPa (150 psi) at the inlet crossbore plug, a static seal. The risk of a leak is therefore a concern.

A key observation is as the sampling chamber fills, the pressure experienced at these most vulnerable locations increases from near zero. Therefore, any leak which occurs will gradually increase in magnitude subject to this pressure, limited only by the circumstance of choked flow should it occur. The effect of such leaks therefore should be apparent in the individual flow-rate measurements, four of which occur in each measurement cycle. The occurrence of a leak can be reasoned to appear as diminishing flow-rate values as measured by the partitions above the leak.

This diagnostic aid availed by the redundancy of flow-rate data is an important feature of the FRACT, essential to fostering confidence in the measurements it provides. Figure 2.9 is a record of the occurrence of such a leak, taken directly from the user interface of the custom FRACT controlling software (to be introduced and described in chapter 6: Control and Data Acquisition Software).

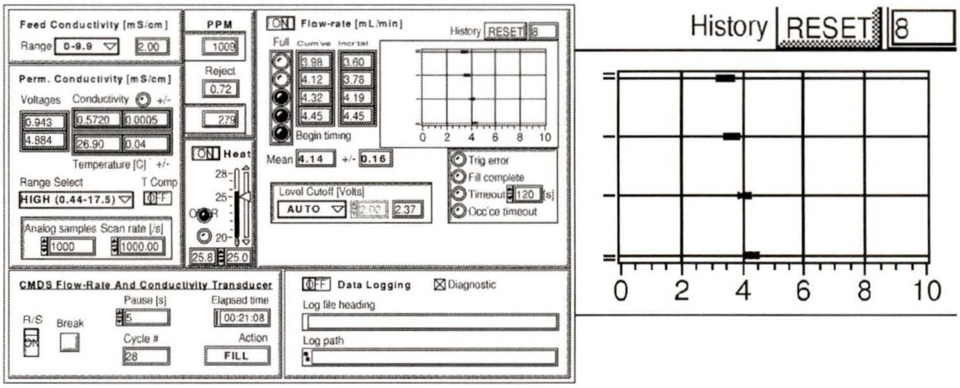

Feed Conductivity [mS/cm]
Range 0-9.9 2.00

Perm. Conductivity [mS/cm]
Voltages 0.943 4.884
Conductivity 0.5720 +/- 0.0005
Temperature [C] 26.90 +/- 0.04
Range Select HIGH (0.44-17.5)
T Comp OFF
Analog samples 1000
Scan rate [/s] 1000.00

PPM
1009
Reject 0.72
279

Heat ON
25.8 25.0

Flow-rate [mL/min] ON
Cum've 3.98 4.12 4.32 4.45
Incr'tal 3.60 3.78 4.19 4.45
Mean 4.14 +/- 0.16
Level Cutoff [Volts] AUTO 2.00 2.37
Timeout 120 [s]

CMDS Flow-Rate And Conductivity Transducer
R/S ON
Pause [s] 5
Elapsed time 00:21:08
Cycle # 28
Action FILL

Data Logging OFF
☒ Diagnostic
Log file heading
Log path

Figure 2.9: Sampling Chamber Leak Evidenced by Redundant Flow-rate Measurement Left: FRACT control software display, to be described in detail later; right: record of lessening flow-rate [mL/min] (abscissa) against increasing chamber fill fraction (ordinate), eight measurement cycles overlaid. This is a close-up of the indicator seen at the upper right of the total display.

2.8 REVIEW OF IMPORTANT DESIGN CALCULATIONS

2.8.1 Stress Regime in the Pendant Valve Spring

The stress regime arising in the valve spring is reasoned to be very nearly a two-dimensional field, owing to the thinness of this component. The spring is placed under tensile load deriving from the centrifugal acceleration acting in part upon the spring but also due to the attached load of the armature and counterweight, affixed by a pair of #1-72 socket head stainless machine screws. These screws are loaded in shear with a magnitude of roughly 21 MPa (3000 psi) in the overspeed situation.

The valve assembly is supported by a pair of stainless steel shoulder screws, also loaded in shear to approximately 27 MPa (4000 psi) at overspeed. These screws fulfill the locational and restraint functions together. It is at their position that, due to the loss of section area associated with the mounting holes and the stress concentration factor affiliated with them, that the spring component is subject to the greatest stress.

Two modes of failure have been examined for this location: rupture occurring under pure tension across the minimum section, and shear failure (tearing) in the web of material adjacent the holes.

Through such a calculation it was learned the component was vulnerable at this location. Additional thickness was specified for this area as a result. Use of thicker material for the entire valve, however, is inadviseable for two reasons: stiffness would be increased, lessening the compressive force applied to the seal, and the mass of additional material would worsen the load levels overall.

2.8.2 Stress Regime in the FRACT Body

The stress regime existent in the FRACT body is most certainly a three-dimensional field. Outside attached loads and various bores, passages and notches which affect cross-sectional areas and incur stress raisers are responsible for this fact.

Despite this, first order estimates of stress levels at key locations, chiefly the minimum section and base, were desired. The need for such estimates emerged when experimental validation of physical integrity of the minimum section under simulated loading was sought.

A computational model was developed in which the FRACT body was hypothetically partitioned into equally spaced sections normal to the loading (R) direction. Pure compressive loading upon these sections was then assumed, the magnitude of which was interpreted to be due to the body forces acting upon the material supported by the section in question, plus any attached loads. Section areas were extracted from AutoCAD drawings of the component and elemental masses calculated by extrusion of these sections through the grid length. The density of Delrin, 1425 kg/m^3 was taken from DuPont product literature. The total body mass of the computational model despite this coarse grid was within 2 grams (5%) of the actual component mass.

A depiction of the model used and a graphical presentation of the main results delivered by this computation are shown in Figure 2.10. A profile view of the FRACT body indicates the one-dimensional "grid". Transverse sections at these grid positions are shown, along with the section area. The compressive stress is plotted as a function of grid position. A maximum stress of approximately 14 MPa (2000 psi) is perceived to occur at the minimum section. This corresponds to 20% of the tensile yield limit of Delrin, within recommended limits for intermittent loading of a failure critical component. These results derive from the overspeed loading case, which exceeds maximum operational loading by a factor of approximately 2.3. Hence, the maximum operational stress expected from this simplified model is roughly 8.3 MPa (1200 psi), 12% of the tensile yield limit of Delrin. This is close to but in excess of the recommended limit of 10% for continuous loading of a failure critical component.

It can easily be envisioned that the stress field proximate to the pole clearance notches and in the immediate vicinity of the valve mounting will differ from the calculated quantities, which assume a uniform purely uni-axial regime across each section. In the vicinity of the two critical areas under scrutiny (minimum section and base-area), however, these convolutions are reasoned to be far-field effects and hence the assumption of uniformity is thought to be largely validated.

The variable load corresponding to the mass of the intermittently captured fluid, between zero and approximately 3 grams, was also computed, giving a rough value of R ~0.10 at the critical section, the ratio used in fatigue studies under cyclic loading. Future studies of component fatigue and reliability might involve this value.

It should be noted that these computations interpret the Delrin body as the only active load bearing member in the model. This is in fact a worst case scenario. In fact, the pole tips, being an interference fit when properly shimmed, convey some load across the pole notch. Additionally, the electromagnet assembly forms a nearly solid entity; again as this component is shimmed in place it certainly conveys some fraction of load causing a resultant lessening of the portion borne by the minimum section.

These points help to assuage any concern over the minimum section operational load being slightly in excess of the recommended. In fact, limitations on the membrane pressure tolerance restrict normal experimental operation to under 1800 RPM. This corresponds to a minimum section peak load of just 6 MPa (880 psi), 9% of the tensile yield strength and therefore within the maximum recommended for continuous loading of a failure critical component, this figure being 10% of the manufacturers data sheet specification of yield strength. The conservatism of these guidelines is in part to address variability of the mechanical properties of engineering thermoplastics such as Delrin. Hence, the results of this calculation evoked optimism that the component will prove serviceable.

The motivation to perform this simplified computational model stemmed from the desire to conceive and execute a simulation of the stress regime borne by the minimum section. This experiment, to be described in detail in chapter 4, Prototype Testing, validated confidence in the calculations. The load magnitude at minimum section area as derived from this model was used a seed value for the experiment.

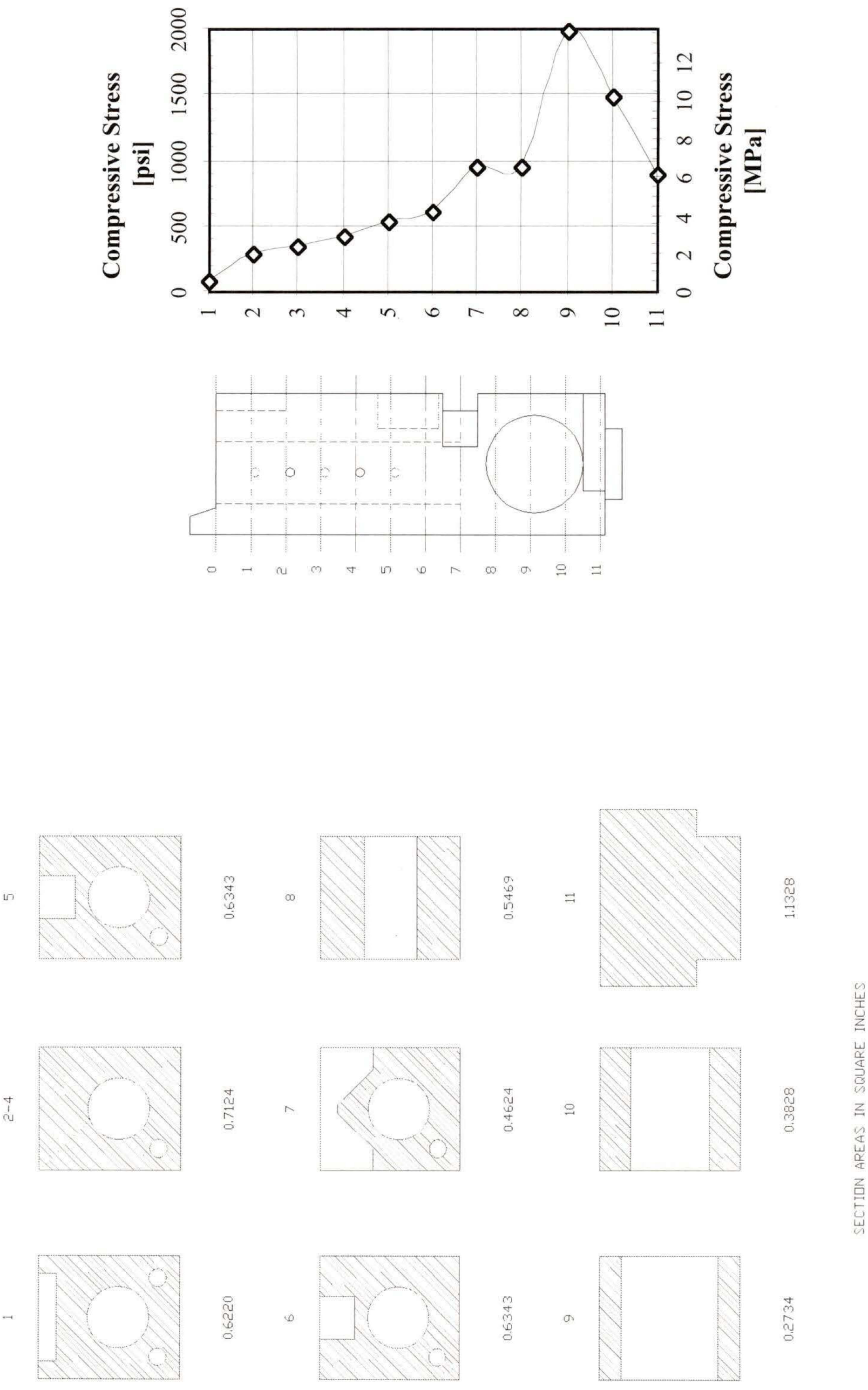

Figure 2.10: FRACT Body Compressive Loading Computation (Overspeed Situation)

2.8.3 Thermal Stability of Sampling Chamber Volume

It is well known that many plastics have greater coefficients of thermal expansion than other engineering materials. Example linear thermal expansion coefficients are given in Table 2.4. An estimate of the volume fractional temperature dependency is availed by Equation 2.2.

Material	**Coefficient [10^-6/°C]**
Delrin 100 (or equiv.)	110
Aluminum	24
Steel	12
Pyrex	3

Table 2.4: Coefficients of Linear Expansion for Various Materials [2.8,2.12]

$$\Delta V = 3\alpha \cdot V \cdot \Delta T$$

$$\Delta V/V = 0.0003\,{}^{\circ}C^{-1} \cdot \Delta T \quad\text{..........................}\quad 2.2$$

The result of 0.03% per degree Celsius propagates to affect flow-rate accuracy, but given that temperature excursions from the 25° ambient are foreseen to be less than ten degrees, this is considered insignificant.

2.8.4 Fluid Mechanical Calculations

As for other aspects of the FRACT design, fluid mechanical calculations were advanced where helpful or necessary, but empirical validation by careful testing was emphasised prior to eventual installation of the device.

2.8.5 Droplet Terminal Velocity

Permeate enters the FRACT at low pressure and immediately experiences a free-fall under centrifuge acceleration until encountering the surface of the entrapped fluid slug within the inlet bore. At centrifuge operational speed, the final velocity of such a droplet depends on the sampling chamber fill-fraction; maximum velocity occurs for the circumstance of an empty chamber and was calculated to be approximately 50 $m \cdot s^{-1}$. Such high impingement velocities justify the inlet design, which is intended to dampen the resulting pulsations.

2.8.6 Maximum Flow-rate Measurement Capability

A method was sought to obtain an estimate of the maximum flow-rate measurement capability early in the design cycle. This was reasoned to be governed by the maximum efflux rate, since the sampling chamber must be capable of draining fully between measurement cycles. The drain orifice is pressurized by the head associated with the fluid sample under centrifuge acceleration. As the chamber drains, the efflux rate decreases, due to decreasing head. Eventually, a steady state is reached where influx and efflux balance. For the flowmeter to function as designed, the surface height for this steady state must be below the zeroth level sensing electrode, whose purpose is to start the timers for the four chamber partition electrodes. Recognizing this fact, this electrode was designed to be situated 3.2 mm above the drain orifice (between centrelines).

Established equations for draining and filling of tanks call upon the basic tenets of mass conservation and quasi-equilibrium. These equations are usually applied to large vessels influenced by normal Earth gravity. For this work, the mass discharge rate equation [2.15] (Equation 2.3) for gravity draining was directly applied substituting centrifuge acceleration for Earth gravity g. Other variables include the fluid density ρ, the discharge coefficient C_d, the discharge orifice area A_d, and the head $(y_L - y_d)$. This equation implicitly assumes that wave action can be neglected, i.e. that the liquid surface may be considered flat. Inequality 2.4 may be evaluated to ascertain this, and for the sampling chamber geometry at centrifuge accelerations indeed this assertion holds. Here, $d/dt\ (m_{net})$ is the net efflux rate, M_{full} the full chamber fluid mass, L the chamber characteristic horizontal length, and y_L the full chamber head. Hence, the results of Equation 2.3 are provisionally justified.

$$dm/dt = \rho C_d A_d \cdot [2g(y_L - y_d)]^{1/2} \quad \text{.........................} \quad 2.3$$

Provided:

$$d/dt\ (m_{net}) << (M_{full}/L) \cdot [g y_L]^{1/2} \quad \text{.........................} \quad 2.4$$

A difficulty arises in the accurate determination of the discharge coefficient, which normally ranges from 0.65 (sharp edged hole) to 1.0 (rounded nozzle). Tabulated values for popular discharge nozzles [2.16] do not include styles resembling the custom nozzle of this embodiment, which includes a straight pipe segment; moreover the valve needle, which resides very close to the outlet is a complicating factor. A static laboratory experiment in which the chamber was allowed to empty under the influence of Earth gravity yielded a dubious coefficient of 0.21. Surface tension, which would be inconsequential at centrifuge loadings, made this experiment very questionable.

To arrive at an estimate of the maximum flow-rate measurement capability, Equation 2.3

To arrive at an estimate of the maximum flow-rate measurement capability, Equation 2.3 was solved using for head (y_L-y_d) the separation between the lower extremity of the zeroth sensing electrode and the upper extremity of the discharge orifice. The efflux rate dm/dt thus determined would correspond to steady state conditions for a permeate flow-rate of equal magnitude. This then may be regarded as the upper bound on measurement capability, for in order to permit a confident detection of the rising fluid surface past this electrode during the fill phase, a small tolerance i.e. a slightly lower steady state fluid surface position, would be desireable. The calculation was performed for a spread of accelerations through the operating range and for three candidate values of the discharge coefficient C_d.These results are depicted graphically in Figure 2.11.

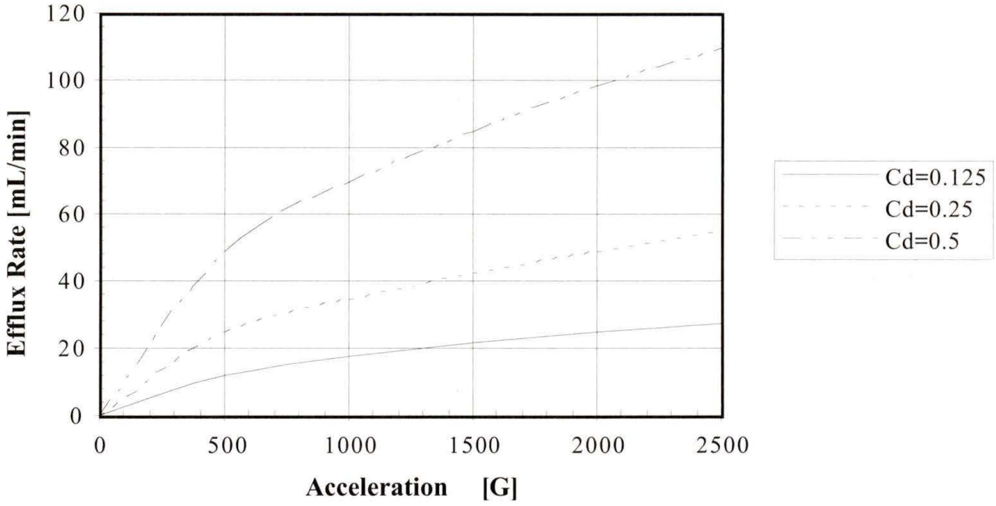

Figure 2.11: Efflux Rate at Maximum Permissible Steady State Chamber Fill Level

Unfortunately, C_d is a poorly known quantity. As a preliminary guide to the maximum flow-rate measurement capability, one can nonetheless glean that for reasonable, even pessimistic estimates to C_d, the operating capability of the FRACT is amenable with the expected permeate flow-rate. The design specification for permeate flow-rate was understood to be up to 20 mL/min, for a full stack of nine membrane modules at nominal maximum operating pressure, which corresponds with approximately 2100 G on the abscissa of Figure 2.9. Many experiments will use fewer than nine modules, and will therefore generate proportionately less permeate fluid.

3 Conductivity Measurement

3.1 GENERAL POINTS

The measurement of conductivity is, next to pH, the most common electrochemical technique, widely used in water monitoring processes. It is a non-selective measurement; all ions present contribute to the extent that their mobility and charge permits. Conductivity measurement employs sensors of the passive type, driven by external voltage.

Kohlrausch investigated the phenomenon of conductivity and its measurement extensively and determined that this quantity ranged, among known substances, over ten orders of magnitude from approximately $5 \cdot 10^{-8}$ S/cm to 1 S/cm [3.1]. The Siemen is equivalent to 1 reciprocal Ohm (Ohm^{-1}).

3.1.1 Temperature Compensation

Conductivity of an ionic solution varies as a function of temperature owing to the effect of temperature on ionic mobility. This effect is most pronounced for aqueous solutions of low concentration, as the proton and OH^- radical possess unusual charge transport mechanisms, and certainly cannot be neglected for permeate conductivity measurements, where the permeate has been depleted of its salts by over 90%. Temperature coefficients, expressed in percent conductivity change per degree Celsius, can be as great as 5%/°C for ultrapure water, while for most ionic salts the coefficient is approximately 2%/°C, decreasing to 1.5%/°C at very high concentration.

Reported specific conductivity figures are usually referenced to the temperature standard of 25° Celsius. To permit this the FRACT is equipped with a temperature-sensing channel. Similar to the conductivity cell, the sensor element is situated to be in steady contact with the entrapped slug of fluid.

A number of temperature sensing elements were considered. To reduce concerns over interchangeability, calibration, and non-linearity (particularly among thermistors), a precision IC temperature transducer, type AD–592CN was selected. This component, housed in a standard TO-92 semiconductor package, provides a linear mapping between output current in micro-Ampères and Kelvin degrees, and is insensitive to supply voltages, making it ideal for the harsh conditions of the centrifuge. Moreover, it is endorsed for remote sensing applications where its high impedance current output virtually nullifies the effects of connecting lead voltage drops and noise, an ideal property for an installation aboard spinning equipment close to electrical noise generating equipment.

The transducer must be placed in thermal contact with the fluid specimen, however hydrostatic pressure at the entrapped volume can reach elevated values during the condition of a full sampling chamber at operating speed. Hence, the transducer must somehow be sealed against leakage, yet its interfacing wires effectively routed.

To address this requirement, and to permit replacement of the transducer IC, a thermally conductive plug, complete with static radial gland O-ring seal and threaded shank, was devised. This plug makes contact with both the permeate and transducer, and exploits the thermal insulating properties of the surrounding Delrin (Table 3.1) to decouple it from other heat flux paths.

Material	Coefficient
Delrin	2.6
Aluminum	1390
Water	3.15

Table 3.1: Heat Transfer Coefficient (20°C) for Various Substances [BTU·i/h·f^2·°F] [2.12,3.2]

The transducer is embedded in this plug, which is made of aluminum to provide optimal thermal conduction properties and light weight. Chemical inertness at the surfaces exposed to permeate flow was accomplished through passivation with NaOH. The component is as small as feasible to minimize the bulk of aluminum used and shorten the response time of the assembly as much as possible.

Signal processing for the transducer exploits its internal precalibration and linearity.

3.2 CUSTOM CELL DESIGN

3.2.1 Commercial Conductivity Cells and Instruments

Commercial conductivity instrumentation, like commercial flow-rate equipment, was found to be generally designed for laboratory, field or production use. As a result, it is unsuitable for installation aboard the spinning rotor for the same chief reasons: size, weight and lack of structural soundness. Several popular commercial conductivity cells were nonetheless investigated, for this is the only portion of the conductivity sensor required to be in the centrifuge environment. None of these cells was deemed suitable for this application. The difficulties in integrating even the most appropriate of these units were incompatible within the strictly constrained overall FRACT design.

The thought of using a commercial meter in conjunction with the custom cell was also entertained, however it was reasoned to be more effective to develop this portion of the device as well. Most meters are sold with the intention for use with a specific cell, and moreover the ability to integrate the performance of this device with the level-sensor system and temperature compensation channel particularly suggested a purpose-built unit be conceived. The use of LabVIEW as the data acquisition platform also negated the need for any stand-alone unit conversion and display capability, strengthening this decision.

3.2.2 Cell Design Requirements and Integration

Required elements for the custom cell stem from the need for structural integrity under severe body accelerations, ability to detect and resolve changes in solution conductivity within the expected target range for typical permeates, and feasibility of manufacture.

The first of these requirements can be synthesized into the goals of imparting no bending loads upon the cell body, and of ensuring that adhesives used in assembly are loaded in pure shear. The second implores that the cell constant be such that for nominal permeate concentrations the cell resistance is amenable to the detection circuitry and that the cell geometry naturally avoids stagnation, gas entrainment or particulate adhesion. The final of these three requirements is an assertion that part geometry and assembly be tractable using available equipment and familiar techniques.

Once discharged, the permeate sample is lost to the environment, therefore conductivity measurement must occur near the inlet. The permeate inlet conduit, an integral feature of the FRACT body, connects to the sampling chamber at its bottom extremity. This was deemed necessary owing to concerns over disturbing the entrapped fluid surface, the presence of which, as it rises due to volume influx, triggers the level sensing channels required for volume measurements. By admitting permeate to the bottom of the chamber, and by maintaining a small slug of fluid there following chamber discharge, the impingement of fluid droplets will be dampened, fostering an undisturbed fluid surface within the sampling chamber.

To permit continuous measurement of permeate conductivity independent of sampling chamber fill fraction, the conductivity cell was designed for installation in this portion of the sampling chamber below the drain orifice. The cell remains, in this manner, fully submerged upon the production of a small initial amount of permeate. Moreover, permeate influx flushes the cell continuously ensuring valid measurements occur.

3.2.3 Cell Design: Engineering Specifics

The conductivity cell was designed as a modular component to permit development and replacement. The cell body consists of a solid cylinder of Delrin sized to have a locational clearance fit within the sampling chamber, and of such height to occupy nearly the full entrapped volume below the discharge orifice.

The sampling volume of the cell consists of an accurately machined slot through part of the cylindrical body. The facing surfaces thus created are used to mount the electrodes and the space between them forms the electrode gap. The uncut web remaining after the machining of this slot supports the gap and lends integrity to the cell.

A useful figure of merit for comparison and selection of conductivity cells is the cell constant K_c. This quantity arises in the conversion of conductance G, the measured property but which entails a relationship to the measuring apparatus, to the conductivity L, a specific property of the specimen (Equation 3.1). The cell constant may be regarded as analogous to a reciprocal gain. For samples of high anticipated conductivity, one seeks a cell of low gain, or high K_c, whereas for samples of low anticipated conductivity, a high gain, low K_c cell is desirable. Being a mapping between instrument output and a physical property, knowledge of the desired cell constant can serve as an aid to the proper design of the sensor.

$$L = G \cdot K_c \qquad 3.1$$

For a basic cell having parallel opposing rectangular plate electrodes the cell constant may be approximated by

$$K_c = l/A \qquad 3.2$$

where l represents the plate separation and A the individual plate area. The dimensions of K_c therefore are reciprocal length, usually cm^{-1}. This equation is not useful however for obtaining accurate conductivity values from conductance data, because the approximation fails to address several significant effects. The electric field between the electrodes for instance is not homogeneous, due to the edge effects of the pair of finite plates. In addition the active area is not that calculated by strictly geometric means. The process of electrode platinization, to be described later, increases the effective electrode area by the deposition of finely divided platinum onto the surfaces.

To accommodate these effects in actual operation the entire conductivity sensor apparatus must be calibrated against a reference. In the design process however the geometric approximation to K_c is useful as a guideline. Given that permeate conductivity was originally expected to be in the 50-150 μS/cm range, a cell constant between 0.1-1 cm^{-1} which yields conductance values easily handled by simple electric circuit elements such as the Wheatstone bridge, was the design objective. This is considered to be a high-gain cell.

3.2.4 Electrode Material Selection

Platinum was selected as the conductivity cell electrode material. Candidate materials included platinum, gold, graphite and 316 stainless steel. Most commercial conductivity meters employ platinum electrodes owing to this material's superior electrochemical properties, including corrosion resistance.

Since the uniformity of the electrode gap (or parallelism of the electrodes) helps assure maximum linearity to the extent possible given the finite plate limitation, platinum sheet stock of 0.010 inch thickness was employed. Of the available grades, this material was seen to provide good compromise between the requirement that the material be sufficiently stiff to allow manufacture, handling and assembly without damage, and avoiding unnecessary material bulk and cost.

The electrodes are situated such that they lie parallel to the centripetal acceleration direction. In this manner, the adhesive is placed in pure shear loading, its strongest condition.

3.2.5 Adhesive Selection

Adhesive selection emerged from tests performed using stainless steel plate samples and a block of Delrin. This included sustained immersion tests, in which bonded specimens were kept immersed in water for seven days. Two different instant bond glues were tested, along with two-part epoxy and Araldite. Both Delrin and stainless steel are considered challenging materials to bond. The joint area and orientation results however in a calculated maximum operational shear stress of 15 psi, well within the expected performance of the glues tested. The outcome of this test indicated Araldite to be the superior adhesive for this application. The instant glues suffered from bond deterioration on sustained exposure to water, and Araldite's slight elasticity was seen to be advantageous compared with epoxy's brittleness, in light of the cyclic loading associated with routine operation.

3.2.6 Electrode Leads

The two electrode plates must be wired to the oscillator and detection circuitry. This joint is required to be electrochemically inert since it shall be immersed within the permeate sample. The use of disparate metals as is often done in generic solder connections is not allowed.

Each electrode was furnished with a small tab to which a length of 0.5 mm (0.02 in) diameter platinum wire was spot welded, its end having been previously peened flat. Subsequently, each of these short leads was conventionally soldered to insulated wire. The resulting solder joints were then sheathed in a compound shrink/melt Teflon encapsulating heat shrink material, whose outer TFE layer provides a chemically inert insulation while the inner melt layer of FEP provides solid encapsulation to withstand moisture, distribute stresses and resist the effects of vibration. The exposed platinum wire to tab weld is chemically inert and should not deteriorate upon exposure to electrolyte.

Two options for routing of the cell wiring were maintained. In one, the wiring was envisioned to pass through the sampling chamber wall via a dedicated port adjacent the conductivity cell. The passage was then intended to be blocked using epoxy. The alternative to this has the wiring disposed between the cell, located at the sampling chamber's bottom, and the top opening of the sampling chamber, where a shallow groove both supports and guides the wire out from under the adapter clamp.

The latter approach has an undeniable advantage: it avoids the irreversible installation of the cell predicated by gluing the dedicated port closed post installation. This port may instead be closed using a small Nylon plug. This approach was chosen for the prototype embodiment. It requires that the wire and its insulation bear the full tensile body force loadings however imparted by the centripetal acceleration. Since the radial distance is small, both these requirements can be met.

3.2.7 Electrode Platinization

The act of electrode platinization serves to increase the effective electrode area while additionally lessening the cell's vulnerability to polarization. This process was affected upon the completed platinum cell following the example of Ives & Janz [3.3].

The process calls for cleaning of the cell using a concentrated nitric acid. The effect of this substance on the Delrin cell body and Araldite adhesive was the source of some concern, motivating a rehearsal using the mock-up stainless steel electrode cell. Dupont literature [2.11] indicates that Delrin is unsuitable for prolonged exposure to either nitric or hydrochloric acids, however the exposure time for these published tests was on the order of tens of days, whereas the act of cleaning the cell required mere tens of seconds. Although the exposed glue became discoloured and the Delrin became chalky, no substantive deterioration was observed to have occurred. Similarly a longer duration test using plain hydrochloric acid (in lieu of the platinization solution largely comprised of this substance) bolstered confidence that the cell assembly would not be harmed by the platinization process.

The 2% platinizing solution was prepared using 2N hydrochloric acid (HCl) and a quantity of Platinic Chloride ($PtCl_4$). A platinum anode was prepared using a small square of plate scrap from the electrode fabrication which, fortuitously, had a short length of platinum wire welded to it; the product of a trial spot weld. Both this anode and the assembled cell were placed in a test tube and immersed in a small amount of the platinizing solution. Using a regulated DC power supply, 0.015±0.005 Ampères were passed by the cell for 1200 seconds, both of whose electrodes served as cathodes during this process and which received as a result approximately 0.313 Coulombs/cm^2 of deposited Pt^+ ions. The process imparted a uniform and dull black coating of finely divided platinum to the electrodes of seemingly negligible thickness.

3.2.8 Determination of the Polarization Resistance of the Platinized Platinum Cell

It was deemed to be of interest to quantify the effect of platinization on the platinum electrode cell. This was accomplished using the procedure of Jones [3.4], which seeks to identify the contribution to total cell resistance arising from the electrode-electrolyte interface. Since the measured cell resistance always includes both this contribution, which can depend on excitation frequency, and the electrolyte resistance, a specific technique is required to obtain this quantity. Equation 3.3 reveals that the measured resistance R_M can be resolved into the electrolyte resistance R_T and a polarization effect dependent on the square-root of the oscillator frequency. This relationship is sometimes called "Warburg's Law".

$$R_M = R_T + k/\sqrt{f} \quad \text{.................................} \quad 3.3$$

A simple four-element resistor bridge was constructed with the cell as one resistance, and a decade resistance box for nulling of the bridge. The cell was immersed in a sample of plain tap water; the procedure requires a single sample be used throughout to assure constancy of R_T. Using a sinusoid function generator with adjustable frequency, the bridge was excited. The null condition was assessed by visual means using an oscilloscope connected across the differential nodes of the bridge; owing to the bridge construction, the null resistance equals R_M.

For a range of frequencies *f*, nulling resistances were recorded. Graphs of null resistance R_M as a function of $f^{-1/2}$ were prepared, depicted in Figure 3.1, and the linear portion, confined to the acoustic range (20-20 kHz), identified. This linear portion was projected to the y-intercept, being the condition of infinite frequency where polarization effects are reasoned to be nil and therefore whose value represents the electrolyte resistance R_T. The slope of this graph, *k*, (summarized in Table 3.2) indicates the cell response with frequency. Appreciable positive slope indicates a significant polarization effect causing measured resistance to be greater than actual electrolyte resistance: an undesirable situation.

A pronounced improvement was perceived between the bright platinum cell and the same cell following platinization. This improvement is apparent by the significant lessening of slope (by a factor of 144) in the relationship, indicating a reduction in the polarization resistance effect. Also, the y-intercept R_T, which is related to the cell constant by

$$K_c = L \cdot R_T \quad \text{.......................................} 3.4$$

given a known sample conductivity (*L*), was reduced by approximately 8%. Since platinization has the effect of increasing the effective electrode surface area this is a consistent result. These beneficial effects affirm the value of investing the effort to platinize the electrodes. For example, at the adopted excitation frequency of 2 kHz ($1/\sqrt{f}$ = 0.022 $s^{-1/2}$), the unplatinized cell exhibits a polarization resistance of 762 Ω whereas for the platinized cell this quantity is a mere 5.3 Ω. In comparison, the electrolyte resistance for a nominal 1 mS/cm sample using the cell constant K_c=0.213 cm^{-1} gleaned from this experiment is 213 Ω.

Cell	RM [Ω]	Kc [/cm]	Eff. Area [cm^2]	Slope [Ω·√s]
Bright Pt	6428±260	0.25±0.01	0.427±0.017	34060±3700
Platinized Pt	5532±34	0.213±0.001	0.498±0.003	237±247
Geometric	-	0.478±0.017	0.222±0.003	-

Table 3.2: Experimental and Calculated Conductivity Cell Particulars

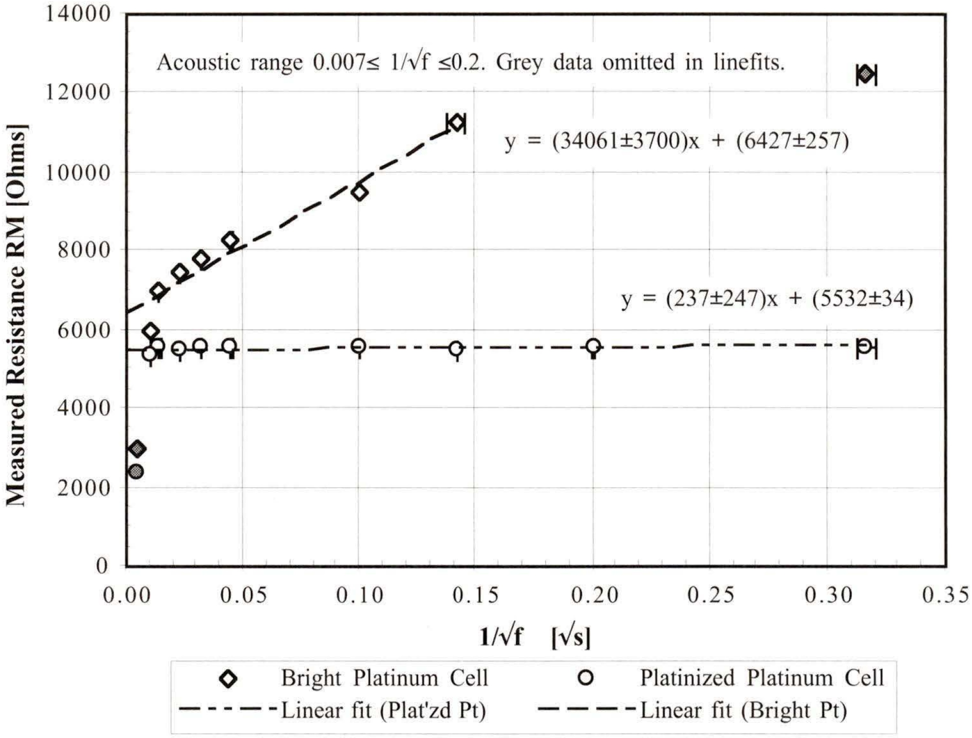

Figure 3.1: Measured Null Resistance vs Frequency$^{-1/2}$, Bright and Platinized-Platinum Conductivity Cells

3.3 ELECTRONICS AND DATA ACQUISITION

3.3.1 The Prototype Circuit and Cell

For development purposes a prototype excitation and detection circuit was devised and constructed following established principles derived from commercial conductivity apparatuses. This prototype circuit is shown in Figure 3.2, and schematically in Appendix III. A mockup cell was made using stainless steel electrodes to precede the manufacture of one using platinum. This was done largely due to the high cost of platinum and the desire to converge on a feasible electrode design before procurement and manufacture using this material.

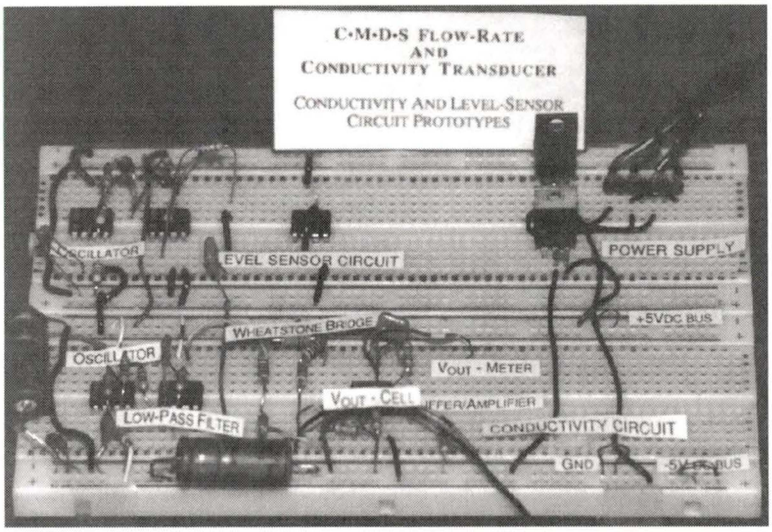

Figure 3.2: Prototype Conductivity and Level-sensor Circuits

The conductivity cell excitation voltage is required to be alternating. Were it direct, ionic migration and the resulting electrochemical processes proximate to the electrodes would quickly influence the electrolytic interaction and lead to spurious readings. The use of an alternating source reverses these processes before this effect develops yielding a zero net migration, provided the frequency is properly selected. This frequency is bounded at the lower end by the time scale required for significant ionic migrations to occur, which is a function of electrolyte concentration. At the upper end, it is bounded by the capacitance of the system, which results in frequency dependent impedance phenomena. Selection of an appropriate frequency drew upon oscillator frequencies used in commercial instrumentation for various conductivity ranges, and was chosen to be 2 kHz.

Oehme demonstrates [3.1] the usable conductivity range of a platinized-platinum electrode cell can reach approximately 100 mS/cm at an oscillator frequency of just 50 Hz. This bodes well for the system developed in this work, whose target range of less than 10 mS/cm using 2 kHz excitation is even less prone to crippling polarization. Concerns over undesirable AC effects arising from complex impedances were assuaged by the awareness that such phenomena seldom materialize within the acoustic frequency range [3.5], which is interpreted as approximately 20-20 kHz.

The prototype circuit therefore included a simple op-amp oscillator generating a square wave of approximately 2 kHz. This output was then supplied to a low-pass filter of the first order active type, and a pair of diodes ensuring that no voltage bias with respect to ground exists. The low pass filter attenuates high frequency components present in the square wave; the resulting output is a smoothed triangle waveform approaching a pure sinusoid. The output from this circuit then drives the Wheatstone bridge, consisting of three identical 10 kΩ resistors and the conductivity cell; the bridge being referenced to ground. The detection circuitry was connected across the differential nodes of the bridge thereby responding to any small resistance change of the cell about the nominal value: that of the bridge resistors.

The detector circuit was a simple differential operational amplifier with feedback gain whose voltage output was measured against a common ground by a Fluke model 76 True RMS Digital Multimeter.

This system permitted the behaviour of the cell and circuit to be studied for a range of specimen conductivities. Typically, as in strain gauge applications, the Wheatstone bridge is used to detect resistance changes of only a few percent about the balanced state. In this application however, the bridge was called upon to sense resistance across a much broader range. This has the undesirable side effect of producing a non-linear response. Without a much more sophisticated circuit (as in the Radiometer CDM3 or most other commercial meters [3.6]) a direct interpretation of the sensor output as a conductivity would be very difficult. In this application though the custom sensor was calibrated against the commercial CDM3 instrument. This mapping function allowed custom circuit voltage outputs to be interpreted as conductivity units.

The non-linear voltage to conductivity mapping has the unfortunate consequence that the instrument sensitivity is reduced for high conductivity samples. This arises in part due to the inherent non-linearity of the cell's behaviour but also due to the current and amplification saturation limits of the allied circuitry. As such, an effective upper limit on the conductivity range is imposed by this ever lessening sensitivity. Later investigations using the final commissioned electronics package and a dynamic calibration served to quantify the range and sensitivity for experiment planning needs.

3.3.2 The Balanced Condition and the Low and High Branch Calibrations

An interesting phenomenon occurs near the balanced bridge condition: the instance where the resistance of the conductivity cell equals that of the bridge resistors. The voltage at the two sensing nodes is said to be nulled. In the DC analogue, by further lowering the cell resistance a polarity reversal of these nodes would be witnessed, with voltage magnitude increasing at diminishing cell resistance anti-symmetric to the situation of cell resistances greater than the bridge resistance. Indeed this is a familiar scenario for strain gage applications, indicating contraction of the specimen. When AC is used, however, as in this application the phenomenon is more subtle. Voltage magnitude responds as for the DC case but polarity has no meaning; a phase reversal of the AC signal is experienced but this is a more difficult property to extract. Hence, there is risk of an ambiguous measurement, for a single voltage reading could be ascribed to two different conductivity values lying either side of this null. Nonetheless, AC excitation of Wheatstone bridges is a common and accepted practice, particularly in conductivity measurement.

Initially this situation was intended to be avoided completely by judicious selection of the bridge resistances such that the cell resistance would never reach equality. In this manner, the calibration mapping could be interpreted as a one to one function. Using the lower branch of the mapping function was deemed inadvisable since one operational requirement of the conductivity sensor must be to flag significant conductivity excursions potentially caused by a membrane rupture. Use of the upper branch was therefore rationalized. Under these assumptions the effective range of the sensor is approximately ten to one.

Later in the development and experiment planning process, this range was deemed unacceptably small, and the goal was altered to range up to approximately 5 mS/cm. Bridge resistors were replaced with 1 kΩ units, moving the null point to a position of higher conductivity. It was decided to exploit the lower branch of the conductivity function, recognizing that experiment planning and membrane performance experience would allow the targeting of permeate conductivity to avoid the null band between branches. Indeed the means to determine which branch of the function is appropriate is possible even during an experiment by perturbing the feed conductivity and noting the resulting correlation or anti-correlation of the voltage perturbation. Therefore with some care the ambiguity of this dual valued function can be avoided, and a much enlarged instrumental range achieved.

3.3.3 Electrolyte Selection to Exploit Instrumental Ranges

In view of the present conductivity measurement range restrictions, later to be characterized fully (chapter 5: Commissioning and Calibration), it is germane to mention one means to achieve expanded experimental results under this constraint.

In many planned C•M•D•S experiments, a range of concentrations of electrolyte will be used. Where such plans threaten to cause exceedence of the usable conductivity range, an electrolyte with lower conductance might be substituted. Two suitable substances whose electrolytic conductances differ in this useful manner are sodium chloride (NaCl) and magnesium sulphate ($MgSO_4$). The latter has a lower conductance than the former, and can therefore be used to perform experiments at higher concentrations.

3.3.4 Conductivity and Level Sensor Coupling Issues

The design and function of the level sensor array and its portion of the prototype electronics hardware has been described in an earlier chapter. Moreover, it has been alluded to that the use of electrical means for fluid level inference couples the measurements of the physically independent phenomena of flow-rate and conductivity. The extent and nature of the signal exchange leading to this coupling was the subject of a test at this stage of FRACT development.

A mockup sampling chamber was made from rod stock Delrin, equipped with a full level sensor electrode array identical to the prototype FRACT. Into this the conductivity cell was installed. The prototype circuit was used to source the 2 kHz, 200 mV triangle wave to the conductivity cell and the 4 Hz, 3 V square wave to the level sensor source electrode. The sampling chamber was filled with water, conductivity ≈50 μS/cm, at that time thought to be typical of permeate conductivity. Using an oscilloscope, the voltage waveform was examined at the level sensor electrodes and at the conductivity cell node.

As expected, mixed signals were witnessed at each channel. The level sensor waveform, whose peak-to-peak magnitude was 2.9 V, contained a superimposed 2 kHz ripple of 50 mV magnitude. This disparate relative magnitude, combined with the broad difference in frequency, led to the conclusion that a simple low-pass filter would suffice to reestablish a clean 4 Hz trace. Indeed for triggering purposes, the level sensor signal need not be exceptionally noise free.

The conductivity signal, being the smaller in magnitude, exhibited 4 Hz offset fluctuations of approximately 1 V. A high-pass filter might be successful in eliminating this offset; this point could not be evaluated using the prototype circuit, because the crude triangle and square waveforms used both contain high frequency components. The use of pure sinusoids of similar 2 kHz and 4 Hz frequencies, as was eventually implemented in the commissioned electronics hardware, is more amenable to band-pass filtering of this kind.

Ultimately, the issue signal mixing was resolved for the conductivity sensor by referencing both cell electrodes to the 4 Hz excitation voltage of the level sensor, such that the differential output arises purely due to the 2 kHz driving voltage intended for conductivity measurement. The level sensor channel, as indicated by the preliminary experiments, benefited from simple low pass filtering.

3.3.5 The Commissioned Electronics Hardware

The prototype circuit described was made available as a guide for the construction of the commissioned electronics hardware, part of an integrated suite of such hardware implementing the various required functions of the FRACT along with numerous requirements allied with the C•M•D•S rig proper.

Final calibration work and all C•M•D•S experiments employ this hardware, but the principles described pertaining to the prototype equipment generally apply, albeit with greater sophistication.

3.3.6 Data Acquisition and Software

Data acquisition (DAQ) is handled by a multi-function I/O board manufactured by National Instruments, installed in a dedicated micro-computer running LabVIEW. Custom Virtual Instruments accept requisite analog buffer reads, perform smoothing, and apply the appropriate voltage-to-conductivity calibration function, based on user input for which calibration branch is desired. Front panel controls give user input of analog port settings such as number of samples and scan rate. Temperature compensation may be toggled; this function exploits the permeate temperature channel availed by the AD-592 transducer and allied circuitry. Chapter 6: Control and Data Acquisition Software explores these matters in greater detail.

3.4 PROPOSED REFINEMENTS

3.4.1 Design of a Low-Gain Conductivity Cell

The possibility exists to improve the conductivity sensor performance across a wider range by the use of a low-gain replacement cell. The potential benefit stems from the observation that the worsening response of the conductivity sensor occurs for samples whose high conductivity causes a lower cell resistance than the initial specification and resulting implementation was intended to handle. This results in increased current being carried by the cell and Wheatstone bridge components, and in a bridge voltage differential far beyond its linear response range. Since the sensor response appears well behaved on the low-range side of the balance (null) value, the possibility of widening this low range while simultaneously extending the high range, is here entertained. The null value could be driven to a higher conductivity value simply by exchanging the bridge resistors for ones with lower resistance, however this would encourage still greater currents. By the use of a low-gain cell (with greater K_c) a similar result could be achieved with the existing 1 kΩ resistors while subjecting the system to no greater current than at present.

The alternative conductivity cell, the design for which is shown in Figure 3.3, has a geometric (approximate) cell constant of 8 cm^{-1}. This results from having a smaller plate area spaced further apart than in the present version. Applying the 14% cell constant reduction exhibited by the original cell solely as a result of platinization, the expected cell constant is approximately 6.9 cm^{-1}. It occupies the same external dimensions of the present cell, and therefore could directly replace it in future versions of the FRACT. Using 1 kΩ bridge resistors, the balance (null) point would occur at approximately 7 mS/cm sample conductivity, at present the practical high extreme of the calibrated range. It should be noted that this cell constant does not include compensation for the enlargement of effective area apparent with the commissioned cell, as manifested by comparison of geometrically calculated and experimentally deduced cell constants. The magnitude of this effect, if any, for the proposed low-gain cell is reasoned to be significantly less, since the design of the cell body confines the fluid sample to a greater extent within the volume directly between the electrodes, changing the nature of any edge effects at play.

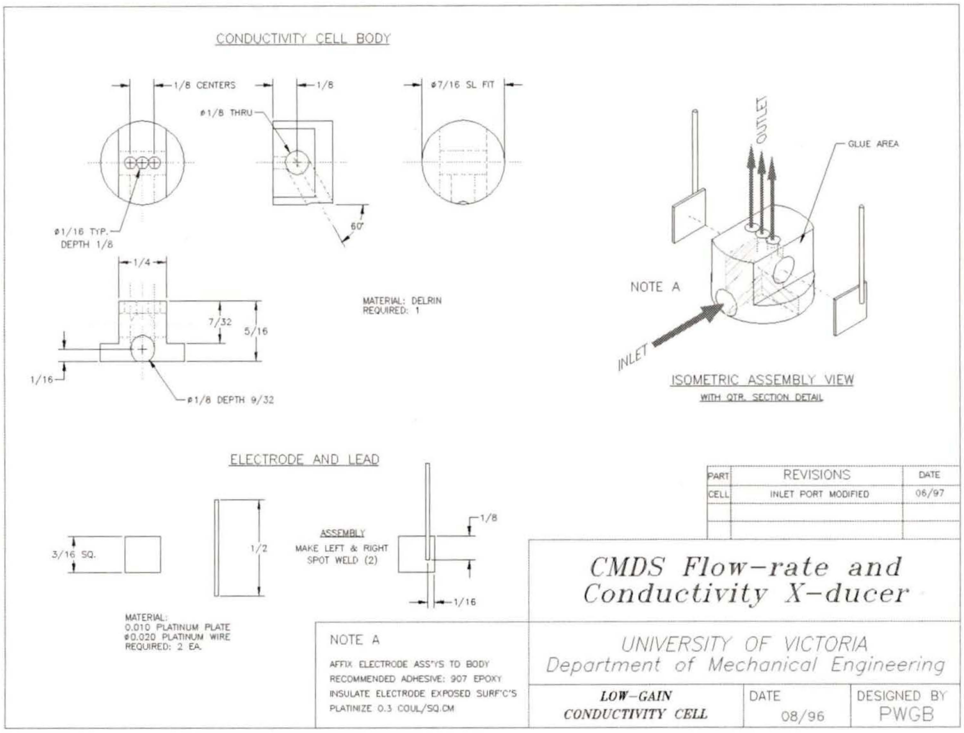

Figure 3.3: Design of Alternative Conductivity Cell with $K_c \approx 6.9\,\mathrm{cm}^{-1}$

3.4.2 Alternative Bridge Configuration

There are many exhaustive treatises on the versatility and usages of the Wheatstone bridge. It is, in the words of Wright [3.7], "an extremely sensitive analog computer at below the one part per million level." In this application, the basic bridge and differential amplifier serve adequately, but the dual-branch conversion function and non-linear response are inconveniences. Horowitz and Hill [3.8] describe an elegant linearized bridge, which is a meritorious candidate to eventually replace the existing circuit. Different or selectable bridge resistors remain as avenues for achieving future conductivity ranging goals either with the existing hardware on in concert with the alternatives mentioned in this section.

4 Prototype Testing

4.1 STATIC TESTING

4.1.1 Rationale and Regimen for Initial Tests

Thorough testing of the FRACT was regarded as a crucial aspect of its development for manifold reasons. Operationally, it was needed to ensure that available development time was productively used and that the FRACT variant ultimately installed on the newly completed centrifuge was prepared to the fullest possible extent for rapid final development and commissioning. The physical survival of the unit in the destructive centrifuge environment was an obvious fundamental objective to meeting this goal, however the larger issue of safety and abatement of risk to the entire apparatus provided increased motivation for pursuit of these tests and calculations. Furthermore, the successful commissioning of the FRACT and all allied instrumentation was an integral part of the commissioning of the C•M•D•S rig proper; its prompt completion was imperative before meaningful experiments could begin.

The various functions of the FRACT were first isolated and tested individually. In many cases, the results of these tests served simply to validate the successful manufacture of a given element of the FRACT, but the outcome of others led to iterative refinement of certain elements. Still others adopted the complexion of detailed characterization of the performance of particular elements.

Further tests explored the interaction of various systems; the level-sensor and conductivity sensor array principally, along with valve pressure and loading tests.

4.1.2 Stages of Development: Hierarchical Perspective

A review of development milestones, both those having already been described and those this chapter delves into, appears below. It enumerates four stages, culminating in the eventual operational version of the FRACT. Though not every development activity is shown, the principal alterations to the physical embodiment are itemized. This hierarchy is also illustrated in Figure 4.1; and is aimed to clarify both the envisioned strategy and its synthesis into a material entity.

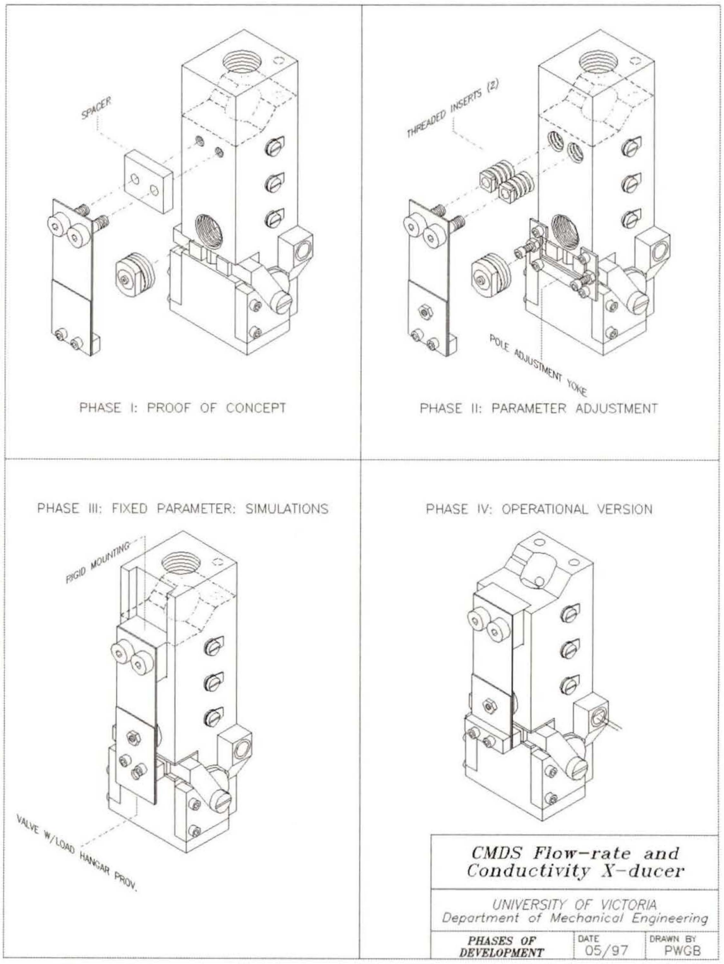

Figure 4.1: Chief Phases of FRACT Development
Dashed lines indicate eventual final form.

Phase I: Proof of Concept

Goal: validate manufacture and assembly

- valve mounting: *spacer and shoulder screw*
    - limited adjustability
    - poor tolerance of repeated assembly/disassembly
    - load bearing ability inadequate
- electromagnet: *cast iron prototype*
    - modest magnetic properties
    - poor corrosion resistance

Goal: demonstrate adequacy of principle of operation

- part interferences checked
- ease of assembly/disassembly demonstrated
- electromagnet servo operation feasibility demonstrated

Goal: satisfy mass and size constraints

- verified

Phase II: Parameter Determination ("Development") Version

Goal: incorporate adjustable parameters for performance evaluation

- valve mounting: *threaded insert receptacles for shoulder screws*
    - allows adjustment of valve relaxed (open) position
- electromagnet: *yoke installation for pole tip locational control*
    - allows adjustment of valve engaged (closed) position

Phase III: Fixed Parameter ("Test") Version

Goal: incorporate fixed parameters for load tolerance assessment

- valve mounting: *fixed mounting block arrangement*
- electromagnet: *post machining of pole length; rigid location by shims*
    - adjustability sacrificed for load capable embodiment
    - optimal parameters from phase II incorporated

Goal: simulate centrifuge loading

- load tolerance tests: *isolate critical locations using various test specimens*
    - valve mounting arrangement proven satisfactory
- centrifuge simulation: *demonstrate operation*
    - valve sealing and actuation proven satisfactory

Phase IV: Operational Version

Goal: deliver developed device for installation on C•M•D•S apparatus

- attachment means implemented
    - static testing capability sacrificed

Table 4.1: Development Hierarchy: Detailed Breakdown

4.1.3 Preparation for Testing

For constructive testing to advance, simulation of the arduous circumstances anticipated in commissioned use was necessary. Since a formidable challenge in implementing this embodiment centred upon the valve and seal system, application of hydraulic pressure to these parts was required to duplicate operational conditions. The initial prototype variant was designed to include an extended body upper portion to allow a hose barb to be threaded into the sampling chamber bore. Ultimately, all vestiges of this adaptation were removed, when this material was machined away to form the upper attachment ear. In addition, the inlet bore vent was capped and the machining of all other vents to atmosphere postponed such that the sampling chamber could be pressurized through the aforementioned hose barb. This embodiment constituted the initial, phase I, prototype.

4.1.4 Phase I: Tests on Initial Prototype Variant

The agenda for initial static tests was drafted while awaiting final manufacture of the prototype. Principal objectives included static seal verification, general performance of actuator, characterization of conductivity sensor, level and temperature sensors; viability of seal assembly and valve operation, and finally simulation of the high-G environment. A summary of these test and objectives is presented in Table 4.1.

Item	**Purpose**
Body	validate integrity of static seals, plugs and gaskets
Actuator	ascertain performance characteristics of electromagnet
Conductivity cell	garner an initial understanding of the sensor behaviour
Level sensor	confirm the adequacy of the level sensor implementation
Temperature sensor	verify the operation of the AD592 sensor
Valve	validate the adequacy of valve operation
Various	confirm structural integrity

Table 4.2: Synopsis of Original Tests and Objectives

The global outcome of these tests was promising. The interim valve mounting arrangement, using long shoulder screws and a spacer block, allowed for valve operation to be tested and evaluated, but was clearly lacking both in ease of adjustment, required for further tests, and in rigidity of locational constraint, required for centrifuge simulation and commissioned use. The actuator was perceived to function adequately, although again the range of adjustment of pole tip position to fully evaluate optimum parameters for final implementation was found to be absent.

4.1.5 Phase II Development and Parameter Determination

To accommodate the stipulations of phase I testing, two principal modifications were affected upon the FRACT. The valve mounting arrangement was modified by discarding the spacer block and replacing it with a pair of threaded inserts designed to accept shorter #4-40 shoulder screws. The FRACT body was retapped to accept these inserts in lieu of the shoulder screws directly. Adjustment of the valve mount offset and hence valve relaxed position was then accomplished by turning these inserts. Integral tool flats were provided to permit this with the assembly in place.

The second principal modification addressed the complementary need to reposition the magnet pole tips. An adjustment yoke was designed which, once attached to the FRACT body, restrained forward movement of the pole tips via a pair of machine screws. The valve closed position and actuator air gap were thereby adjustable by simply turning these screws. The pole clearance notch afforded enough range of movement to converge on an appropriate position that worked in harmony with the valve mount offset position described above. Although a misalignment between pole tip and armature could be caused by this arrangement, for the range of positions explored this misalignment was small.

Assessment of parameter settings was based on consistency of actuator closure and pressure bearing integrity of the dynamic seal. This phase of testing succeeded in converging upon the key parameters required for reliable valve operation. Locked-in implementation of these parameters was then sought, both for load tolerance testing and eventual commissioned use.

4.1.6 Phase III: The Fixed Parameter Variant

The actuator pole tips were designed and manufactured with a small excess of material in order to permit their eventual machining to final size. Therefore, the implementation of the desired dimension as determined earlier was merely a matter of having these tips ground down.

The implementation of an improved valve mounting arrangement using the results of phase II testing recognized the need for contact stress abatement where metal-plastic joinery was attempted. The avoidance of threaded joints involving plastic was also a goal.

This was accomplished by providing an intermediate component, the valve mounting block, which redistributes the load imparted to the FRACT body by the pendant valve assembly and moreover assures rigid positioning and fastening of this assembly. The block, made from aluminum in the interest of mass reduction, has a pair of tapped and counterbored holes to receive the shoulder screws. Its face forms the contact area defining the pendant valve offset position; this offset, 4.3 mm (0.17 in) having been ascertained in the previous phase of testing. The block was designed to engage within a pocket to be machined into the FRACT body, and itself restrained against the resulting moment by a #2–56 machine screw passing through a clearance hole to a contoured nut residing against the wall of the sampling chamber. The design calculations concerning this feature have already been alluded to.

Prior to affecting the irreversible machining of this new feature on the FRACT body, a test specimen exactly duplicating this geometry was prepared, and used to conduct experiments leading to the conclusion this avenue would prove successful for the commissioned device.

4.1.7 Loading Tests on Pendant Valve and Valve Mounting

To ascertain both the adequacy and behaviour of the valve mounting arrangement under anticipated loads, a test fixture and specimen were configured as shown in Figure 4.2. The fabrication of the custom load hanger rack allowed 44, 22, and 11 Newton (10, 5 and 2.5 lb) plates lacking a slot to be added individually to the rack in order to perform the desired experiment. An assembly view of the specimen can be seen in Figure 4.3, showing the loading coupon which replicates the attachment of the pendant valve assembly to the mounting block.

Vertical deflections of the loading coupon were measured as load was applied. Load magnitude was related to centripetal acceleration by regarding the valve assembly as a lumped mass of 4.6 grams subject to a uniform acceleration. The actual situation differs slightly in that the acceleration diminishes in magnitude nearer the rotor axis. Therefore the simulation includes a margin of approximately 8%.

The specimen experienced a small rotational displacement arising from the holding clamp's ineffectiveness to react to the moment imparted the specimen. On the actual FRACT this is not expected to pose difficulty because of a more robust clamp design. The effect of this displacement was nulled from the experiment by forcibly returning the specimen to its original position after completion of the tests, and observing that the vertical displacement of the coupon was thereby returned to zero. The results of this experiment are shown in Figure 4.3, and indicate the tolerable deflection of the valve mounting under operational loading.

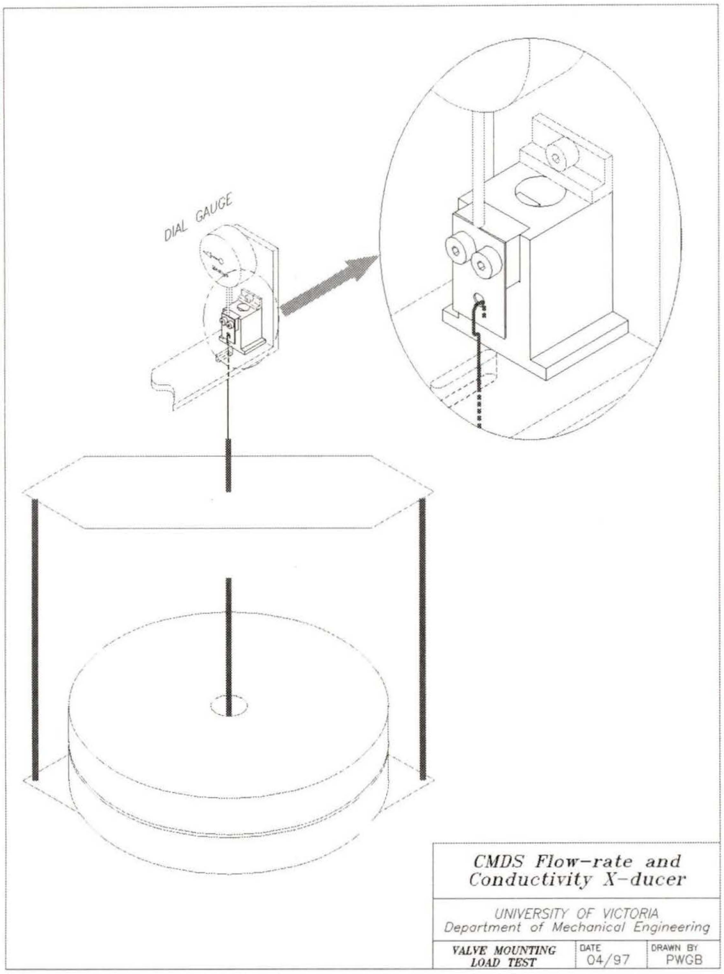

Figure 4.2: Valve Mounting Load Tolerance Test

A further test was performed in like fashion wherein load representing the accelerated lumped mass equivalent of the entire valve assembly and mounting hardware was applied to the loading coupon. This served not only to test the mounting's ability to bear both its own plus the attached load, but also verified the loading coupon's strength and hence that of the pendant valve spring to a higher than operational level.

With this espousal in hand, the FRACT prototype was reconfigured, engendering the phase III configuration for full simulation of the centrifuge operating environment.

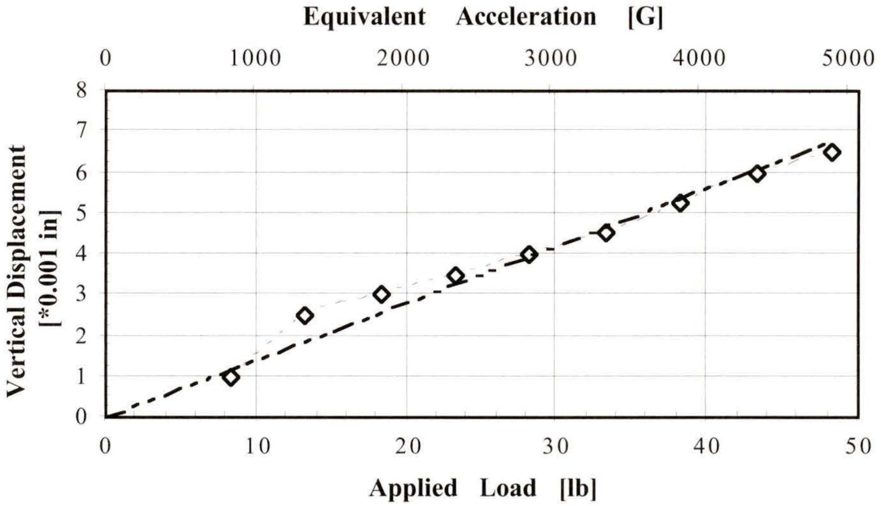

Figure 4.3: Valve Mount Vertical Displacement vs Simulated Centrifuge Loading

4.1.8 Experimental Validation of Load Bearing Minimum Section

The behaviour of the portion of the FRACT body surrounding the highly stressed minimum section was studied experimentally. This was accomplished by application of compressive load to a sacrificial specimen. The specimen was prepared duplicating the bottom portion of the FRACT body; it and the valve mounting specimen are depicted in Figure 4.4. Testing of the entire body in this manner would not have been meaningful since actual centrifuge induced body forces result in a cumulative load regime in the radial direction. External application of a compressive force roughly simulates a given centrifuge loading only at a specific section. Therefore, this experiment was confined to examining the minimum, or critical, section. The specimen replicated not only the electromagnet bore but also the pole clearance notch and square bottomed sampling chamber in order to encompass the influences of these stress raisers and subject the minimum section to the most accurate attainable stress field.

The MTS machine of the Love Laboratory was used in conjunction with a pair of steel plates to subject the specimen to a compressive load. Three separate trials were conducted. Approximate load levels required for the set up of the MTS were extracted from the uniaxial model stress calculation, described in chapter 2 Flow-rate Measurement. This model was also exploited to yield a nominal load value of 2225 N (500 lb) for a sustained loading test. Finally, the specimen was loaded destructively and the mode of failure examined.

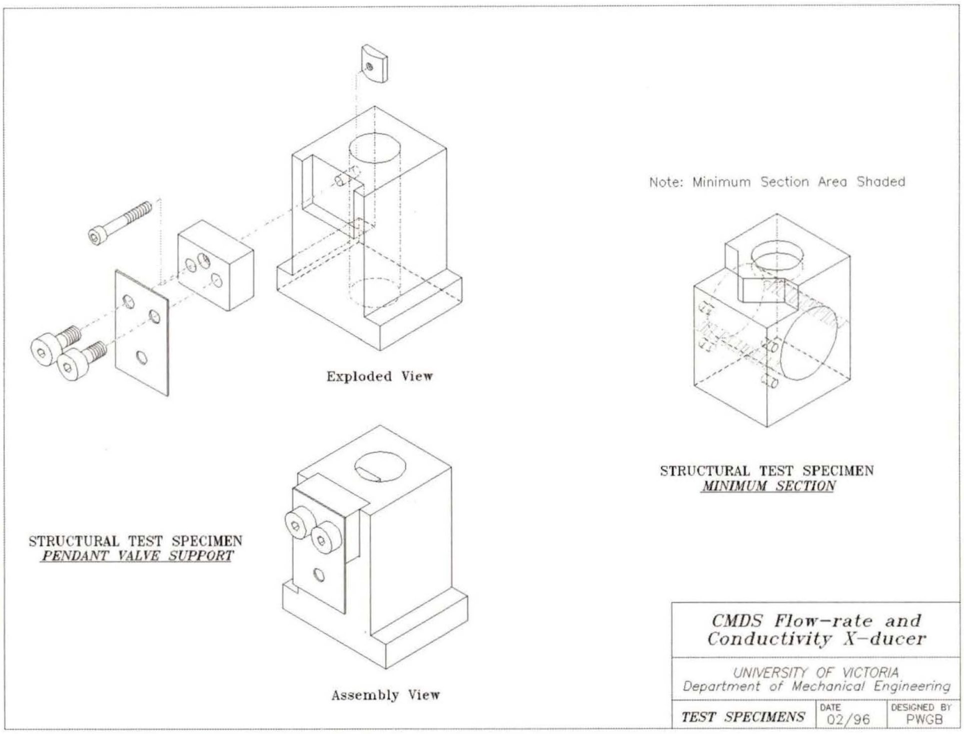

Figure 4.4: Specimens Used in Load Tolerance Testing
Left: isometric exploded and assembly views of the valve mounting test specimen; right: the minimum section (shaded) test specimen for compressive load tolerance validation. These specimens exactly replicate specific portions of the FRACT, and are made of identical materials.

Results of these experiments are depicted in Figures 4.5 and 4.6. The displacement control mode of the MTS machine was used initially to avoid damage to the apparatus if an unexpected specimen failure occurred. In this mode, applied load is the dependent variable while ram displacement is controlled and varied. This test verified that 2775 N (624 lb) could be supported by the minimum section, giving confidence that the sustained loading test could safely performed.

In the sustained loading test, load control was used to subject the specimen to 2225 N force for five minutes, bracketed by a ramp program of 22 N/second (5 lb/second). The ram displacement was recorded, giving a measure of both elastic and plastic deformation. Measurable, but small, plastic deformation occurred: approximately 6% of the elastic deformation. This is typical for Delrin, which exhibits slight creep at highly elevated loads.

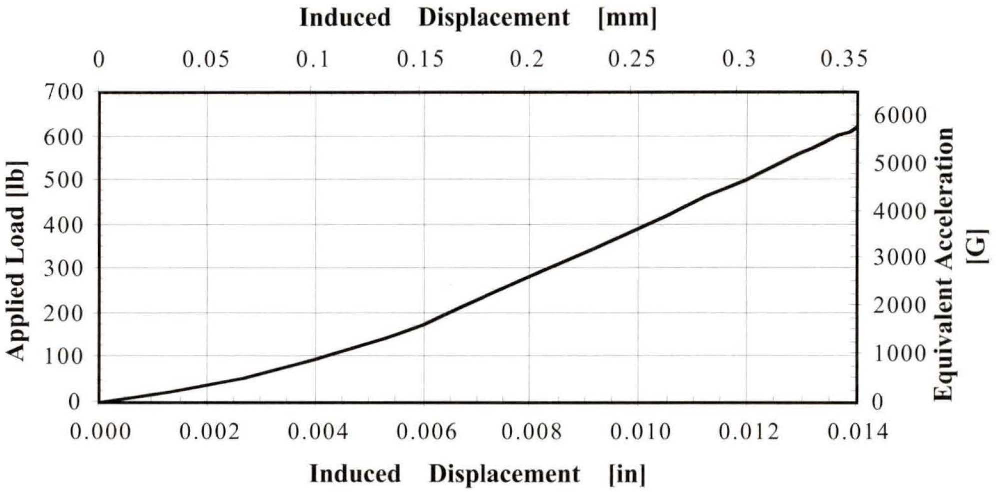

Figure 4.5: Specimen Compression under Induced Displacement
MTS machine operating in displacement control mode (load the dependent variable).

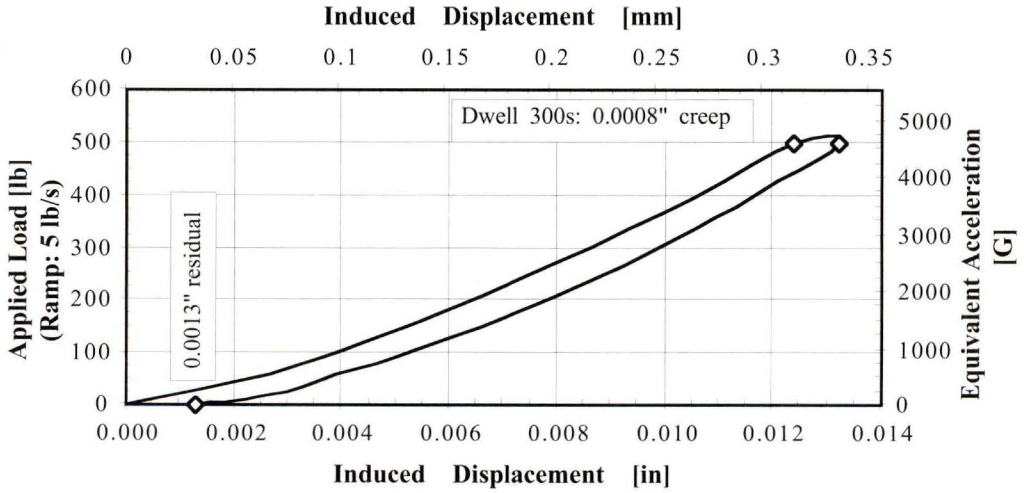

Figure 4.6: Specimen Compression under Applied Load
MTS machine operating in load control mode (displacement the dependent variable).

Finally, again under displacement control to protect the apparatus, the specimen was compressed with over 10200 Newtons (2300 pounds) force. Rupture did not occur but significant plastic deformation developed. Permanent stress damage was apparent both from significant residual deformation and visible stress damage.

In actual service the presence of the electromagnet coil and poles will redistribute and share the load supported entirely by the body webs in this test, and will impart additional load to the base area. This lessens the stress borne by the minimum section.

4.1.9 Efflux Rate

Under optimal steady state draining conditions, the sample fluid surface height must lie at or less than approximately 1.5 mm above the outlet centreline. This ensures the zeroth level sensing electrode will not be triggered prematurely. For operational centrifuge conditions, this upper limit corresponds to a discharge pressure of roughly 50 kPa (21 psi). Using the leak valve and gear pump, this pressure was brought to bear on the apparatus while the valve was open. Capture of the exhausted fluid yielded a efflux rate of 174 mL/min. This suggests the released discharge valve is capable of passing considerably more fluid than required to ensure adequate and full drainage necessary for permeate flow-rate measurement in the desired range.

4.1.10 Procedure for Valve Adjustment

Although the valve mounting offset dimension, having been locked in by the phase III implementation, can no longer be freely adjusted, thin stainless steel shims may be installed giving a small latitude of adjustment if desired. Initial and routine adjustment to accommodate component (such as seal assembly) replacement, is affected via the valve needle.

If the pendant valve assembly has been removed, the first stage of readjustment must be to recentre the valve needle such that it cleanly penetrates the tubular seal element. This is accomplished by slackening the valve restraint shoulder screws, affording the ability to reposition the valve spring very slightly, then re-securing the screws.

To initially set the seal compression the actuator must be engaged, and the valve needle gradually tightened. Resistance will be encountered as the seal is compressed, eventually leading to a sudden release of the armature. This is an indication the needle has been driven too far. With some alacrity, the procedure can be repeated such that proper seal compression is obtained but actuator pull strength not exceeded. The achieved setting should be tested by cycling the actuator several times. If it fails to engage fully, the needle should be withdrawn in no more than 1/8 turn increments until it does.

Occasionally this procedure will fail to establish a satisfactory seal. The needle should then be tightened in similar increments. If a working valve cannot be attained through such adjustment, an investigation of the cause will likely be required.

4.1.11 Simulation of the Centrifuge Environment

The gamut of sub-system testing was an essential part of the "development helix" but confidence in the operational viability of the FRACT could only be gained by simulation of the pressure and loading conditions to be experienced on-board the spinning rotor.

Exact simulation of these conditions is effectively impossible. The behaviour of the fluid surface for example cannot be reconciled in laboratory experiments, since the ratio of surface tension to body forces is very much smaller on the centrifuge. It was deemed sufficient to subject specific questionable aspects of the FRACT to realistic pressure and loading conditions. This approach took the form of subjecting the sampling chamber to hydraulic pressurization while simultaneously imparting the pendant valve assembly with tensile load. In doing so, the critical seal activation and integrity functions were strenuously exercised.

The complete sealing of the sampling chamber drain is paramount to the success of this device. The pressure against which this seal must occur may be calculated reliably, and a means to apply this pressure easily implemented, however the radial pressure gradient within the sampling chamber cannot be statically duplicated in the laboratory. This is not a serious encumbrance however because the application of merely static pressure subjects the article in question to desired conditions, while greater than expected pressure is experienced elsewhere in the device.

Active control and monitoring of the FRACT was not possible since the computer system and LabVIEW software had not yet been acquired nor devised. Manual control of the actuator instead was made possible using a 6 W variable hobby transformer in series with the Fluke 76 DMM in the DC current mode.

Faucet pressure, typically less than 300 kPa (45 psi), initially was used for hydraulic tests. Higher test pressures, up to 550 kPa (80 psi), were later attained by charging the FRACT with water followed by the application of pressurized nitrogen. This method was sufficient for cursory validation of seal adequacy but was inconvenient for thorough testing. Confirmed in this manner was the seal activation and integrity under expected chamber pressure, in the absence of tensile loading of the pendant valve member.

The phase III prototype was affixed to a jig which in turn was clamped to the laboratory bench overhanging a sink (Figure 4.7). A special pendant valve was prepared which included a short integral extension, allowing a length of 150 pound-test stainless steel multistrand wire to dangle below the armature. This in turn passed through a slot in the jig to a terminal snap-swivel fastener. The purpose of this arrangement was to permit the movable valve parts to be imparted with a controlled tensile loading by the suspension of known weights.

An Ismatek variable speed gear pump drawing water from a reservoir was plumbed into the FRACT testing adapter, equipped with a tee connected to the following panel mounted components: an analog pressure gauge (0-160 psi range) and a NuPro "S"-Type Precision Metering Valve, venting to the reservoir. This valve was selected based on its well documented pressure-drop to flow-rate and discharge coefficient to number-of-turns-open relationships, and has a maximum discharge coefficient of 0.004.

Adjustment of the pump speed and leak rate permitted pressures ranging to 800 kPa (115 psi) to be imparted to the FRACT. Make-up water continually replenished the reservoir. Weights of 2.3, 3.2, and 4.5 Newtons (5, 7 and 10 pounds) were suspended, supported entirely by the pendant valve, and activation and sealing effectiveness examined. Valve activation was cycled, and current requirements both for initiation and sustain of valve closure (within the limitations of the equipment) were investigated.

An important corollary: application of suspended mass serves to duplicate the centrifuge's effect in establishing the stress regime within the pendant valve assembly. In addition, this mass simulates the additional work required of the actuator to raise the centre-of-mass of the pendant valve assembly through some small displacement against the centrifugal acceleration. Two further aspects of this simulation however result in meaningful differences with the centrifuge scenario.

Through the addition of the suspended mass the total inertia of the system will have been increased by several orders of magnitude. The actuator therefore is caused to contend with a greater inertia than it would do in the centrifuge; hence, this test is more severe than required. The length of wire rope, with its flexile terminations, buffers the actuator from the full brunt of this effect by allowing the suspended mass to experience a less abrupt acceleration than the armature. Estimation of the net magnitude of this effect was not attempted but the observation that it results in a more strenuous test is asserted.

Additionally, the potential energy gain of the pendant valve assembly is greater in the simulation than in actual operation. This is because although the loads in both cases are equal, in the simulation the suspended mass is raised against gravity by a larger amount than the pendant valve assembly's centre-of-mass is raised against the centrifugal acceleration. The suspended mass displacement is approximately 58% greater, due to its application at the extremity of the assembly, 1.58 times further from the geometrically deduced effective hinge point.

The results of this test unambiguously implied that the seal, valve and actuator embodiment would ultimately operate as intended aboard the spinning rotor.

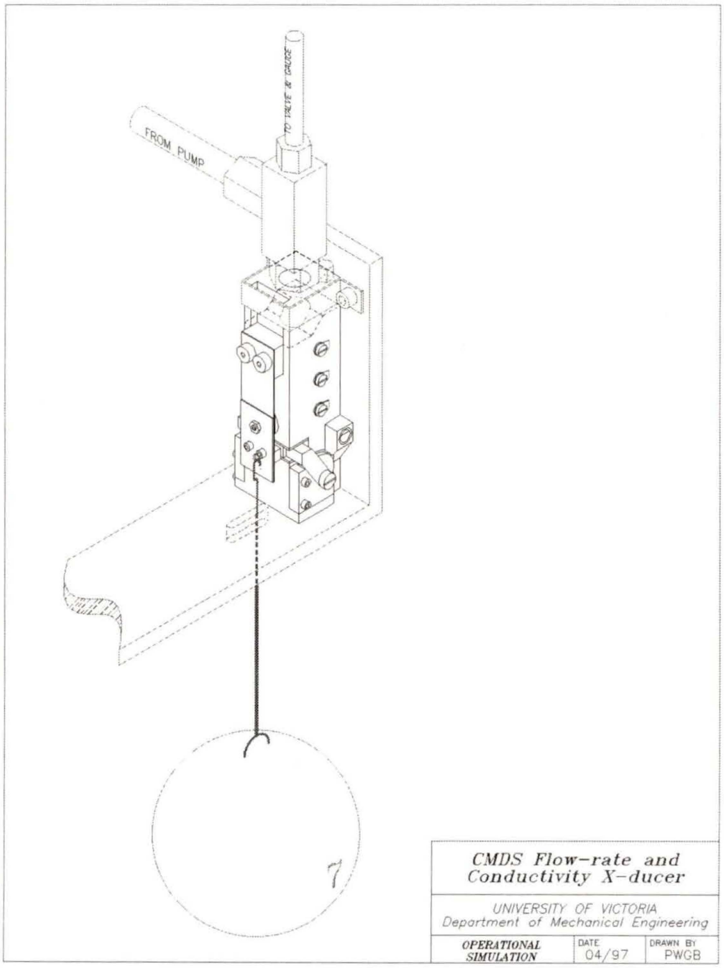

Figure 4.7: Full Simulation of Centrifuge Operation
The phase III prototype, mounted on a restraining fixture, is plumbed to a variable speed pump, in parallel with a throttling valve and pressure gauge. Vents to atmosphere are blocked. A lead weight is shown imparting load to the pendant valve spring. This set-up simulates centrifuge operating conditions experienced by the discharge valve.

4.2 THE DEVELOPED FLOW-RATE AND CONDUCTIVITY TRANSDUCER

The FRACT in its final form prior to installation on the C•M•D•S rig cell holder is shown from three perspectives in Figure 4.8. Machining of the attachment ears and drilling of the vent and overflow ports committed the device irrevocably to installation, since testing fixture attachments were effaced at that time.

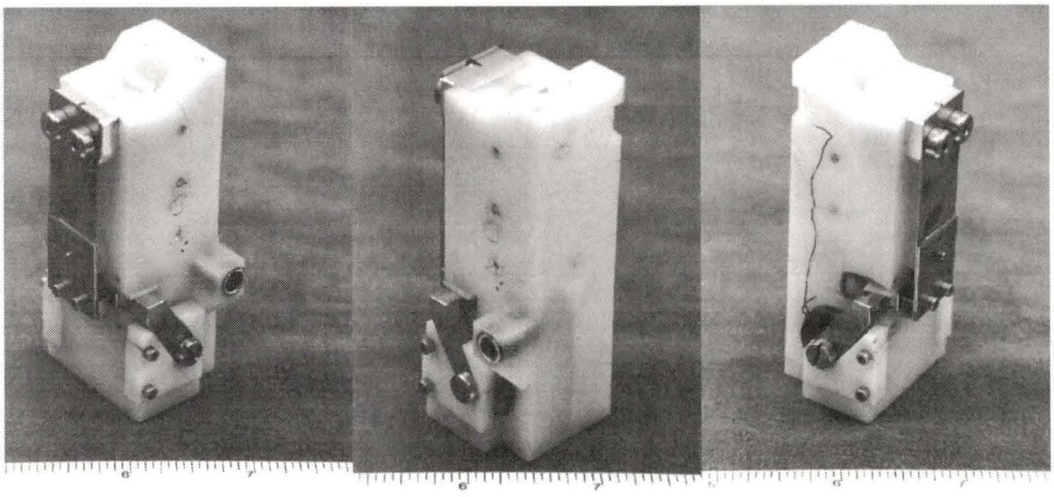

Figure 4.8: Three Views of the Completed FRACT Ready For Installation

4.2.1 Installation: Restraint and Interfacing

In the isometric quarter section view of Figure 4.9, the engagement of both the FRACT upper mounting ear and the bottom boss into their counterparts on the RO cell holder, can be seen. The FRACT is fully restrained against all translations and rotations by this arrangement; its entire centrifugally induced weight, which reaches 3000 Newtons (660 pounds) during normal operation, is borne by the protruding titanium tab on which it rests. Also, the permeate inlet path is shown in this view. Figure 4.10 depicts this hardware during a trial fitting

The fluid passages within the RO cell can be examined in the sequence that a parcel of newly produced permeate traverses. As in most spiral-wound and other commercial membrane cartridges, the fluid is collected from the membrane area by a fine mesh spacer. Thereafter it is directed through the membrane stack by ports within each stack element, aligned by a pair of screws and separated from the bulk flow by O-rings in face seal configuration. From these passages it enters a shallow annular channel which ducts it into a port within the RO cell holder; this annular channel allows the cell to be indexed through several yaw orientations if desired.

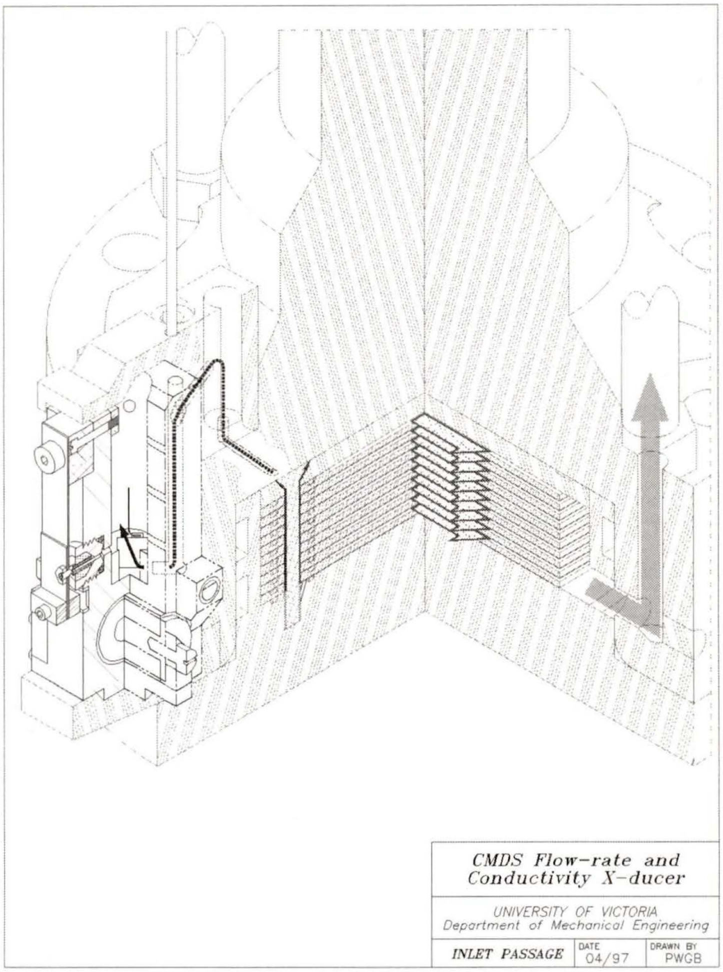

Figure 4.9: Isometric Quarter Section View of FRACT Installation
The FRACT support and restraining provisions can clearly be seen, as can the permeate inlet path. Permeate is channeled from the RO cell into the adapter clamp by an inclined passage. Within the adapter clamp it may optionally be routed into a header capillary (not shown), before entering the FRACT near its rear upper extremity. Thereafter, an integral conduit delivers the permeate to the temperature sensor and conductivity cell en route to the sampling chamber. The electrical conduit can be seen extending vertically from the adapter clamp. The outflow of retentate fluid from the RO cell is also shown (grey arrow).

From the RO cell holder port the permeate enters the adapter clamp, whose design was dictated by the FRACT, flows into a header capillary (if desired) to establish controlled process back pressure, and thereafter enters the FRACT at low pressure via through a small O-ring face seal at the interface plane.

All permeate produced ultimately is released into the rotor enclosure through the discharge orifice, either in a sudden burst when the valve opens following a measurement cycle, or more steadily at other times. An overflow port is provided but seldom required.

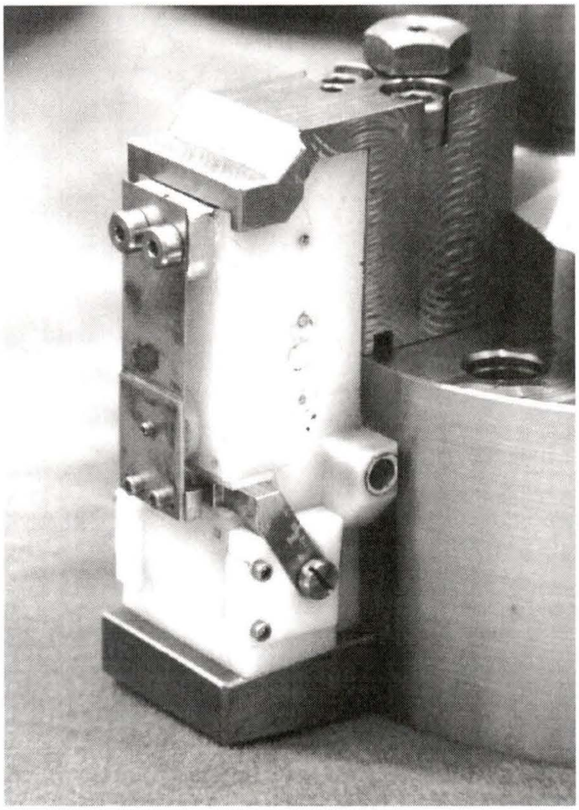

Figure 4.10: Trial Fitting of FRACT on Cell Holder
Level sensor electrodes, temperature sensor and allied electrical wiring not in place.

4.2.2 Electrical Signal Conveyance to Stationary Frame

From the various terminals of the FRACT, insulated 30 gauge stranded wire passes into the adapter clamp on each side, then is led to the rotor axis through a slender conduit. This wiring bundle passes within the shaft to its rearward extremity outside the rotor enclosure.

The duty of conveying data signals between the spinning rotor and the laboratory frame is performed by a Litton ten-channel slip ring assembly. This component features three brushes per ring and is rated to 1 Ampere peak per channel and 10000 RPM. It is specifically designed for maintaining low-noise transmission of data-level signals under the taxing conditions such as are found in this application.

The current capacity of the Litton assembly was deemed too low to deliver sustained electromagnetic servo power. Therefore a dedicated pair of power slip rings, each equipped with two brushes, was provided on the shaft stem for this purpose. The entire slip ring assembly is shown in Figure 4.11.

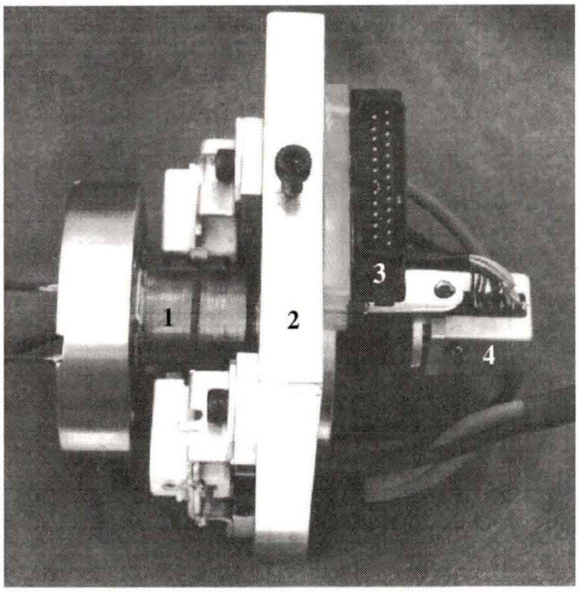

Figure 4.11: Electrical Slip Ring Fixture
1) Power slip rings, 2) mounting frame, 3) data connector, 4) Litton 10-channel assembly.

4.2.3 Alternative Signal Interface Concepts

The shaft has sufficient space within its bore to accommodate a small circuit board which by virtue of its proximity to the rotation axis, avoids being subject to any excessive centrifuge loadings. Such a circuit board might be designed to perform much of the signal generation and processing, its output being encoded data. In this scenario, it would be possible to transmit data from the rotor to a receiver in the stationary frame using infrared emitter-detector pairs located on the axis of rotation. This approach completely eliminates any fear of electrical noise introduction by the Litton slip ring assembly. It, however, accomplishes this at the price of simplicity, and moreover places the electronics in a nearly inaccessible place where they must operate in vacuo. Slip rings, though perhaps not so numerous, would still be required to supply power for both control and for the electronics. In future embodiments if more ambitious data treatment is desired, this avenue remains open as an elegant option.

4.3 DYNAMIC TESTING

4.3.1 Overview

Dynamic testing ensued once the C•M•D•S rig was complete and the FRACT installed and interfaced (Figure 4.12). Software development had progressed to the state of readiness for trials and the allied electronics hardware was in place though still under development.

It must be borne in mind that the initial dynamic testing of the FRACT was closely enmeshed with the first operational testing of the C•M•D•S rig proper. The various operating functions of the C•M•D•S rig had previously been individually validated, including drive tests of the hub and shaft assembly sans rotor, fluid handling pumps, chamber vacuum integrity and control systems. The MONITOR.VI software was prepared and exploited specifically for these tests.

The need for exact rotor balancing, inclusive of the FRACT and allied wiring, prohibited any precursory tests of the C•M•D•S rig complete with rotor, RO cell and membrane inserts to proceed in the absence of the FRACT unit. This was exacerbated by the relative awkwardness of installing the FRACT wiring following rotor installation. Hence, the FRACT was installed onto the rotor unit and its wiring connected prior to the final installation of this complete assembly within the containment housing.

This incurred the situation of simultaneously pursuing the numerous vagaries of the FRACT and allied electronics together with uncertainty over even the successful production of permeate.

Once electronics filtering, grounding and power isolation challenges had been overcome, it was possible to demonstrate by way of the FRACT instrumentation that successful production of permeate was occurring at a rate of flow consistent with expectations from the static rig. This benchmark confirmed, it remained to properly calibrate the sensors and incorporate fully automatic control features into the LabVIEW software.

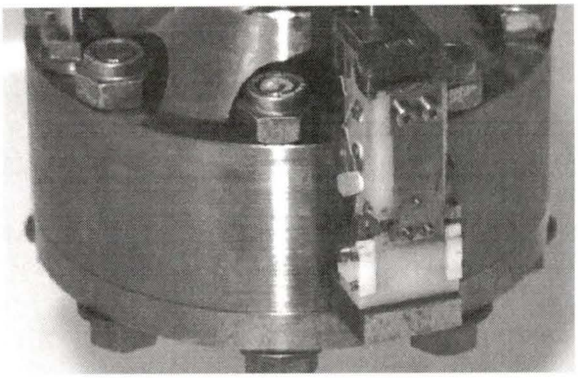

Figure 4.12: Final Installation of FRACT on the Centrifuge Rotor
Electrical connections emanating from two level sensor electrodes and their routing into the adapter clamp can be seen in this view.

4.3.2 Restriction Imposed on C•M•D•S Rig Ancillary Function Duty Cycles

The FRACT demands power for the dedicated electronics hardware suite and, intermittently, for the electromagnetic actuator, supplied from a common rail in the main electrical junction box. In addition, an array of eight relays in the centrifuge control panel support manual override or remote control over many C•M•D•S rig ancillary functions. These functions include feed, vacuum and clean-up pumps, rotor inverter power, air brake and vacuum valve solenoids, and heat exchanger functions.

Although the power for these functions is absolutely independent from the FRACT, the drains on the low-voltage supply rail by the control relays of these devices can affect the sensitive detection and amplification electronics of the FRACT. This quickly became apparent during initial testing: certain C•M•D•S rig ancillary functions (for example the vacuum pump) are not required to operate continuously; when cycled, excursions in voltage output from the conductivity sensor were witnessed.

Solution of this problem might have involved the requisition and installation of an isolated power supply, however since the offending intermittent functions were also capable of continuous duty without damage, it was decided simply to ensure all such functions were kept on both during calibration and subsequently during experiments. Thereby, the supply voltage stability was maintained and unreconcilable deviations in important output data avoided.

The FRACT electromagnetic actuator, however, is required to cycle during normal operation; it too can impart fluctuations to the conductivity output owing to power supply drain. As a consequence of the actively synchronized approach to level sensor state latching, analog voltage data acquisition, which includes conductivity, must be sacrificed during the flow-rate measurement phase. Detrimental effects of the actuator manifested at the conductivity sensor therefore are confined to a brief, approximately two second interval, following the release of the actuator. This was accommodated by a programmed pause in software, occurring between the drain phase and the acquisition of voltage data. Five seconds was determined to be an appropriately conservative duration of this pause, and although the operator can adjust this duration it has not been required to do so.

4.3.3 Synopsis of First Dynamic Test

The first measurements obtained using the FRACT came after a series of painstaking exercises to complete and test the supporting electronics package, and to establish continuity between it and the many channels of the remotely located FRACT.

Since the issue of latching the alternating level-sensor array output had not yet been solved, the prototype version of the control and data acquisition Virtual Instrument (VI) did not encompass automatic control or fill-time and flow-rate processing. Instead, by manually engaging the actuator from the VI front panel and observing the displayed level sensor array state information, it was possible to glean fill-time and hence flow-rate results (Figure 4.13) for a series of trials. These trials occurred at rotor speeds between 590 and 1150 RPM; the lower limit of this range corresponding to the onset of permeate production, the attainment of osmotic pressure in the cell.

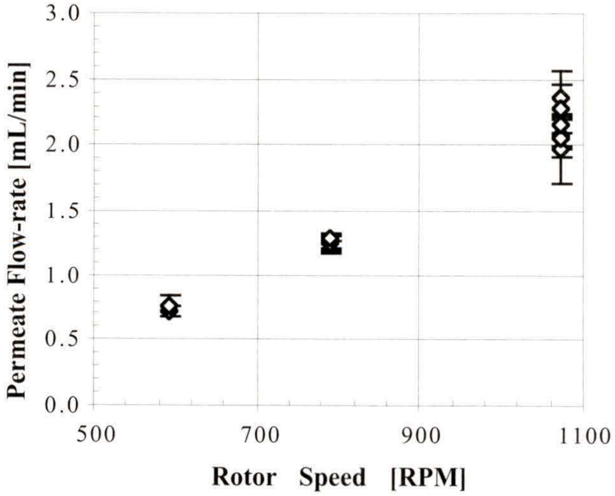

Figure 4.13: First Results from FRACT

During these first tests a number of faults, such as the overloading of the actuator power supply due to inductive back emf generation upon magnetic field collapse, were revealed. Many of these faults were quickly rectified, while others such as the solution of the level sensor latching issue required considerable evaluation. Nonetheless, the mechanical viability and flow-rate measurement capability of the FRACT were aptly demonstrated which, at such an early stage of testing, was a welcome event.

4.3.4 Isolation of an Unforeseen Grounding Problem

During these initial tests a curious and perplexing phenomenon was observed. Following the indication of fluid presence by the uppermost level sensor, the indications of all level sensors became sporadic. Under steady operating conditions, an average flow-rate of 1.4 mL/min was observed. Furthermore, it was noted that the onset of sporadic indications occurred approximately 15 seconds after the final level sensor gave positive detection. From sampling chamber geometry and the average flow-rate, it was perceived that the fluid surface had attained a height 3 mm above the upper level sensor electrode in that time. This was seen to correspond with the position of the valve mounting retaining nut. It was thereby deduced that the fluid sample was completing an electric circuit to ground by contact with the nut, through the valve block to the adapter clamp. This eventuality was not anticipated, in part because original projections for the design of the clamp did not bring it into proximity of these conductive parts. With active control of the flow-rate measurement cycle, this occurrence is unlikely, since immediately upon sample detection by the top level sensor the sampling chamber is voided; moreover further chamber influx is discharged through an overflow. Nonetheless, measures were taken to isolate the valve mounting block from the adapter clamp. A future solution to this problem might involve the manufacture of the valve mounting block from a non-conductive tough plastic such as Lexan.

4.3.5 Level Sensor Array Latching: Candidate Solutions

The necessary use of an alternating excitation voltage for the level sensor array predicates the need to rectify, or latch, the response signals and provide steady binary state information. The original approach, assumed during early VI development, was expected to be performed electronically in hardware. This implementation was reasoned to function in the following manner: an array of registers, one associated with each level sensor channel, would respond to any input voltage excursion above a set threshold, thereafter delivering a true logic level to the digital input port of the DAQ board. Following a complete measurement cycle, a "clear" pulse would reset the registers in preparation for another cycle. The raw level-sensor signal would be buffered and amplified before becoming the register inputs.

A similar implementation was considered with latching handled fully in software. Rudimentary VIs for this purpose were developed and tested.

These approaches are simple and feasible yet flawed. Since the register states are irrevocably latched until forcibly reset, the occurrence of a noise spike could spuriously invoke triggering. Moreover, the sensor array would fail to indicate the falling fluid level within the chamber during the drain phase. A more responsive and less error prone implementation was sought.

Since meaningful level sensor state information is present only during a portion of the alternating excitation voltage phase, it was decided to use this excitation voltage to trigger the acquisition of data from the level sensor array. In this manner, the state information would be representative of fluid continuity between the source electrode and the sensor electrodes. Two strategies for the implementation of this approach were pursued.

4.3.6 Software Approach to Level Sensor Synchronization

The 4 Hz excitation voltage was tapped and returned to an unused analog input line on the DAQ board. A set of custom VIs were devised whose purpose was to calculate the excitation waveform period. This function was encoded into the FRACT control and data acquisition VI to take place each measurement cycle. Once the period, and a time stamp associated with an excitation voltage maximum, were known, thereafter during the flow-rate measurement cycle synchronism would be maintained predictively, with timed gating of the digital level sensor state data.

The excitation voltage period was calculated by acquisition of a high temporal resolution ($1000 s^{-1}$) array of voltage data. This array was then differentiated and smoothed. The negative slope zero-crossings of this result array were then thresholded (to filter any noisy multiple crossings) and the indicial values of the crossings stored. These indicial values correspond with voltage maxima and were then used, in conjunction with the actual sampling period returned by the analog-read VI, to define the location of the voltage maxima in the time domain. An average period for the sample in question was then extracted from this information. The front panel of the excitation period VI is portrayed in Figure 4.14 with a typical excitation waveform displayed; the period calculated in this instance was 262.3±0.5 ms.

Unfortunately, this approach proved inadequate. The accurate and robust timer-counters of the DAQ hardware were unavailable, having been allocated for motor control purposes, so the more fallible Windows tick-counter was employed for prediction. Greater detail on the vagaries of this feature appears later; for the sensitive task of gating the digital data acquisition this implementation was not satisfactory: synchronism was unreliable.

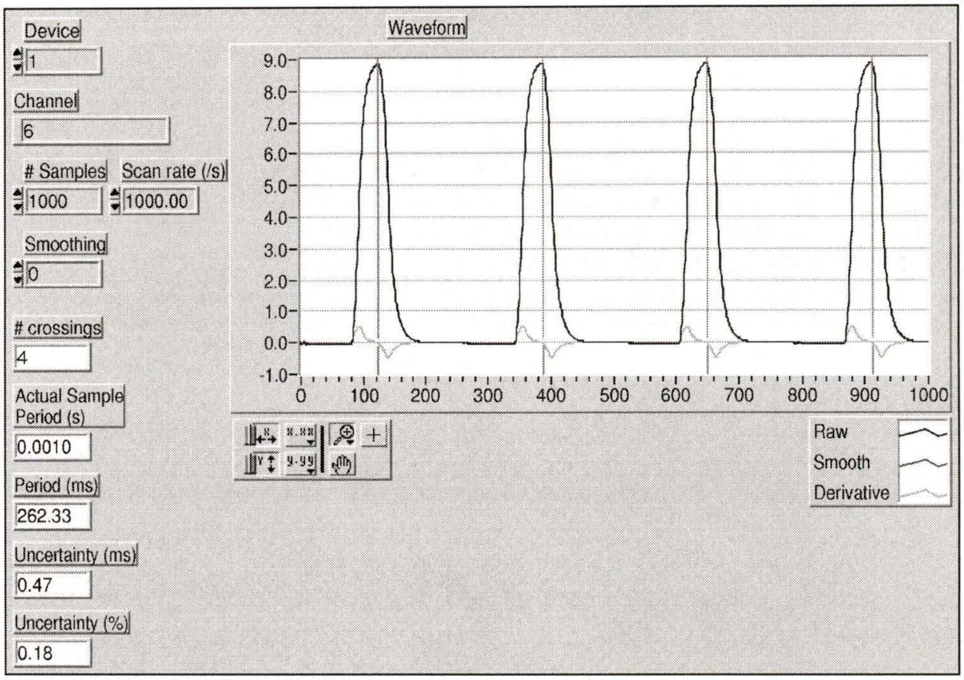

Device
1
Channel
6
Samples
1000
Scan rate (/s)
1000.00
Smoothing
0
crossings
4
Actual Sample Period (s)
0.0010
Period (ms)
262.33
Uncertainty (ms)
0.47
Uncertainty (%)
0.18

Figure 4.14: Front Panel of Custom Period Extraction Virtual Instrument

4.3.7 Hybrid Hardware/Software Approach to Level Sensor Synchronization

The adopted method of establishing reliable level sensor state information was deceptively sophisticated, involving a suite of supporting signal processing features to be incorporated into the electronics hardware, and resourceful use of some advanced level VI programming. The results were, however, eminently satisfactory, and resolved the quandary of level sensor state latching for flow-rate deduction and cycle control.

The commissioned electronics package, its development, and construction, diverged from the prototype with the inclusion of these features, and therefore cannot be considered part of the work of this thesis. The novel LabVIEW programming and concurrent testing however, which are the domain of this work, link the subjects and are the thrust of this section.

The hardware implementation works by summing the excitation waveform with a variable negative cutoff voltage and amplifying the positive resultant. The resultant waveform is delivered to an analog input of the data acquisition board. This signal is a smooth but sharply rising pulse, and is used to trigger the act of reading the digital level sensor data.

A custom sub-VI oversees the reconfiguration each cycle of the analog input port for its role in triggering the acquisition of digital level sensor array state data. This act renders the analog port unusable for voltage data acquisition while the triggering function is in scope. Hence, all other data acquisition activity ceases during the flow-rate measurement cycle. This is however not a great encumbrance, since the act of reading any sizable array of analog data from the DAQ board buffer would upset the crucial timing of digital data acquisition anyhow.

A unique data type is supported by LabVIEW: the occurrence. The purpose of this data type is to allow unrelated actions to be associated. The "DAQ Generate Occurrence" VI applies specified triggering conditions, and sources an occurrence which is routed to a structure containing a "wait-on-occurrence" node. The function of this node is to suspend further execution until the analog input channel to which the pulse waveform described above is sourced, operating in indefinite scan mode, witnesses the fulfillment of triggering conditions. Thereafter, execution resumes at that node, and the digital port associated with the level sensor array is read. By this method, digital data acquisition is kept in strict synchronism with the excitation voltage.

The data flow involved in this process is depicted in Figure 4.15. An important but latent feature of the hardware implementation is the buffering of raw level sensor signals so that stable TTL levels are read by the digital port. This approach overcomes all the obstacles associated with the various candidate solutions described earlier, and its conception and development paved the way for eventual bona fide C•M•D•S experiments using the FRACT.

4.4 CONCLUSION

4.4.1 A Proposed Means for Post-Installation Static Testing

Unfortunately, it was not possible to implement the means to conveniently separate the FRACT from the rotor once installed. A scheme had been envisioned whereby this ability would be retained, allowing the FRACT to be transferred intact to a testing fixture similar to that used during the preliminary static tests. This fixture would have added sophistication, however, to fulfill the requirement of sealing the open sampling chamber, inlet and vent ports, a function necessitated by the physical modifications to the device subsequent to the testing programme. Through the use of this fixture it was envisioned that performance and reliability questions could be effectively diagnosed and rectified, using the procedure of static pressure application and suspended weight loading to simulate operational conditions. This scheme had proved successful during static testing.

The decision to hard wire the FRACT to the rotor made its removal an impossibility: too great was the risk of damage to the wiring loom, potentially requiring replacement of this assembly through to the hub, a procedure both difficult and costly in time. Henceforward therefore, any diagnosis of sealing problems, for example, would be achieved deductively, for direct examination of the pressurized device was no longer possible.

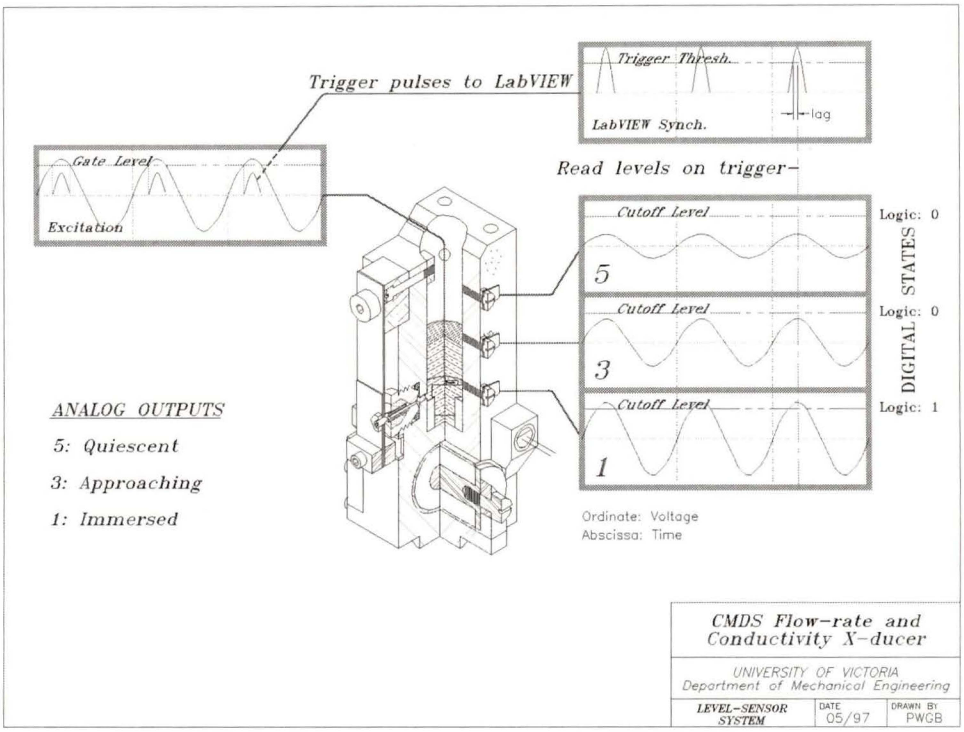

Figure 4.15: Pictorial Representation of Actively Synchronized Digital Data Acquisition

The waveform labeled "Excitation" is both delivered to the source electrodes and gated by the DC voltage "Gate Level"; the amplified resultant is then directed to LabVIEW (top right). Triggering conditions, specified by "Cutoff Level" are applied to this pulse, and digital state information from the level sensor electrodes (1,3,5) is acquired in synchronism as shown. Three important cases are depicted: 1) this electrode is immersed and indicates a positive detection (Logic: 1); 3) the fluid surface is approaching this electrode, and detection conditions have not yet been met (Logic: 0); 5) the signal at this electrode is the quiescent signal (Logic: 0). The amplitude of the level sensor signals is correlated with sample conductivity therefore "Cutoff Level" is automatically tuned to discriminate between quiescence and positive detection.

A recommendation for future embodiments is to resurrect the idea of having available a test fixture, and to endow the FRACT with removability through the use of an electrical junction near the cell. This connector would have to be impervious to moisture invasion and resistant to structural harm, these challenges being the reason the idea was rejected originally. The benefit of experience has fostered the belief that a solution would be possible, and effective. Costly downtime and uncertainty which has been a continuing annoyance to the research agenda might thereby be lessened.

5 Commissioning and Calibration

5.1 INTRODUCTION

The resolution of the issue of synchronizing digital data acquisition with the alternating level-sensing array output by software heralded a critical phase of FRACT development. With flow-rate, conductivity and temperature measurement now fully enabled, progress could be made on commissioning, characterization and calibration.

5.1.1 Initial Rotor Speed Limitation on Flow-rate Measurement and its Rectification

The mechanical operation and effectiveness of the discharge valve, thoroughly tested in the laboratory to a simulated 3000 G was displayed to be satisfactory for centrifuge operation up to a rotor speed of 800 RPM. This corresponds to a G_r of approximately 440 experienced by the FRACT. Beyond this speed valve sealing was inadequate to permit capture of permeate. A phenomenon not simulated in the laboratory was therefore reasoned to be responsible. The bimodal magnet control logic delivers a draw current which is sustained for a brief interval, followed without interruption by a lesser sustaining current. This permits peak field intensity to establish closure of the air-gap, while avoiding needless heat generation during idle. A first attempt to solve this difficulty involved experimenting with the current and dwell time settings; adjustment of these parameters was not sufficient.

The pendant valve assembly in use at this time was a minimal mass configuration and employed an armature but no counterweight. Early analysis of this design indicated that deflection of the valve spring might be caused by a moment imparted by the unbalanced armature. This deflection would conspire to misalign the needle and seat by a slight amount. Despite this knowledge, it was decided initially to try the minimal mass configuration, particularly in light of the advantage it propagates in lessening the stress levels proximate to the valve retaining screws. The simulated application of this unbalanced load to the installed valve assembly was impossible in the laboratory setting and its effect could not be tested.

An experiment using the centrifuge gave a further clue to the reason for the limited performance envelope. It was learned that by closing the valve at an arbitrary speed not exceeding 800 RPM, then accelerating the rotor to speeds up to 1700 RPM (the maximum rotor speed attained to that date), sealing was sustainable through the measurement cycle but could not be repeated. Apparently, the properly seated needle established at the lower speed permitted the armature to be drawn into contact with the poles and full sealing force to be achieved. Once released, the unbalanced moment of the armature caused a small deflection which likely prevented subsequent full translation of the armature and hence prevented full sealing force to be developed. The mis-alignment of the needle, interfering with the seal periphery, might have been the sole cause of this effect, or the mere lack of parallelism between the armature and pole faces might have been responsible.

The solution of this problem was to add a counterweight to the valve spring opposite the armature. Dimensionally and materially this component is identical to the armature (being adapted from a spare), but has clearance holes for the #1-72 fasteners used. A review of stress calculations confirmed that load simulations corresponding to 3300 G for the minimal mass configuration assured safety to over 2000 G for the balanced configuration. This benchmark (1700 RPM) was achieved without difficulty indicating a successful diagnosis and rectification of this problem.

5.2 DYNAMIC FLOW-RATE CALIBRATION

Preliminary flow-rate estimation using the FRACT was possible having determined the sampling chamber partition volumes geometrically (and statically confirming this in a rudimentary test). The normal operation of the FRACT cannot be faithfully duplicated in static testing, therefore rigorous calibration and validation in the dynamic setting was required to establish confidence in the flow-rate data validity before experiments could proceed.

Flow-rate calibration under any circumstances is a challenging enterprise. Sophisticated flowmeter calibrators are commercially available [5.1] at considerable expense; these devices can provide accuracies within 0.1% of a United States National Institute of

Standards and Technology. flow standard. The use of any such device in conjunction with flow-rate measurements on board the spinning rotor is, however, impossible.

5.2.1 Calibrated Leak Approach

The approach championed for this goal involved the development of a cell insert which implemented the means to establish a steady leak of feed fluid into the permeate conduit at a representative flow rate within the expected range of the FRACT. The careful manufacture and testing of such inserts using the static rig would establish a flow-rate specification; presumeably a set of such inserts spanning the desired calibrated range would be produced. By conducting tests using these inserts on the dynamic rig, flow-rate calibration could take place.

Independent work addressed the matter of developing these inserts according to the following method. Modules were made using thin shim stock in place of membrane. These were statically tested for unwanted leaks, then a minute perforation was inflicted on the shim stock with a sharp tool. Again, each module was statically tested to establish its flow-rate.

Although seemingly foolproof, this implementation was infeasible for flow-rate calibration. It proved extremely difficult to achieve acceptably low flow rates. Those modules which were successfully made to deliver acceptable flow rates exhibited a vulnerability to flow-rate attenuation due to fouling of the orifice, possibly caused by permeate spacer mesh extrusion, and hence were not considered reliable. The useful subset of these modules were eventually exploited in conductivity calibration procedures.

A second attempt at this problem was inspired by the suggestion that the workings of a high-quality precision metering valve could be adapted to be installed in the process cell. The embodiment spawned by this suggestion was a dedicated cell insert “puck” which included a shimstock disc, retainer and seal, along with a needle and screw advancer, and permeate porting. This embodiment allowed the easy replacement of pierced discs with fresh ones to more rapidly converge on an appropriate leak rate. The screw advancer allowed accurate control over location and penetration depth of the orifice for consistency.

Although better than the earlier embodiment, difficulties still ensued whereby flow-rate stability was insufficient for calibration purposes.

5.2.2 Calibrated Membrane Approach

Flow-rate validation was eventually possible once concentration polarization and the relationship between static and dynamic experiments on identical membrane stacks was understood. The concentration polarization experimental agenda calls for a series of tests at different feed concentrations. Each of these tests encompasses a range of process pressures, resulting in a corresponding range of permeate flow-rates. Each series is performed on both the static and dynamic apparatusses; the RO process cell is transferred undisturbed between them to ensure peerless consistency. The concentration polarization phenomenon is understood to occur in correspondence with the feed concentration. Dynamic effects are reasoned to influence this phenomenon, however at very low feed concentrations polarization is expected to occur in neither dynamic nor static tests. Experiment confirms this point, therefore the flow-rate measurements for low feed concentration can be correlated for the static and dynamic cases using reliable membrane modules.

This fact permits the dynamic flow-rate measurement using the FRACT, at a range of rates (corresponding to a range of process pressures imparted by various rotor speeds), to be compared with the manual direct volume method results of the static rig. This approach served to demonstrate the FRACT flow-rate output was valid, as can be seen by the close agreement between permeate flow-rate versus pressure curves shown in Figure 5.1. Four thoroughly tested membrane modules comprised the stack for these experiments; they occupied the four middle positions in the array of ten. During this set of calibration tests, feed temperature was strictly controlled within the bounds 25°C$\leq T \leq$25.3°C, eliminating any unwanted temperature effects. A 500 ppm NaCl solution was used, and both relevant dynamic membrane module orientations were tested to validate that concentration polarization was not occurring. The $+R$ orientation refers to the instance of membrane active face normal parallel to the centrifuge radial direction (outward); $-R$ refers to the opposite orientation (inward).

The error bars shown in Figure 5.1 were obtained as follows. Uncertainty in process pressure for the static apparatus was estimated at ±10 psi, owing to pressure transients induced by the reciprocating high-pressure pump, only partially damped by an accumulator in the system, and apparent at the analog pressure gauge as needle fluctuations. For the dynamic apparatus this uncertainty was regarded to arise wholly due to the radial span of the active portion of the membrane module and its basic radial positional uncertainty, $r_{calc}= (0.61\pm0.01)$ m; dynamic process pressure is a calculated value (Equation 1.1) and uncertainty in the r^2 term was thought to dwarf the density and angular velocity contributions. Uncertainty in permeate flow-rate was interpreted as the standard deviation of the mean in both situations. The absolute uncertainty in a typical static measurement was estimated as ±0.2 mL against the volume captured in a 25 mL graduated cylinder in 120 s. Least squares fits were performed on both data sets and are shown; the equations thereby obtained are:

Dynamic slope: (0.0161±0.0003) mL/min/psi................ 5.1(a)

Static slope: (0.0158±0.0003) mL/min/psi.................. 5.1(b)

Since the slope estimates fall within one another's bounds of uncertainty, the FRACT results may be regarded as calibrated to absolute to within less than 2%.

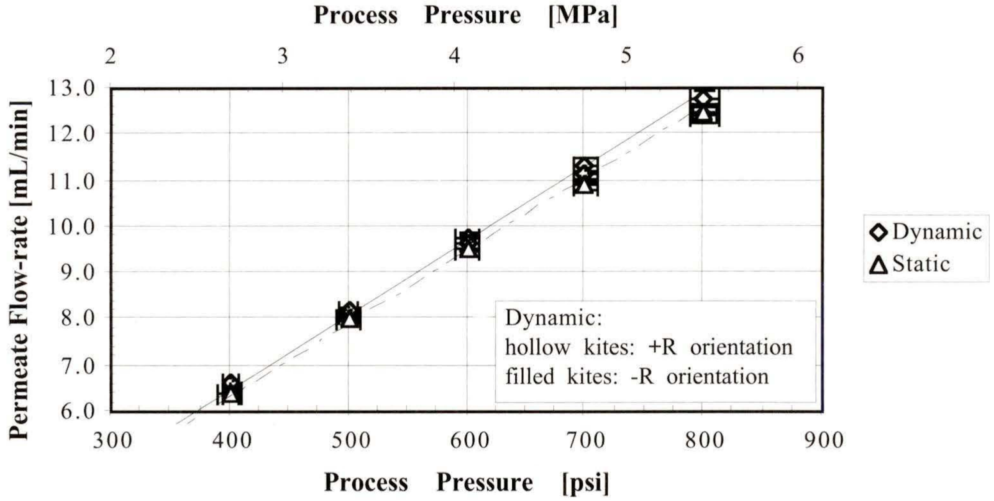

Figure 5.1: Correlative Static and Dynamic Flow-rate Measurements

500ppm NaCl feed (no concentration polarization) 2L/min, 4 active-module membrane stack.

5.3 CHARACTERIZATION OF FLOW-RATE RANGE AND RESOLUTION

Each measurement cycle includes one fill phase, during which five triggers permit four flow-rate data to be gleaned. Flow-rate values in mL/min are obtained by evaluating the quotient of the relevant sampling chamber partition swept volume with the elapsed time to fill that partition. These data have uncertainty originating with both the divisor and dividend, and the magnitude and nature of these uncertainties must be grasped to fully characterize the FRACT.

5.3.1 Uncertainty Attributable to Partition Volume (Dividend)

The partition volume is known from the chamber section area, calculated from its radius (manufactured to close tolerance), and from the partition height. The latter quantity can possess significant uncertainty owing to the diameter of the level-sensing electrodes, which is a sizeable fraction of the partition height. This is witnessed in Table 5.1. The electrode size was minimized insofar as possible while maintaining the desired fulfillment of liquid pressure sealing capability and manufacture concerns. Also, the consistency of the thresholding trigger circuitry with conductivity compensation lessens the operational uncertainty in fluid surface height further.

The relationship among uncertainties associated with the four flow-rate values resulted in the decision to generate a weighted cycle mean flow-rate value, by weighting each individual cumulative flow rate by the square of its ratio to the incremental partition volume. In this manner, all individual flow-rate data are utilized, but the cycle mean (and its standard deviation) are perturbed to a lesser extent by the inherently noisier constituent values, and any associated skewness is thereby resolved.

Partition	**Electrode Centre ht. [mm]**	**Height Uncertainty [mm]**	**Partition Volume [cu.cm]**	**Volume Uncertainty [%]**
0	0.0	0.85	-	-
1	6.3	1.7	0.7	26.8%
2	12.7	1.7	1.3	13.4%
3	19.1	1.7	2.0	8.9%
4	25.4	1.7	2.6	6.7%

Table 5.1: Partition Height and Uncertainty

This results in a cycle mean flow-rate uncertainty of ±8.9% deriving from the positional uncertainty of the rising fluid level as detected by the electrodes of finite dimensions. The lower boundary of all cumulative partition volumes is common, defined by the start timer trigger provided by the bottom level-sensing electrode which has identical dimensions to the others. The calculation accounts for this by including two contributions of equal magnitude to the height uncertainty.

The uncertainty arrived at by this calculation is a very pessimistic estimate and is regarded as the worst case outcome for the situation of a properly functioning FRACT. Steady state dynamic experiments have displayed much higher cycle to cycle consistency of flow-rate values, lending strong support to the notion that the level sensing circuit signal conditioning results in triggering conditions being met at a consistent fractional immersion of each level sensing electrode. This achievement arose from much careful testing and adjustment of the electronics package during actual centrifuge operation. Individual level channel gains were selected to deliver this consistency, which is maintained throughout the conductivity range of the device by a threshold compensation applied to all channels alike.

5.3.2 Uncertainty Arising from Elapsed Fill Time (Divisor)

This uncertainty can be resolved into two components: a portion associated with timing resolution of the LabVIEW program, and a portion imparted by the alternating excitation voltage frequency of approximately 4 Hz. The tick resolution and software loop execution timing comprise the former portion.

5.3.3 Tick Resolution

The tick resolution is 55 ms and can be reduced only at peril of causing nefarious operating system difficulties. It arises due to the necessity of using the Windows 3.1 timer via supporting LabVIEW functions, since the more accurate and robust data acquisition board timing operations had been allocated for eventual motor control purposes. Under other operating systems, the tick resolution is improved: for example, resolutions of 10 ms, 3 ms and 1 ms can be had with Windows NT, Macintosh (Quicktime installed) and Unix systems respectively [5.2]. Appraisal of the software loop execution timing is untenable, save to state that the loop concerned is optimized; the sub-program call overhead amounts to “tens of microseconds” and the I/O and display overhead “milliseconds to tens of milliseconds” [5.2]. LabVIEW’s data-flow programming syntax also makes possible the artificial dependency of the less time critical sub-programs; in this way, execution order can be prioritized.

A brief investigation of the effect of tick resolution is in order. Tick resolution rounds timing values to the nearest tick and therefore a timing interval, which is bracketed by an initial and a final tick, has up to 110 ms uncertainty. Considering a permeate flow-rate near the FRACT upper operating range, for example 20 mL/min, the fluid surface speed during the fill phase may be calculated:

$$v_{surface} = d/dt\,(h_{surface}) \quad = \quad 0.344 \text{ cm/s} \ldots\ldots\ldots\ldots\ldots 5.2(a)$$

Hence,

$$\Delta h_{surface} = v_{surface} \cdot \Delta t \quad = \quad 0.034 \text{ cm} \ldots\ldots\ldots\ldots\ldots 5.2(b)$$

Expressing this result as a volume uncertainty:

$$\Delta V = \Delta h_{surface} \cdot A_{sect} = 0.033\ cm^3 \ldots\ldots\ldots\ldots\ldots\ldots\ldots\ldots 5.2(c)$$

This absolute uncertainty applies uniformly to the four volume partitions, resulting in relative uncertainties of 5%, 2.5%, 1.25% and 0.65% and a weighted cycle average relative uncertainty of 1.2%. These estimates imply a worst case scenario of both initial and final ticks being inaccurate by the full tick resolution amount for all four individual flow-rates.

The aggressive level sensing signal processing circuit does not exact any remedial effect on this uncertainty as it does for the previous discussion regarding electrode dimensions.

5.3.4 Alternating 4 Hertz Excitation Signal: Discretization Effect

It will be seen that this effect dominates any timing uncertainties and is therefore regarded as the principal limiting factor in establishing the FRACT flow-rate resolution.

Fluid level sensing by electrical means requires an injection of electrical energy. In like manner to the more sophisticated conductivity cell, an alternating excitation signal is required to avoid electrode polarization. In addition, it is desireable to have this excitation signal at a sufficiently different frequency from the conductivity circuit to ensure decoupling of these channels by electronic filtering.

Preliminary experiments using the level-sensing and conductivity prototype circuit revealed that the impedance of the sampling chamber and level sensing electrode configuration promoted a rather low excitation frequency of approximately 4 Hz. The factor of 500 disparity between this and the 2 kHz conductivity oscillator also allows straightforward filtering to decouple these channels, as desired.

Software latching of fluid levels states was accomplished, however the synchronization of channel polling with the excitation waveform exemplifies how this affects flow-rate resolution. State information is communicated at no greater than the 4 Hz rate. Hence, flow-rates are resolved only within 250 ms time intervals. This results in the FRACT flow-rate resolution being not only discretized, but also variably so with respect to flow-rate: greater resolution is achieved at lower flow-rates when a greater number of detection phases occur during the filling of a given volume partition. Fortunately, it is straightforward to characterize this effect.

The resolution capability of each partition is a linear function of flow-rate. It can be estimated for any given flow-rate by calculation of the relevant partition fill time for that rate and observing the relationship of this value to the discretization interval. Clearly, the smaller partitions exhibit reduced resolution for a given flow-rate since fewer detection phases occur. In like fashion to the electrode position resolution however, the cycle mean flow-rate resolution deriving from this effect can be obtained for the weighted mean. Figure 5.2 indicates this relationship, with resolution expressed in relative terms: resolution is 5% or better for flow-rates of up to 20 mL/min, and approximately 2.5% at a nominal 10 mL/min. Better resolution is achievable if only the full sampling chamber individual rate is chosen; this does not detract from the utility of the three less well resolved rates as indicators of instrumental performance, but mitigates their potential deleterious effect on data precision.

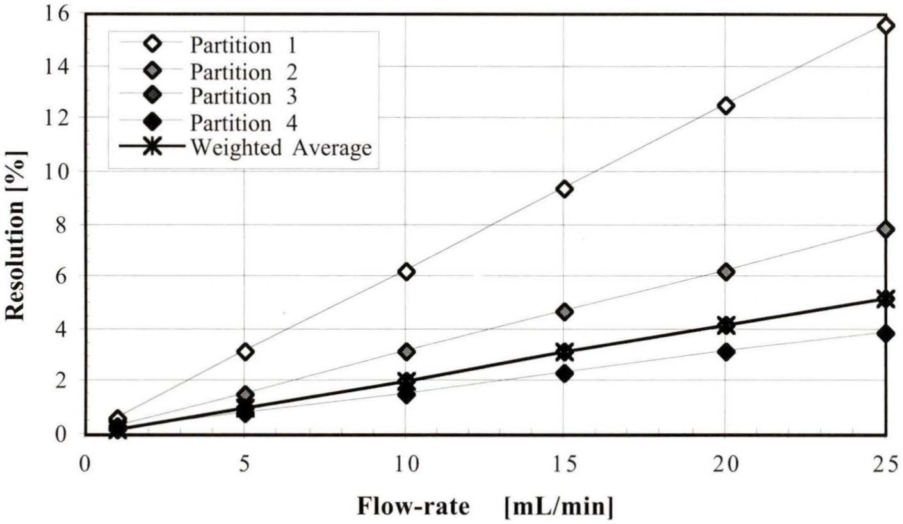

Figure 5.2: Predicted Flow-rate Resolution vs Flow-rate

This study assumes no relationship between fill phase initiation and alternating excitation signal phase, since none is invoked by the controlling software. The resolution figures quoted portray again a worst case scenario; over an extended run some cycles will achieve better than expected precision by virtue of fortunate coincidence in phase synchronization between actual fluid surface arrival and excitation signal phase. The reported cycle mean will reveal this through atypically small standard deviation.

5.3.5 Summary of Flow-rate Uncertainty Contributors

The uncertainty in flow-rate data has been reasoned to arise from three contributors: partition volume uncertainty, timing uncertainty and 4 Hz state discretization. Of these, 4 Hz discretization has the greatest damaging influence on data precision. Partition volume uncertainty, though serious in the worst-case scenario, has been witnessed to be demonstrably better in actual operation through the remedial influence of the electronics signal conditioning.

5.4 PROBABILISTIC INVESTIGATION OF TYPICAL EXPERIMENTAL FLOW-RATE DATA

Data from a typical early experiment were scrutinized with the goal of uncovering any unexpected biases and of validating the understanding of flow-rate resolution. Using an approximately constant feed stock concentration, a series of rotor speeds between 877 and 1755 RPM provided eleven intervals of data associated with their corresponding process pressures (ranging from 1.4 to 5.5 MPa). These intervals each were sustained for approximately thirty minutes (1800 seconds), delimited by speed changes. Permeate flow-rates fell between 3 and 14 mL/min, causing each interval to contain a different number of data points, corresponding to the number of cycles (governed by flow-rate) occurring in each interval. This is shown in Figure 5.3.

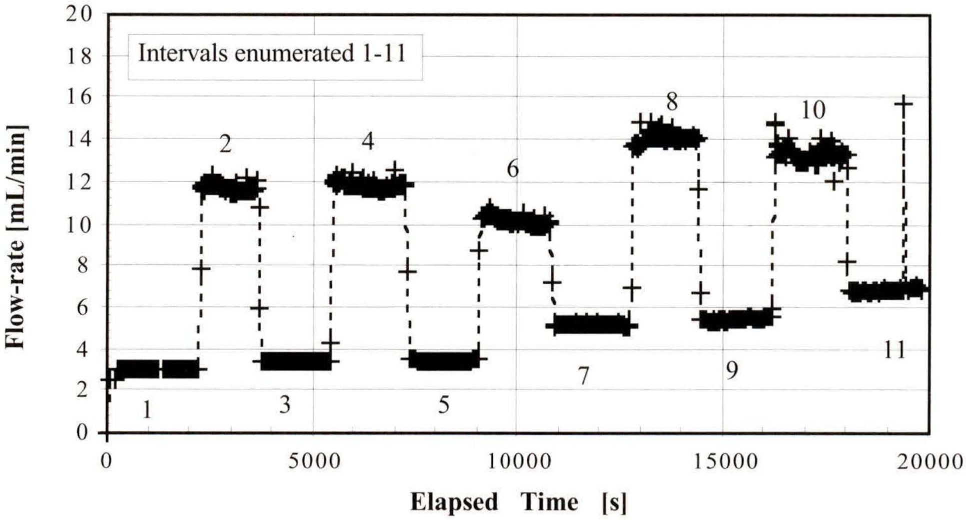

Figure 5.3: Raw Data: Cycle Mean Flow-rate vs Elapsed Time

Within each interval, actual permeate flow-rate was reasoned to be constant. In fact, reconciling this with later knowledge that flow-rate is subtly related to process temperature, controlled by a heat exchanger with a coarse duty cycle, this might not be absolutely true. At 877 RPM, the lowest rotor speed in this experiment, twenty-six data points were recorded, therefore to avoid biasing of results by the weighting of more points in intervals conducted at higher speeds, twenty-six middle points from each interval were used in subsequent analysis. These groups of points form eleven bins of data, two bracketing examples of which are isolated in Figure 5.4.

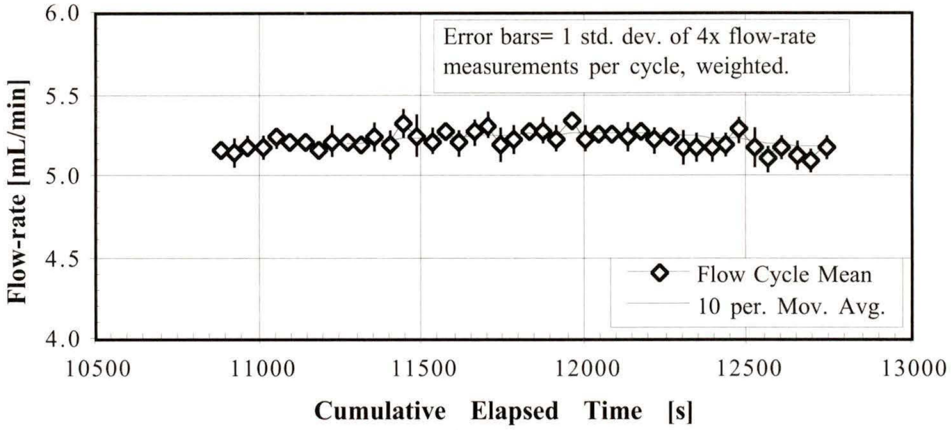

Figure 5.4(a): Cycle Mean Flow-rate vs Elapsed Time: Bin 7

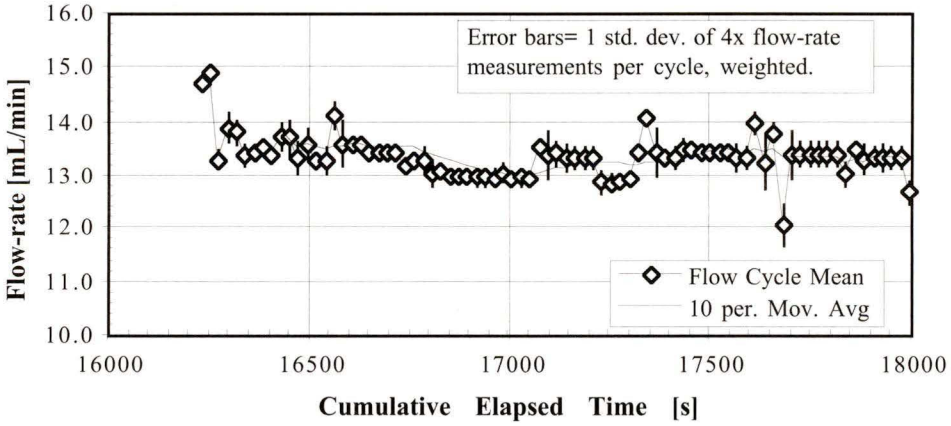

Figure 5.4(b): Cycle Mean Flow-rate vs Elapsed Time: Bin 10

For each bin, a mean flow-rate and standard deviation were computed. The standard deviation was graphed against the bin mean and this scatter compared with the predicted resolution, as seen in Figure 5.5. For all but one bin, the standard deviation was observed to be lower than predicted. Indeed, the trend observed suggests that for high flow-rates the predicted resolution is increasingly pessimistic.

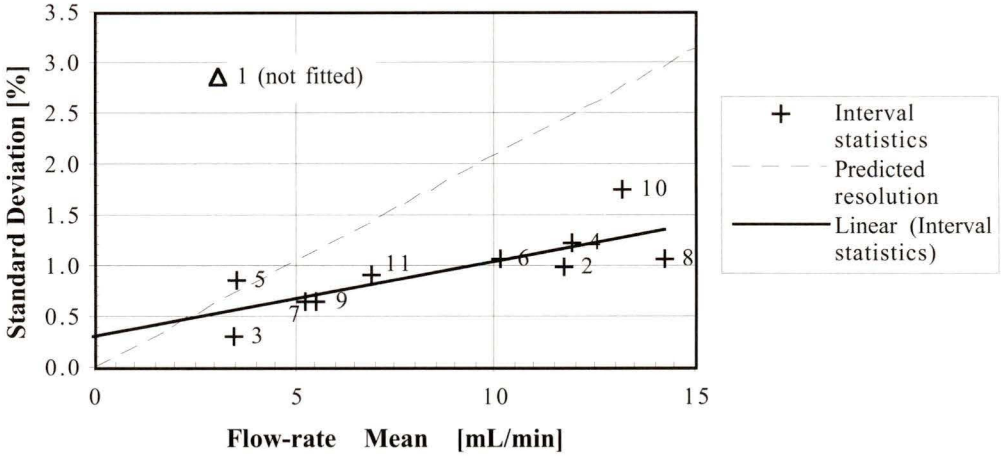

Figure 5.5: Standard Deviation vs 26-point Bin Mean Flow-rates

Histograms with a 0.25s grid were prepared displaying the four constituent individual fill times within an interval, and the data spread was observed to be stochastic. This assertion would be more compelling with a larger data population. Two such histograms for data at each extreme of the flow-rate range investigated are presented in Figure 5.6. Modal values for each partition were extracted from the histograms, and compared with predicted fill-times in Table 5.2. The predicted fill times were calculated from the mean flow-rate value for the interval in question given the individual partition volumes. Uncertainty in these predictions, being individual measurements, is the average uncertainty of the raw data, whereas the uncertainty in the mean flow-rate is the standard deviation of the mean, and accordingly far smaller. Predicted and modal values showed excellent agreement in this comparison.

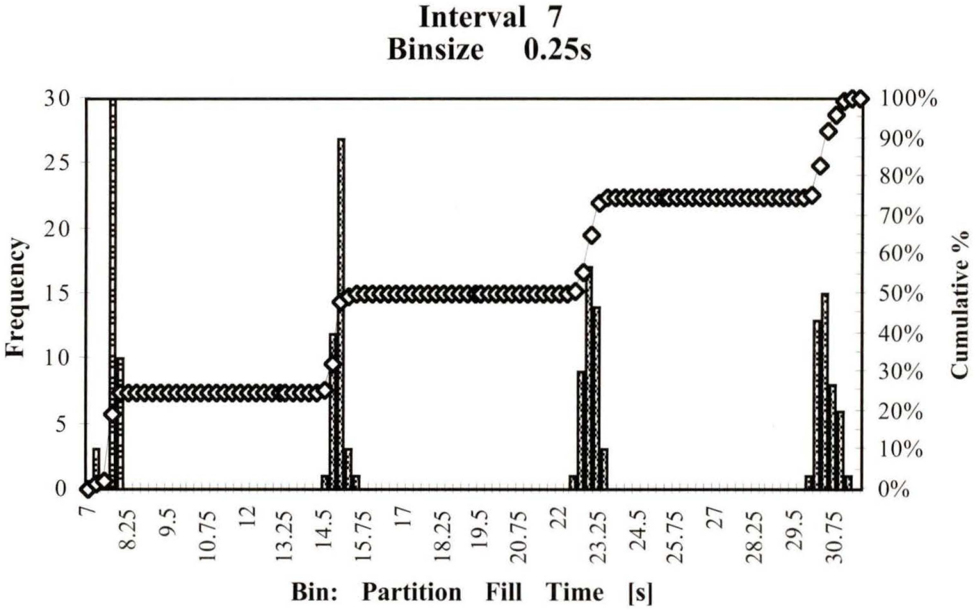

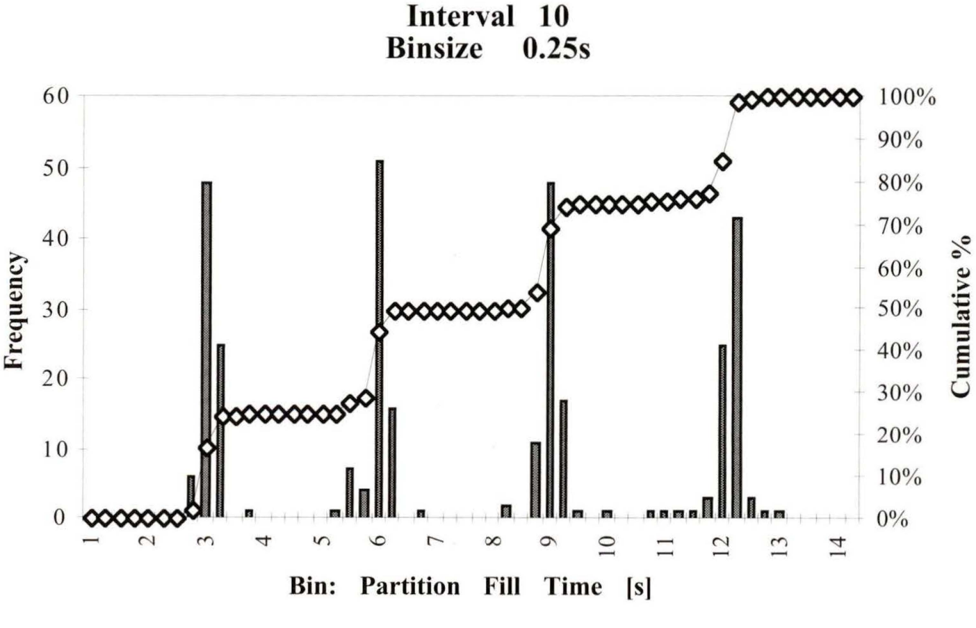

Figure 5.6 (a&b): Partition Fill-time Histograms (0.25s bin-size)

Mean flow-rate	5.22±0.01	[mL/min]
BIN 7	Predicted	Histogram
Partition	Fill-time [s]	Modes [s]
1	7.7±0.07	7.75
2	15.4±0.15	15.00
3	23.1±0.22	23.00
4	30.8±0.30	30.50

Mean flow-rate	13.4±0.04	[mL/min]
BIN 10	Predicted	Histogram
Partition	Fill-time [s]	Modes [s]
1	3.01±0.09	3.00
2	5.02±0.18	6.00
3	9.03±0.27	9.00
4	12.04±0.36	12.25

Table 5.2 (a&b): Predicted Individual Fill-times and Histogram Modes
The uncertainties stated for mean values are the standard deviations of the means; that of the individual values the basic standard deviations.

These investigations reinforce the suggestion that flow-rate resolution is dominated by the 4 Hz discretization effect and that through its expected range of operation the FRACT faithfully delivers unbiased results subject to documented performance limitations.

5.4.1: Ultimate Usage of Flow-rate Data: Time Independence

The eventual synthesis of FRACT generated flow-rate data with comparative data originating with static experiments will often, if not usually, be time-independent. A set of experimental conditions will be prescribed and many data points over time spans of tens of minutes to several hours accumulated. Such data sets will be averaged, or at a minimum smoothed, to provide, usually, a single representative flow-rate value and associated uncertainty for comparison to a similar figure obtained using the static apparatus.

The act of assimilating a population of data in this manner tends to override the uncertainty of individual members of the population, provided such uncertainty is normally distributed. FRACT flow-rate data indeed appears to fulfill this requirement. Hence, the uncertainty eventually reported will be the standard deviation of the mean; a better estimate to the global uncertainty in individual constituent measurements, should the need for such a figure arise, can be reasoned to be the basic standard deviation, calculated for this mean. The standard deviation of the mean, an estimator to the uncertainty in the mean value is, by contrast, this basic standard deviation scaled by the factor $1/\sqrt{N}$, where N is the number of members comprising the mean [5.3].

With this knowledge it can be observed that the accumulation of excessive data has diminishing returns on the accuracy of its mean. This is quite divorced from the vulnerability of assimilating unresolved time dependent drift, which could arise for many reasons. The desired accuracy can be used to determine a suitable population size and hence to optimize the time economics of an experiment. It should be noted however that since the temporal density of data is directly related to permeate flow-rate, the time interval to accumulate this population often cannot be accurately foreseen.

5.5 TEMPERATURE SENSOR CALIBRATION

Temperature calibration was a high priority due to its significant effect on conductivity and the desire to calibrate and characterize that important measureand promptly and properly.

Although the AD-592CN Precision IC Temperature Transducer is inherently calibrated and manufactured to a high standard for interchangeability, the associated custom built electronics package, which affects a current-to-voltage conversion, has gain and offset characteristics that require the completed system to be calibrated. Fortunately, the behaviour of this system is linear, making the use of calibration data straightforward. Unfortunately, the necessity of performing this calibration on the fully assembled and installed system makes the procedure somewhat complicated. The AD-592CN manufacturer's specification for accuracy over temperature is shown in Figure 5.7.

The location of the AD-592 and the conductive socket in which it is embedded subject to heat transfer not only from the permeate, but undesireably from the large thermal mass of the RO cell nearby. This might be an insurmountable problem were it not for the permeate being subject to an exchange of heat with this body also, resulting in its thermal equilibration. On inspection of the circuitous path taken by the permeate through porting of small dimensions within the RO cell and associated metal parts it is apparent, and heat transfer calculations [5.5] confirm, that after steady state has been reached permeate and RO cell temperatures should agree within 0.3°C. The convolution of temperatures registered by the AD-592 in its present manner of installation is therefore not an obstacle; nonetheless future FRACT variants will take strides to better isolate the chip from all but permeate thermal energy transfer.

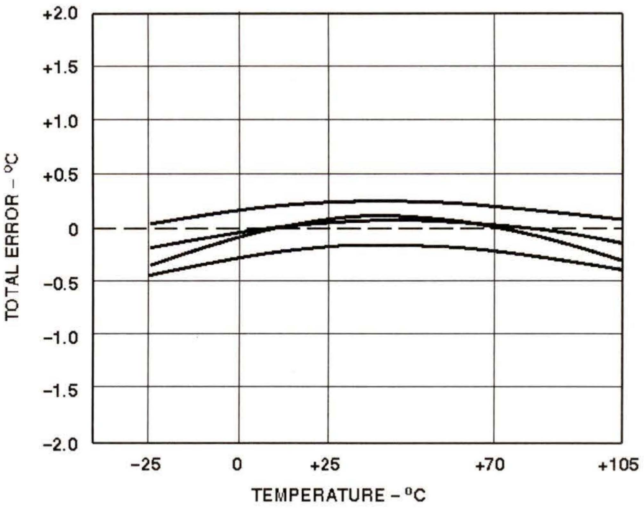

AD592CN Accuracy Over Temperature

Figure 5.7: Temperature IC Accuracy Chart [5.4]

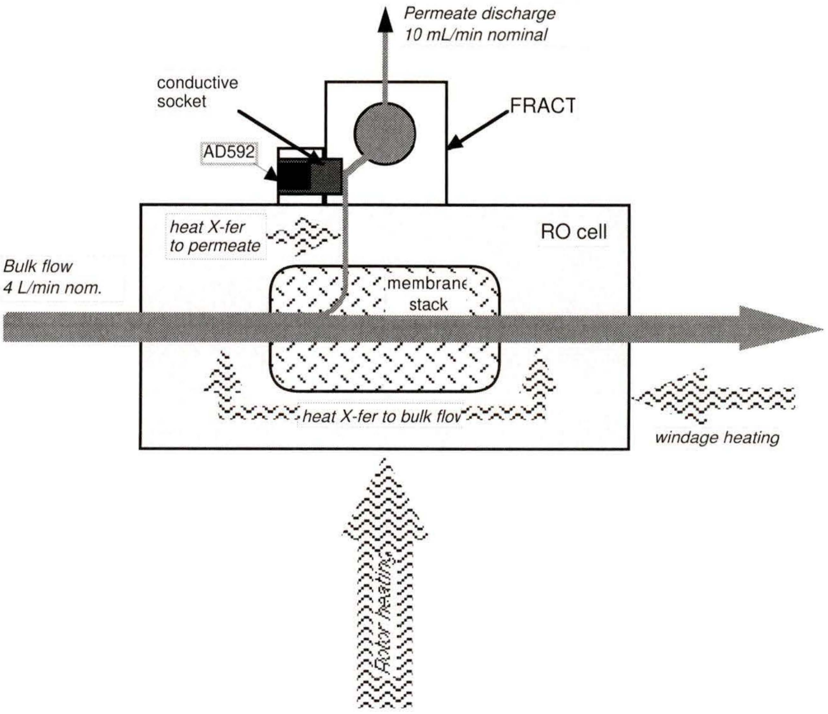

Figure 5.8: General Heat Transfer Paths: RO Process Cell

A water bath incorporating an insulated reservoir, circulation pump and thermostatically controlled heater/agitator was prepared. An inlet adapter fitting which, with the RO cell removed, may be affixed to the RO cell holder, allows fluid to be ducted into the permeate transfer port from an external source. Thereafter, flow proceeds through the usual conduit into the FRACT. Using a small variable speed constant displacement pump plumbed into this adapter fitting, it was possible to establish steady flow at a typical rate into the sampling chamber via the inlet porting which brings flow into contact with the AD-592 socket. A 3 mm Nylon hose barb installed in the disused sampling chamber side-port directed the drain fluid into a small test tube where an accurate thermometer was placed to record fluid temperatures at a location as close as possible to the transducer. The overflow was then collected and dripped back to the reservoir.

To eliminate the temperature convolution mentioned earlier, the entire RO cell holder and FRACT was wrapped in a 10 metre length of 6 mm ID PVC tubing, then boxed and surrounded by styrofoam chips. A contact thermocouple, having been attached to the RO cell holder, gave direct readings of that temperature. A large positive displacement pump was required to circulate fluid through this heat-exchange jacket. It was plumbed into the bath.

Using both ice and the thermostatically controlled heater, it was possible to achieve temperatures ranging from 2°C (well below the desired calibrated range) to 38°C, the upper limit. Bath, thermocouple, outlet temperatures and LabVIEW voltage were recorded at five minute intervals over five hours as the system was underwent a gradual temperature increase (Figure 5.9).

Subsequently, the thermocouple and outlet temperatures were graphed against LabVIEW input voltage (Figure 5.10) providing two well correlated linear relationships. The slopes and intercepts of these relationships were then averaged to yield a single calibration function (Equation 5.3).

$$T(°C) = (-\,2.325\ °C/V)\cdot V_{LabVIEW} + 38.548\ °C \quad\ldots\ldots\ldots\ldots\ldots\ldots 5.3$$

This relationship, encoded via a formula node into LabVIEW, makes possible real time temperature output in degrees Celsius, which is in turn needed to correct conductivity data to the reference temperature of 25°C.

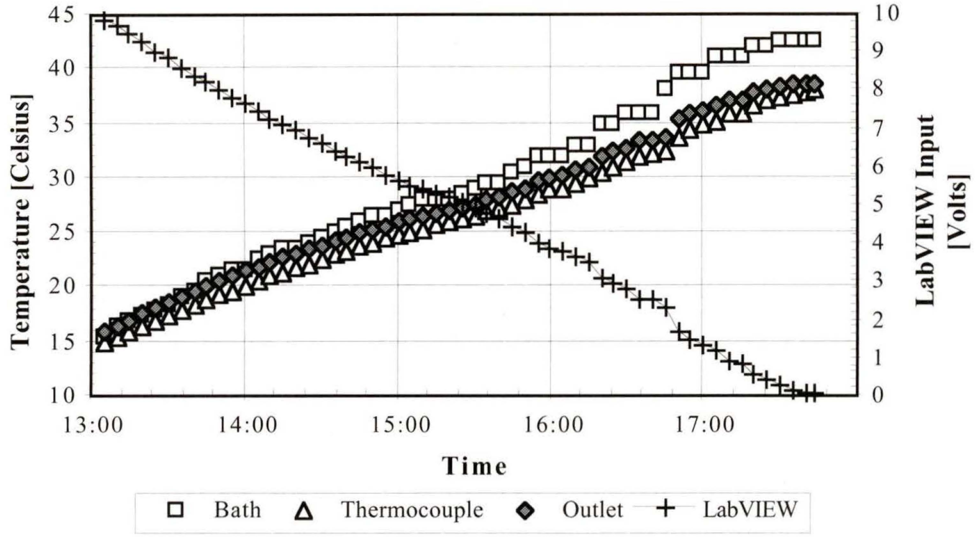

Figure 5.9: Time Series: Temperature Calibration Data

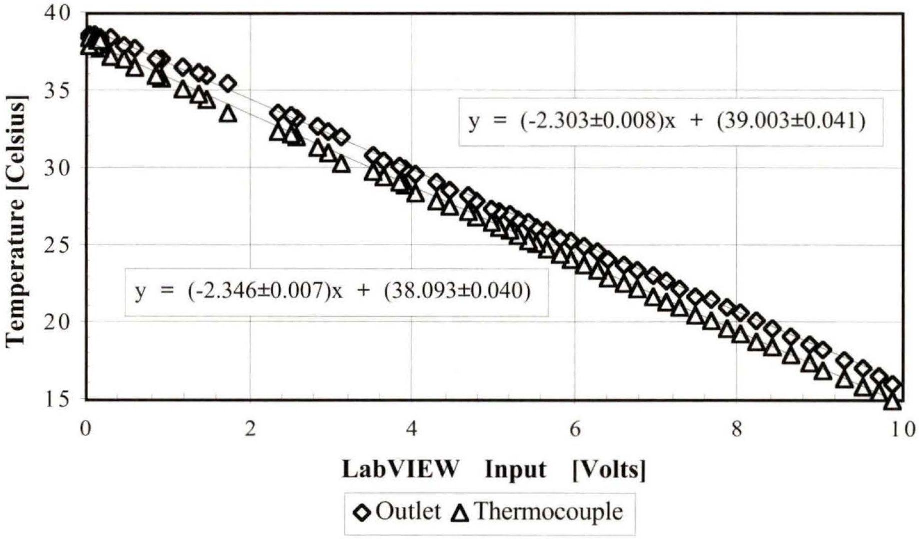

Figure 5.10: Temperature Calibration Relationships

5.6 CONDUCTIVITY SENSOR CALIBRATION

The calibration of the conductivity sensor was performed in two stages. The first, a detailed calibration of the complete instrument as installed while stationary, delivers an instrument function to be used subsequently to relate the output voltage to conductivity units. A second stage of calibration, performed under controlled conditions of centrifuge operation, serves the purpose of truthing the initial calibration and assures that the assumption of similar operation under centrifuge conditions is valid.

Both these calibration procedures involve the use of a benchtop laboratory conductivity meter to furnish correlative measurements and permit the voltage-to-conductivity units mapping to be extracted. Prior to final calibration of the custom conductivity sensor therefore, a procedure to establish the absolute accuracy of the benchtop meter was performed.

It must be emphasized that conductivity is an inferred property, defined by the use of primary standard solutions. It is against such solutions that the benchtop meter is calibrated; hence conductivity measurements availed by the FRACT, being in turn referenced to this secondary standard, are subject to the resulting propagation of uncertainty.

5.6.1 Calibration of Radiometer Type CDM3 Conductivity Meter to Absolute

To ensure the calibration of the custom instrument is absolute, confidence in the accuracy of the Radiometer CDM3 conductivity meter is vital. The CDM3 (Figure 5.11) is a precision instrument which, although old, rivals expensive modern instrumentation for accuracy and precision. Occasional recalibration, however, of this venerable machine is required, according to detailed instructions provided by the manufacturer.

The CDM3 meter is furnished with an immersion type conductivity cell, type CDC304. This delicate glass and platinum cell has a nominal constant of 1.00 cm^{-1}, with a specification of +3.0% inscribed by the manufacturer. A control on the CDM3 faceplate allows the user to apply this offset yielding accurate conductivity indication on the analog display. Accommodation of gradual drift in the measurement system is accomplished by experimental assessment of this drift and adjustment of the cell constant correction control to annul it.

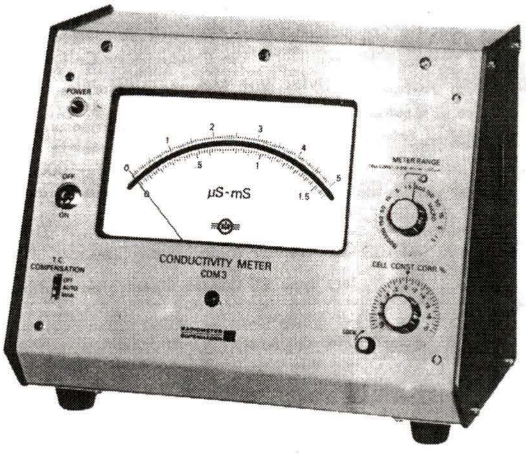

Figure 5.11: The Radiometer CDM3 Benchtop Conductivity Meter

The accepted procedure for calibration of conductivity instruments, originating with Kohlrausch, is the use of standard solutions, usually potassium chloride, with accurately documented conductivity values. Such a standard solution, 0.01000 Normal concentration, was prepared for the purpose of recalibration of the CDM3. A quantity (1.4911 grams) of analytical grade potassium chloride (KCl) was diluted in triply-distilled water to make 2000.0±0.5 mL. The use of triply-distilled water ensures that the solution conductivity arises wholly due to the solvated ions; the procedure stipulates a maximum solvent conductivity of 1 μS/cm. The conductivity of the triply-distilled water used was 1.2 μS/cm.

To ensure temperature constancy, a small vessel was arranged in circuit with a circulation pump and thermostatically controlled bath set to 25°C. Within this vessel, filled with the 0.01000 N KCl solution, the cell was placed and left to soak for 24 hours. This cleanses the cell in preparation for calibration. Following the procedure outlined in the CDM3 instructions, fresh standard solution conductivity was measured (with no cell constant correction effective) on the 1.5 mS/cm range. It was found to be 1.338 mS/cm at 25.3°C.

Via this procedure the cell constant was determined to be the nominal 1.00 cm^{-1} plus a correction of (6.20±0.08)%, i.e.1.062±0.001 cm^{-1}. This value having been then invoked using the cell constant correction control of the CDM3, subsequent correlative conductivity measurements were assured to be of acceptable accuracy and precision.

5.6.2 Remarks on CDM3 Performance Specifications

The CDM3 meter has twelve manually selected ranges, the lowest being 0-1.5 μS/cm and the highest 0-500 mS/cm; when used in conjunction with the provided cell (K_c=1.00 cm^{-1}); each order of magnitude is supported by two ranges having multipliers 1.5 and 5.0. The measuring accuracy is stated as ±0.6% of full-scale-deflection (F.S.D.) +0.002 μS/cm in each range, except the 500 mS/cm range, whose accuracy is ±1.5% F.S.D. Error bars appearing in graphs containing CDM3 derived data represent these accuracies. It should be noted that, for measurements within a given range, the relative uncertainty falls between 0.6-2%, the latter value applicable to measurements near the upper bound of the next lowest range.

A secondary ±0.05%/°C error due to ambient temperature variations is also documented by the manufacturer, however significant temperature excursions were not experienced during any usage of the CDM3 in this work.

The cell constant correction control is graduated in 0.5% divisions and the calibration procedure yields the cell constant to two decimal figures of accuracy. The applied cell constant correction is merely as accurate as the operator's positioning of the control which is reasoned to be approximately ±0.1%.

Although both automatic (via a separate compensating cell) and manual temperature compensation features are supported by the CDM3, in most usages it was found preferable to simply record temperature data during a given procedure and apply the correction during post-processing.

5.6.3 Stationary Calibration of Custom Sensor

The stationary calibration was performed using an adapter which, when the cell holder has been removed, allows fluid to be admitted to the permeate port and thereafter, flowing through the passages within the rotor components, into the flowmeter in like fashion to the flow under operating conditions. This ensures that the conductivity cell is flushed through as samples of different known conductivities are admitted for correlative voltage measurements.

Allied inlet plumbing consisted of a fill tube and funnel; drain plumbing made use of the disused side port on the meter and was configured to avoid siphoning fluid from the sampling chamber. A drip guide allowed for the easy collection of the exhausted samples and avoided contamination of same.

Bulk NaCl solutions of bracketing the desired conductivity range were prepared. Conductivity possesses a strong temperature dependence, approximately 2%/°C for the solutions in question[1]. Therefore the calibration of conductivity requires steady, or at least known, temperatures. Hence these solutions, plus bulk amounts of tap and distilled water, were left to equilibrate to room temperature. Blinds were drawn in the lab to reduce ambient temperature variations, and ambient, as well as sample temperatures were recorded throughout the procedure.

Tests began with the low concentration solution. Approximately 400 mL of solution were decanted and the sample conductivity and temperature measured accurately before gradually being poured into the funnel. Care was taken to avoid aerating the sample and a slow pour was required to ensure drainage occurred through the intended channel; overflow would result in spillage. Once a minimum of 200 mL was flushed through the device a beaker was positioned to capture further 100 mL passed through the device. This exhaust was immediately subjected to conductivity and temperature measurements, while simultaneously LabVIEW data was recorded. Thereby, confidence in the actual conductivity and temperature at the cell was ensured. A second LabVIEW value was recorded five minutes later.

By combining correct proportions of the two bulk solutions samples of intermediate conductivity were obtained. The above procedure was followed for each, culminating with a measurement at 5 mS/cm. The data thereby gathered, once corrected for temperature, forms the calibration mapping from output voltage to conductivity units of mS/cm.

5.6.4 Dynamic Calibration of Custom Sensor

The dynamic calibration requires less set-up effort than the static calibration, but the procedure requires similar attention to detail. A leak insert replacing the membrane stack is required; the desired rate of flow is approximately 10 mL/min to permit effective flushing of the conductivity cell.

A feed solution having conductivity at the high limit of the useful conductivity range was prepared in the bulk feed tank. The CDM3 conductivity cell was placed in this feed stock, and temperature monitored. At a moderate rotor speed, the FRACT conductivity voltage output and "permeate" temperature were monitored. Once cell flushing resulted in stable conductivity channel output, correlative data was recorded. Sample conductivity was then reduced by the addition of tap water to the feed stock. Care was taken to inject water of

---

[1] Established earlier by an independent experiment, described in appendix IV: Temperature Compensation Coefficient

similar temperature; throughout this procedure it was endeavoured to maintain all temperatures close to 25°C to minimize required corrections. The procedure was repeated; distilled water was used to extend the calibrated range below that attainable using tap water.

Post-processing to compensate for temperature effects resulted in the generation of a reliable data set, seen in Figure 5.12, which deviated insignificantly from the previous static calibration. The dynamic calibration procedure, encompassing all potential influences of actual centrifuge operation, is less troublesome to execute than the static procedure, and is recommended for future occasional re-calibration as warranted.

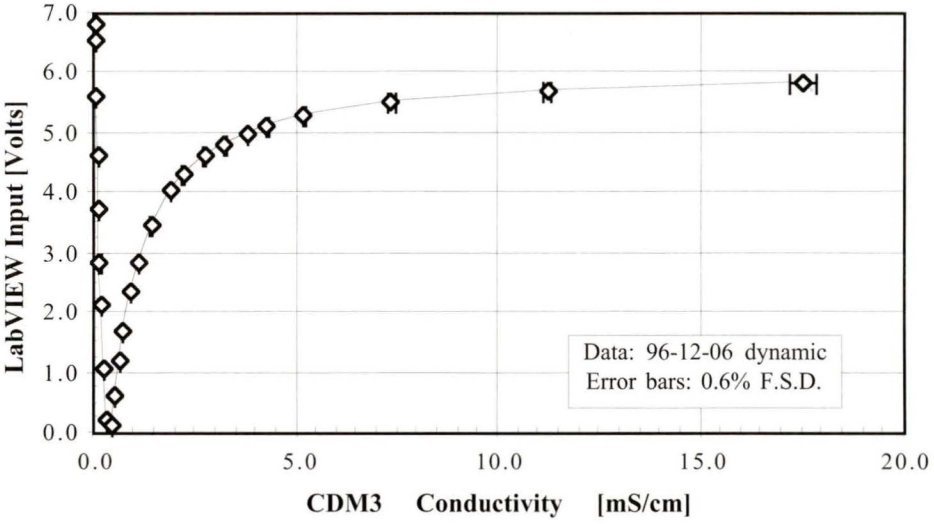

Figure 5.12: Conductivity Calibration: Full Range

5.6.5 Voltage Conversion Algorithms

Calibration data gathered by the previously described procedures permits automatic voltage to conductivity unit conversion in LabVIEW. The two branches of the mapping function are handled separately and differently: the low-branch was found to be amenable to a polynomial fit whereas analytic curve fitting was more difficult for the high branch, leading to the use of a simple piecewise linear interpolation method.

The cubic polynomial coefficients for low range conversion were obtained using a popular general purpose graphing program, and subsequently entered as user input into the appropriate LabVIEW sub-program. Thereafter, given a voltage value the calibrated conductivity is evaluated and returned.

Polynomial fitting was investigated for high-range conversion but, through the full range desired an adequate fit, with monotonic derivative, was not attainable. A simple piecewise linear interpolation routine was implemented; this approach has the benefit that calibration data is entered directly into the relevant sub-program without pretreatment of any kind.

The chordal error associated with this method was found to be smaller than residuals magnitude and related difficulties with the various analytic, including non-linear regression, fits attempted. Constant, linear, exponential and quadratic terms comprise the most promising non-linear regression results obtained, depicted in Figure 5.13. This graph also shows the residuals calculated against the calibration data, expressed fractionally with respect to conductivity. The residuals magnitude clearly indicates this function is inadequate for conversion purposes: it well exceeds the estimated uncertainty of the calibration data.

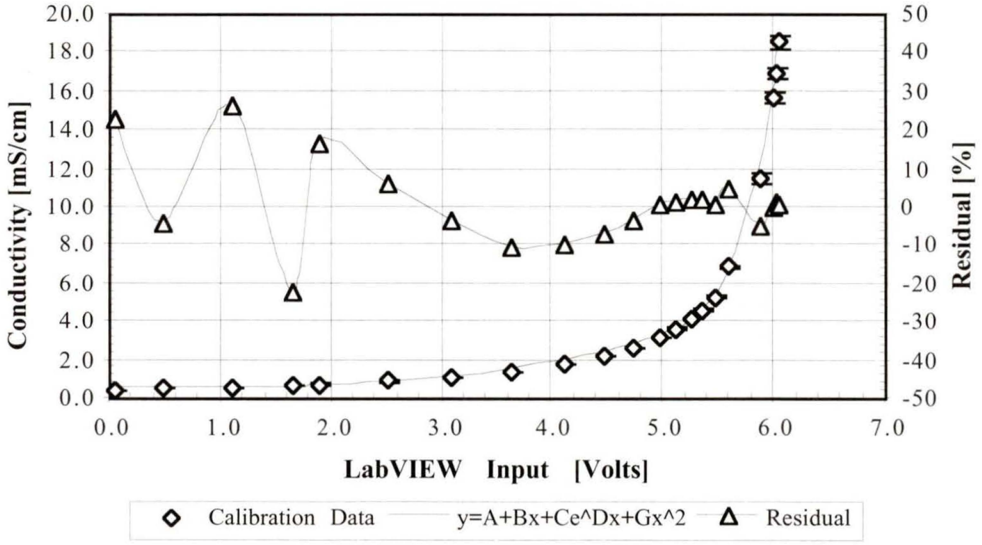

Figure 5.13: High-range Calibration: Non-linear Regression Results

Cubic spline interpolation offers perhaps the optimum voltage conversion means for the high range calibration. It operates much like the piecewise linear approach, differing in that the piecewise functions are third-order (cubic) rather than first-order (linear) polynomials.

The algorithm that determines the polynomial coefficients is empowered to ensure that continuity in slope occurs; the resulting function is constrained, as is the linear, to pass through all calibration data, but avoids the clearly non-physical slope discontinuities of the simpler approach. Moreover, for a globally concave, monotonically increasing function such as the calibration curve, the cubic spline is expected to resemble very closely the true continuous function.

For investigative purposes, a cubic spline curve fit was performed using Matlab on a set of calibration data. Then, the resulting piecewise polynomial was evaluated and compared with the linear interpolation at one-hundred intervals within their common domain. The results of this comparison are shown in Figure 5.14, expressed fractionally with respect to conductivity. This approach, it is claimed, offers the best available insight into the approximate chordal error of the piecewise linear interpolation method. Implicit to this statement is the assertion that the cubic spline method is the preferable approach for unit conversion.

This residual function has zeroes at all node (data) points however the equipartitioning of the domain does not ensure these points appear in the figure. Residual maxima correspond to the chordal error occurring between node points. It can be seen that through the serviceable sensor range, this error is usually approximately 1% or less. A marked improvement would be apparent with denser calibration data, however 1% is reconcileable with other sources of uncertainty in the system.

This investigation leads to the championing of cubic spline interpolation for future implementation as the means to accomplish improved high range voltage to conductivity units conversion. This could be accomplished in one of three ways. The piecewise polynomial coefficients could be calculated, as was done in this study, by existing third-party software, to be encoded subsequently into a custom LabVIEW sub-program which would be very similar to the piecewise linear interpolation sub-program devised in this work. Alternately, the cubic spline algorithm could be programmed into LabVIEW, requiring only that the calibration data be supplied; the piecewise polynomial would then be generated and subsequently evaluated during routine operation. An adjunct to this option would be the use of the cubic spline module of the Advanced Analysis VI library, available commercially [5.6]. A third option would be to synthesize a denser data set using the cubic spline interpolation, but to apply piecewise linear interpolation using this data for real-time conversion in LabVIEW.

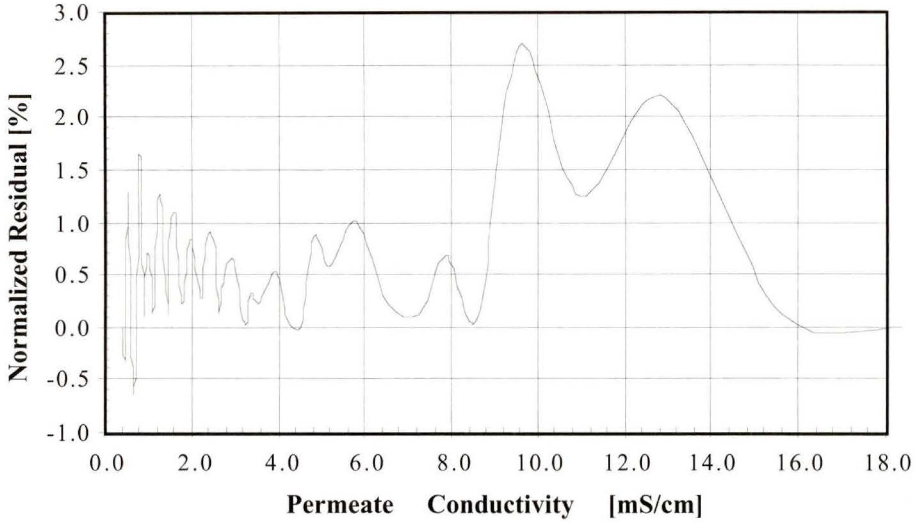

Figure 5.14: Approximate Chordal Error of Piecewise Linear Interpolation
This plot was achieved by subtraction of interpolated values from two approaches: piecewise linear and cubic spline. The cubic spline, owing to the data's uniform concavity, was reasoned to be an accurate interpolant for comparison. The opportunity exists to codify the piecewise polynomial function for improved accuracy, or to extract from it a denser mesh of points for continued use of the linear method.

5.6.6 Implementation of Temperature Compensation Function

Given the measured conductivity L_M at arbitrary temperature T, the temperature difference ΔT is calculated as:

$$\Delta T = 25 - T \quad [°\text{Celsius}] \ldots\ldots\ldots\ldots\ldots\ldots\ldots\ldots\ldots \quad 5.4(a)$$

and the specific conductivity, referenced to 25° Celsius in adherence to convention, is given by the formula:

$$L_{25} = L_M / [1 - \Delta T \cdot \Gamma_T] \ldots\ldots\ldots\ldots\ldots\ldots\ldots\ldots\ldots \quad 5.4(b)$$

where Γ_T is the temperature compensation slope, having units %/°Celsius. The application of this compensation function is a user selectable option in the FRACT control VI. Figure 5.15 illustrates how, in LabVIEW's graphical syntax, Equation 5.4(b) appears. More detail on the niceties of graphical programming will be uncovered in chapter 6: Control and Data Acquisition Software.

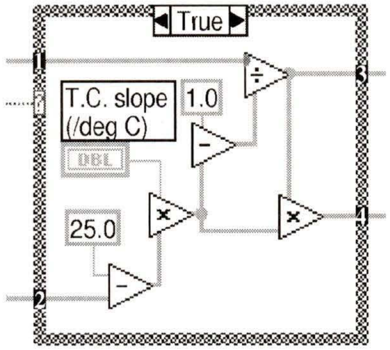

Figure 5.15: LabVIEW 'G' Representation of Equation 5.3(b).
Data flow is generally left-to-right. Wires extending beyond the picture are: 1) uncompensated conductivity, 2) permeate temperature, 3) compensated conductivity, 4) compensation, and 5) to the ? terminal of the conditional frame, the Boolean state enabling temperature compensation. Within the frame the input for Γ_T, labeled 'T.C. slope' can also be seen.

5.6.7 Sensitivity Characterization: Conductivity Resolution

To provide insight into the conductivity sensor resolution, sensitivity functions were produced for both low and high branch ranges. Analog to digital quantization is the ultimate limitation to instrument resolution, but noise present in the raw signal must also be investigated as a contributor to the operational resolution.

The analog to digital conversion supported by the AT-MIO-16DE10 multi-function board is 12-bit resulting in a 1 in 4096 quantization, which when applied to the 0-10 V gain range option in use, yields a 2.44 millivolt precision [5.7]. Examination of data spanning the whole calibrated range of the conductivity sensor allowed the extraction of a nominal full-width (one standard deviation) 25 mV noise level. Use of this figure in resolution estimation, however, is unduly pessimistic. Usually, uncertainty in such averaged values is stated as the standard deviation of the mean. To resolve adjacent measurements of this sort, it is often asserted that a minimum spacing need exist of three times the standard deviation of the mean. Given N =1000, this resolution limit is found to be 2.4 mV. Coincidentally, this is also the quantization limit.

For the low range branch, the polynomial transfer function was differentiated yielding a response slope through this conductivity range. Taking the nominal voltage resolution limit to be ΔV= 2.5 mV, a conductivity resolution function for this range was produced, and is shown along with other relevant curves in Figure 5.16. It indicates a resolution of better than 0.1% across most of the range, decreasing to approach 0.8% close to the null-band.

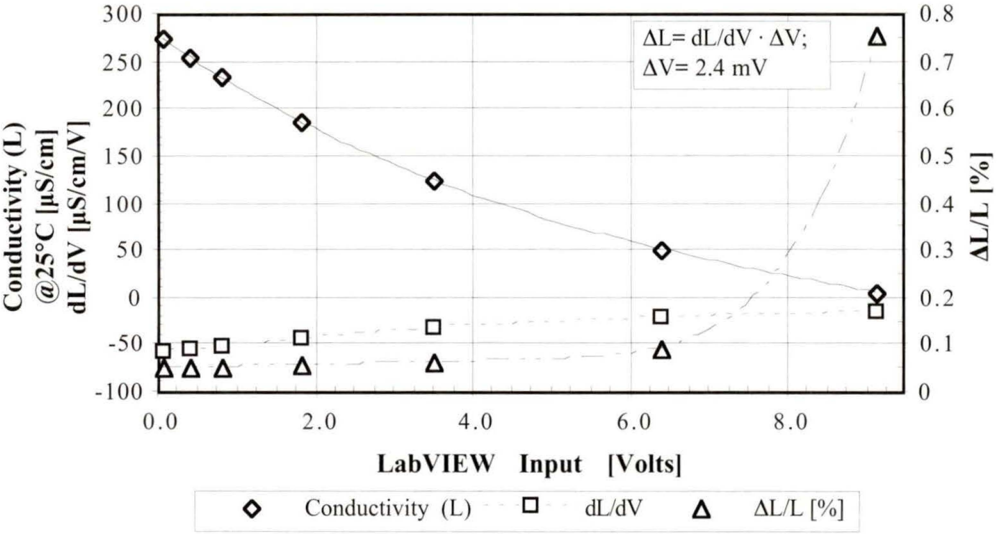

Figure 5.16 (a): Low-Range Calibration, Sensitivity, and Fractional Resolution Calibration Data: 97–04–11.

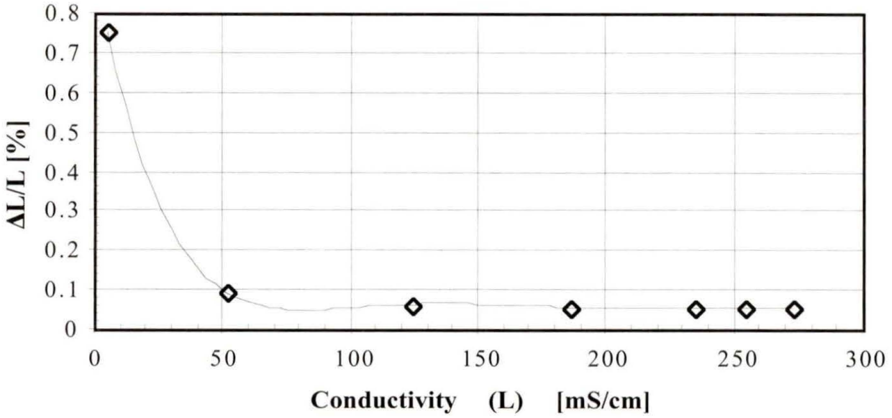

Figure 5.16 (b): Low-Range Fractional Resolution vs Conductivity

The response function for the high range was generated by a central difference discrete differentiation approach. This is shown in Figure 5.17. Again, ΔV= 2.5 mV, resolution was expressed as a percent fraction of conductivity, and achieves values of 0.3% or less through the original target range up to 5 mS/cm, and 1% or less throughout the extended range to 15 mS/cm.

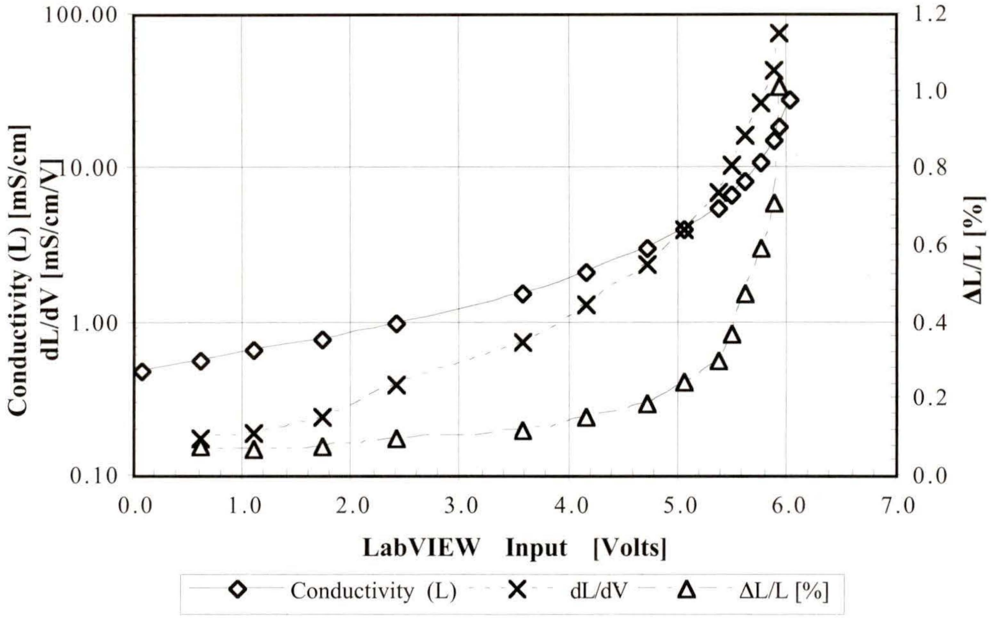

Figure 5.17: High-range Conductivity Sensitivity and Fractional Resolution Calibration Data: 97–04–11.

This information has considerable utility in the planning of meaningful experiments, to ensure that output variables may be resolved sufficiently to substantiate objectives.

5.6.8 Summary of Conductivity Uncertainty Contributors

The foregoing investigation of uncertainty contributors to conductivity measurement leads to the following conclusions. Uncertainty in the CDM3 meter, used to reference the FRACT to a primary standard may be stated (for a mid-range case) as ±1.3%. FRACT accuracy cannot be quoted to better than this value.

The linear interpolation voltage conversion algorithm of the high range, through comparison with a cubic spline interpolation, is seen to impart roughly +1.5/-0.5% within the serviceable portion of its range. This uncertainty can be reduced by accumulating a greater number of calibration data points or by using a better mapping function; options for this have been suggested. Combined with the preceding figure, this places FRACT accuracy at +2.8/-1.8% (high range).

Resolution investigations suggest a small uncertainty contribution of just 0.1% in the low range and 0.3% in the high range. This is ultimately manifested in the precision, rather than the accuracy, of FRACT output, since it is a variance upon the predicted value which has already been subject to all the preceding accuracy stipulations.

5.7 LONG-TERM STABILITY OF CONDUCTIVITY SENSOR

To assess the long term stability of the conductivity sensor, data from two calibration procedures are required spaced by a long interval of time. Although a second dynamic calibration took place several weeks after the commencement of the C•M•D•S experimental agenda, adjustments to the electronics hardware were also performed at that time. Hence, the temporal behaviour of the intact sensor could not be deconvolved. This behaviour includes a component due to the electronics hardware and one associated with the conductivity cell. It is reasoned that the conductivity cell, owing to its situation in a harsh environment, is the greater contributor to any long-term drift in the sensor.

An opportunity to judge the long-term stability of the sensor was provided after several months of service, when a renovation of the entire FRACT system occurred. At this time, the conductivity cell was removed, cleaned and re-platinized in like fashion to the original platinization process. The procedure of removing and reinstalling the cell may have introduced additional small perturbations between the two calibration data sets; unfortunately it is impossible to rationalize these. Such perturbations might be associated with the resistance of the various electrical joints involved in reconnecting the cell to the electronics board, and confidence that these connections were excellent both before and after suggests any associated perturbations would be small.

Since it was not possible to obtain a pair of data sets spanning an interval within which the sensor was untouched, the later (post re-platinizing) data here represents the cell in its pristine state, while the earlier data set represents the deteriorated condition. Some tens of hours of experiments were performed between these calibrations. Notably, a similar or greater amount of usage occurred prior to the generation of the earlier dynamic calibration data set. Therefore, the deterioration, if any, of the cell between these data sets corresponds to the total usage of the sensor from initial installation to the earlier dynamic calibration.

The voltage conversion functions for both calibrations are shown in Figures 5.18 (a&b). The ratio between the calibration data sets is also presented. Through the high range of the sensor, agreement within 2% is witnessed up to approximately the 6 mS/cm level, beyond which the agreement progressively worsens. This bound corresponds to the lessening sensitivity of the instrument at high conductivity, a phenomenon previously described.

The low range comparison shows a discrepancy of similar magnitude, but the drift ratio is less well behaved than in the high range case. As before, the stability of the sensor is worse in that range corresponding to its lessening sensitivity as the output voltage grows higher.

Compromised as it is by some generous assumptions, this investigation is offered only as a benchmark for the magnitude of conductivity sensor drift, and is suspected to be a pessimistic one.

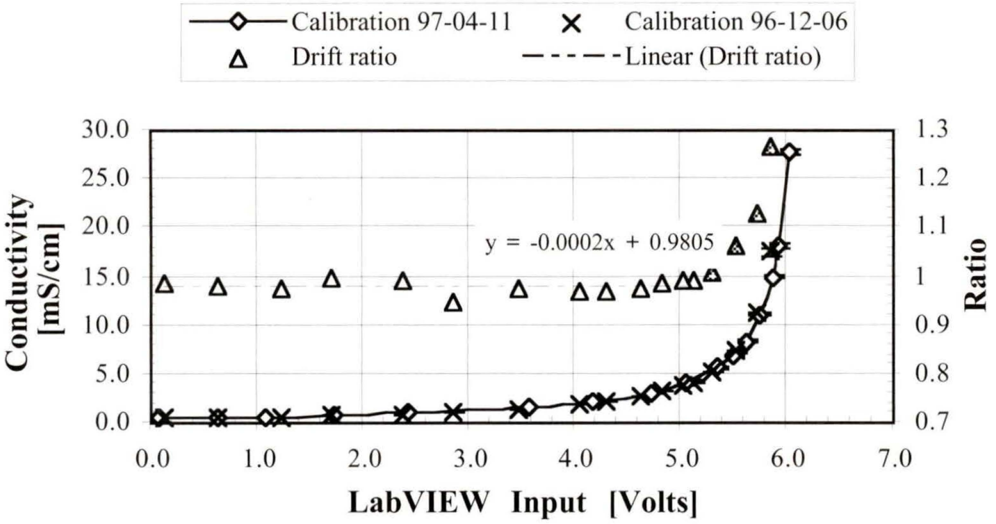

Figure 5.18 (a): High-range Conductivity Calibration Long-term Effects
Note: grey data omitted from linefit.

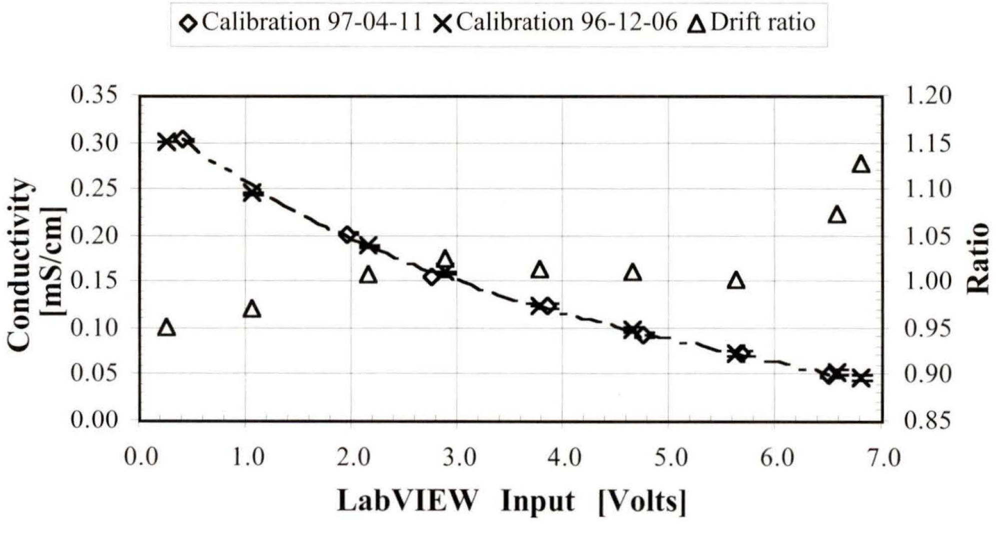

Figure 5.18 (b): Low-range Conductivity Calibration Long-term Effects

6 Control And Data Acquisition Software

6.1 INTRODUCTION

Mention has already been made several times of enabling, novel programming solutions relevant to a number of topics, such as synchronous level sensor state data acquisition. A broader view of the programming activity undertaken as part of the development and commissioning of the FRACT is to be presented in this chapter.

6.2 OVERVIEW OF DATA ACQUISITION AND CONTROL SYSTEMS

6.2.1 Computing Hardware

The FRACT, from its inception, was envisioned to be a passive device, relying on external control and data processing. The need for a computer with I/O capabilities was also mitigated, however, by the wish to eventually have automated experiment capability with data logging of C•M•D•S rig specific physical information. Clearly, the merging of these two principal functions is an effective use of resources.

The 486 PC-compatible running LabVIEW 3.1 under the Windows 3.1 environment was selected, along with a National Instruments AT-MIO-16DE-10 interface board. This board includes digital and analog input and output ports, counter/timers and buffering, making it ideal for present and foreseeable system requirements. The graphically intensive LabVIEW interface further is best served by a good-quality colour monitor.

6.2.2 The Rudiments of LabVIEW

LabVIEW is a graphical programming environment specifically aimed at the experimental and process control user. Its principal virtue is the clarity and visual impact of the programs created with it, both to the end user and to the programmer. LabVIEW programs are referred to as "virtual instruments", or VIs, for good reason: they resemble and behave in close analogy with actual physical instruments. Being a National Instruments product, LabVIEW works harmoniously with the DAQ hardware.

The programmer devises a VI from a functional perspective. User inputs are considered and their implementation represented by virtual controls placed on one of two forks of the programming hierarchy: the "Front Panel". This is the display framework on which the end user will make selections and invoke actions via mouse and keyboard, and on which results will be presented. The latter role is fulfilled by placement of virtual indicators. Both the indicators and controls are selected from a palette of many possible types and variations. Most resemble actual physical controls and indicators, such as toggle switches, rotary knobs, gauges, LEDs and charts. Their positioning, size, colour and other attributes are chosen by the programmer, allowing for the creation of a visually striking and ergonomic Front Panel.

Functionality is endowed the Front Panel by a source-code equivalent known as the "Block Diagram". As its name suggests, this second fork of the programming environment contains the logic and data flow paths required to interpret inputs, execute actions, and generate outputs; it is the editor for the graphical programming language "G" unique to LabVIEW. It is a symbolic language, made to resemble a schematic, or wiring diagram. Iconic representations of the Front Panel objects appear on the diagram; the programmer links these "terminals" with those of many other icons representing a panoply of available functions [6.1], even other custom VIs, on the diagram using "wires". Familiar structures governing execution, such as for and while loops, and case structures are available. These are complemented by the concept of "dataflow programming" wherein execution order is determined by the flow of data as it becomes available. Superimposed on this, if required, is the sequence structure, a way to programmatically assert execution sequence. This assemblage allows one to achieve any desired programming objective. Conventional programming variables are not used explicitly, rather the flow of data between sources and sinks (inputs and outputs) fulfills a similar role. The colour and pattern of wires represents the data type in question. This paradigm promotes the development of hierarchical, modular VIs, which in turn accelerates and enhances the development of robust and powerful applications.

Documentation is also accomplished in a powerful and useful manner. Entities both on the Front Panel and Block Diagram possess description attributes which appear in a help bubble when the cursor is placed on them. Likewise, each sub-VI, be it from the extensive library or custom written, is endowed with this feature; its input and output terminals, respective data types and icon are also made known this way.

The strength of this environment is its intuitiveness both to the programmer and the end user. Furthermore, a meaningful, professional appearance to the Front Panel can be achieved, allowing custom applications using the full power of today's graphical user interface to be rapidly devised by the programmer, and quickly grasped by the end user.

6.3 ROLE OF SOFTWARE IN DATA ACQUISITION AND CONTROL

Although the chief control output delivered to the FRACT is a single DC voltage governing the magnet state, the control logic governing this draws upon real-time data acquisition and as such is a significant part of the programming exercise. The act of timing the capture of fluid is a fundamental functional requirement of the device, and this too is handled by the LabVIEW software. Other functions include the processing of analog input data, and manipulations of data to perform scaling, filtering and calibration operations. User inputs are monitored, which control various functions and allow choice among options. Both raw and processed results are displayed, and data sets are written to a disk archive for later interpretation.

6.4 FUNCTIONAL OVERVIEW OF FRACT.VI

6.4.1 Introduction to the Virtual Instrument FRACT.VI

A compendious top-level virtual instrument entitled FRACT.VI was designed prior to the commencement of commissioning tests. It was desired to minimize the development time between initial testing of the installed FRACT and the tasks of commissioning and calibration; this skeleton VI provided the basis for rapid progress, much of which (for example the convergence on a viable level sensor data acquisition scheme) could not constructively progress prior to FRACT installation and initial testing. FRACT.VI and its suite of allied sub-VIs naturally grew in sophistication as functions were added, and made more robust and comprehensive.

In routine operation of the C•M•D•S centrifuge, the operator is presented on the computer screen with the following Front Panel (Figure 6.1), compiling all FRACT related controls and indicators plus those for feed conductivity and heat exchanger functions, which are required to operate simultaneously during most experiments. It is through this interface, using mouse and keyboard, that all controlling options are selected and all results are indicated. Routine operation is nearly fully automatic.

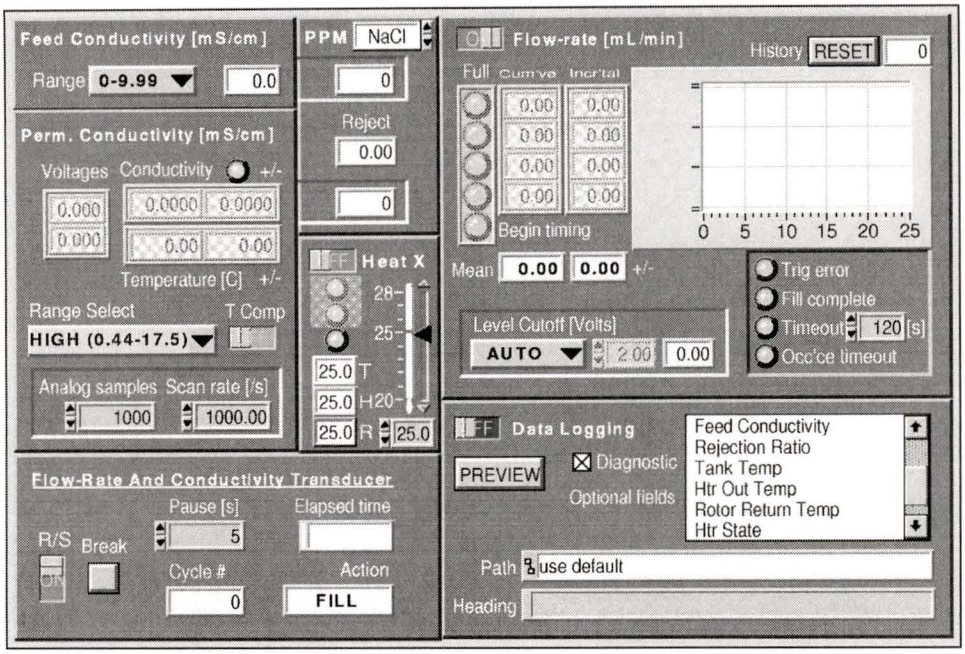

Figure 6.1: FRACT.VI Front Panel

6.4.2 Programming Conventions

The collective of displayed items associated with each principal function is to be found on an individual tile, the title for which appears in the top-left corner of said tile in bold print. Where applicable, physical units are also shown on this line of text in square brackets. If the function in question can be overridden, a horizontal slide-switch is provided to the immediate left of the title. Although all such switches have as their OFF condition the left or lower slider position, the Boolean state is also indicated by cyan coloured text hovering over the switch. In addition, the overridden state is often made more obvious by appearance of a red background, to avoid accidental oversights by the operator.

Numeric indicators and controls can be easily distinguished due to adherence to the following convention: controls have default grey colouration whereas indicators have a white field, surrounded by the usual grey frame. Exceptions to the general physical units are shown next to the relevant item in square brackets. Significant figures of indicators have been specified, in some cases dynamically so, given range selection information if applicable. Meaningful default values have been programmed. Most controls also have range checking and default increments, often with coercion if out-of-range inputs might have harmful consequences. When, within a tile, certain items have a deeper functional association, this is highlighted by their being surrounded by a recessed frame.

The author has striven to organize this Front Panel, and all the tiles it consists of, in a clear yet compact fashion, avoiding redundant information without obfuscating meaning. It is possible to select any control on the panel by use of the TAB key; the selected control then appears bordered within a black rectangle. Ordering of controls has been organized to facilitate this method, however the preferred mode of operation involves using the mouse.

It is effective to describe the normal sequence of operations in parallel with this functional organization, following approximately the operating sequence. In addition, exhaustive documentation is available on-line; the user merely needs to place the pointer on an item with the "Help" window visible and a description of the item will be presented.

6.4.3 FRACT.VI General Management

In the lower left corner can be found those controls and indicators not associated strictly with any specific hardware function (Figure 6.2). The *R/S* (Run/Stop) control is used to stop VI execution at the conclusion of an experiment, and ensures all active operations including termination routines are completed. The *Break* control can be invoked to interrupt the loop structures involved in flow-rate measurement; sometimes this is necessary during testing or in the event of a failure. The *Pause [s]* control is used to prescribe the length of pause, in seconds, to occur each cycle between flow-rate and conductivity measurements; this can be required to allow voltage transients to stabilize.

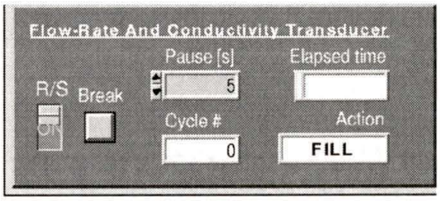

Flow-Rate And Conductivity Transducer

Pause [s]: 5

Elapsed time:

Cycle #: 0

Action: FILL

Figure 6.2: FRACT.VI General Management Tile

Complementing these three controls are three indicators. The *Cycle#* indicator maintains a non-decreasing record of cycles completed during an experiment. This is useful for associating noteworthy events with the FRACT.VI data log at a later time. The *Elapsed time* indicator is updated each cycle with the cumulative experiment elapsed time in clock format. Finally, the *Action* indicator displays the instantaneous state of activity of the FRACT and/or of the controlling software. It therefore indicates the following sequence or subset thereof: FILL-DRAIN-PAUSE-ANALOG-HEATX-LOGDATA-PREVIEW-STOPPED.

6.4.4 Flow-rate

Occurring first in the normal sequence of operations governed by FRACT.VI, permeate flow-rate measurement, its control and data acquisition requirements, are the principal tasks of this VI. The relevant tile is to be found in the upper right of the Front Panel, and is presented in Figure 6.3.

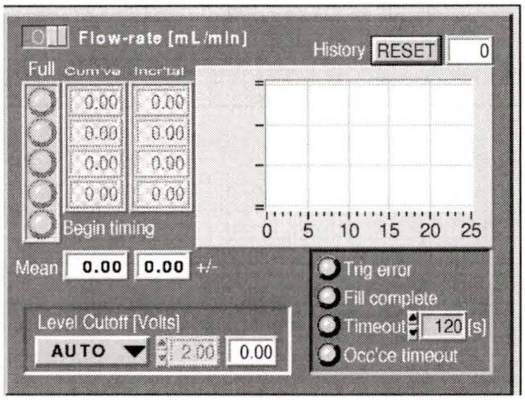

History RESET 0

Cum've	Incr'tal
0.00	0.00
0.00	0.00
0.00	0.00
0.00	0.00

Mean 0.00 0.00 +/-

Level Cutoff [Volts] AUTO 2.00 0.00

Timeout 120 [s]

Figure 6.3: FRACT.VI Flow-rate Measurement Tile

A conglomeration of four important indicators spans the width of this tile. Three of these indicators are arrayed vertically, and consist of five Boolean indicators associated with the five fluid level sensing channels, and a pair of numeric array indicators, four elements in size, displaying cumulative and incremental flow-rate measurements. To the right of these lies a chart style indicator entitled *History*, the ordinate of which has ticks aligned with the four flow-rate value fields and whose abscissa is flow-rate. Each cycle the incremental flow-rate values are mapped onto this chart and retained. Above this chart are two associated items, a pushbutton *RESET* which erases the chart contents, and an indicator which shows the number of cycles worth of data displayed on the chart.

During a typical cycle, the *Begin timing* indicator lights cyan, followed in turn by the four further level sensor indicators above it, mimicking the rising surface of the volume sample, until *Full* is reached. After this, the *Cum've* (cumulative) and *Incr'tal* (incremental) numeric flow-rate indicators along with the *History* chart are updated. The Boolean array of level sensor state indicators quickly extinguishes as the chamber is then caused to drain.

The weighted mean flow-rate is displayed each cycle by an indicator entitled *Mean*, aligned below the column of cumulative values which comprise it. The uncertainty in this value is displayed next to it; this indicator is named *+/-*, as are all other similar indicators on the whole Front Panel. Values in this pair of indicators appear in bold text to identify them as the principal outputs of this function.

Below, two associations of items are delimited by recessed frames. To the left appear the *Level Cutoff* features. A menu-ring control (pull-down list) both indicates and allows selection of the cutoff mode: manual or automatic. In manual mode, a voltage setting is taken from the numeric control adjacent; in automatic mode the calculated voltage is shown by a nearby indicator. One of these items shall appear greyed, and in the case of the control, be disabled, when the other is in use.

Four Boolean indicators disposed vertically are clustered with a numeric control in a recessed frame to the right. *Trigger error* glows yellow to warn of a (possibly transient) error in the sequence of level sensor detections. *Fill complete* glows green following achievement of a full sampling chamber. *Timeout* glows red if chamber filling time exceeds a specified interval; this interval is specified by the numeric control having units of seconds adjacent. *Occ'ce timeout* glows blue if the level sensor synchronization routine encounters a timeout situation. This timeout interval is prescribed in the relevant sub-VI.

The flow-rate measurement phases are then concluded and attention turns to the measurement of conductivity.

6.4.5 Permeate Conductivity

Several functions take place immediately subsequent to flow-rate measurement, the most important of which fulfills the second chief functional requirement of the FRACT system, that of permeate conductivity measurement. The tile grouping items relevant to this function, shown in Figure 6.4, can be found on the left side of the Front Panel.

As with the *Flow-rate* tile, horizontal continuity is used to associate separate numeric fields. In this case, a columnar array of two elements named *Voltages* displays the averaged analog voltages for permeate conductivity and temperature. Next to this indicator are stacked a pair of row arrays of two members each, used to display the *Conductivity* and *Temperature*, and their uncertainties. These are aligned with the voltage values used to obtain them. There is a small Boolean indicator next to the conductivity indicator label which glows red and shows the overlaid caption OOR if the conductivity goes out of range.

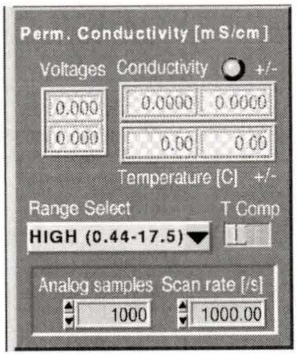

Perm. Conductivity [m S/cm]

Voltages: 0.000, 0.000

Conductivity: 0.0000 +/- 0.0000

Temperature [C]: 0.00 +/- 0.00

Range Select: HIGH (0.44-17.5)

Analog samples: 1000

Scan rate [/s]: 1000.00

Figure 6.4: FRACT.VI Permeate Conductivity Measurement Tile

Below are disposed two controls. A menu-ring both displays and controls the current range selection, while a simple horizontal slide-switch toggles conductivity temperature compensation. The latter is entitled *TComp*, while the former, entitled *Range Select*, incorporates a novel feature requiring further narrative.

The range select menu-ring text labels are generated dynamically according to the conductivity calibration ranges at the users disposal. These labels represent the options recognized by the control; the selected option shown in Figure 6.4 is, for example, "HIGH (0.44-17.5)". At initialization, FRACT.VI examines the calibration data contained within the relevant sub-VI and extracts range extremes. These numeric values are then converted to text strings and parsed to yield the required menu-ring labels. Via an attribute node, a LabVIEW feature permitting programmatic changes to Front Panel items, the available ranges are thus displayed. The virtue of this exercise is that following occasional recalibration the conductivity range options shown on this control are assured to be correct without requiring any LabVIEW programming.

The last items on this tile to be discussed are associated by a recessed frame and are the controls for the number of voltage samples per channel to be acquired (*Analog samples*) and the *Scan rate [s]*. It should be noted that these settings affect all analog input operations handled by this VI, not just those for permeate conductivity and temperature.

6.4.6 Feed Conductivity and PPM

Found in the top-left corner of FRACT.VI, these two tiles, shown together in Figure 6.5, support related functions. Feed conductivity exploits analog voltage data gathered simultaneously with the permeate conductivity and temperature data, which is converted into a conductivity value using a simple algorithm furnished by the sensor manufacturer. This sensor has two operating ranges, chosen via the *Range* menu-ring control which additionally prescribes the number of significant figures displayed by the adjacent indicator.

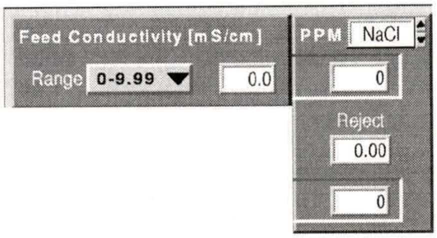
Feed Conductivity [mS/cm]
Range 0-9.99 0.0
PPM NaCl 0
Reject 0.00
0

Figure 6.5: FRACT.VI Feed Conductivity and Rejection Ratio Tiles

The *PPM* tile has a custom text ring control located close to the tile title, so as to appear part of the title. This text ring's contents are, like the permeate conductivity *Range Select* control, programmatically generated, and reflect the currently available set of solute species. A set of polynomial coefficients are employed to execute conversion between conductivity units and parts-per-million, a unit of concentration more familiar to many experimenters. The sub-VI responsible for this conversion, ppm.vi, generates a list of solutes for which such coefficients have been recorded, and this list is subsequently used to generate the ring control contents. The ppm concentrations of both feed and permeate are displayed by two of this tile's indicators, and are given visual association with their conductivities by recessed frames aligned with the relevant indicators on the adjacent tiles. In addition, the rejection ratio, which indicates the proportion of solute rejected by the membrane process, is shown by the *Reject* indicator.

6.4.7 Heat Exchanger

This tile, found roughly in the middle of the FRACT.VI Front Panel and presented in Figure 6.6 , encompasses the display of bulk fluid temperatures, heat exchanger activity and its control. These functions have no direct relationship with the FRACT device, but rather are important process control functions which, in the interests of experimental consistency, cannot be neglected.

Along its right edge is a vertical slide control with an associated numeric control directly below; this control establishes the set point for the heat exchanger algorithm. This slide is positioned parallel to a thermometer style indicator having identical size and scaling, immediately to its left, the scale for which applies to both items and whose range bounds normal operating conditions. The thermometer style indicator has three pointers of different colours: yellow, cyan and magenta. This allows the three bulk temperatures, tank, heater out and rotor return, to be displayed on the sole indicator. As an aid to clarity, a vertical stack of three small numeric indicators with similarly coloured frames simultaneously echo the temperature values in Celsius degrees. These bear the legends T, H and R, abbreviations for tank, heater and rotor, to aid in recognizing the coloured pointers of the thermometer.

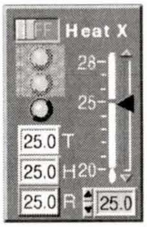

Figure 6.6: FRACT.VI Heat Exchanger Functions Tile

Also arranged in a single column are three Boolean indicators. For compactness, their identification appears only when a true state is displayed, by text superimposed on the lit indicator. From top to bottom, they are COOL (green), HEAT (yellow) and OVER (red), and indicate cooler activity, heater activity and exceedence of the bulk temperature tolerance bounds. The former two remain active but are greyed over when heat exchanger control has been overridden by the user. In this role they indicate the controlling algorithm's output even in the absence of controlling action.

6.4.8 Data Logging

FRACT.VI boasts "experiment to spreadsheet" capability, meaning recorded experimental data may be saved directly in a tab-delimited ASCII file, complete with column labels, for interpretation by any popular spreadsheet or graphing program. This action, if invoked by the operator, is the last of the cycle, and this final tile to be described (Figure 6.7) is found in the lower right corner of the FRACT.VI Front Panel.

Required user input is minimal, and relevant only at the commencement of an experiment. Provision for a descriptive line of text at the top of the log file has been included, and this is entered into the *Heading* string control at the bottom of this tile. Above it is an indicator called *Path* which displays the log file path once it is known. A default filename and path is automatically parsed from the calendar date, and a dialog box gives the operator the chance to accept or change this path; in the latter case a conventional Windows type file control dialog box is generated. A checkbox labeled *Diagnostic* facilitates selection between two datalogging modes: a core data set which includes all required fields and, when checked, a superset of data fields including many required only for troubleshooting purposes. As a future enhancement to this feature, a multiple-selection listbox has been incorporated, endowing the operator the means to select exactly relevant data fields for logging, and appears at the upper right of the tile.

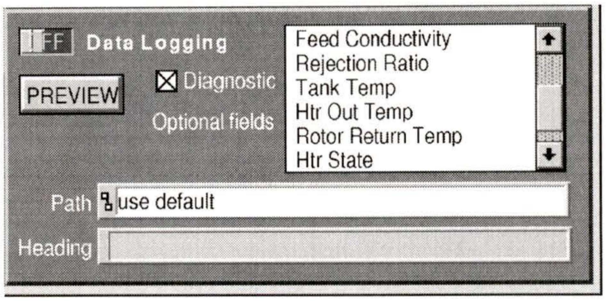

☒ Diagnostic

Path use default

Figure 6.7: FRACT.VI Data Logging Control Tile

During an experiment it may be useful to preview flow-rate, conductivity or temperature trends while FRACT.VI is running. This is supported by the *PREVIEW* pushbutton control, which appears grey and is disabled, until the log file exists. Invoking this control brings up the preview.vi Front Panel, which displays this data in chart form while other activities continue.

6.5 ALGORITHMIC SYNOPSIS OF FRACT.VI

6.5.1 Sequenced Actions

In LabVIEW parlance, a virtual instrument is endowed with functionality by its Block Diagram, on which Front Panel controls appear as terminals and act as data sources while indicators behave as data sinks. In between, one finds many familiar operators, and iconically represented entire sub-VIs, all connected with "wires" which represent data type and transfer.

A number of novel programming solutions were undertaken in the development of FRACT.VI, some of which are not readily apparent to the operator during normal use. In describing the important features of the virtual instrumentation portion of this thesis, it remains to highlight some of these features.

During execution, the major actions governed by FRACT.VI proceed sequentially. Some of these actions, such as sampling chamber fill and drain, are compelled to occur in sequence by their nature. Other operations, such as conductivity measurement, are less strictly required to occur in any rigid sequence, but are integrated into the cyclic flow-rate measurement structure as members of a regular sequence of actions. Execution sequencing is represented on the Block Diagram by sequence frames; concurrent activities are contained within a frame, subsequent frames can occur only when all preceding activity is complete. Most other functions are caused to be suspended during the flow-rate measurement phase, even though they may be physically unrelated, having been so compelled by the chosen level sensor implementation involving the full capacity of the analog input hardware.

The use of the sequence structure is scorned by some LabVIEW programmers for its supersedence of data dependency and its innate capacity for execution sequencing. In this application however, deliberate avoidance of the sequence structure would have endangered the clarity of the Block Diagram, not only by concealing the action sequenced but also by causing the diagram to scroll far off the limited screen area. A single screen Block Diagram is an enormous aid to its easy interpretation.

Each iteration of the totality of sequenced actions is defined as a cycle; the constituent groupings of actions, each contained within a frame, are referred to as phases. Table 6.1 clarifies the phases comprising a cycle of FRACT.VI.

Frame	**Phase**	**Major Actions**
0	Refresh	Refresh indicators at start of cycle
1	*Fill*	Engage actuator, register filling of samp. chamber
2	*Drain*	Release actuator, register drainage; calc. flow-rates
3	Clear AI	Release analog input port from triggering role
4	*Pause*	Pause: allow input voltage transients to decay
5	*Analog*	Acquire and process analog voltage data
6	Feedback	Calculate feedback voltage and update output line
7	*Heat X*	Actions relating to feed temperature stabilization
8	*Log Data*	Concatenate and log data to spreadsheet file
9	Sundry	Sundry tasks to conclude cycle
Note: italics denote this entry is enunciated in the "Action" indicator.		

Table 6.1: Synopsis of Essential Logical Structure of FRACT.VI

6.5.2 FRACT.VI Logical Structure: Salient Points

Once initializations have successfully occurred and indicators have been updated a measurement cycle is ready to begin. If not overridden, flow-rate measurement occurs first. The actuator is drawn closed: maximum initial current is supplied to develop full pulling capability despite maximum air gap, followed by the lesser sustaining current required to hold the valve shut. The level sensor excitation voltage is exploited to synchronize the level sensing system; upon fluid detection at the zeroth level sensor, chamber filling is deemed to have begun. Absolute time is registered as each level sensor in turn indicates arrival of the fluid surface. When the chamber is indicated to be full, the magnet is released; instantly the chamber begins discharging.

The level sensor array continues to be monitored awaiting indication of a fully discharged chamber. Meantime, the individual cumulative fill times are employed to calculate flow-rate values. These values, and their weighted mean, are displayed, and the history chart, which maintains a record of incremental flow rates for diagnostic purposes, is updated. Once chamber emptiness is confirmed, execution proceeds to the next phase in the sequence.

The analog input hardware is reassigned to serve in its customary capacity: voltage data acquisition. Data for permeate conductivity and temperature and for feed conductivity is scanned and buffered. The FRACT.VI then acquires this data from the DAQ hardware, and processes it: the data is averaged, and voltage to unit conversion performed using recorded calibration results. Temperature compensation of permeate conductivity may be applied, conversion of feed and permeate conductivity to concentration units takes place (given the dissolved species coefficients) and results are indicated. To ensure reliable flow-rate measurement on the following cycle, the new permeate conductivity datum is used to compute a level sensor cutoff-voltage; this is then delivered to the electronics hardware package via an analog output line.

Several ancillary functions, though unrelated to FRACT operations, take place at this stage under the governance of FRACT.VI. Data from three temperature transducers in the feed and retentate streams is acquired and exploited by a custom sub-VI to determine heat exchanger action, which is then invoked via a pair of digital states routed to the C•M•D•S rig main controller. The temperatures and heat exchanger activity are displayed. User override and temperature setting is accepted from this module of FRACT.VI.

Data logging to disk file, if enabled by the user, concludes the salient activities handled by FRACT.VI in a typical cycle. Unless the user has chosen to terminate execution, another cycle begins anew.

6.5.3 Example Block Diagram: An Enabling Programming Novelty

The formulation of read levels on occurrence.vi was a watershed achievement in solving the conundrum of synchronized digital port data acquisition in real time; its Block Diagram is presented in Figure 6.8. The principal task of this sub-VI is the prescription of configuration and triggering conditions settings to a quartet of intermediate-level and configuration National Instruments DAQ-library VIs [6.2]. Thereafter a simple sequence structure with a wait-on-occurence node embedded, ensures that execution advances to the read levels.vi digital data acquisition and filtering sub-VI only after triggering conditions are met and a specified lag interval has elapsed. The occurrence descriptor is retained at the uninitialized shift register for future calls to this sub-VI.

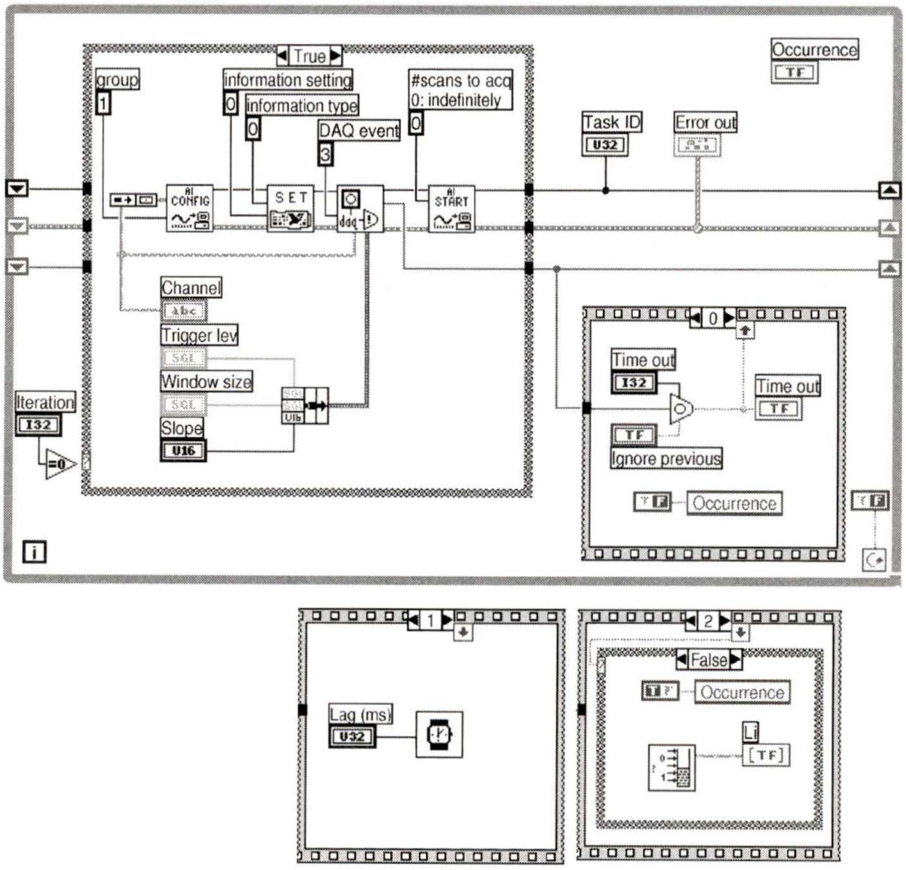

Figure 6.8: read levels on occurrence.vi Block Diagram.
Within the grey rectangle and to the left is a case structure (True) showing the four steps to initializing the triggering function; in the lower right corner is the initial (0) member of the sequenced actions: wait-on-occurrence. The remaining members, shown below are: (1) wait (lag ms), and (2) proceed to read levels, if triggering time out is False.

Lacking sufficient hardware resources to employ the more exact timer/counter capabilities of the NI DAQ board, the Windows millisecond clock was used to formulate a sub-VI whose function mimics that of a stopwatch with four registers, stopwatch array.vi.

6.6. INFREQUENTLY REQUIRED USER INPUTS

The routine operation of FRACT.VI is nearly fully automatic. Often, starting and stopping the VI and enabling data logging at the desired time is the only required user input; the controls affecting these, and many occasionally used functions, has been described earlier. It remains only to highlight certain rarely used, but critical, controls requiring only occasional attention. These controls appear on the Front Panels of various sub-VIs and are not normally seen.

Nearly all sub-VIs have controls and indicators, much like FRACT.VI does: they are the conduits through which data is exchanged with the calling routines, and can be likened to the parameter list found in conventional programming. In some cases, data does not arrive from outside the sub-vis scope; the control is set strictly from the sub-VI Front Panel whereafter this default value continues to apply. It is a subset of such latter controls which will be the topic of discussion.

Of the controls in question many, such as the electromagnet current settings, have proven satisfactory in demanding operation over long intervals of time. Although the existence of these controls is intended to allow occasional adjustment, attention will be confined to those controls requiring occasional adjustment following recalibration. This primarily affects the conductivity sensor.

6.6.1 Conductivity Conversion Low-Range Coefficients

The low-range voltage to conductivity units polynomial coefficients, and the high-range calibration data pairs, must be updated following occasional recalibration of the sensor, a topic discussed in chapter 5: Calibration and Commissioning. These two sets of values are to be found on different sub-VIs, a consequence of the desire to facilitate the option of implementing different high range conversion algorithms. The low range polynomial coefficients are found on the Front Panel of unit convert.vi; the order of the polynomial is arbitrary: any number of coefficients may be entered. To ensure that the newly encoded values remain in effect, the user must invoke the "make current values default" command upon the control using the right mouse button, and subsequently re-save the sub-VI.

6.6.2 Conductivity Conversion High-Range Data

The high range calibration data pairs are associated with the Front Panel of interpolate.vi in a two-dimensional array. Any number of data pairs may be entered, but the array must contain only the most current data: any old data not overwritten must be deleted. Null entries appear grey. Again, the "make current values default" command is required to assert the continued availability of this new data.

6.6.3 PPM Conversion Coefficients

The conversion of conductivity (mS/cm) to concentration (ppm) units requires a set calibration coefficients which usually are generated experimentally. These polynomial coefficients reside in the sub-VI ppm convert w/species.vi in an array of clusters; this portion of its Front Panel is shown in Figure 6.9. A cluster is simply a data type representing a conglomeration of several items of non-specific data type. In this case the cluster includes a character string containing the chemical abbreviation for the species, and a numeric array in which the coefficients are stored. To revise an existing coefficient set, one merely indexes through the array until the desired species is current, then edits the coefficient control. A new species may be added by indexing to the end of the array and entering the abbreviation and calibration data into a blank member. When FRACT.VI is next run, a dialog box will inform the user that the species list has been rebuilt, making it known that the species control now contains new members available to be chosen.

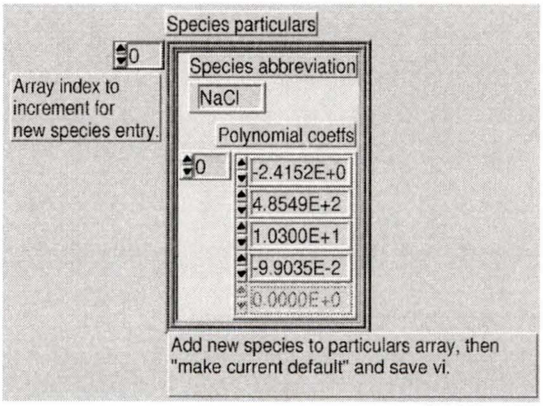

Species particulars
0
Array index to increment for new species entry.
Species abbreviation
NaCl
Polynomial coeffs
0
-2.4152E+0
4.8549E+2
1.0300E+1
-9.9035E-2
0.0000E+0
Add new species to particulars array, then "make current default" and save vi.

Figure 6.9: "Species particulars" Control from ppm.vi Front Panel

6.6.4 Bulk Fluid Temperature Control Settings

Control of bulk fluid temperature emerged late as a crucial requirement for experimental consistency. This feature was incorporated into FRACT.VI via the sub-VI Tcontrol w/2ndary cntl.vi. Principal set point input is accepted via the FRACT.VI Front Panel, however the controlling algorithm has seven additional input parameters found on the Tcontrol w/2ndary cntl.vi Front Panel. Experience has led to a workable set of parameters and it is inadvisable to adjust these settings without due care and attention.

6.6.5 Bulk Fluid Temperature Conversion Coefficients

The three bulk temperature transducers are commercial pre-calibrated linear devices. To arrive at Celsius degrees from voltage data, each transducer was calibrated to provide slope and intercept coefficients for linear conversion. These coefficients are found in the sub-VI TConvert.vi, and may be amended on its Front Panel. Furthermore, the algorithm can accommodate further channels for simultaneous conversion if new coefficients are appended to the existing set.

6.6.6 Automatic Level-cutoff Voltage Settings

As stated earlier, routine FRACT.VI operation is mostly automatic; one sub-VI whose task it is to permit this is level cutoff.vi, whose purpose it is to calculate the required level sensor cutoff voltage based on recent conductivity results. Setting of two voltages which take effect outside the bounds of the conversion function is imparted via Front Panel controls. If it becomes necessary to adjust these, the conversion formula itself, found within a Formula Node on the Block Diagram, will likely require revision.

6.7 INTRODUCTION TO THE ALLIED VIRTUAL INSTRUMENT MONITOR.VI

MONITOR.VI predates FRACT.VI but has received limited usage. Its purpose is to monitor, and optionally log, C•M•D•S rig specific data, to affect control of rotor speed and feed flow rate, to indicate numerous warnings and to invoke software control over many switchable functions of the apparatus. The physical parameters monitored are: feed flow-rate and pressure, rotor speed, chamber vacuum, brake servo pressure and vibration amplitude. Several of these variables are displayed using large analog gauge type indicators, as can be seen in Figure 6.10.

The utility of this VI has been hampered by FRACT.VIs intensive hardware demands, particularly as pertaining to analog voltage triggering of digital data acquisition. For them to operate harmoniously, measures must yet be implemented to integrate these VIs. The potential usefulness of MONITOR.VI would be further enhanced with the anticipated inclusion of a control feature to allow lengthy experiments to be preprogrammed. This desireable development, however, invites the serious task of developing a robust trouble handling sequence, which would glean from available data (such as vibration amplitude) the worsening of a potential problem, and execute a planned sequence of actions to safely end the automated experiment.

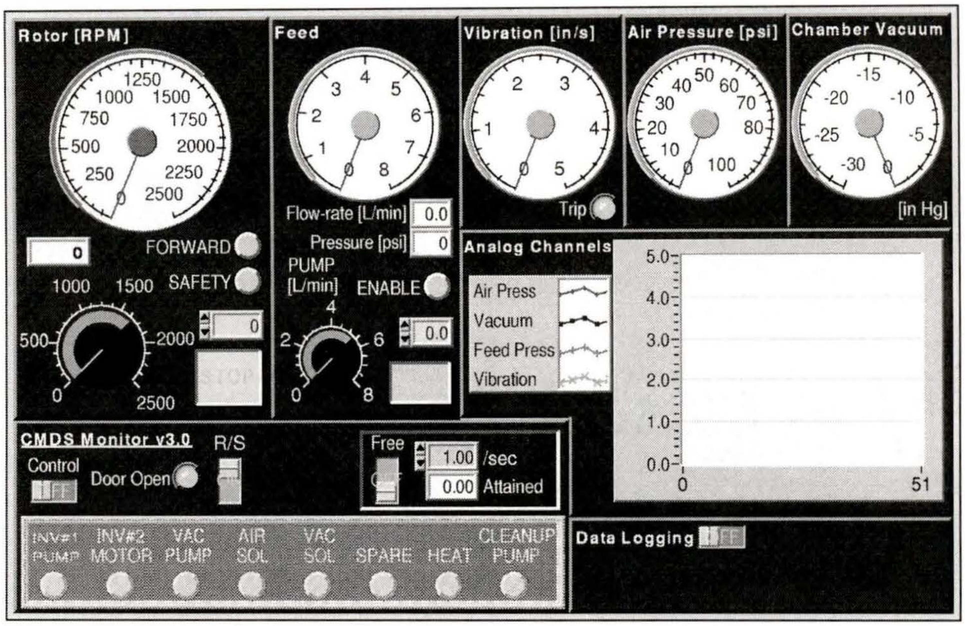

Figure 6.10: MONITOR.VI Front Panel

As for FRACT.VI, related information is clustered on tiles. From top left proceeding clockwise these are: rotor speed indication and control, feed fluid flow-rate and pressure indication and control, vibration amplitude, air brake pressure, chamber vacuum, charted data, data logging, and general operation controls.

7 Example Results from C•M•D•S and Conclusions

7.1 ENGINEERING ISSUES EMERGENT DURING FRACT SERVICE

Through the processes of dynamic testing, characterization and calibration, the FRACT device, its subtleties, and those of the supporting electronics and computer software came to be well understood. This experience was assimilated in the detailed planning of numerous experiments involving both the static and dynamic (centrifuge) apparatuses. These experiments immediately yielded illuminating results, but also revealed difficulties both with the FRACT and with other aspects of the newly commissioned equipment. Ultimately, growing confidence in both the instrumentation and the body of equipment led to sound and resourceful solutions to most outstanding matters.

Validity of FRACT flow-rate data is strongly reliant on the total capture of permeate; any leakage in the sampling chamber causes spurious measurements. Redundant flow-rate data, a design feature described in Section 2.7.5, yields real-time evidence of chamber leaks. This diagnostic aid has been invaluable, revealing, on occasion, compromised performance and in turn leading to its solution. A few such examples are highlighted.

7.1.1 Deterioration of Valve Needle and Seal Seat

Deterioration of the needle and seal seat after prolonged usage was indicated by monotonic decline in flow-rate with sampling chamber fill-fraction, and confirmed by later inspection of these parts. The permeate discharge impinges at high velocity upon the originally stainless needle; this is the presumed root cause of the problem. The Viton elastomeric seal also appears to suffer damage, perhaps through interaction with the pitted stainless needle.

Clearly, use of a needle with greater corrosion resistance in the presence of ionic solutions is a probable solution. A variety of Nickel alloys are often used in marine and chemical applications; threaded fasteners made of one such alloy, Monel, are readily available. The fabrication of a suitable needle merely involves turning of a point, 60° interior angle, onto a commercial #2-56 setscrew (Allen) fastener. The alternative pursued, however, involved the use of a Nylon setscrew. This material is non-corrosive but is mechanically weaker than the candidate metals. Despite this, it has functioned well and imparted improved durability to the critical valve assembly.

A related modification sought to overcome the possibly related damage, resembling spalling, to the Viton seal. Tygon tubing, which has has somewhat greater hardness than Viton, was available having suitable dimensions. A seal assembly using this material has served in unison with the Nylon needle, the pair exhibiting greater life than the original combination of stainless and Viton.

7.1.2 Level Sensor Electrodes

The six (five detector and one source) electrodes of the level sensing array each offer a potential conduit for leakage. Those members nearer the chamber bottom are more vulnerable due to greater hydrostatic pressure there. Thread engagement depth is approximately 6 mm, and although care must be exercised to avoid stripping the #1-72 tapped holes, adequate gasket compression is attainable. This, coupled with the sparing use of thread sealant, was proven in static testing to bear without leakage the full expected hydraulic pressure.

Leakage has been traced nonetheless to these sources on occasion. It is speculated that minor channeling of the FRACT body beneath the electrode gasket was the culprit on these occasions. This channeling is surmised to have originated due to heat damage during soldering at an early testing stage, and to have worsened through erosion while leaking during service. The solution, which has been satisfactory, was to spot face the gasket seat area before careful reassembly.

7.1.3 Inlet Crossbore Plug

There are nine sites penetrating the sampling chamber; six of these have been discussed. The remaining three are the AD-592 socket, the disused side port and the inlet crossbore plug. It is the latter of these which gave rise to the most vexing and evasive chamber leak experienced. The former are reliably sealed by a static radial O-ring gland and a Nylon #10-32 taper thread plug respectively.

To connect the parallel sampling chamber and inlet bore, the inlet crossbore is drilled, from the normal surface afforded by the pole clearance notch, through the sampling chamber wall to the inlet bore beyond. Depth control during drilling avoids this bore passing through the far wall of the FRACT body. The open end of this bore requires permanent sealing. A taper plug such as the one used for the side port was initially desired, and would have been most satisfactory. These commercially available plugs have a hex head, and to permit installation in this location of minimal clearance, it was envisioned that the head be machined to suitable dimensions. This was, however, discovered to be impossible, the plug being hollow. A custom threaded plug with gasket was therefore improvised; a permanent sealing compound was understood to have been used. One goal of initial static testing was to validate this seal, with a knowledge that its integrity has paramount importance; such tests indicated positively the seal was sound, and were trusted until, while investigating a leak, all other possible sites had been eliminated. Indeed, on this occasion, the crossbore plug was the culprit, and its secure replacement using epoxy has resolved this problem.

To assuage any doubt concerning the integrity of this plug, on future FRACT variants it is recommended that spin-welding be used to install a permanent plug. This approach, once statically tested, should be inviolable, since the plug and FRACT body become materially fused. The process is simple, but requires the correct application of joint pressure, choice of rotation speed and of spin time. Recommended pressure is 4.8 MPa, and tangential speed is to be in the range 3-12 m/s; where joint diameter causes prohibitively high rotation rates, greater time and/or pressure may be used. Nominal spin times are stated as 0.25–0.5 s [7.1].

Though used in mass production, spin welding is feasible for purpose built contrivances like the FRACT. Overrun should be avoided, and so production equipment features a clutch to disengage the drive mechanism from the workpiece. Toward this end, an application specific plug and chuck have been designed. A high speed drive such as a Dremel tool, mounted on a press fixture, should attain sufficient speed and accommodate the chuck. This allows for torque and pressure to be applied, and the drive swiftly retracted to complete the weld. It is suggested that the procedure be rehearsed on a dummy workpiece before being attempted on an actual part. Post machining is envisioned to remove the shank of the plug.

7.2 SOME EXAMPLE EXPERIMENTAL RESULTS

7.2.1 Concentration Polarization

Investigation of concentration polarization was the first major experimental objective in which the FRACT played a role, indeed the first cell holder was designed fundamentally with this in mind. Using a stack of pretested membranes, dynamic and static experiments were performed across a range of pressures, with various solute concentrations and two solute species. Dynamic tests were conducted for both *+R* and *-R* orientations. For each such test date was rendered to yield a set of points relating permeate flux to process pressure. The relationships between comparable dynamic and static results were compared.

One example of such an experiment has already been discussed: the calibrated membrane approach to FRACT flow-rate validation (Section 5.2.2). In this experiment, concentration polarization was deliberately eliminated by using a weak solute concentration. To illustrate the nature of typical FRACT raw data and to highlight the compelling results it delivers, raw and processed data from an experiment in which concentration polarization was witnessed is presented in this section.

Permeate flow-rate, conductivity and temperature data, extracted directly from the automatically generated spreadsheet data file, are shown in Figures 7.1 and 7.2. This data spans nearly four hours of centrifuge operation, during which time a series of five rotor speeds delivered process pressures between 2.7 and 5.4 MPa to a stack of four membrane modules using 35000 ppm NaCl feed. The membrane orientation was *+R* (active face outward), hypothesized to maximize the concentration polarization abatement afforded by centrifugal effects.

To quantify any such effects, this data was compared to similar data acquired during a static experiment, the dynamic (titanium) RO cell having been transferred intact between apparatuses. Average flow-rate values for each interval of constant pressure are compared in Figure 7.3. Both data sets exhibit a linear relationship between flow-rate and process pressure. The existence of a centrifugal phenomenon is gleaned by observing the significant augmentation, up to 40%, of permeate production with the dynamic apparatus.

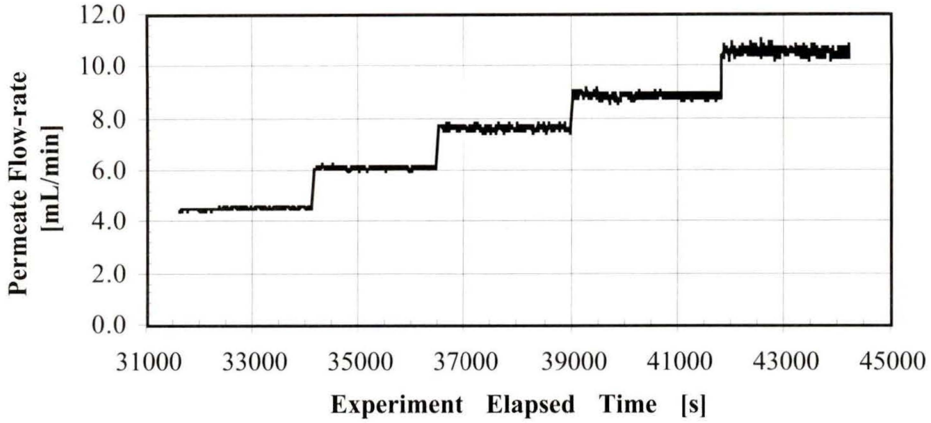

Figure 7.1: Typical Permeate Flow-rate Raw Data from FRACT
The steps apparent in this graph correspond to five rotor speeds developing process pressures of 2.7, 3.4, 4.1, 4.8 and 5.4 MPa (400 to 800 psi). Four membrane modules, +*R* (active face outward) orientation, 35000 ppm NaCl feed, 2 L/min.

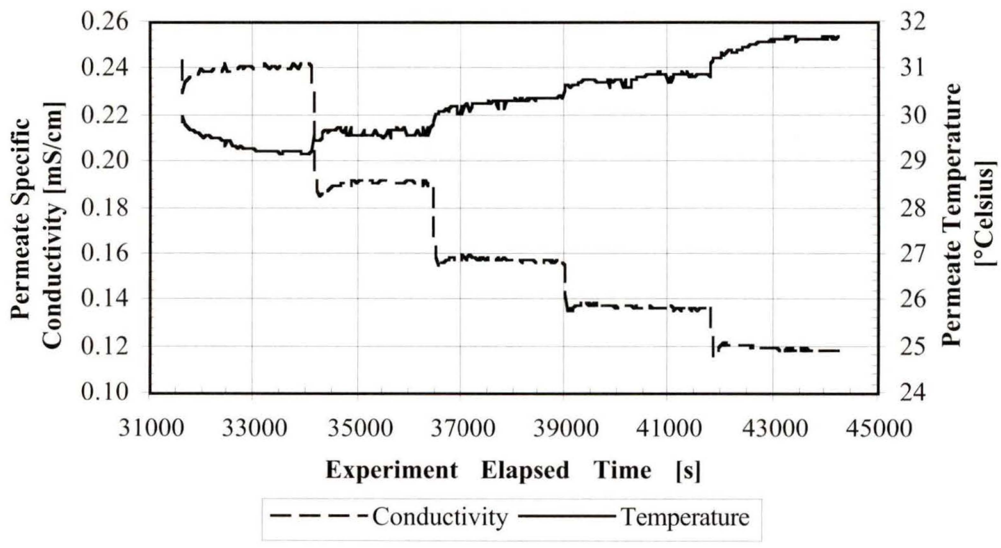

Figure 7.2: Typical Permeate Temperature and Specific Conductivity Raw Data
Permeate temperature is witnessed to generally increase with increasing rotor speed owing to windage, bearing and fluid coupling heating. Specific conductivity generally decreases due to an inverse relationship with permeate production rate. Four membrane modules, +*R* (active face outward) orientation, 35000 ppm NaCl feed, 2 L/min.

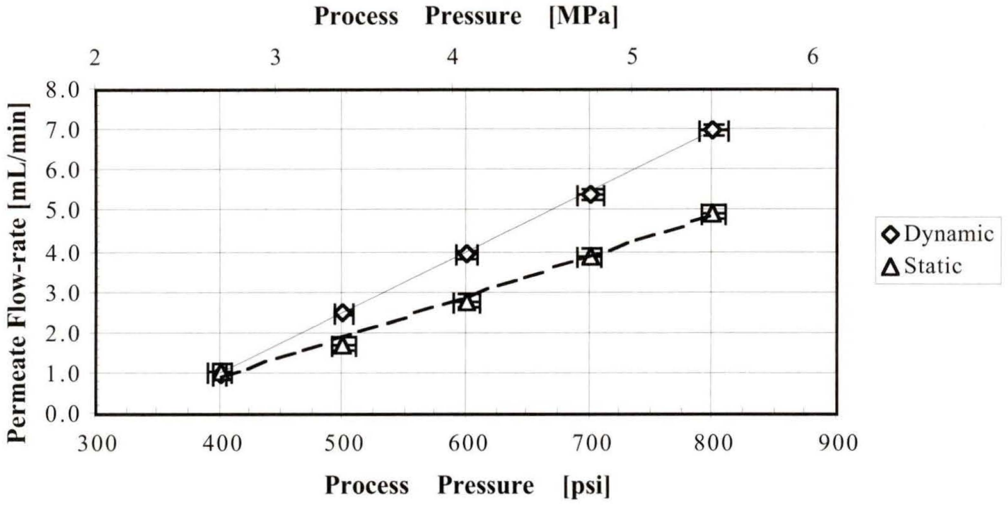

Figure 7.3: Dynamic and Static Permeate Flow-rate vs Process Pressure
An example of concentration polarization abatement by C•M•D•S. A flux improvement of 40% is apparent at 5.4 MPa due to centrifugal effects in this orientation. This is in direct analogy to the hatched area depicted in Figure 1.5. Four membrane modules, +*R* (active face outward) dynamic orientation, 35000 ppm NaCl feed, 2 L/min.

7.2.2 Silicate Fouling

A preliminary study of colloidal membrane fouling has been undertaken using silica as the fouling agent. Such fouling is more tractable intuitively than the polarization effect: a tangible layer of foulant develops against the membrane. This study indicates that, compared with the static experiment, the C•M•D•S approach exerts a considerable lessening of deleterious effects, manifested by permeate flux attenuation and attributable to fouling.

7.2.3 Numerical Modeling

In parallel with the experimental research only fleetingly described here, extensive work on the formulation of a numerical modeling technique has been performed [7.2]. Initial applications of this technique have been confined to the present membrane cartridge style and its feasible orientations. Much enlightenment as to the possible mechanisms behind the centrifugally induced phenomena, such as were outlined earlier in this chapter, have already been gained. There is little doubt, however, that the benefits of this work will become ever more apparent as innovative future rotor configurations are proposed and developed.

7.3 REVIEW OF DEFINITIVE OBJECTIVE AND SUGGESTIONS FOR FUTURE ROTOR-BORNE INSTRUMENTS

"Flow-rate measurement in situ aboard the spinning rotor is undeniably the main challenge attempted by this work." This statement, made in Section 1.7.4, was recast in Section 2.2.4 to read "The formulation and development of design parameters satisfying each of these requirements[1] under the stipulated constraints has been the definitive objective of this thesis."

It has been demonstrated, through extensive dynamic testing, calibration and characterization, that this objective has been met. On a lesser plane, the physical survival of the FRACT in the punishing centrifuge environment was achieved, if not foretold, by the thorough prototype testing during the development phases. Indeed the basic FRACT embodiment was forged with a view to facilitating laboratory simulation of the loading and operating situations expected to occur in the centrifuge. It is asserted that this was an important step toward ensuring a high probability of success with the rotor borne device.

Measurement of conductivity and temperature, albeit challenges of lesser magnitude, have also been achieved. Although opportunities for improvement of all three FRACT functions have been revealed, these should not be construed as deficiencies in the FRACT, given that a new arena of measurement capability has been broached.

7.3.1 Alternate Level-Sensing Strategy

Fluid level sensing by electrical means is both simple and effective: reasons why it was chosen in this work. It is conditional, however, on a conductive fluid sample being present. Even weak ionic solutions, as the permeate stream often is, are adequately conductive. Nevertheless, greater versatility could be afforded by a level sensing means that functions independently of sample conductivity. Restated, this would amount to the fundamental uncoupling of flow-rate and conductivity measurement. In the current embodiment, these functions are not innately independent, but have been rendered so by the superimposition of electronics filtering and information feedback: this is therefore a "decoupled" design. Electronics filtering can be regarded as an extra design parameter that could be eliminated by promoting a truly uncoupled design.

Level sensing by optical means is the most obvious alternative.Various implementations can be envisioned; one that can be melded with the present FRACT embodiment with minimal alteration is discrete reflective optical level sensing. It is briefly outlined here.

---

[1] $FR_{1.1}$: drain valve permitting control and repetition of fluid capture;
$FR_{1.2}$: fluid level sensing means for volume mensuration;
$FR_{1.3}$: data acquisition and processing means.

In a second bore, similar to the inlet bore but located where the vent and overflow ports presently exist, a 3 mm polypropylene sphere (specific gravity 0.91) will float on a column of the permeate sample. An infrared LED will shine from the top of this bore onto the float. Several infrared detectors will be arrayed vertically and installed such that they "see" the rising float. With proper conditioning, the resulting analog signals will yield discretized sample volume information much like the present electrical arrangement, but independently of sample conductivity and devoid of the 4 Hz resolution this system entails. Computer activity will no longer involve triggered synchronism, freeing the DAQ hardware for service in its usual capacities. Installation of the detector components should involve reliable O–ring seals and threaded retainers or, more ambitiously, these provisions could be machined directly into the detector component [7.3]. Permeate specific gravity not less than 0.91 is a chief constraint of this novel system.

7.3.2 Improved Temperature Sensor Installation

To better isolate the precision IC temperature transducer from convoluting heat transfer paths, future FRACT embodiments should adopt a reoriented socket receptacle boss.

7.3.3 Valve Restraint for Orientation Flexibility

Certain future C•M•D•S experiments may be performed with the RO cell and holder, either the present or a new design, in different "yaw" orientations. FRACT operation to date has occurred at one orientation which places the pendant valve spring, held in a state of tension by the centrifugal acceleration, in a relaxed position with appropriate actuator air gap for discharge and valve closure requirements. Variation of the yaw angle will cause this part to assume a position causing greater distance between the armature and the electromagnet poles. It is unclear whether the actuator will remain capable of engaging the valve under these more demanding circumstances. A simple design modification which should ensure satisfactory operation is a restraining provision to delimit the maximum opening displacement. This could be implemented on future versions by including on the FRACT body a lug into which a spring or dowel pin is pressed, spring movement being constrained by contact with this pin.

7.3.4 Self Activating Discharge Valve Option

Use of a self-exciting discharge valve was considered at the conceptual design stage (Section 2.2.5) but was overruled in favour of the current design. Main reasons for this decision were greater difficulty in manufacture, inaccessibility of critical elements for testing and adjustment purposes, and more demanding performance requirements for the actuator. In addition, laboratory testing was viewed more awkward if not impossible for the alternative embodiment envisioned.

Given the fruitful experience garnered by the success of the FRACT, an embodiment featuring a self-exciting valve with high probability of success can now be envisioned.

7.3.5 Installation on Other RO Cell Holders: The Future of FRACT

Eventually, investigation of membrane orientations not achievable with the current cell holder will be attempted. To do so the FRACT, or its descendant(s), will be installed on a new RO cell holder constructed for this purpose.

Owing to the high level of integration between the rotor-borne instrumentation package and the overall centrifuge infrastructure, but particularly the RO cell holder, it may be necessary to adapt the present design to this new configuration; a wholly new FRACT may even be required. Said new design might exploit some of the suggestions for refinement of the current design. This thesis will have served its purpose if it can aid in such an effort.

Literature Cited

1.1 Wild, Peter M. Development, Optimization and Implementation of the Design for a Centrifugal Reverse Osmosis Desalination System. Doctoral dissertation, University of Victoria, 1994.

1.2 Lycon, D.S.; Fyles, T.M. Manuscript in Preparation, 1997.

2.1 DeCarlo, J.P. Fundamentals of Flow Measurement. Instrumentation Society of America, 1984.

2.2 Upp, E.L. Fluid Flow Measurement. Gulf Corp., 1993.

2.3 Thermal Pulse Flow Meter. Molytek, Inc., Pittsburgh, 1991.

2.4 Rheotherm Precision Flow Instruments, Bulletin 895-1. Intek, Inc., Westerville, OH, 1989.

2.5 Miller, T.E., Jr.; Small, H. Thermal Pulse Time-of-Flight Liquid Flow Meter. *Analytical Chemistry*, 54:907-910, 1982.

2.6 Harpster, J.W. Thermal Technique for Measuring Fluid Flow. *Sensors*, 10:25-28, 1984.

2.7 Suh, N.P. The Principles of Design. Oxford University Press, 1990.

2.8 Green, R.E., Editor. Machinery's Handbook, 25th Edition. Industrial Press Inc., New York, 1996.

2.9 Alloy Data: Soft Magnetic Alloys. Carpenter Technology Corp., Reading, PA, 1992.

2.10 Dietrich, D.W. Magnetically Soft Materials. *Properties and Selection: Non-Ferrous Alloys and Special Purpose Materials, Volume 2, ASM International Metals Handbook, 10th Edition.* ASM International, 1990.

2.11 Messler, R.W., Jr. Joining of Advanced Materials. B/H, Inc., Boston, 1993.

2.12 Delrin Acetal Resin Design Guide - Module III. DuPont, 1995.

2.13 Loctite Technology Document LT-284. Loctite Corporation, 1989.

2.14 Ciba-Geigy Araldite 2041 Product Data Sheet. Ciba-Geigy, 1995.

2.15 Moody, F.J. Introduction to Unsteady Thermofluid Mechanics. Wiley, New York, 1990.

2.16 Blevins, R.D. Applied Fluid Dynamics Handbook. Krieger, Inc., New York 1992.

3.1 Oehme, F. Liquid Electrolyte Sensors: Potentiometry, Amperometry, and Conductometry. *Sensors: A Comprehensive Survey, Volume 2, Part 1: Chemical and Biochemical Sensors.* Göpel, W.; Hesse, J.; Zemel, J.N., Editors. VCH Verlag GmbH, Weinheim, FRG, 1991.

3.2 Shortley, G.; Williams, D. Elements of Physics, Fifth Edition. Prentice Hall, Inc., New Jersey, 1978.

3.3 Ives, D.G.; Janz, G.J. Reference Electrodes. Academic Press, Inc., 1961.

3.4 Jones, G.; Bollinger, D.M. The Measurement of the Conductance of Electrolytes, VI, on Platinum. *Journal of the American Chemical Society*, 57:280-284, 1935.

3.5 Malmstadt, H.V.; Enke, C.G. Electronics for Scientists. W.A. Benjamin, Inc., New York, 1962.

3.6 CDM3 Conductivity Meter Service Manual. Radiometer, A.S., Copenhagen Denmark, 1972.

3.7 Wright, C.P. Applied Measurement Engineering. Prentice-Hall, 1995.

3.8 Horowitz, P.; Hill, W. The Art of Electronics, Second Edition. Cambridge University Press, New York, 1989.

5.1 Precision Flowmeter Calibrators. Cox Instrument Corporation.

5.2 LabVIEW for Windows User Manual. National Instruments Corporation, Austin, TX, 1994.

5.3 Taylor, J.R. An Introduction to Error Analysis. University Science Books, Mill Valley, CA, 1982.

5.4 Analog Devices Product Data Sheet AD-592. Analog Devices, 1996.

5.5 Djilali, N. CMDS Research internal communication, October, 1996.

5.6 Base Analysis VI Reference Manual. National Instruments Corporation, Austin, TX, 1994.

5.7 AT-MIO E Series User Manual. National Instruments Corporation, Austin, TX, 1994.

6.1 LabVIEW Function Reference Manual. National Instruments Corporation, Austin, TX, 1994.

6.2 LabVIEW Data Acquisition VI Reference Manual for Windows. National Instruments Corporation, Austin, TX, 1994.

7.1 Engineering Polymers Design Handbook, Module I: General Design Principles. DuPont, 1992.

7.2 Pharoah, J.G. Computational Modeling of Centrifugal Membrane and Density Separation. Master's thesis, University of Victoria, 1997.

7.3 Bennett, N.R. Private communication, 1996.

IV.1 Shedlovsky, T.; Shedlovsky, L. Conductometry. *Techniques of Chemistry, Volume I: Physical Methods of Chemistry, Part II-A, Electrochemical Methods.* Weissberger, A.; Rossiter, B.W., Editors. Wiley Interscience, New York, 1971.

Appendix I: Isometric Exploded View of Membrane Module and RO Cell

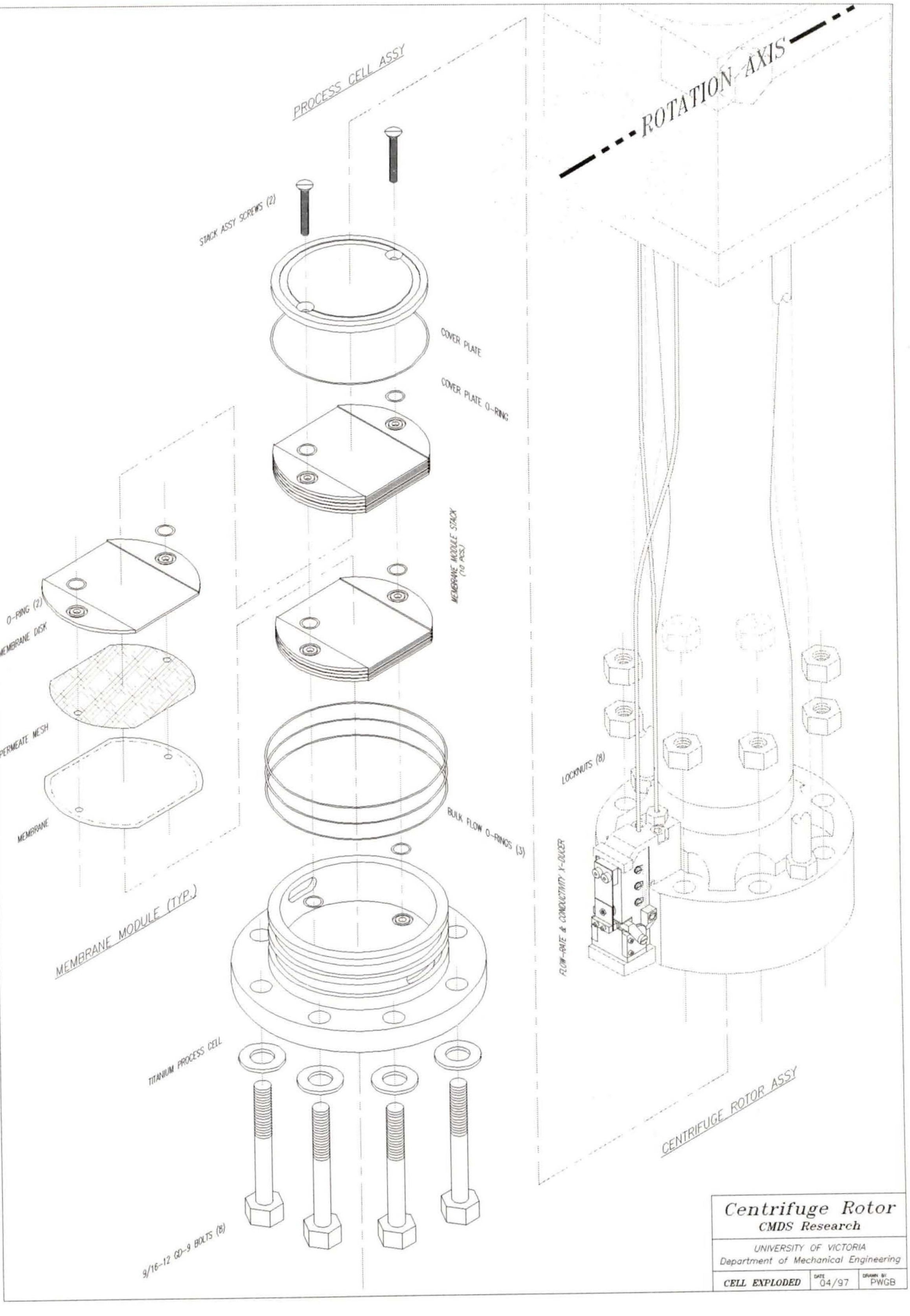
PROCESS CELL ASSY
ROTATION AXIS
STACK ASSY SCREWS (2)
COVER PLATE
COVER PLATE O-RING
MEMBRANE MODULE STACK (10 PCS.)
O-RING (2)
MEMBRANE DISK
PERMEATE MESH
MEMBRANE
MEMBRANE MODULE (TYP.)
BULK FLOW O-RINGS (3)
LOCKNUTS (8)
FLOW-RATE & CONDUCTIVITY X-DUCER
TITANIUM PROCESS CELL
9/16-12 GD-9 BOLTS (8)
CENTRIFUGE ROTOR ASSY
Centrifuge Rotor
CMDS Research
UNIVERSITY OF VICTORIA
Department of Mechanical Engineering
CELL EXPLODED
DATE
04/97
DRAWN BY
PWGB

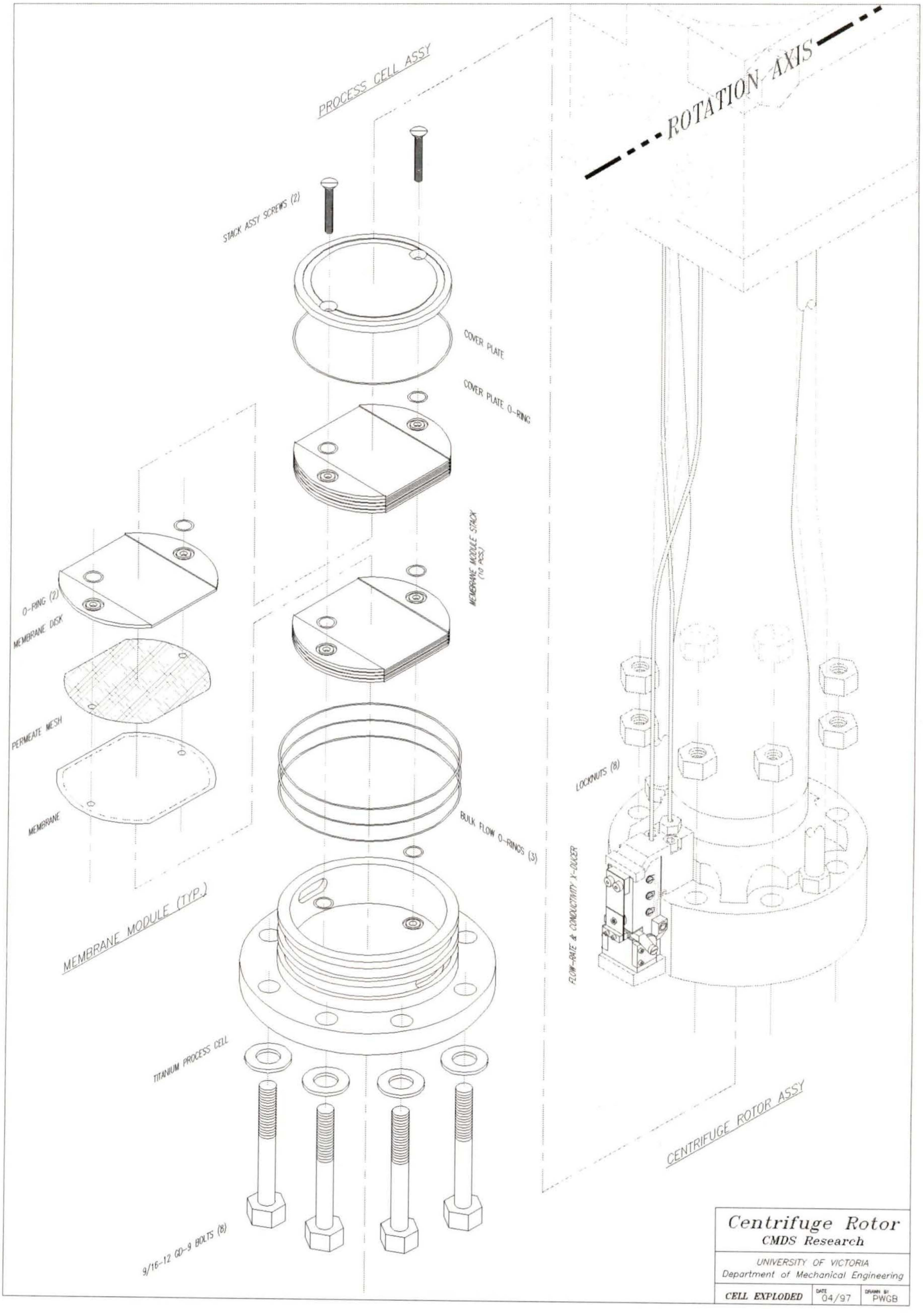
PROCESS CELL ASSY
ROTATION AXIS
STACK ASSY SCREWS (2)
COVER PLATE
COVER PLATE O-RING
MEMBRANE MODULE STACK (10 PCS.)
O-RING (2)
MEMBRANE DISK
PERMEATE MESH
MEMBRANE
MEMBRANE MODULE (TYP.)
BULK FLOW O-RINGS (3)
LOCKNUTS (8)
FLOW-RATE & CONDUCTIVITY X-DUCER
TITANIUM PROCESS CELL
CENTRIFUGE ROTOR ASSY
9/16-12 GD-9 BOLTS (8)
Centrifuge Rotor
CMDS Research
UNIVERSITY OF VICTORIA
Department of Mechanical Engineering
CELL EXPLODED
DATE
04/97
DRAWN BY
PWGB

Appendix II: Isometric Exploded, Assembly and Quarter Section Views of FRACT

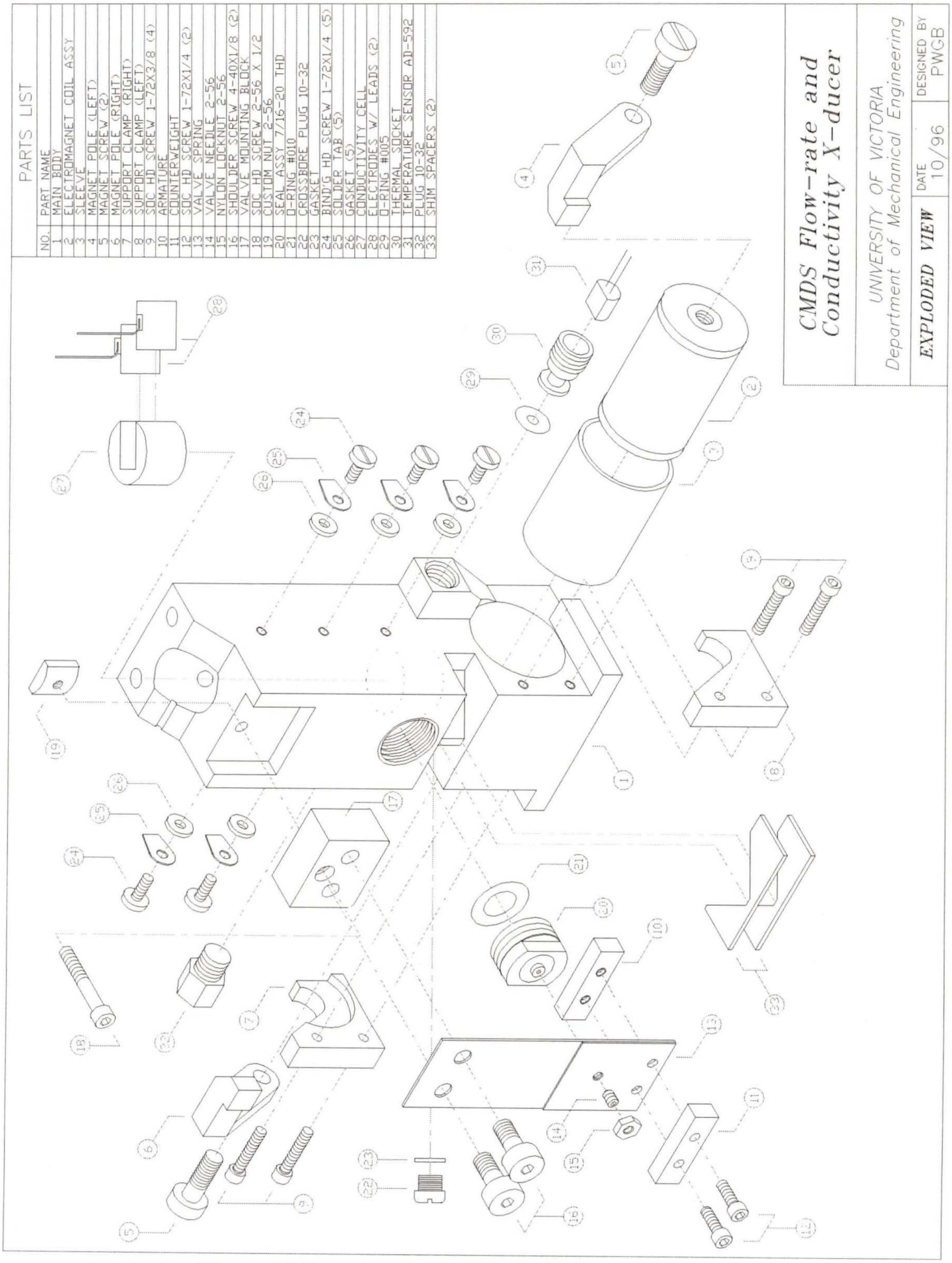

PARTS LIST

NO.	PART NAME
1	MAIN BODY
2	ELECTROMAGNET COIL ASSY
3	SLEEVE
4	MAGNET POLE (LEFT)
5	MAGNET SCREW (2)
6	MAGNET POLE (RIGHT)
7	SUPPORT CLAMP (RIGHT)
8	SUPPORT CLAMP (LEFT)
9	SOC HD SCREW 1-72X3/8 (4)
10	ARMATURE
11	COUNTERWEIGHT
12	SOC HD SCREW 1-72X1/4 (2)
13	VALVE SPRING
14	VALVE NEEDLE 2-56
15	NYLON LOCKNUT 2-56
16	SHOULDER SCREW 4-40X1/8 (2)
17	VALVE MOUNTING BLOCK
18	SOC HD SCREW 2-56 X 1/2
19	CUSTOM NUT 2-56
20	SEAL ASSY 7/16-20 THD
21	O-RING #010
22	CROSSBORE PLUG 10-32
23	GASKET
24	BIND'G HD SCREW 1-72X1/4 (5)
25	SOLDER TAB (5)
26	GASKET (5)
27	CONDUCTIVITY CELL
28	ELECTRODES W/ LEADS (2)
29	O-RING #005
30	THERMAL SOCKET
31	TEMPERATURE SENSOR AD-592
32	PLUG 10-32
33	SHIM SPACERS (2)

CMDS Flow-rate and
Conductivity X-ducer

UNIVERSITY OF VICTORIA
Department of Mechanical Engineering

EXPLODED VIEW	DATE	DESIGNED BY
	10/96	PWGB

Figure A-II.1: Isometric Exploded View of FRACT

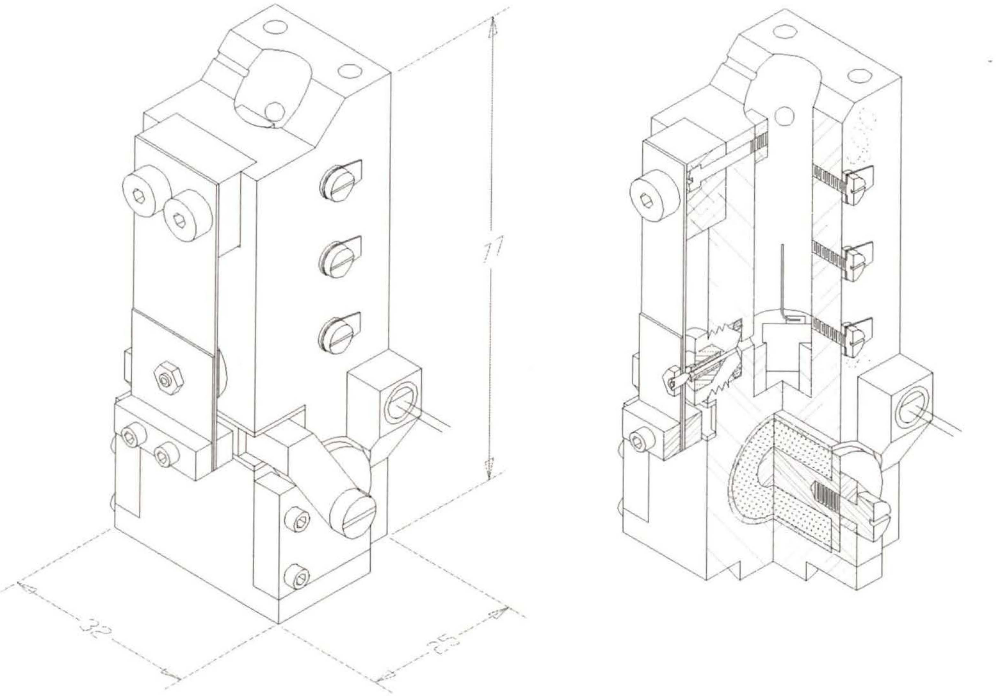

LEGEND	
▨	DELRIN 100 (OR EQUIV.)
░	#28 AWG DUAL INS. MAGNET WIRE
▨	SS TYPE 430FR SOLENOID QUAL.
▨	ALUMINUM
▤	M-S 907 EPOXY
▩	VITON
▨	ABS

NOTES:

(1) DIMENSIONS: MM

CMDS Flow-rate and Conductivity X-ducer

UNIVERSITY OF VICTORIA
Department of Mechanical Engineering

ISOMETRIC ASSEMBLY & QTR. SECTION VIEWXS	DATE 12/96	DESIGNED BY PWGB

Figure A-II.2: Isometric Assembly and Quarter Section Views of FRACT

Appendix III: Prototype Circuit Schematic

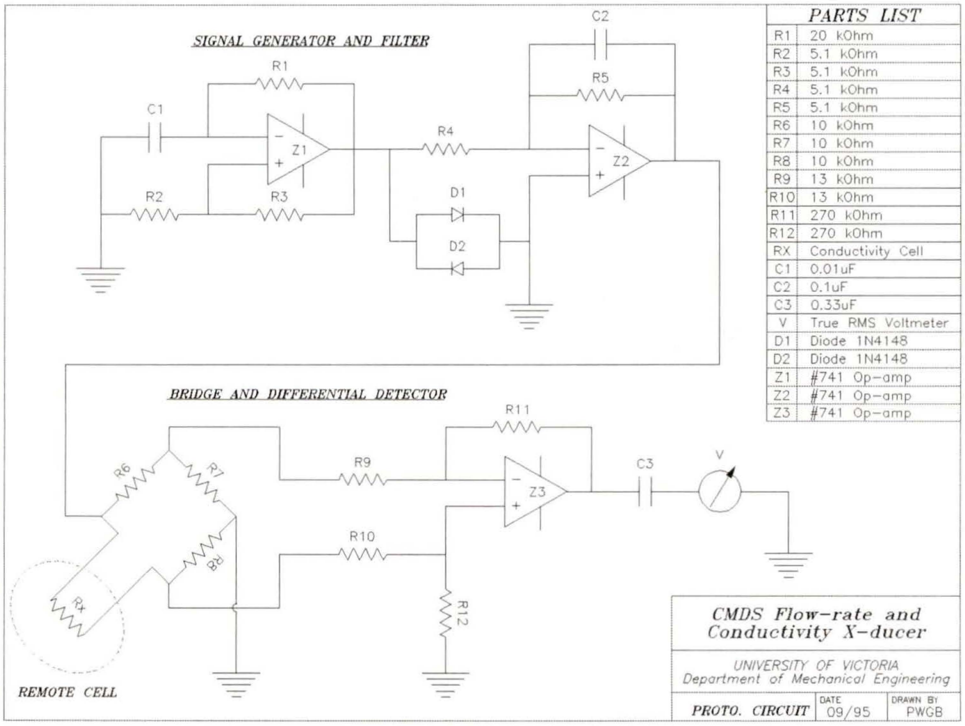

PARTS LIST	
R1	20 kOhm
R2	5.1 kOhm
R3	5.1 kOhm
R4	5.1 kOhm
R5	5.1 kOhm
R6	10 kOhm
R7	10 kOhm
R8	10 kOhm
R9	13 kOhm
R10	13 kOhm
R11	270 kOhm
R12	270 kOhm
RX	Conductivity Cell
C1	0.01uF
C2	0.1uF
C3	0.33uF
V	True RMS Voltmeter
D1	Diode 1N4148
D2	Diode 1N4148
Z1	#741 Op-amp
Z2	#741 Op-amp
Z3	#741 Op-amp

Figure A-III.1: Prototype Conductivity Circuit Schematic

Appendix IV: Temperature Compensation Coefficient

Conductivity is known to be related to temperature for many solutions. This is due to ionic mobility being influenced by temperature, a measure of mean kinetic energy of the matter comprising a solution.

Typical temperature coefficients for aqueous solutions fall within the bounds of 1 to 3 %/°C [3.1]. Interestingly, the magnitude of this temperature dependence is greater for purer solutions; since the permeate has been depleted of solute by as much as 99% this is particularly relevant.

In order to properly implement temperature compensation of permeate conductivity, a procedure was devised to provide the temperature coefficient for the solute(s) to be used in C•M•D•S experiments. Initially, common salt, sodium chloride (NaCl) was of interest.

Five solutions of NaCl having approximate conductivities between 0.25 and 15 mS/cm were prepared. In turn, each specimen was placed in a beaker on a heater stirrer, and the CDM3 meter conductivity cell and an accurate thermometer immersed in the specimen. Through a range of temperatures, uncompensated conductivity and temperature readings were taken.

A graph showing the measured conductivity versus temperature for each solution was generated, and is presented in Figure A-IV.1. The abscissa was offset, indicating temperature referenced to 25°C. Thereby, least-squares fits to the five data sets provided both specific conductivity at the reference temperature 25°C and temperature dependence information. Uncertainties in both values were obtained.

Equation A-IV.1 formally portrays the goal of this exercise: the inference of Γ_T, the temperature compensation coefficient from L, the sample conductivity, and dL/dT, its responsivity to slope. Both these variables were, as has been mentioned, extracted from the experimental data

$$\Gamma_T = L^{-1} \cdot (dL/dT) \qquad \text{A-IV.1}$$

The five data pairs (slope, conductivity) arising from this experiment were then graphed, relating dependence to absolute conductivity (Figure A-IV.2). A least-squares fit to this data was performed, with the y-intercept constrained to be zero, the slope of which is the desired temperature coefficient Γ_T , found to be (0.0199 ± 0.0002) $°C^{-1}$, or 2%/°C. Shedlovsky [IV.1] tabulates "Approximate Temperature Coefficients" for numerous cations and anions. Averaging those cited for Na^+ (0.0209 $°C^{-1}$) and Cl^- (0.0188 $°C^{-1}$) yields 0.0199 $°C^{-1}$, engendering some confidence in the experimental result. This value was then encoded into the relevant LabVIEW sub-VI to permit automatic temperature compensation of conductivity data.

This procedure is recommended to establish temperature correction coefficients for different species as they are needed for future experiments.

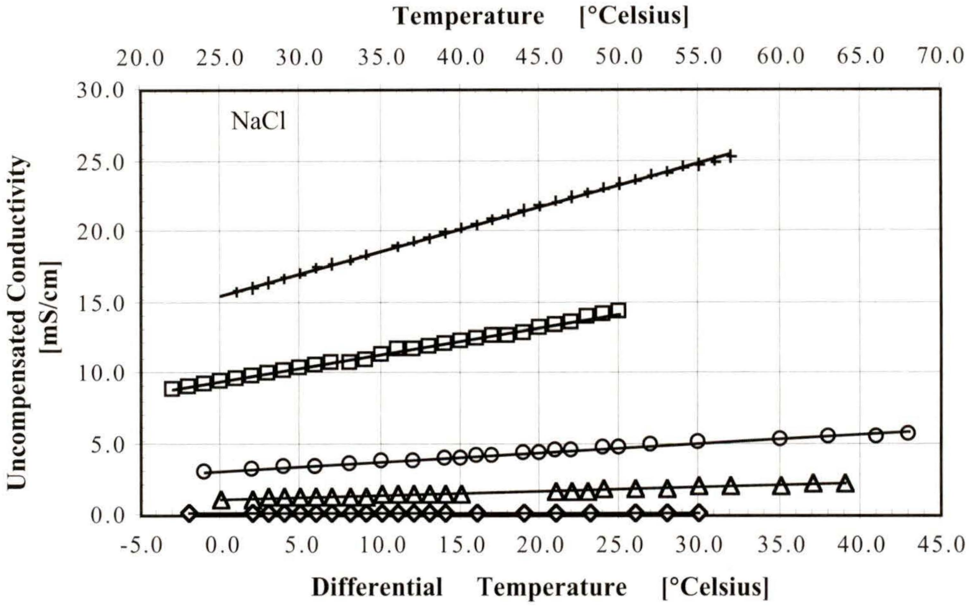

Figure A-IV.1: Five Data Series Relating Conductivity to Temperature for NaCl

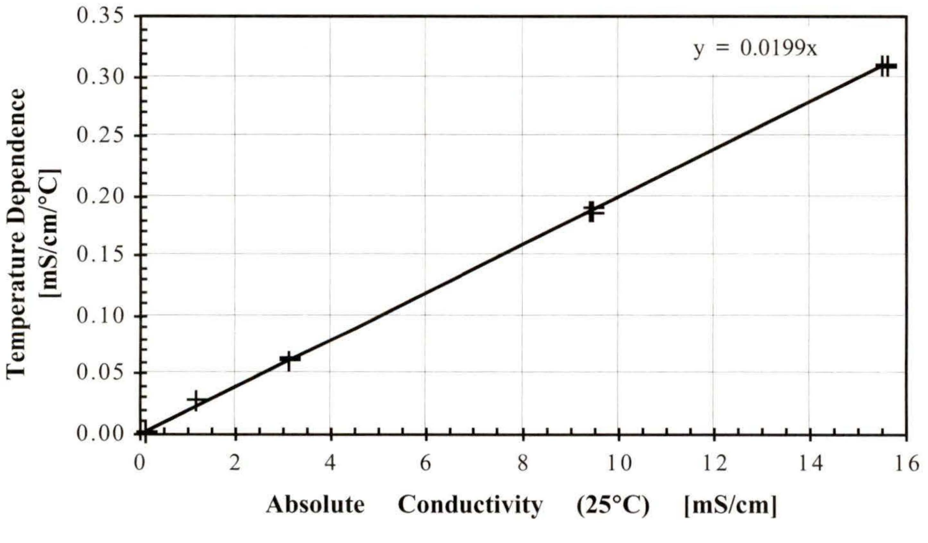

Figure A-IV.2: Temperature Dependence vs Specific Conductivity for NaCl

Appendix V: FRACT Specifications

Overall Dimensions

Height	80	millimetres
Width	38	millimetres
Depth	35	millimetres

Mass and Capacity

Mass	103	grams
Total Capacity	3.3	millilitres
Dynamic Capacity	2.7	millilitres

Electrical Requirements

Actuator	4-9	DC volts; ground
AD-592 IC Temperature Sensor	4-30	DC Volts; ground
Level Sensor Excitation	10	4 Hz AC Volts
Conductivity Sensor Excitation	0.2	2kHz AC Volts
Level Sensor Signal	5	TTL
Signal Ground	1	

Measurement Capabilities

Flow-rate.........0.5-20 mL/min
Accuracy.........better than ±2%
Precision.........better than ±2.5% (@ 10mL/min)

Conductivity
Low Range.........0-0.34 mS/cm
Accuracy.........±1.3%
Precision.........±0.1%

High Range (nominal).........0.44-5 mS/cm
Accuracy.........+2.8/-1.8% (linear conversion)
Precision.........±0.3%

High Range (extended).........5-15 mS/cm
Precision.........±1%

Temperature.........15-45 °Celsius
Accuracy.........±0.4 °C
Precision.........±0.5% (estimated)

Appendix VI: FRACT Virtual Instrumentation Documentation

Connector Pane

fract.vi

Front Panel

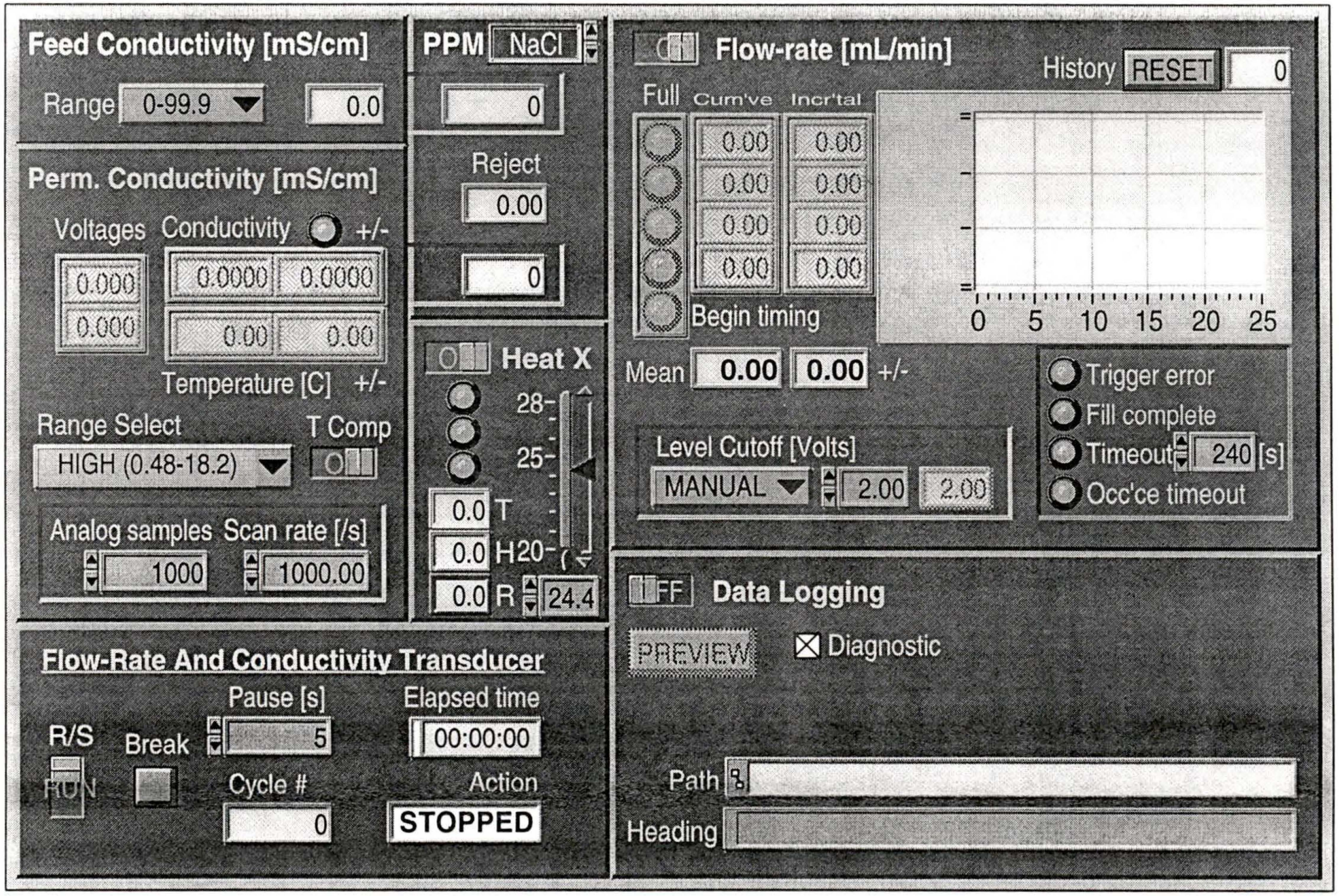

Feed Conductivity [mS/cm]

Range 0-99.9 0.0

Perm. Conductivity [mS/cm]

Voltages 0.000 0.000

Conductivity 0.0000 0.0000 +/-

Temperature [C] 0.00 0.00 +/-

Range Select HIGH (0.48-18.2)

T Comp

Analog samples 1000

Scan rate [/s] 1000.00

PPM NaCl 0

Reject 0.00

0

Heat X

0.0 T

0.0 H20

0.0 R 24.4

Flow-rate [mL/min]

History RESET 0

Full	Cum've	Incr'tal
○	0.00	0.00
○	0.00	0.00
○	0.00	0.00
○	0.00	0.00
○	Begin timing	

Mean 0.00 0.00 +/-

Level Cutoff [Volts] MANUAL 2.00 2.00

○ Trigger error

○ Fill complete

○ Timeout 240 [s]

○ Occ'ce timeout

Data Logging

☒ Diagnostic

Path

Heading

Flow-Rate And Conductivity Transducer

Pause [s] 5

Elapsed time 00:00:00

Cycle # 0

Action STOPPED

Controls and Indicators

TF **R/S**
Run-Stop control for termination of vi main loop execution.

TF **Break**
Break control to abort loops within the vi.

TF **Flow-rate**
Toggles the permeate Flow-rate function.

TF **History**
Resets the Incremental Flow-rate History display and counter.

U16 **Level Cutoff [Volts]**
Governs whether level cutoff signal filtering is automatically determined or manually set by the

SGL **Manual**
Sets the user-controlled level sensing signal cutoff threshold.

U32 **Timeout [s]**
Governs the time allotted for sampling chamber fill/drain before timeout.

U16 **Range**
User-selected feed fluid conductivity range control.

U16 **Range Select**
Governs which branch of the conductivity calibration is used for voltage to conductivity conversion. Labels are updated automatically at run-time from actual calibration data to properly reflect available options.

TF **T Comp**
Toggles temperature compensation of permeate conductivity.

I32 **Analog samples**
Controls the number of analog voltage samples to read, buffer, and average to yield conductivity and temperature values.

SGL	**Scan rate [/s]** Controls the scan rate of analog voltage reads.
U32	**Pause [s]** Controls pause length (each cycle).
U16	**Species** User-selection of feed stream species (from available options) for conductivity to ppm conversion function.
TF	**Tank Heat** Governs whether tank heater activity is controlled by software.
SGL	**Temp setting** Prescribes target feed fluid temperature.
TF	**Data Logging** Toggles state of data-logging function.
TF	**Diagnostic** Toggles inclusion of diagnostic (additional) fields in the logged data array.
abc	**Heading** User input of heading inserted in data log file.
TF	**Preview** Launches previewer, allowing examination of data recorded during current run (datalogging must be on.)

SGL **Feed Conductivity**
Displays feed fluid conductivity.

SGL **Voltages**
Mean analog input voltages for permeate temperature and conductivity.

- SGL **Celsius**
  see documentation for array.

SGL **Conductivity**
Converted conductivity value with attached uncertainty (1 standard deviation of averaged array).

- SGL see documentation for array.

SGL **Temperature [C]**
Converted temperature value with attached uncertainty (1 standard deviation of input array).

- SGL see documentation for array.

SGL **PPM [feed]**
Indicates feed fluid concentration in ppm.

SGL **Reject**
Indicates process rejection ratio as derived from feed and permeate concentrations.

SGL **PPM [permeate]**
Indicates permeate concentration in ppm.

TF **Overheat**
Indicates feed fluid temperature has exceeded target window.

TF **Heat**
Indicates feed-fluid heater activity.

Feed temp
Displays feed fluid temperatures:
YELLOW: tank
CYAN: heater out
MAGENTA: rotor return

[TF] **Level trig**
Depicts the fill-fraction of the sampling chamber as extracted from the filtered and synchronised level-sensing array.

TF see documentation for array.

[SGL] **Cum've**
The flow-rate as calculated for the portion of sampling chamber volume swept from the zeroth level to the level in question.

SGL see documentation for array.

[SGL] **Incr'tal**
The flow-rate calculated for the swept volume between adjacent level sensors.

SGL see documentation for array.

U32 **Displayed**
Indicates the number of cycles currently displayed on the Incremental Flow-rate History chart.

Incremental Flow-rate History
Relates the incremental flow-rate to fill-fraction (level sensor array element).

SGL **Mean**
The weighted mean of the cumulative flow-rate values for the current cycle. This mean accounts for the inherently different uncertainty in each of the four cumulative values by weighting the values by their proportional volume.

SGL **+/-**
Displays the standard deviation of the weighted mean of flow-rate values.

TF **Trigger error**
Indicates the level-sensing array did not trigger monotonically increasing by element.

TF **Fill complete**
Indicates all elements of the level-sensing array have triggered, implying a full chamber.

TF **Timeout**
Indicates the sampling chamber failed to fill or empty in the allotted time.

TF **Occ'ce timeout**
Indicates the synchronism of level-sensing array reads was not possible owing to a failure to obtain occurrence criteria from the analog voltage feedback line.

SGL **Cutoff [V]**
Displays the automatic level sensing signal cutoff threshold.

Path
Indicates data logging path presently in use.

abc **Elapsed time**
Indicates experiment elapsed time.

◂▸ **Action**
Indicates present activity of the vi.

I32 **Cycle #**
Indicates the elapsed number of cycles

TF **OOR**
Indicates permeate conductivity has exceeded tolerable limits.

TF **Cooler**
Indicates cooling valve open.

Block Diagram

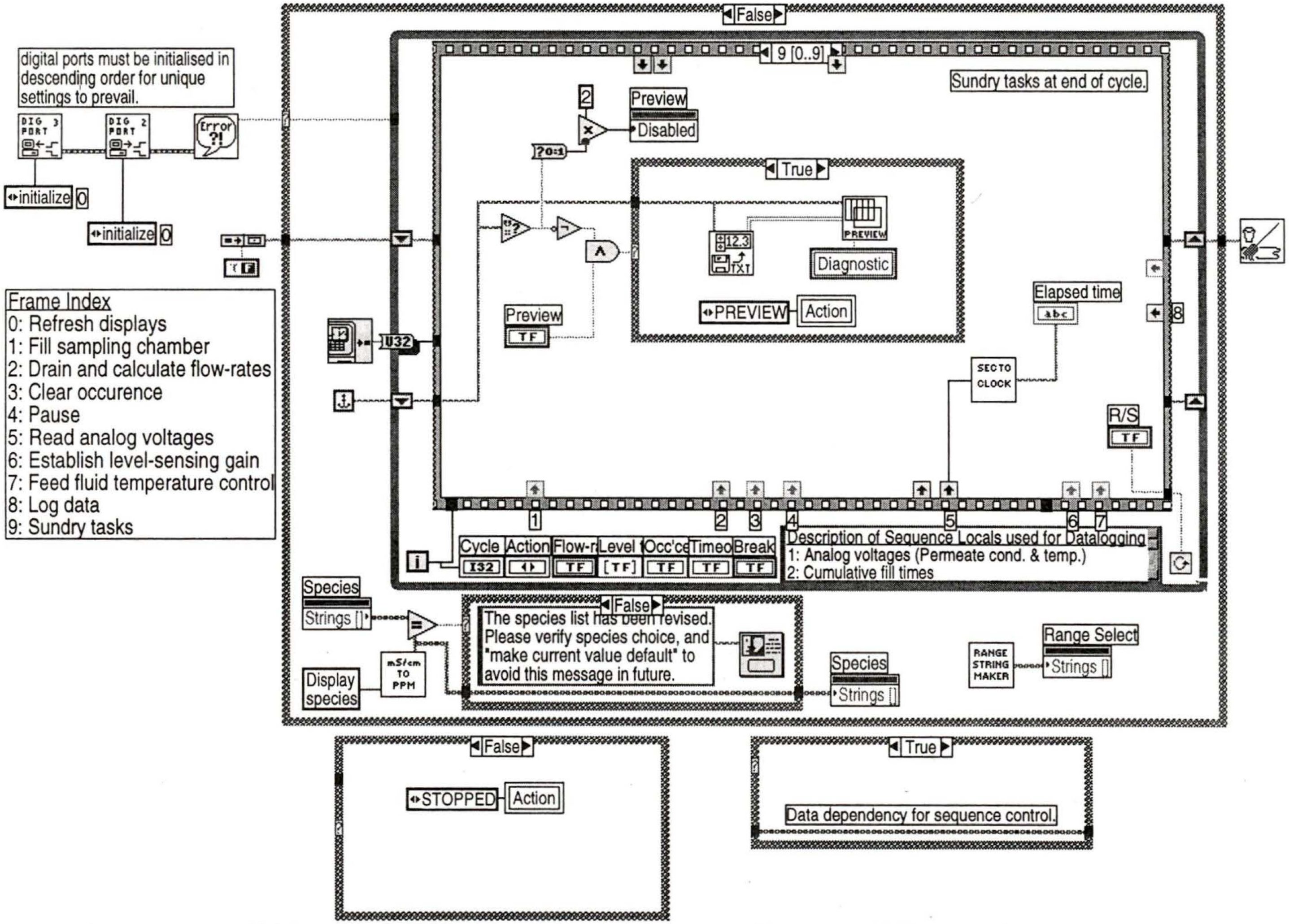

digital ports must be initialised in descending order for unique settings to prevail.

Frame Index
0: Refresh displays
1: Fill sampling chamber
2: Drain and calculate flow-rates
3: Clear occurence
4: Pause
5: Read analog voltages
6: Establish level-sensing gain
7: Feed fluid temperature control
8: Log data
9: Sundry tasks

Sundry tasks at end of cycle.

Description of Sequence Locals used for Datalogging
1: Analog voltages (Permeate cond. & temp.)
2: Cumulative fill times

The species list has been revised. Please verify species choice, and "make current value default" to avoid this message in future.

Data dependency for sequence control.

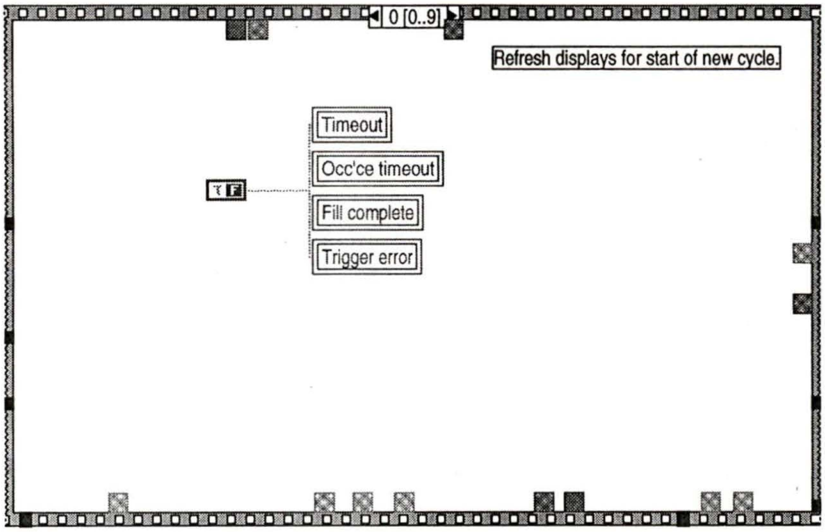
0 [0..9]
Refresh displays for start of new cycle.
Timeout
Occ'ce timeout
Fill complete
Trigger error
F

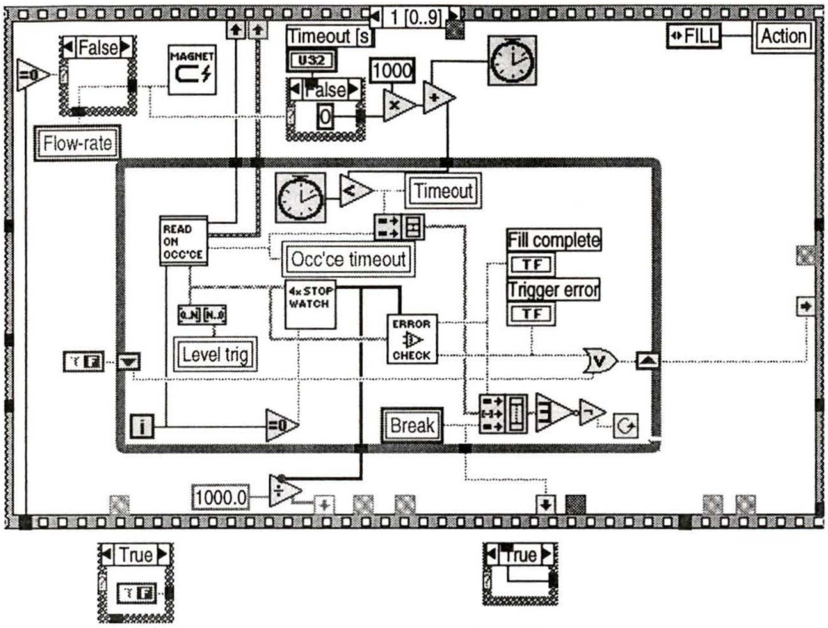
1 [0..9]
False
MAGNET
Timeout [s]
U32
1000
False
0
FILL
Action
Flow-rate
Timeout
READ ON OCC'CE
Occ'ce timeout
Fill complete
TF
Trigger error
TF
4x STOP WATCH
ERROR CHECK
Level trig
Break
1000.0
True
True

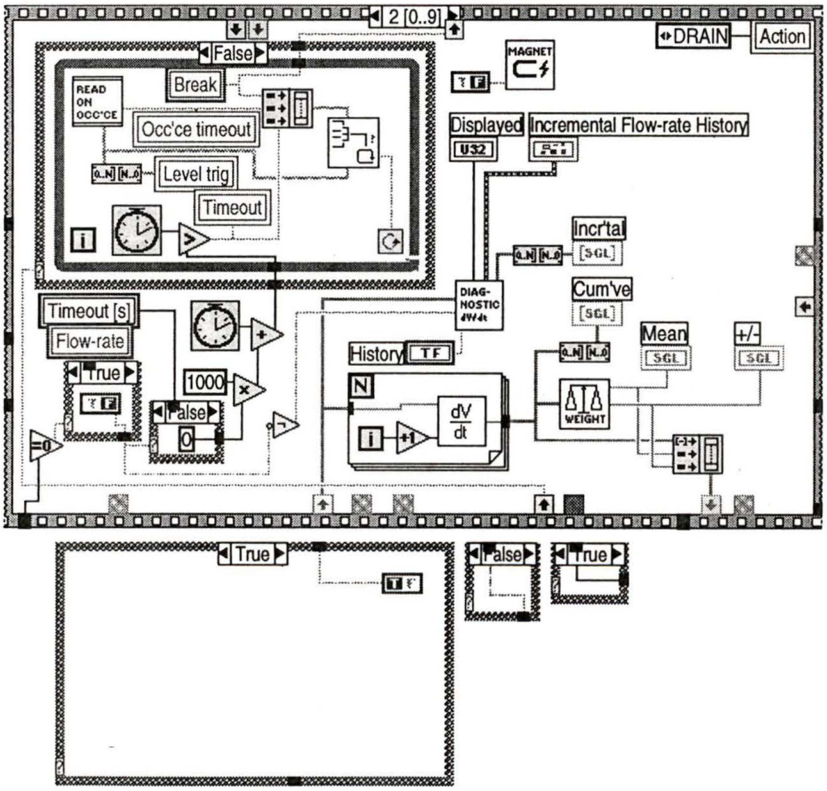
2 [0..9]
DRAIN
Action
False
MAGNET
READ ON OCC'CE
Break
Occ'ce timeout
Level trig
Timeout
Displayed
U32
Incremental Flow-rate History
Incr'tal
SGL
Cum've
SGL
DIAG-NOSTIC dW/dt
Mean
SGL
+/-
SGL
Timeout [s]
Flow-rate
True
1000
False
0
History
TF
N
dV/dt
WEIGHT
True
False
True

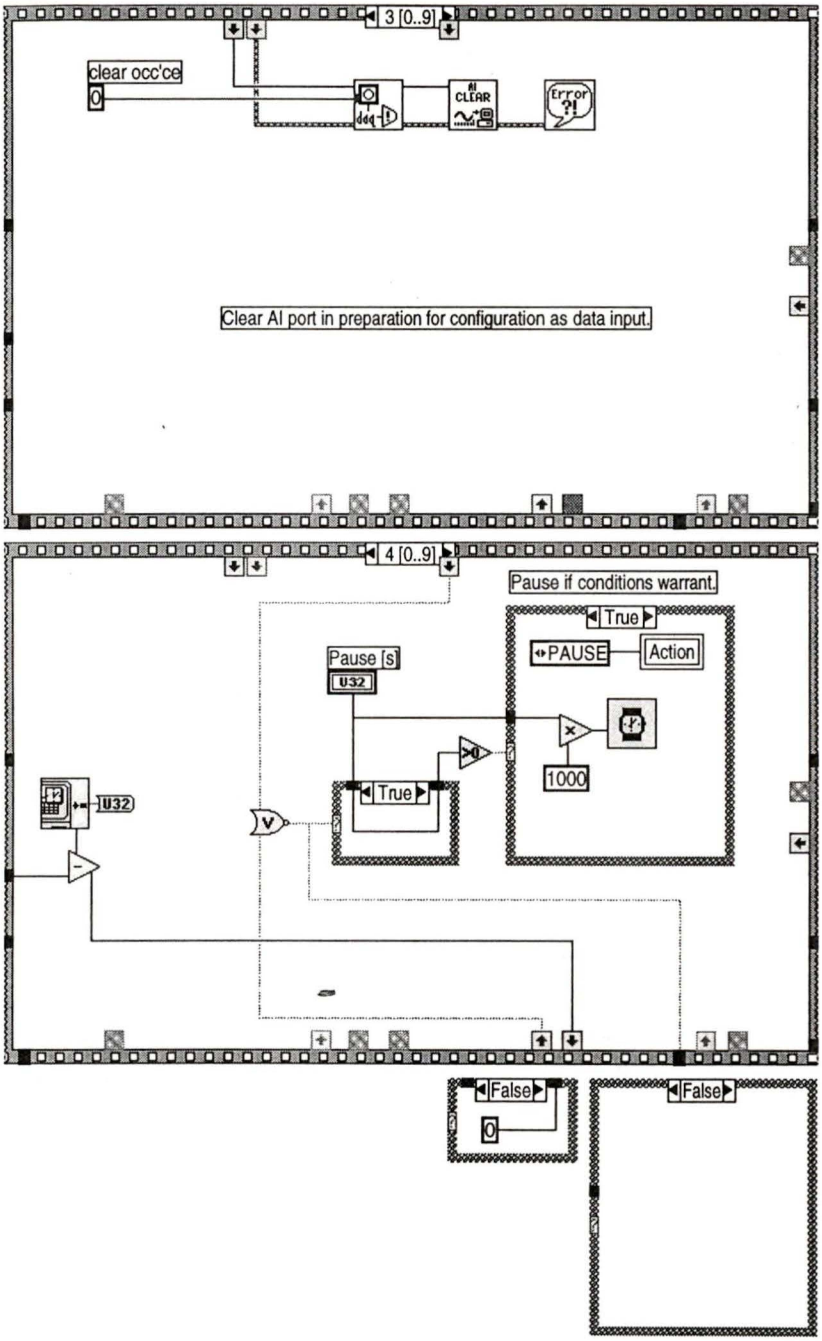
3 [0..9]
clear occ'ce
0
AI CLEAR
Error ?!
Clear AI port in preparation for configuration as data input.
4 [0..9]
Pause if conditions warrant.
True
PAUSE
Action
Pause [s]
U32
1000
True
U32
False
0
False

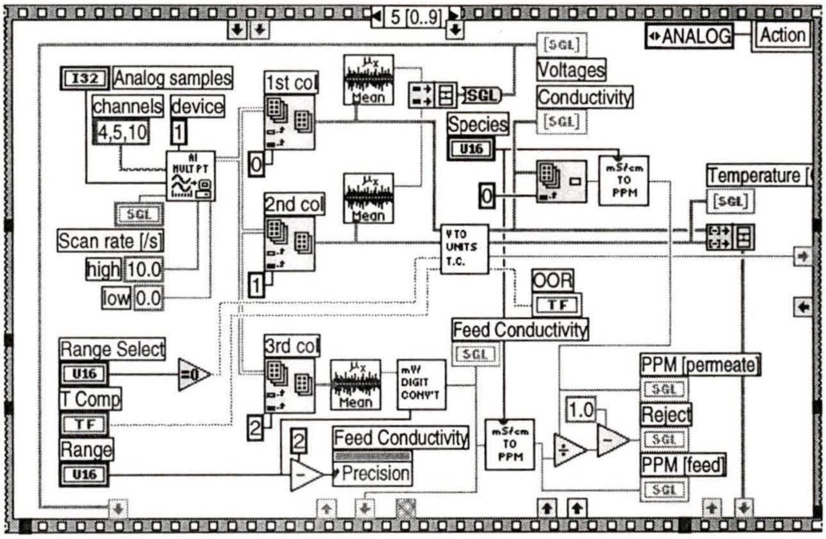
5 [0..9]
ANALOG
Action
I32
Analog samples
channels
device
4,5,10
1
AI MULT PT
SGL
Scan rate [/s]
high
10.0
low
0.0
1st col
0
Mean
2nd col
1
Mean
SGL
SGL
Voltages
Conductivity
SGL
Species
U16
0
mS/cm TO PPM
Temperature
SGL
V TO UNITS T.C.
OOR
TF
Feed Conductivity
SGL
Range Select
U16
=0
T Comp
TF
Range
U16
3rd col
2
Mean
mW DIGIT CONV'T
2
Feed Conductivity
Precision
mS/cm TO PPM
1.0
PPM [permeate]
SGL
Reject
SGL
PPM [feed]
SGL

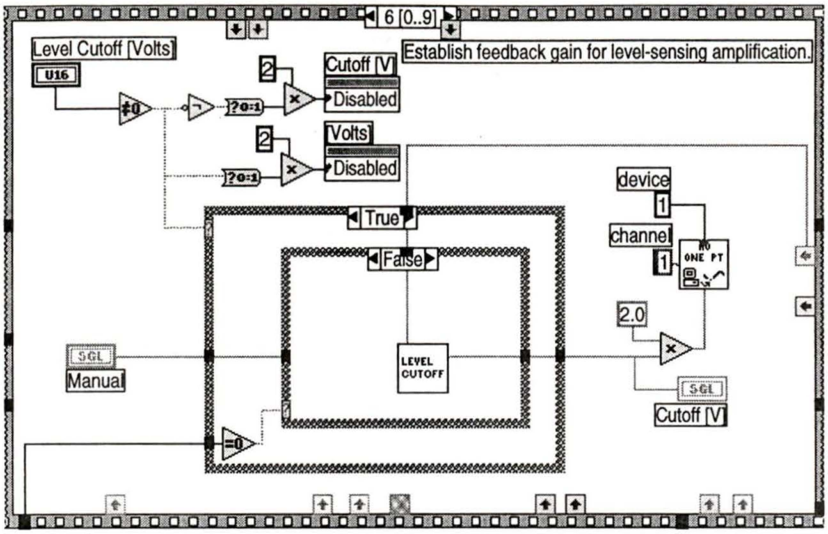
Establish feedback gain for level-sensing amplification.

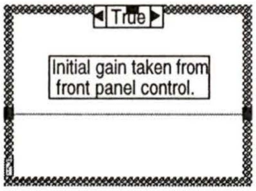
Initial gain taken from front panel control.

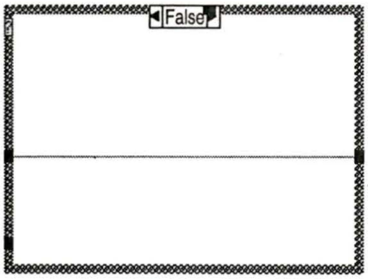

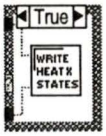

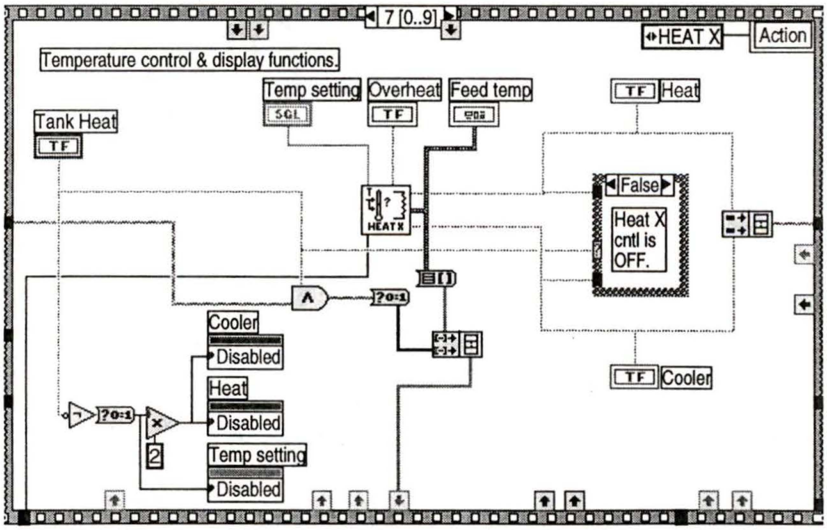
Temperature control & display functions.

Heat X cntl is OFF.

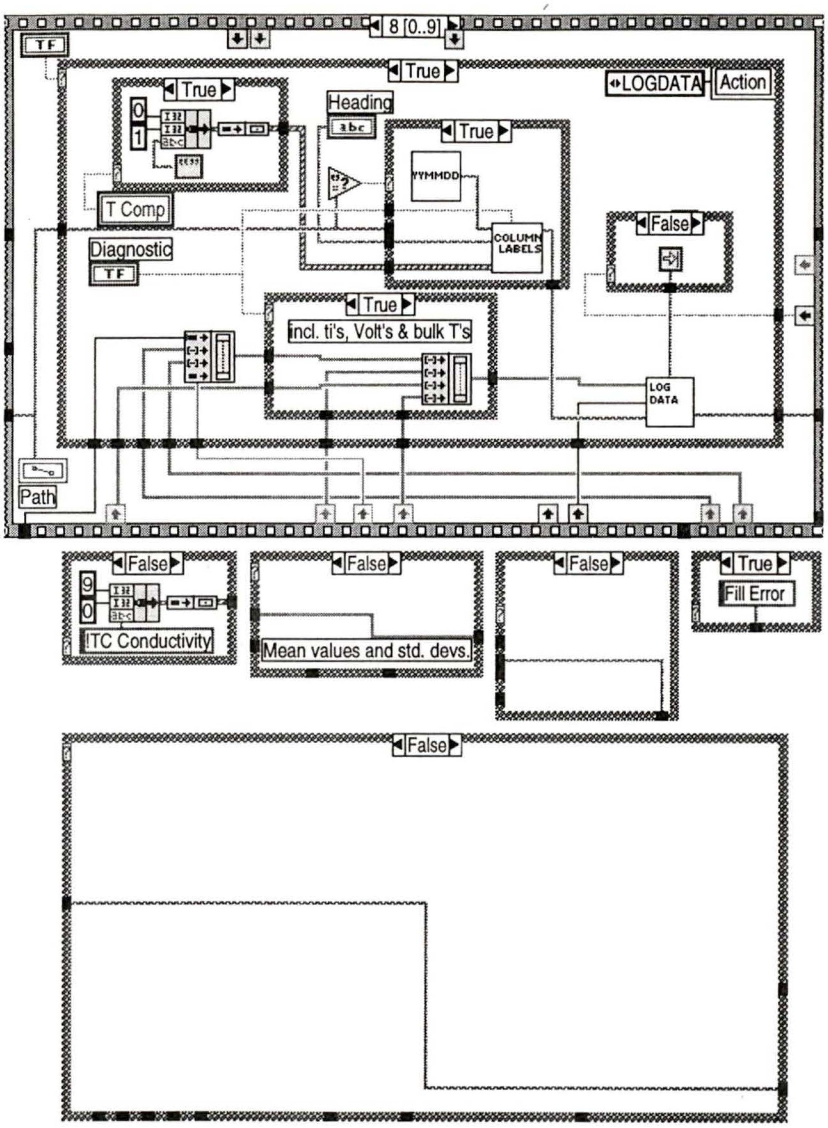
8 [0..9]
TF
True
LOGDATA
Action
True
0
1
Heading
abc
True
YYMMDD
T Comp
COLUMN LABELS
False
Diagnostic
TF
True
incl. ti's, Volt's & bulk T's
LOG DATA
Path
False
9
0
!TC Conductivity
False
Mean values and std. devs.
False
True
Fill Error
False

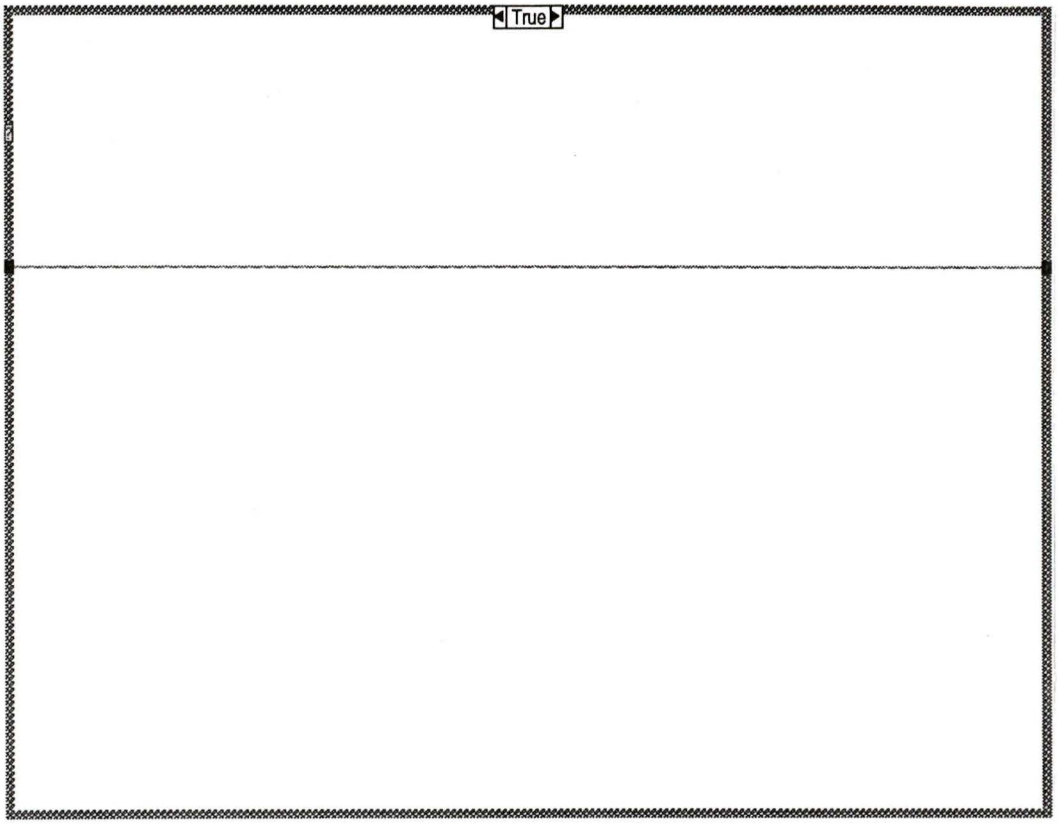
True

List of SubVIs

magnet drive.vi
A:\Pwgb.llb\magnet drive.vi

error check.vi
A:\PWGB.LLB\error check.vi

flow diagnostic.vi
A:\PWGB.LLB\flow diagnostic.vi

log data.vi
A:\PWGB.LLB\log data.vi

unit convert.vi
A:\PWGB.LLB\unit convert.vi

read levels on occurrence.vi
A:\PWGB.LLB\read levels on occurrence.vi

AI Clear.vi
D:\LABVIEW\vi.lib\DAQ\AI.LLB\AI Clear.vi

Simple Error Handler.vi
D:\LABVIEW\vi.lib\UTILITY\ERROR.LLB\Simple Error Handler.vi

Mean.vi
D:\LABVIEW\vi.lib\ANALYSIS\5STAT.LLB\Mean.vi

AO Update Channel.vi
D:\LABVIEW\vi.lib\DAQ\1EASYIO.LLB\AO Update Channel.vi

DAQ Occurrence Config.vi
D:\LABVIEW\vi.lib\DAQ\MISC.LLB\DAQ Occurrence Config.VI

stopwatch array.vi
A:\PWGB.LLB\stopwatch array.vi

column labels.vi
A:\PWGB.LLB\column labels.vi

parse filename.vi
A:\PWGB.LLB\parse filename.vi

AI Acquire Waveforms.vi
D:\LABVIEW\vi.lib\DAQ\1EASYIO.LLB\AI Acquire Waveforms.vi

mV digit conversion.vi
A:\PWGB.LLB\mV digit conversion.vi

level cutoff.vi
A:\PWGB.LLB\level cutoff.vi

weight cumulative values.vi
A:\PWGB.LLB\weight cumulative values.vi

dig port 2 handler.vi
A:\PWGB.LLB\dig port 2 handler.vi

dig port 3 handler.vi
A:\PWGB.LLB\dig port 3 handler.vi

loop control.vi
A:\PWGB.LLB\loop control.vi

clean up.vi
A:\PWGB.LLB\clean up.vi

seconds to clock.vi
A:\PWGB.LLB\seconds to clock.vi

flowcalc.vi
A:\PWGB.LLB\flowcalc.vi

preview.vi
A:\PWGB.LLB\preview.vi

Read From Spreadsheet File.vi
D:\LABVIEW\vi.lib\UTILITY\FILE.LLB\Read From Spreadsheet File.vi

Tcontrol w/2ndary cntl.vi
A:\PWGB.LLB\Tcontrol w/2ndary cntl.vi

write heat X states patch.vi
A:\PWGB.LLB\Write Heat X states patch.vi

ppm convert w/species.vi
A:\PWGB.LLB\ppm convert w/species.vi

range string maker.vi
A:\PWGB.LLB\range string maker.vi

Position in Hierarchy

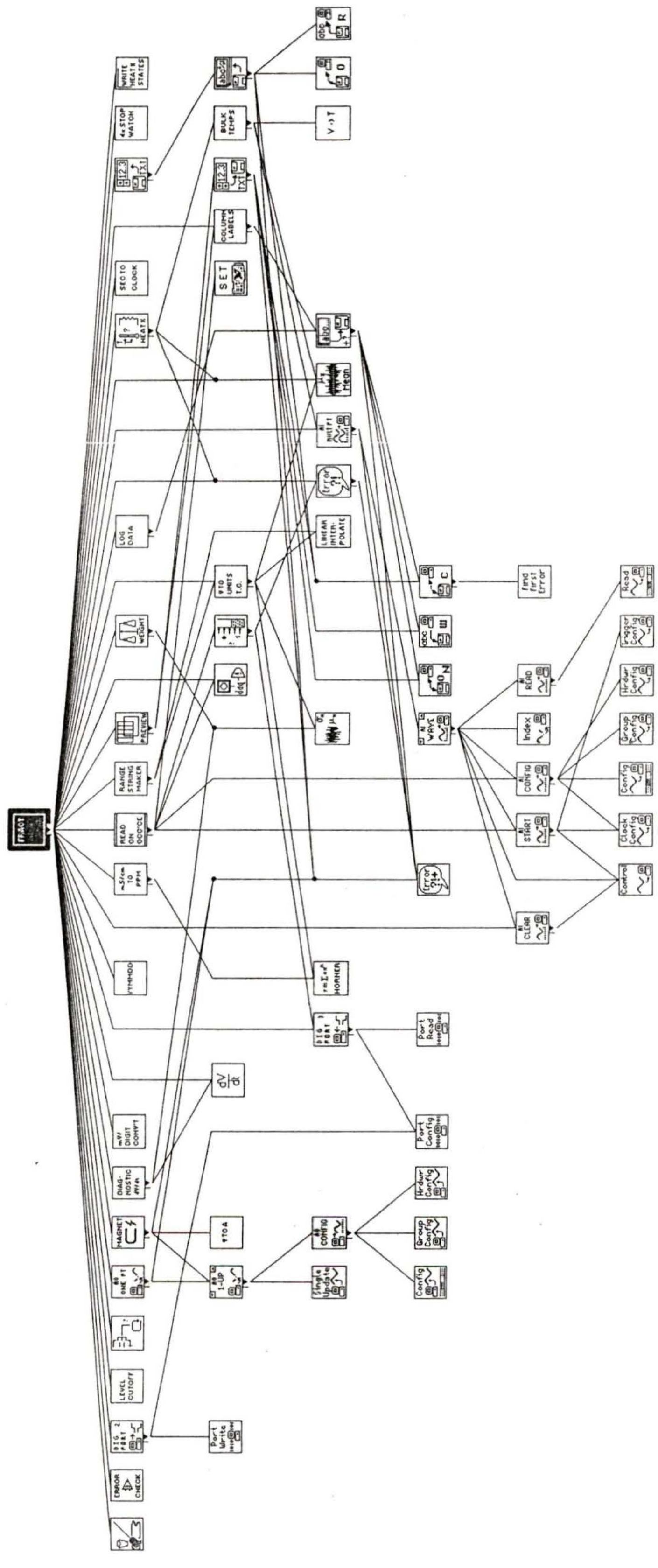

Vita

Surname:	Byrnes	**Given Names:**	Peter William George
Place of Birth:	Ottawa, Ontario, Canada	**Date of Birth:**	20 December, 1964

Educational Institutions Attended:

University of Victoria	1982-1984 1987-1989 1994-1997
University of Toronto, Victoria University	1985-1987

Degrees Awarded:

B.Sc.	University of Victoria	1989

Honours and Awards:

British Columbia Post-Secondary Scholarship (1982)
Austrian Government Prize for Excellence in Beginner's German (1984)
University of Victoria Graduate Teaching and Research Fellowship (1996)

Publications:

"The C•M•D•S Flow-Rate And Conductivity Transducer: A Custom Measurement System With Virtual Instrumentation Using LabVIEW," in *Proceedings, NIWeek97: The Worldwide Conference on Virtual Instrumentation*, Austin, Texas, USA, 1997.

Partial Copyright License

Title of Thesis:

The CMDS Flow-Rate and Conductivity Transducer:
Design, Manufacture, and Testing

Author:

[redacted]

Peter William George Byrnes
3 September, 1997

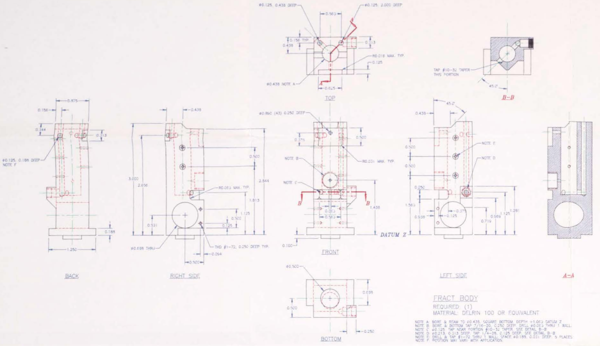

FRACT BODY
REQUIRED: (1)
MATERIAL: DELRIN 100 OR EQUIVALENT

NOTE A: BORE & REAM TO ⌀0.438, SQUARE BOTTOM, DEPTH +1.063 DATUM Z
NOTE B: BORE & BOTTOM TAP 7/16-20, 0.250 DEEP, DRILL ⌀0.063 THRU 1 WALL
NOTE C: ⌀0.125, TAP NEAR PORTION #10-32 TAPER, SEE DETAIL B-B
NOTE D: ⌀0.213, 0.313 DEEP, TAP 1/4-28, 0.125 DEEP, SEE DETAIL B-B
NOTE E: DRILL & TAP #1-72 THRU 1 WALL; SPACE ⌀0.188, 0.031 DEEP, 5 PLACES
NOTE F: POSITION MAY VARY WITH APPLICATION

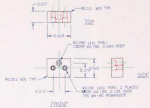

VALVE MOUNT
REQUIRED: (1)
MATERIAL: STAINLESS 316

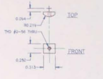

RETAINING NUT
REQUIRED: (1)
MATERIAL: STAINLESS 316

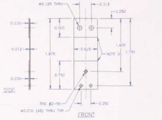

VALVE LEAF SPRING
REQUIRED: (1)
MATERIAL: STAINLESS 301 PLATE

NOTE G: REINFORCE TO 0.025 AS SHOWN
SILVER SOLDER OR SPOT WELD

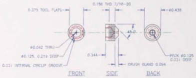

INTERCHANGEABLE SEAL BLANK
REQUIRED: (1)
MATERIAL: DELRIN

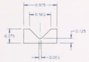

POLE SHIM
REQUIRED: (2)
MATERIAL: 0.063 PLASTIC SHIMSTOCK

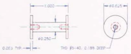

CORE
REQUIRED: (1)
MATERIAL: STAINLESS 430FR

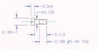

SHOULDER SCREW
REQUIRED: (2)
MATERIAL: STAINLESS 430FR

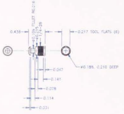

TEMPERATURE IC SOCKET
REQUIRED: (1)
MATERIAL: ALUMINUM

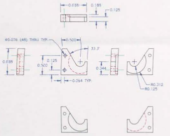

CLAMP
REQUIRED: (2): LEFT & RIGHT
MATERIAL: DELRIN

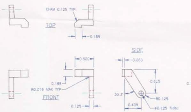

MAGNET POLE
REQUIRED: (2): LEFT & RIGHT
MATERIAL: STAINLESS 430FR

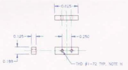

ARMATURE
REQUIRED: (2)
MATERIAL: STAINLESS 430FR

NOTE H: REPLACE THD #1-72 WITH CLEARANCE ⌀0.076 (48)
ON ONE PART, 2 PLACES

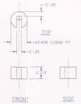

CONDUCTIVITY CELL
REQUIRED: (1)
MATERIAL: DELRIN

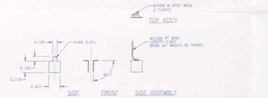

CONDUCTIVITY CELL ELECTRODE
REQUIRED: (2): LEFT & RIGHT
MATERIAL: 0.010 PLATINUM PLATE, ⌀0.020 PLATINUM WIRE

DATE	PART	REVISION DETAILS
97-04	MOUNT	STAINLESS REPLACES ALUMINUM
96-12	SEAL	CIRCLIP GROOVE INCLUDED
96-12	CORE	END WASHERS MADE INTEGRAL
96-11	BODY	CHAMBER SIDE PORT ELIMINATED
96-05	BODY	INSTALLATION FEATURES INCORPORATED

Flow-Rate And Conductivity Transducer

CMDS Research

NOTES:
FULL SIZE
DIMENSIONS:
INCHES ±0.005

UNIVERSITY OF VICTORIA
Department of Mechanical Engineering

DRAWING NUMBER	SHEET	DATE	DESIGNED BY	DRAWN BY
CMDS-01-26	1/1	02/97	P&B	P&B